DISSOLUTION AND MEMBRANE MASS TRANSPORT OF SUPERSATURATING DRUG DELIVERY SYSTEMS

by

Siddhi Santosh Hate

A Dissertation

Submitted to the Faculty of Purdue University

In Partial Fulfillment of the Requirements for the degree of

Doctor of Philosophy

Department of Industrial and Physical Pharmacy

West Lafayette, Indiana

May 2020

THE PURDUE UNIVERSITY GRADUATE SCHOOL
STATEMENT OF COMMITTEE APPROVAL

Dr. Lynne Taylor, Chair

Department of Industrial and Physical Pharmacy

Dr. Gintaras Reklaitis

Department of Chemical Engineering

Dr. Zoltan Nagy

Department of Chemical Engineering

Dr. Rodolfo Pinal

Department of Industrial and Physical Pharmacy

Dr. Susan Reutzel-Edens

Eli Lilly and Company

Approved by:

Dr. Rodolfo Pinal

To Mom, Dad and Saurin

ACKNOWLEDGMENTS

TABLE OF CONTENTS

LIST OF TABLES

LIST OF FIGURES

13

15

ABSTRACT

Supersaturating drug delivery systems are an attractive solubility enabling formulation strategy for poorly soluble drugs due to their potential to significantly enhance solubility and hence, bioavailability. Compendial dissolution testing is commonly used a surrogate for assessing the bioavailability of enabling formulations. However, it increasingly fails to accurately predict *in vivo* performance due its closed-compartment characteristics and the lack of absorptive sink conditions. *In vivo*, drug is continually removed due to absorption across the gastrointestinal membrane, which impacts the luminal concentration profile, which in turn affects the dissolution kinetics of any undissolved material, as well as crystallization kinetics from supersaturated solutions. Thus, it is critical to develop an improved methodology that better mimics *in vivo* conditions. An enhanced approach integrates dissolution and absorption measurements. However, currently-used two-compartment absorptive apparatuses, employing a flat-sheet membrane are limited, in particular by the small membrane surface area that restricts the mass transfer, resulting in unrealistic experimental timeframes. This greatly impacts the suitability of such systems as a formulation development tool. The goal of this research is two-fold. First, to develop and test a high surface area, flow-through, absorptive dissolution testing apparatus, designed to provide *in vivo* relevant information about formulation performance in biologically relevant time frames. Second, to use this apparatus to obtain mechanistic insight into physical phenomenon occurring during formulation dissolution. Herein, the design and construction of a coupled dissolution-absorption apparatus using a hollow fiber membrane module to simulate the absorption process is described. The hollow fiber membrane offers a large membrane surface area, improving the mass transfer rates significantly. Following the development of a robust apparatus, its application as a formulation development tool was evaluated in subsequent studies. The dissolution-absorption studies were carried out for supersaturated solutions generated via anti-solvent addition, pH-shift and by dissolution of amorphous formulations. The research demonstrates the potential of the apparatus to capture subtle differences between formulations, providing insight into the role of physical processes such as supersaturation, crystallization kinetics and liquid-liquid phase separation on the absorption kinetics. The study also explores dissolution-absorption performance of amorphous solid dispersions (ASDs) and the influence of resultant solution phase behavior on the absorption profile. Residual crystalline content in ASDs is a great concern from a physical

stability and dissolution performance perspective as it can promote secondary nucleation or seed crystal growth. Therefore, the risk of drug crystallization during dissolution of ASDs containing some residual crystals was assessed using absorptive dissolution measurements and compared to outcomes observed using closed-compartment dissolution testing. Mesoporous silica-based formulations are another type of amorphous formulations that are gaining increased interest due to higher physical stability and rapid release of the amorphous drug. However, their application may be limited by incomplete drug release resulting from the adsorption tendency of the drug onto the silica surface. Thus, the performance of mesoporous silica-based formulations was also evaluated in the absorptive dissolution testing apparatus to determine the impact of physiological conditions such as gastrointestinal pH and simultaneous membrane absorption on the adsorption kinetics during formulation dissolution. Overall, the aim of this research was to demonstrate the potential of the novel *in vitro* methodology and highlight the significance of a dynamic absorptive dissolution environment to enable better assessment of complex enabling formulations. *In vivo*, there are multiple physical processes occurring in the gastrointestinal lumen and the kinetics of these processes strongly depend on the absorption kinetics and *vice-a-versa*. Thus, using this novel tool, the interplay between solution phase behavior and the likely impacts on bioavailability of supersaturating drug delivery systems can be better elucidated. This approach and apparatus is anticipated to be of great utility to the pharmaceutical industry to make informed decisions with respect to formulation optimization.

CHAPTER 1.   INTRODUCTION

1.1   Research Significance, Specific Aims and Hypotheses

Oral administration is the most common route of drug administration, wherein the drug is first dissolved in the gastrointestinal fluids and then is absorbed across the gastrointestinal membrane to reach the systemic circulation. The compendial dissolution test, defined by the United States Pharmacopeia (USP), simulates the formulation dissolution process and is an important formulation development tool for oral formulations.[1] Along with its application to understand the physicochemical properties of drug substance, as well as product attributes, its link to drug absorption and hence, bioavailability has been increasingly explored.[2–4] However, with the rise in the number of poorly water soluble drugs in the drug discovery pipeline over the past two decades, the optimization of drug delivery systems using solubility enabling formulation strategies has become increasingly important.[5,6] These formulation strategies are extremely complex and sensitive to the dissolution environment. Interestingly, even though formulation science has evolved over the past few decades, standard (i.e. closed compartment) dissolution testing is still widely used to assess formulation performance. For increasingly complex formulations containing poorly soluble drugs, it is often difficult, if not impossible, to predict *in vivo* performance from such measurements.[2] Thus, obtaining meaningful dissolution data for better prediction of drug product performance is imperative to optimize pharmaceutical formulation development and there is a substantial need for improving release testing methodology.

Over the past few years, several designs have been proposed to overcome known challenges of dissolution testing with respect to hydrodynamics, fluid volume, environment pH, gastric emptying and fluid composition (i.e. use of biorelevant fluids).[2,7–9] Although these developments include modifications to the dissolution conditions, they do not incorporate an absorptive sink environment. The presence of an absorptive compartment in dissolution studies is important for testing solubility enhancing formulations, particularly those that supersaturate and potentially undergo precipitation during gastrointestinal (GI) transit. This is because the mass transport rate of drug from the dissolution compartment into the receiver compartment not only provides information about the solution thermodynamics, but as the drug is continuously removed,

it will also impact the supersaturation profile, which in turn will impact dissolution kinetics of any undissolved material, as well as crystallization kinetics.

Therefore, the goal of this research was to develop a dissolution methodology that can incorporate absorption in combination with dissolution, to provide *in vivo*-relevant information about formulation performance, and enable better discrimination between complex formulations based on differences in mass transport profiles and total amount of drug transferred, relating these factors to different solution phase behaviors. **The first aim of this study was to design and construct a large membrane surface area, flow-through absorptive dissolution testing apparatus to achieve faster and substantial membrane mass transfer in order to study formulation performance over biorelevant time frames.** The central component of the apparatus is a hollow fiber membrane to simulate the absorption process. The large surface area of the membrane increases the rate of mass transfer while the flow-through operation of the apparatus offer potentially more *in vivo*-relevant conditions. *It was hypothesized that faster mass transfer in the hollow fiber membrane-based apparatus as compared to conventional side-by-side diffusion apparatus would provide superior prediction of formulation performance.*

Supersaturated solutions impart higher membrane flux, particularly when the system does not undergo crystallization over biorelevant time frames, due to the higher thermodynamic activity of the drug species.[5,10,11] A highly supersaturated solution of a hydrophobic compound may undergo liquid-liquid phase separation (LLPS), when the solute concentration exceeds the amorphous solubility of the drug in the aqueous medium, leading to the formation of drug-rich nanoparticulate species.[12–15] In the absence of crystallization, these drug-rich nanodroplets can serve as a drug reservoir, replenishing drug to the aqueous phase from which absorption across the membrane occurs, until the drug-rich phase ultimately depletes.[10] The drug-rich phase can be obtained by instantaneous addition of concentrated stock solution of the drug into the aqueous medium or by dissolution of amorphous solid dispersions (ASDs). **The second aim of this study was to evaluate the absorption behavior of solutions undergoing LLPS using the new absorptive dissolution testing apparatus and assess enhancement in absorption due to dissolution of amorphous solid dispersions.** *It was hypothesized that the formation of a drug-rich phase via LLPS would result in higher mass transport across the membrane due to the*

reservoir effect of the drug-rich nanodroplets and enhanced absorption would be observed for ASDs undergoing LLPS upon dissolution.

Amorphous solid dispersions often improve the oral bioavailability of poorly soluble drugs. However, drug crystallization may occur either during manufacturing or storage, particularly at elevated temperature and humidity.[16–19] The resultant residual crystallinity would be anticipated to diminish the solubility and bioavailability advantage offered by these formulations. Therefore, accurate *in vitro* evaluation of such formulations is of paramount importance at several levels of drug product development such as bioavailability assessment, process development, process validation, quality control or bioequivalence testing. Compendial dissolution testing, due its closed-compartmental setup, large dissolution volume and lack of absorptive sink conditions, has poor discriminatory power to assess complex formulations. Therefore, **the aim of this study was to utilize the apparatus developed herein to study the dissolution and absorption behavior of amorphous formulation with varied amounts of residual crystallinity, using different volumes of dissolution fluid.** Residual crystalline content is expected to seed crystal growth from the supersaturated solution. *It was hypothesized that simultaneous absorption of drug across the membrane would lower the supersaturation in the dissolution compartment, thereby reducing the risk of crystallization of drug in a crystal seeded environment.*

Amorphous formulations are attractive formulation strategies to improve bioavailability of poorly soluble drug compounds. One such strategy includes mesoporous silica-based drug delivery systems wherein the drug compound is encapsulated into the silica pores. The large specific surface area of silica offers high drug loading[20,21] and due to confinement of drug molecules in the nanopores, drug exists in the amorphous state, providing solubility and bioavailability advantages.[22–26] Although mesoporous silica-based formulations offer better physical stability, dissolution often results in incomplete drug release.[27] Therefore, **the next aim of this study was to understand the potential reason for incomplete drug release from silica formulations and the impact of absorptive dissolution measurements on drug release profile.** *It was hypothesized that incomplete release of drug was due to adsorption of the drug molecule onto the silica surface. As a result, the dissolution performance of mesoporous silica-based formulations may be enhanced in the presence of an absorptive compartment as the simultaneous removal of*

drug across the membrane would alter the adsorption kinetics of the drug-silica system due to a reduction in the solution concentration.

The performance of mesoporous silica-based drug delivery systems is dependent upon the strength and type of interactions that exists between drug molecules and silica in the solid and solution state.[28–30] The surface chemistry of silica is very complex. The silica surface has isolated silanol groups that typically interact with functional groups of drug molecules via hydrogen bonding or electrostatic interactions. When suspended in aqueous medium, surface silanols protonate or deprotonate, and exist in a positive, negative or neutral charged state, depending upon the pH of the solution. As drug-silica interactions and drug solubility are important driving forces for drug release and drug adsorption, both processes can be controlled by the solution pH, particularly for ionizable poorly soluble drugs as pH alters drug ionization and solubility. **The aim of this study was to evaluate the effect of solution pH on the adsorption tendency of weakly basic drugs onto the silica surface, as well as the dissolution of drug-loaded mesoporous silica formulations, at different physiologically relevant pH values to assess formulation performance during gastrointestinal transit.** *It was hypothesized that weakly basic drugs that are ionized at intestinal pH conditions will result in poor drug release due to electrostatic interactions between the positively charged drug molecule and the negatively charged silica surface, and hence suboptimal drug release may occur.*

1.2   Dissolution Testing

For oral solid dosage forms, the dissolution profile is an important *in vitro* characteristic of a formulation under development. Dissolution testing is widely used to obtain several types of information during drug product development process such as selecting appropriate excipients or a suitable solid form of the compound for the desired dissolution profile.[4] Hence, it is typically used to understand the physicochemical properties of a drug substance and the drug product attributes.[2] Dissolution testing plays an important role in determining whether the dosage will dissolve in the patient's gastrointestinal tract. Even if the solid form disintegrates immediately, it is the dissolution rate of the solids that will ultimately determine the amount of drug available for absorption.[1] As a quality control test, dissolution testing confirms batch-to-batch reproducibility, that manufacturing procedures are followed for a given batch, and a consistent product

performance throughout the shelf-life. Dissolution testing typically provides quality assurance and is critical in determining the effects of processing parameters on stability and bioavailability. Hence, it is an important part of the approval process for a new solid oral dosage. With the FDA's specification to minimize bioavailability testing in humans, clinical scientists place increasing reliance on *in vitro* dissolution testing in combination with mathematical modeling to predict *in vivo* performance. Physiological conditions such as fluid volume, media composition, hydrodynamics and transit time can have significant influence on the rate of dissolution and concentration of drug available for absorption.[4] Hence, if the tests are not performed under appropriate conditions, the *in vitro* predictions will be inaccurate, potentially delaying the development process. It is, therefore, imperative to develop an *in vitro* dissolution test that can mimic gastrointestinal conditions and give the desired information in a relevant time frame.

1.2.1 Dissolution-Solubility Relationships

1.2.1a. Solubility

Attaining the equilibrium solubility of an organic solute following dissolution of the solid depends on a series of events. The first step includes breakage of solute-solute bonds, the strength of which depends on the extent of attractive forces in the solids. These are typically higher for electrolytes than for nonelectrolytes, and for crystalline solids than for amorphous solids. This is followed by the formation of a void in the solvent to accommodate a solute molecule. The solute molecule then enters the solvent void. Thus, the extent of solubility depends upon how energetically favorable these processes are.[31] In terms of a crystalline solid, the solubility is the concentration of the solute in the solution in equilibrium with the solid.[32] Crystalline solubility is given by equation 1.1:

$$\ln(x^c \gamma^c) = \frac{\mu^c - \mu^0}{RT} \tag{1.1}$$

where x^c is the mole fraction solubility of crystalline drug, γ^c is the activity coefficient of the drug at saturation, R is universal gas constant, $(\mu^c - \mu^0)$ is the difference in the chemical potential between crystal and the standard state (supercooled or pure liquid) at temperature, T. The process of breaking of crystal lattice is considered analogous to the melting of crystal and hence, solubility X follows a van't Hoff type equation,

$$\ln X = \frac{\Delta H_f}{R}\left[\frac{1}{T_m} - \frac{1}{T}\right] \tag{1.2}$$

where ΔH_f is the heat of fusion and T_m is the melting temperature. The above equation is the ideal solubility where the mixing of solute and solvent molecules results in no net energy change, and the activity coefficient is unity. However, in the case of non-ideal solution behavior, equation 1.2 becomes as follows,

$$\ln X = \frac{\Delta H_f}{R}\left[\frac{1}{T_m} - \frac{1}{T}\right] - \ln\gamma \tag{1.3}$$

The activity coefficient can be given by regular solution theory and is a function of the difference in the solubility parameter of solvent (δ_1) and solute (δ_2), the molar volume of the solvent (V_1) and the volume fraction of the solute (φ_2) as shown below,

$$\log\gamma = \frac{V_1\varphi_2^2}{2.303\,RT}(\delta_1 - \delta_2)^2 \tag{1.4}$$

The thermodynamic driving factors of solubility for a particular compound can be determined from the above equations.[6] Hence, the solubility of a poorly soluble drug can be limited either by the strength of the crystal lattice, or unfavorable solute-solvent interactions, or both. Compounds that are hydrophobic show poor solubility in water. If these compounds have strong intermolecular forces, they will be poorly soluble in both aqueous and non-aqueous solvents, whereas if they are limited only by poor affinity to water, they can be soluble in non-aqueous solvents.

1.2.1b. Dissolution Rate

The rate of dissolution of a drug is defined in terms of the change in concentration of dissolved drug, *dc,* in a specific time interval *dt*. The first introduction of the dissolution rate was in the seminal work by Noyes and Whitney in 1897, wherein the dissolution of a solute from the solid is based on a simple process of diffusion.[33] The rate of dissolution of a substance is given as follows:

$$\frac{dC}{dt} = k(C_s - C) \tag{1.5}$$

where k is a constant, C_s is the saturation solubility, and C is the instantaneous concentration at time, t. The dissolution is governed by diffusion of molecules across a thin diffusion layer formed on the solid surface into the bulk aqueous phase, shown in Figure 1.1.
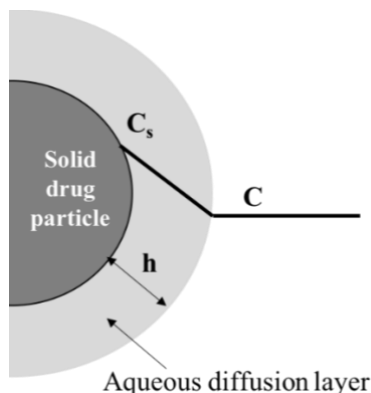
Figure 1.1: Graphical representation of dissolution mechanism.

Equation 1.5 was further modified by Nernst-Brunner based on the diffusion layer model and Fick's second law to incorporate specific relations between the constants involved as follows:

$$\frac{dC}{dt} = \frac{DS}{Vh}(C_s - C) \tag{1.6}$$

where D is the diffusion coefficient, S is surface area of the solid, h is the thickness of the diffusion layer and V is the volume of the dissolution medium.[34]

In relation to the prediction of oral absorption, the solubility of the compound in bulk solution, C_s, determines two characteristics of the dissolution profile (1) the slope of the dissolution profile ($D.S.C_s/h$) (2) the plateau concentration, which indirectly determines oral absorption.[35] Therefore, the rate at which drug is released into the aqueous media and the equilibrium solubility are critical, as the time available for dissolution and absorption is limited in the GI tract.[6,36] Both solubility and dissolution rate can be increased by reducing intermolecular forces in solid-state,

increasing the strength of solute-solvent interactions in solution or increasing the surface area of the solid available for dissolution.

1.2.2   Types of dissolution testing apparatus

1.2.2a. USP 1/2 Apparatus

The conventional dissolution testing setup, USP 1/2 systems, are simple paddle/ basket systems providing a well-stirred, medium-rich environment for evaluating disintegration and dissolution of solid dosage forms.[1] The apparatus is used for all types of oral solid dosage. The basket is useful when the dissolution test includes a change of media from gastric to intestinal fluid. However, changing the media is difficult and this lack in flexibility may result in poor prediction for drugs undergoing changes in solution concentration with change in location in the GI tract.[7] Considering body temperature, dissolution tests are typically carried out at 37 °C. The fluid volume used in the apparatus ranges from 500-1000 mL, a volume corresponding to the fed state of stomach. The large volume of fluid also helps sink conditions to be incorporated during testing. The hydrodynamics in the dissolution vessel are controlled by paddle rpm. However, these hydrodynamics do not mimic GI conditions due to inherent variability and formation of dead zones in the dissolution vessel.

Due to certain limitations of the USP 1/2 apparatus, such as poor hydrodynamics, lack of flexibility of fluid compositions and high fluid volumes, dissolution testing may be unrepresentative of true *in vivo* performance. Several designs have been proposed to overcome challenges suffered by compendial dissolution testing methods.

1.2.2b. Reciprocating Cylinder

The reciprocating cylinder apparatus is similar to a disintegration tester with an open cylinder containing the solid dosage form placed in a vessel that is maintained at 37 °C. The cylinder is moved up and down at a speed that can generate *in vivo*-relevant hydrodynamics. The mesh at the bottom of the cylinder also controls the hydrodynamics. The main advantage of the reciprocating cylinder over the basket/paddle method is the flexibility to study dissolution in different media and the absence of hydrodynamic dead zones. However, the operating volume is low and hence it is difficult to maintain sink conditions in this apparatus.[7]

1.2.2c. Flow-through cell, USP 4

The Pharmacopeia has standardized a flow-through cell for studying dissolution of solids. It consists of a reservoir with dissolution media maintained at 37 °C. The dissolution media is continuously circulated either in open or closed loop using a pump. The cell has a filter system that prevents escape of undissolved particles from the top and bottom of the cell which is filled with glass beads.[37] A tablet holder is used to hold the tablet in the center of the apparatus. The flow profiles generated in the apparatus are more uniform compared to other USP apparatus. The flow-through operation of the apparatus allows flexibility in controlling hydrodynamics, maintaining sink conditions and mimicking change in fluid compositions during GI transit.[7] It is attractive tool for testing dissolution of poorly soluble drug compounds.

1.2.2d. Artificial Stomach Duodenal Model

Compendial dissolution techniques have been modified to accommodate certain physiological conditions that mimic the GI tract, however, due to methodology constraints, it is difficult to predict physical processes during dissolution such as crystallization or supersaturation occurring due to changes in media and pH during the transit. To overcome these limitations, several non-compendial dissolution methodologies have been proposed. The most *in vivo*-relevant is the artificial stomach duodenal model.[38] The apparatus consists of two compartments, mimicking stomach and duodenum. Gastric emptying is incorporated by controlling the rate of transfer of solution from the stomach compartment to the duodenal chamber, where the pH of the media is at the intestinal pH. The concentration of drug in the duodenum chamber is correlated to *in vivo* bioavailability. However, the bioavailability predicted by this apparatus may not be well correlated with *in vivo* performance if it is permeability-limited or the formulation is a controlled-release type with some residence time in lower gastrointestinal region.[2]

1.2.3 Failure of *In Vivo* Prediction by Dissolution Testing

Solubility is key to dissolution and bioavailability. A significant increase in the number of candidates exhibiting poor water solubility in past two decades has resulted in the evolution of several solubility enhancing formulation strategies. The most common approaches used in marketed products include cosolvents, salts, polymorphs, co-crystals, surfactants, cyclodextrins, particle size reduction, lipid-based systems, and amorphous solid dispersions.[6] These strategies

result in enhanced solution concentration in two ways: by creating supersaturated solutions or by adding components that solubilize the drug.[5] Formulation strategies such as addition of surfactants or cyclodextrins solubilize the drug by partitioning of drug in micellar structure or formation of inclusion complexes. A large increase in the solubility however impacts the free concentration of the drug in the solution and hence, the thermodynamic activity of the drug. This may result in the decrease in amount of drug available for absorption and reduce bioavailability.[39] If these formulations are studied using dissolution testing to assess the *in vivo* performance, the results may not correlate with the *in vivo* data. This is because enhanced solubility in the presence of additives does not necessarily increase the free drug concentration. Miller et al.[40] demonstrated the effect of surfactant on the permeability of progesterone. With an increase in sodium lauryl sulfate and sodium taurocholate concentration beyond the critical micelle concentration, a decrease in permeability of progesterone in a single-pass rat jejunal perfusion model was observed. Thus, in addition to dissolution testing, formulations containing solubility-enhancing additives should be tested for apparent permeability changes and flux.

Formulation strategies such as amorphous solid dispersions, on the other hand, generate supersaturated solutions, where the thermodynamic activity of solute exceeds that of the crystalline drug. Hence, these strategies enhance the free drug available in the solution. However, supersaturation is thermodynamically metastable and system is susceptible to crystallization in order to lower the free energy of the system. Dissolution testing in a well-stirred, simple, one-compartment apparatus often fails to predict *in vivo* performance of supersaturating formulations as it is does not reflect the impact of physical processes such as crystallization, true supersaturation or phase separations occurring during dissolution of supersaturating formulations. DiNunzio et al.[41] studied the dissolution performance of Sporanox and amorphous solid dispersions (ASD) of itraconazole with cellulose acetate phthalate (CAP). The *in vitro* dissolution studies showed that ASDs with CAP dissolved more slowly as compared to Sporanox pellets, indicating Sporanox was a better formulation, since drug release was faster. However, *in vivo* plasma concentration showed higher C_{max} and area under the curve (AUC) for ASDs with CAP. Hence, the conclusions drawn from *in vitro* studies did not correlate with the *in vivo* results. In addition to poor correlation of the dissolution profile and the *in vivo* concentration profile, supersaturated solutions undergo crystallization, the kinetics of which can be altered by subsequent removal of drug from the

dissolution compartment due to simultaneous absorption. Bevernage et al.[42] demonstrated that precipitation of drug from a supersaturated solution was less extensive when dissolution studies were carried out in the presence of an absorptive compartment.

The evaluation of dissolution and mass transfer to estimate overall drug absorption can provide formulation scientists with better sensitivity of the product performance to formulation changes.[43] Hence, considering the limitations of dissolution testing to predict the performance of solubility enhancing formulations, it is important to consider mass transfer or flux measurements to discriminate between formulations and improve understanding of the true bioavailability advantage from such formulations.

1.3 Mass Transfer Measurements

1.3.1 Membrane Mass Transport

The mass transport per unit surface area of a membrane has two principle components: convection, transport by bulk motion and diffusion, transport by molecular displacement. Herein, only diffusive mass transport is discussed.

1.3.1a. Diffusion

Any perturbations in temperature or concentration of a chemical species results in a gradient that tends to disappear over time. The spontaneous dissipation of such gradients is by movement of energy, mass and momentum from a region of higher concentration to lower concentration, generally known as *diffusion*, and is characterized by small-scale molecular displacements.[44] The diffusion process is defined using Fick's first law,

$$J = -D\frac{\partial C}{\partial x} \tag{1.7}$$

where J is mass flux or the rate of mass transfer per unit area, D is the diffusion coefficient, and dC/dx is the gradient in the concentration in a direction, x. The diffusivity or diffusion coefficient of a molecule in a liquid is dependent on the hydrodynamic force acting on the molecule and is given by Stokes-Einstein equation,

$$D = \frac{kT}{6\pi\eta r} \tag{1.8}$$

where k is the Boltzmann constant, T is temperature, η is dynamic viscosity and r is radius of the molecule.

Thermodynamically, diffusion occurs so as to minimize the free energy of the system and as free energy is a function of chemical potential, the gradient in the chemical potential is the true driving force for diffusion. The chemical potential (μ_i) is given as,

$$\mu_i = \mu_i^o + RT \ln a_i \tag{1.9}$$

where μ_i^o is reference chemical potential and a_i is activity of the species, such that $a_i = c_i \gamma_i$. Hence diffusive flux is given as,

$$J = -D\left(1 + \frac{\partial \ln \gamma}{\partial \ln C}\right)\nabla C \tag{1.10}$$

The diffusion coefficient is affected by solution non-ideality.

In terms of general conservation equations, the steady-state diffusion is given by Fick's second law where the change in concentration over time in one dimension is given by the change in flux across the diffusion barrier:

$$\frac{\partial C}{\partial t} = -\frac{\partial J}{\partial x} \quad \text{or} \quad \frac{\partial C}{\partial t} = D\frac{\partial^2 C}{\partial x^2} \tag{1.11}$$

1.3.1b. Steady State Diffusion in Thin Films and Membrane Barrier

A typical mass transfer across a membrane includes an aqueous barrier in addition to the membrane barrier, as shown in Figure 1.2.[45] The solutions on both sides of the membrane become less and less stirred as they approach the membrane surface.
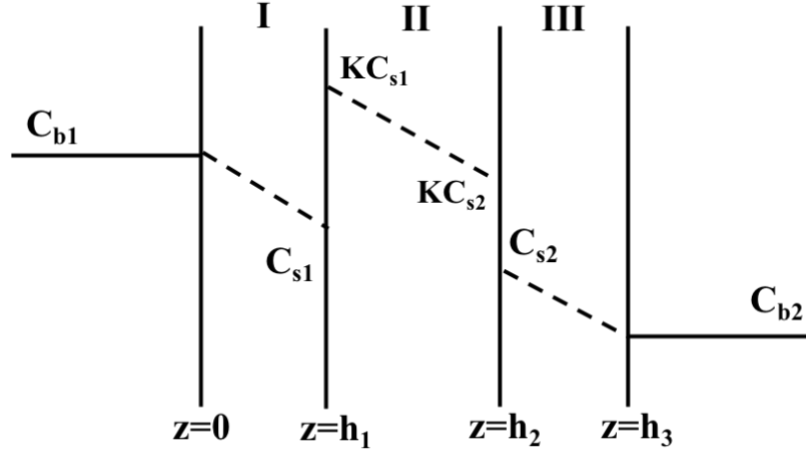
Figure 1.2: Schematic of diffusion barriers in membrane mass transport. Region I and III represent aqueous diffusion layer and Region II represent membrane.

The mass balance across the aqueous diffusion layer is given by,

$$Accumulation = (rate\ of\ diffusion)_{in} - (rate\ of\ diffusion)_{out} \tag{1.12}$$

At steady state, the accumulation is 0, hence in a small element of thickness Δz ,

$$0 = A\ (J_z - J_{z+\Delta z}) \tag{1.13}$$

Using Fick's first law and gradient of flux across the thin film, at steady state,

$$0 = -D\frac{d^2C}{dz^2} \tag{1.14}$$

Boundary conditions can be defined,

$$z = 0, C = C_{b1}\ and\ z = h_1, C = C_{s1}$$

Solving equation 1.14 and substituting boundary conditions,

$$C = C_{b1} + (C_{s1} - C_{b1})z/h_1 \tag{1.15}$$

And flux is given by,

$$J_I = \frac{D}{h_1}(C_{b1} - C_{s1}) \tag{1.16}$$

Similarly, the flux across region III can be written as,

$$J_{III} = \frac{D}{h_3}(C_{s2} - C_{b2}) \tag{1.17}$$

The steady state flux across the membrane is determined similarly using mass balance across the membrane and is given by,

$$J_{II} = \frac{KD_m}{h_2}(C_{s1} - C_{s2}) \tag{1.18}$$

The overall flux across the membrane is typically written in terms of overall or effective permeability P_{eff},

$$J = P_{eff} (C_{b1} - C_{b2}) \tag{1.19}$$

such that,

$$\frac{1}{P_{eff}} = \frac{1}{P_I} + \frac{1}{P_{II}} + \frac{1}{P_{III}} \tag{1.20}$$

where $P_I = \frac{D}{h_1}$, $P_{II} = \frac{KD_m}{h_2}$ and $P_{III} = \frac{D}{h_3}$ and the mass transport barriers are treated as resistance in series.

1.3.2 Dissolution-Absorption Studies of Pharmaceutical Formulations

The importance of mass transfer studies to determine true drug concentration and in turn, bioavailability is reasonably well established. One of the simplest approaches to incorporate absorption measurements during dissolution studies is biphasic dissolution testing. An organic layer is added to the aqueous medium and drug dissolved in the aqueous medium partitions into the organic layer at the top.[46] A biphasic test offers three main advantages. There is no accumulation of drug in the aqueous phase, the free drug concentration can be measured by evaluating the concentration in the organic phase and reduced analytical challenges due to the formation of a solution free of undissolved solids. Gao et al.[47,48] incorporated biphasic dissolution with the USP IV apparatus for evaluating the performance of poorly soluble drug compounds. They illustrated the importance of an absorptive compartment in evaluating supersaturation generated during dissolution, obtaining a better discrimination between formulations. A lower supersaturation was generated for formulations due to simultaneous partitioning of drug into the organic layer and these results correlated well with *in vivo* performance. Frank et al.[49] included a pH-shift into the biphasic dissolution test leading to improved prediction of formulation performance as compared to single phase dissolution. Although the biphasic system provided interesting findings, the use of organic solvent and the lack of a physical barrier between the two phases limits its applicability. Solvent volatility, emulsion formation with surfactant-enriched biorelevant media or blocking of sampling lines due to viscous solvents are some of the issues that have been reported for the biphasic system.[46]

An alternative approach to performing dissolution-absorption measurements is the use of a two-compartment system separated by a membrane barrier, wherein drug present in the donor compartment diffuses across the membrane into a receiver compartment. Several studies have been performed to develop an *in vitro* methodology using dissolution-permeation systems and to correlate the results with *in vivo* performance. Ginski and Polli[43] were one of the first to develop a dissolution/Caco-2 system to predict formulation performance. They evaluated fast and slow dissolving immediate release formulations and correlated the performance with the clinical data. Since then several modifications have been made to the membrane, fluid composition or configuration of the apparatus. Kataoka et al.[50,51] carried out simultaneous dissolution and absorption studies of solid oral dosage forms in a side-by-side diffusion cell with a Caco-2 monolayer mounted in between, to predict oral absorption. They also studied the rate-limiting step in oral absorption and distinguished formulations based on dissolution, solubility or permeability limited.[52,53] Motz et al.[54] demonstrated use of a flow-through diffusion cell to study permeation of drug dissolved from tablets across a Caco-2 monolayer. A double artificial membrane permeability assay was also developed to incorporate an intracellular compartment in absorption measurements while maintaining the appropriate pH in apical, intracellular and basolateral compartments.[55]

Some absorption studies have been performed using artificial membranes as well. The most standard membrane model is the parallel artificial membrane permeability assay (PAMPA) wherein the setup consists of 96-well microtiter plate containing hydrophobic filters that are saturated with a lecithin – organic solvent mixtures.[56,57] A number of studies have demonstrated the use of artificial membranes to study membrane flux and to evaluate formulation performance of poorly soluble drug compounds.[10,11,58,59]

1.3.3 Limitations of Conventional Mass Transport Apparatuses

The currently used *in vitro* apparatuses to determine the mass transport of poorly water-soluble drugs, however, have certain limitations which impact their usefulness for absorptive dissolution testing. The most important limitation is the small surface area of the membrane available for absorption in a typical side-by-side setup. The small surface area results in slower mass transfer and a long experimental duration to obtain significant information about formulation performance. The small volumes of the apparatus result in analytical detection limits, particularly

for poorly soluble drugs and concentration measurements in the receiver compartment. The poor hydrodynamics in most of the mass transport apparatuses increase the unstirred water layer barrier adjacent to the membrane surface. This aqueous layer can further slow the mass transfer if the drug compound is lipophilic. Moreover, the small volumes of the apparatus can result in non-sink conditions in the receiver compartment and this may result in back diffusion of drug molecule into the donor compartment. Poorly soluble compounds have a high tendency to generate non-sink conditions during mass transfer measurements. The conventional apparatuses also fail to capture the pH dynamics in the GI tract as experiments have to be carried out at fixed pH. This is an important consideration while studying performance of weakly basic drugs. All of these limitations can alter the rate of mass transfer and also impact the dissolution rate in an *in vitro* setup, resulting in failure in the prediction of *in vivo* performance.

1.4 Hollow Fiber Membranes

1.4.1 Configuration and Properties

A typical hollow fiber membrane module is shown in Figure 1.3. A single module contains a bundle of hollow fibers which are encapsulated at each end forming tubesheets. This allows direct flow of fluids in and out of the lumen of the fibers. A circumferential header adjacent to the tubesheets allows flow of fluid on the outer or shell side. The module is geometrically similar to a shell-and-tube heat exchanger.[60]

Figure 1.3: A hollow fiber membrane module offering surface area of 100 cm[2].

The hollow fiber membrane design has widespread application for separation processes in liquids such as liquid-liquid extraction or dialysis. The membrane module is easy to manufacture, and its compactness and reliable performance makes it advantageous over other membrane configurations. Moreover, a large surface area of the membrane is available due to the presence of

several membrane fibers in a single module.[61] Several varieties of hollow fiber membranes with different membrane materials, pore size distribution and surface area are available. The membrane material properties and device dimensions play an important role in mass transfer efficiency of the module and hence, selection of the appropriate module lies in its application.[62] The membrane material that can be used for studying absorption of a pharmaceutical drug should be hydrophilic in nature such that it is wetted by the aqueous media used in the study. *A priori* prediction of the material selection is difficult due to adsorption of drug on the membrane. The pore size distribution in the membrane should be such that pore size is able to exclude suspended particles in the fluids. Moreover, the pore size distribution is the determining factor in mass transport mechanism. The mass transport across membranes with smaller pore size is typically diffusion-controlled, while membranes with larger pore size will have significant contribution of both convection and diffusion. For this particular application, membranes with a pore size lower than 20 nm were chosen to study diffusive flux across the membrane. There is a lower limit to the number of fibers in a single module and the diameter and thickness of the individual fibers. Selection of the module should also consider the overall surface area and thickness of the fibers to achieve the desirable rate of mass transfer. The flow of fluids inside the lumen of fibers and in the shell-side of the module can be co-current or countercurrent depending upon uniformity of the flow in the channels and overall mass transfer performance. Flow of fluids in the hollow fiber membrane allows design of a flow-through setup, thus providing an important advantage over other configurations.

1.4.2   Hollow Fiber Membranes to Simulate Intestinal Absorption

A hollow fiber membrane module was first used to simulate intestinal absorption in a multi-compartmental, dynamic, computer-controlled model of human upper gastrointestinal tract (TIM-1) to assess the amount of digested food or drug substance available for absorption.[63] Hydrodynamics in this apparatus are controlled by altering the water pressure on the flexible membranes containing luminal contents, thus mimicking mixing created in *in vivo*. However, most of the studies using TIM-1 have been reported for digestion and bioaccessibility of nutritional compounds, with only limited data available for evaluating drug product performance.[2,7] Blanquet et al.[64] studied the impact of transit time and food effect on oral absorption and the results were consistent with the *in vivo* data. However, the complexity of the apparatus and lengthy experimental setup time are important limitations of using this system for evaluating drug

performance.[2] Another study developed a dissolution-absorption setup, simulating dissolution in the USP 2 apparatus and absorption in a hollow fiber membrane, to assess oral absorption of theophylline.[65] However, the authors did not thoroughly explore the potential of the membrane module for mass transport measurements or as an *in vitro* tool for formulation development of supersaturating dosage forms.

1.5   Supersaturating Drug Delivery Systems

1.5.1   Supersaturation

A solution is said to be supersaturated when the solution concentration exceeds the saturation solubility of the compound. Mathematically, it is expressed as:

$$\ln S = \frac{\ln x^S \gamma^S}{\ln x^* \gamma^*} \tag{1.21}$$

Here x^S and γ^S are mole fraction solubility and activity coefficient of the solute in the supersaturated solution respectively while x^* and γ^* are mole fraction solubility and activity coefficient of solute in the saturated solution respectively. For an ideal solution, the activity coefficient is unity and supersaturation is typically expressed as a concentration based ratio for supersaturated (C) and saturated solution (C^*),

$$S = \frac{C}{C^*} \tag{1.22}$$

Supersaturation is also a driving force for crystallization as supersaturated solutions are thermodynamically metastable and any system perturbations can lead to desupersaturation, i.e. crystallization of drug from the solution.[66]

1.5.2   Amorphous Solids and Amorphous Solubility

An amorphous solid has short-range ordering of molecules, limited to a few neighboring molecules.[67]   However, unlike crystalline solids, it lacks long-range order of the molecular packing.[68] When a crystalline material is melted and rapidly cooled back to a lower temperature, the liquid melt becomes amorphous in nature, losing any long-range ordering.[69] The amorphous solid has higher free energy, enthalpy, entropy and free volume as compared to its crystalline

counterpart and as a result, they are metastable in nature. When a liquid melt is cooled rapidly below its melting temperature such that there is no formation of crystal nuclei, the amorphous solid formed is referred to as supercooled liquid as it retains equilibrium properties of liquid. The cooling of a liquid melt results in the increase in viscosity and decrease in molecular mobility. Thus, below a certain temperature, due to increased viscosity, the material deviates from the equilibrium line to accommodate for excess free energy and results in the formation of glassy material.[68] This transition temperature is called as glass transition temperature (T_g). The glass material is thermodynamically unstable and hence, susceptible to gradual relaxation over time to a more stable solid form. The physical stability of amorphous materials can also be lost due to an increase in the molecular mobility at higher temperature and humidity.[16] Typically, higher configurational entropy and lower free energy difference between amorphous and crystalline state may the reduce probability of crystallization of the amorphous solid.[69]

Owing to the lack of a crystal lattice and high free energy of amorphous solids, the amorphous solubility is higher than the crystalline solubility. The solubility of an amorphous solid is the solution concentration achieved due to solid-liquid equilibrium between the amorphous solid and a solution phase. The thermodynamic equilibrium between the amorphous solid and an aqueous phase is often difficult to achieve as it is thermodynamically unfavorable. Thus, it can be achieved only when the crystallization is slow or inhibited for a prolonged time period.[5,70] The amorphous solubility (X_a) is typically expressed in terms of crystalline solubility (X_c) and free energy difference (ΔG) between the two solid states[71],

$$X_a = \exp\left(\frac{-\Delta G}{RT}\right) X_c \tag{1.23}$$

where the difference in the free energy is given by the Hoffman equation;

$$\Delta G = \frac{\Delta H_f (T_m - T) T}{T_m^2} \tag{1.24}$$

The water absorption tendency of amorphous solids can alter the activity and free energy of the solid. Hence, amorphous solubility prediction involves estimation of the activity of the amorphous solute saturated with water ($-I(a)$) along with experimental crystalline solubility and free energy difference between crystalline and amorphous forms[72,73],

$$X_a = \exp[-I(a)] \exp\left(\frac{-\Delta G}{RT}\right) X_c \tag{1.25}$$

The amorphous solubility is also estimated by assuming it to be a supercooled liquid, however, only if the glass transition temperature of drug is lower than temperature of interest.[5]

1.5.3   Phase Separation in Supersaturated Systems

A highly supersaturated solution of a drug compound is thermodynamically metastable and prone to crystallization. However, it is observed that sometimes, instead of crystallization, species of a second liquid phase are formed in the solution. This phenomenon is called liquid-liquid phase separation (LLPS).[12] LLPS is observed as a precursor to crystallization and can impact the nucleation process by either hindering or accelerating the step.[13] It is a metastable zone wherein liquid phases exist as solute rich and solute lean. The two liquid phases are in equilibrium with each other, hence the solute chemical potential or supersaturation of solute is identical in both phases.[74] The free energy of mixing (ΔG_{mix}) is a function of the chemical potential of the two species. For a drug (D) – water (W) mixture,

$$\Delta G_{mix} = x_D(\mu_D - \mu_D^*) + x_W(\mu_W - \mu_W^*) \tag{1.26}$$

For partially miscible liquids, the free energy of mixing as a function of composition shows negative net ΔG_{mix} for all mixture compositions as shown in Figure 1.4. However, there exits two compositions where the ΔG_{mix} is at a minimum, generating a miscibility gap in the free energy phase diagram.
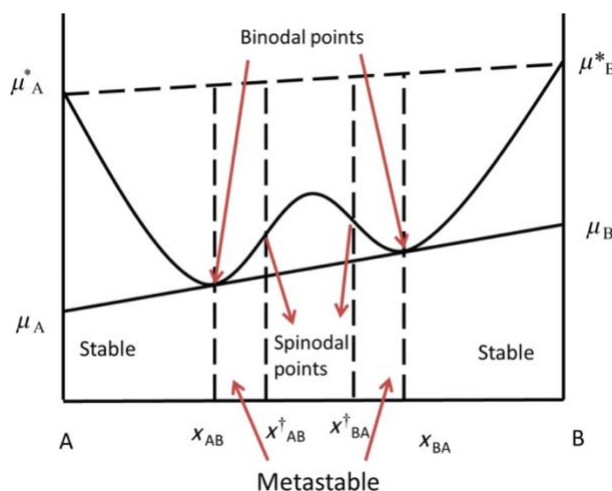
Figure 1.4: Free energy of mixing as function of composition of two liquids with a miscibility gap. D is drug and W is water.[5]

For a mixture of pure water (W) and amorphous drug (D), the free energy is at a minimum for compositions x_{DW} and x_{WD}. The compositions can be attained by either starting with amorphous drug and addition of water or vice-a-versa. At these compositions, the net overall ΔG_{mix} is the lowest and the chemical potential of each species is equal in both the phases. These points are called as binodal points. The region below x_{DW} or above x_{WD} are stable with respect to demixing. Any composition between x_{DW} and x_{WD} is thermodynamically unfavorable and the overall free energy can be lowered by phase separation into two liquid phases. Between x_{DW} and x_{DW}^* and x_{WD} and x_{WD}^*, the system is metastable such that phase separation will occur if energy barrier is overcome. Beyond x_{DW}^* and x_{WD}^* the system is unstable and can undergo spontaneous phase separation into two liquid phases of equal chemical potential. These compositions are called as spinodal points and phase separation occurs by spinodal decomposition, which is a diffusion-controlled process.[5,75]

In an amorphous drug and water mixture, the concentration at which LLPS occurs, has been observed to be equal to the amorphous solubility of the drug.[10,11,15,76] This relation can be explained based on equal activity of species in the two phases. The chemical potential or activity of drug is equal in the water-rich phase (W) and the supercooled liquid-rich phase (L),

$$\ln x_D^W \gamma_D^W = \ln x_D^L \gamma_D^L \tag{1.27}$$

The amorphous solubility is equal to x_D^W, concentration of drug in water-rich phase.[5]

1.5.4   Mass transport advantage of supersaturated systems

The mass transport of a drug across the gastrointestinal membrane typically involves passive diffusion. As the diffusion process is driven by the chemical potential gradient of the species across the barrier, supersaturated systems can show a higher mass transfer as compared to saturated systems, thus translating to higher oral bioavailability, particularly for BCS Class II compounds. The highest concentration or thermodynamic activity of species in the solution that can be achieved is the amorphous solubility. Beyond the amorphous solubility, additional supersaturation will result in LLPS and formation of drug-rich and water-rich phases, with thermodynamic activity equivalent to the amorphous solubility. In the absence of crystallization, a highly supersaturated phase separated systems will maintain the highest solution concentration

until the drug-rich nanodroplets are depleted. Hence, during absorption, the drug absorbed from the aqueous phase will be replenished by the drug-rich nanodroplets and show highest flux for longer periods of time. This effect of nanodroplets replenishing absorbed drug in the aqueous phase is termed as the reservoir effect of LLPS, schematically shown in Figure 5. In the presence of LLPS, the thermodynamic activity is maintained at the maximum and hence more drug diffuses through the membrane. In the absence of LLPS and subsequent crystallization, the thermodynamic activity decreases with a subsequent decline in driving force due to absorption and crystallization, resulting in less drug transferred.
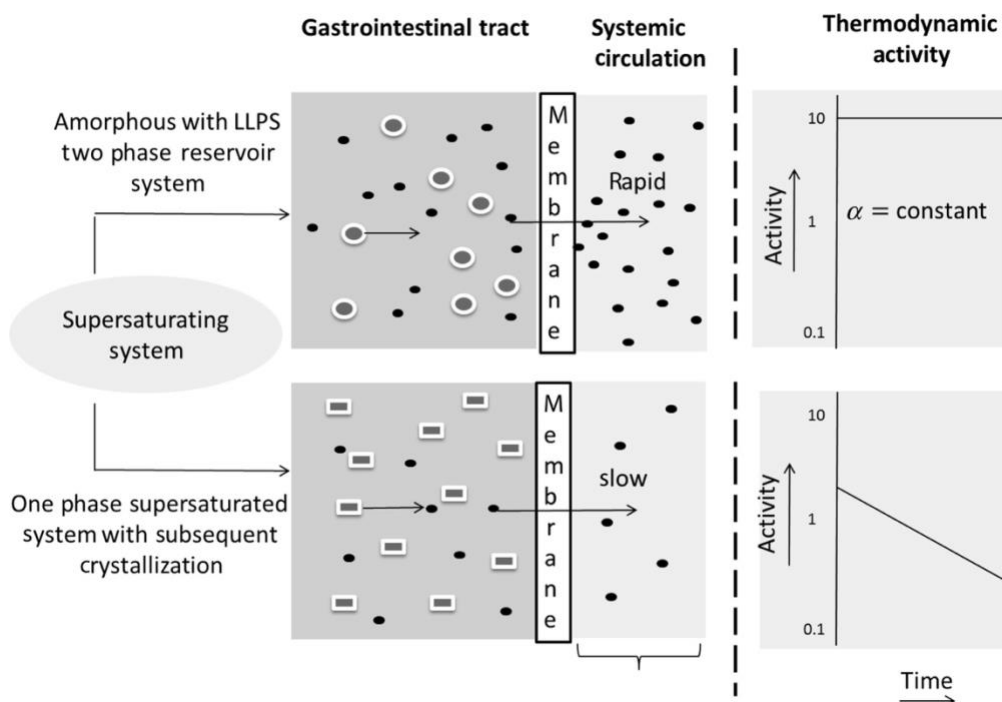
Figure 1.5: Schematics of passive diffusion across membrane in presence and absence of LLPS in supersaturated systems.[11]

As the membrane flux is proportional to the thermodynamic activity of a species, it is expected that constant flux is observed for concentrations above the amorphous solubility, undergoing LLPS. The effect was experimentally demonstrated using a side-by-side diffusion cell, Figure 6a. The constant driving force for mass transfer across the membrane due to the presence of drug-rich nanodroplets was also demonstrated experimentally using a flow-through side-by-side diffusion cell, Figure 6b. The non-cumulative concentration measurement from the receiver

compartment allowed visual representation of the reservoir effect of nanodroplets, until they depleted over time.
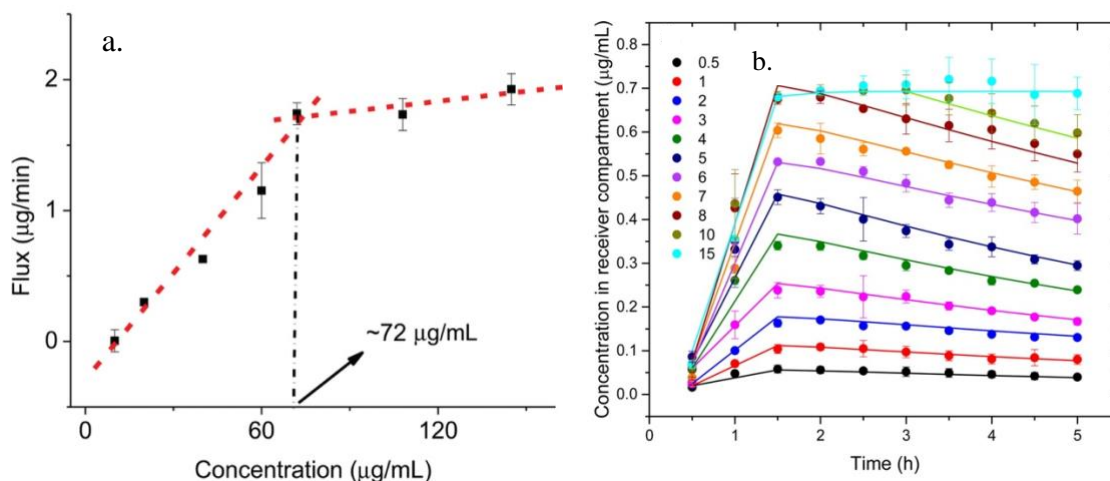
Figure 1.6: (a) Diffusive flux of nifedipine for concentrations below and above amorphous solubility (72 μg/mL).[11] (b) Receiver concentration profile of clotrimazole for concentrations below and above amorphous solubility (7.5 μg/mL).[10]

1.5.5 Amorphous Solid Dispersions

Amorphous solid dispersions are an attractive formulation strategy for poorly soluble compounds to improve their bioavailability by improving solubility and dissolution rate. An amorphous solid dispersion is a multi-component system wherein drug is molecularly dispersed in the polymer matrix. They are typically prepared by melt extrusion of drug and polymer mixture or dissolution of the mixture in a solvent followed by spray drying or lyophilization.(ref) The dispersion of drug in a polymer matrix at a molecular level provides two main advantages from the presence of the polymer: (1) inhibiting crystallization of drug in the solid formulation and (2) maintaining the supersaturation generated upon dissolution of the amorphous formulation by inhibiting crystallization in the aqueous phase.[77] The drug-polymer miscibility is critical to the development of a stable amorphous solid dispersion. According to the Gordon-Taylor equation, the mixing of two materials with different T_gs results in an intermediate value for the T_g of the mixture, which in turn would depend on the individual T_g's, weight fraction of drug and polymer and level of interaction between the two components. Thus, mixing low-T_g drug with high-T_g polymer results in an amorphous solid dispersion with a T_g that is higher than that of the drug. As a result, the presence of the polymer slows down the molecular mobility and crystallization of

41

amorphous drug as compared to the amorphous drug alone, improving the physical stability.[78] Strong intermolecular interactions between drug and polymer can also slow down the drug molecular mobility. Amorphous solid dispersions may phase separate and undergo crystallization over time if the drug loading exceeds the drug-polymer miscibility limit.[77] This extent of drug and polymer miscibility can be altered by environmental factors such as temperature or moisture. Low temperature can result in crystallization due to favorable thermodynamic factors for nucleation, while higher temperature can increase the molecular mobility and induce crystallization.[16,79] Additionally, depending upon the phase behavior as a function of temperature, drug and polymer can undergo mixing and demixing with changes in the temperature.[80] Similar to the temperature effect, water absorption by an amorphous solid can result in an increase in molecular mobility due to plasticization by water, thus significantly lowering the T_g of the mixture and increasing the tendency of the mixture to crystallize or phase separate.[81]

The bioavailability enhancement offered by amorphous solid dispersions (ASDs) is primarily determined by its dissolution performance. Dissolution of ASDs often results in a 'spring and parachute' effect which is associated with supersaturation generated by dissolution of amorphous drug and maintenance of supersaturation by the polymer.[82] Thus, ASDs have great potential to improve the bioavailability of poorly soluble drugs by generating to higher thermodynamic driving force for membrane absorption.[5] Based on the properties of ASDs such as drug loading and polymer type, dissolution of ASDs can result in the formation of drug-rich nanodroplets, further enhancing bioavailability by the reservoir effect of these colloidal species as mentioned in the above section.[58] Typically, ASDs with low drug loading have been observed to undergo LLPS upon dissolution.[58,83,84] This is associated with faster, polymer-controlled dissolution of the formulation. The high dissolution rate can result in a solution concentration in excess of the amorphous solubility followed by precipitation of the excess drug as amorphous nanodroplets.[85] At higher drug loadings, the drug-rich layer on the surface of ASDs may slow down the release due to the poor solubility of the drug.[86] The critical drug loading to obtain LLPS upon dissolution of ASD varies with drug and polymer type and is hence, an active area of research.[87]

1.5.6 Mesoporous silica-based drug delivery systems

Another type of widely researched amorphous formulation strategy is mesoporous silica-based formulations. The development of nanostructured materials for biomedical applications resulted in the synthesis of mesoporous silica materials and was proposed as a drug delivery system for the first time in 2001.[88] These materials can be prepared by templating of a silica surface with supramolecular assemblies of surfactant.[89] Surfactant is later removed by pyrolysis or dissolution with suitable solvent resulting in the formation of an ordered pore network, high pore volume and high surface area material.[88,90] The pore volume can be as high as 1 cm^3/g and specific surface area is typically in the range of 500-1500 m^2/g. These properties make mesoporous silica materials an attractive carrier for drug delivery. The most commonly studied mesoporous silica materials include MCM-41 and SBA-15, which have a hexagonal pore structure. The typical pore size in these materials lies between 2 to 15 nm. SBA-15 also has additional micropores (< 2 nm) which are located in the walls between adjacent mesopores and are dead end pores.[91] Drug encapsulation in the mesopores can result in the formation of a stable amorphous solid if the pore size is smaller than the critical nuclei radius required for the crystallization of drug and if the pore filling is low.[25,92] The amorphization of drug in silica-based formulations can, thus, offer solubility and bioavailability advantages.[93] Therefore, there is a growing interest in formulating poorly soluble drugs using mesoporous silica materials.[94]

The drug encapsulation in the silica matrix is carried out by immersing silica in a highly concentrated solution of drug, therefore the extent of drug loading mainly depends on the adsorption tendency of drug.[90] Similarly, drug release from the silica matrix is a diffusion-controlled process and the displacement of drug from the silica surface by competitive adsorption of water molecules significantly controls the drug release.[93,95] The drug adsorption on silica and subsequent release can, thus, be influenced by several factors. For the drug molecule to effectively adsorb on the silica surface, the pore size of the material should be considerably larger than the molecular size of the drug. The pore size also controls the drug release rate, with faster drug release observed for larger pore sizes.[88] This is typically attributed to more efficient penetration of water molecules or wetting of the formulation to release the drug adsorbed and faster drug diffusion out of the pores. As the pore size controls the diffusion of drug molecules, depending on the size of the drug molecule, a critical pore size exists below which the drug release would be hindered.[93]

The specific surface area of the silica material can alter the achievable drug loading by improving drug adsorption for higher surface area materials. In addition to the pore structure properties, the silica surface is rich in silanol groups that allow molecular interactions with the guest molecule, promoting drug encapsulation and immobilization of molecules in the pores.[29] Hence, drug-silica interactions can also alter the drug adsorption tendency and drug release behavior. The drug molecules interact with silica surface either via hydrogen bonding or electrostatic interaction, with the latter being the stronger interaction. Strong interactions between drug molecules and the silica surface have been observed to improve the drug adsorption, thereby enhancing drug loading capacity, however, this slows down the drug release significantly.[90] Therefore, mesoporous silica materials are often functionalized to deliver drug in a sustained-release manner.[96,97] Weaker molecular interactions typically result in a rapid burst release of the drug.[90] Owing to the activity of the silica surface, drug release in an *in vivo* environment can also be altered by gastrointestinal pH or fluid components. The pH of the media can modify surface chemistry of silica due to deprotonation of silanol groups with the increase in pH.[98] This can influence drug-silica interactions as well as drug solubility during gastrointestinal transit of the formulation. The gastrointestinal fluid components can competitively adsorb onto the silica surface or improve wetting of the formulation, thereby improving the drug release. Mesoporous silica-based formulations are inherently complex formulations and the impact of pore structure properties and experimental conditions on the drug release behavior makes the prediction of formulation performance a complex process.

1.6 Summary

In conclusion, the membrane mass transport is essentially governed by the thermodynamic activity of species in the solution. Therefore, solubility and dissolution rate are important descriptors of the rate of mass transfer across the membrane. As a result, solubility enabling formulation strategies that undergo supersaturation upon dissolution are increasingly considered as a formulation approach to develop poorly soluble drugs. Amorphous solid-based formulations are one such approach. This chapter discusses how higher free energy of the amorphous solid results in higher solubility and hence, faster dissolution rate. The increase in thermodynamic activity due to supersaturation generated upon formulation dissolution enhances the driving force for mass transfer, improving the absorption behavior. In addition to supersaturation, dissolution of

amorphous solid dispersions also results in liquid-liquid phase separation in the solution, which can further improve the bioavailability of drug due to the reservoir effect of drug-rich phase. Since the extent of supersaturation generated determines the formulation performance of these complex enabling formulations, an accurate assessment of supersaturation is critical. Compendial dissolution testing apparatus is typically used for optimization and performance assessment of these formulations. The chapter describes several commonly used dissolution methodologies that have been developed over several years to additionally incorporate dynamic *in vivo* environment. However, the lack of absorptive sink in these *in vitro* apparatuses either overestimates or underestimates the performance of complex formulations, resulting in poor *in vitro-in vivo* correlations. This is because in the dynamic environment that exists *in vivo*, drug dissolution is accompanied by the simultaneous absorption across gastrointestinal membrane. Since only free, molecularly dissolved drug gets transferred across the membrane, the dissolution of enabling formulations in the closed-compartmental setup can show concentrations higher than what is truly available for the absorption. Similarly, for supersaturated solution, as supersaturation is thermodynamically metastable, the drug may crystallize over time and the extent of supersaturation observed *in vitro* may vary with that observed *in vivo*. Incorporation of an absorptive compartment during dissolution test, hence, is an effective approach to better predict formulation performance of complex formulations. The absorption measurements can provide insights into the amount of drug that is freely available for absorption and can also help in deducing the influence of simultaneous absorption process on the solution phase behavior in the lumen. For instance, the absorption kinetics can be altered by crystallization of supersaturated solutions or liquid-liquid phase separation in highly supersaturated drug solution. At the same time, absorption process can reduce the driving force for crystallization by the continuous removal of drug and lowering of the supersaturation. Dissolution rate may also vary in the presence of absorptive sink as the depletion of drug due to absorption can alter the driving force for dissolution. Hence, assessing the absorption behavior of a formulation and obtaining insights into the complex interplay between different solution phase behavior and absorption kinetics is pivotal. However, this is a great challenge with existing mass transport apparatuses due several limitations discussed in this chapter, most importantly slow mass transfer rates due to small membrane surface area. Slow mass transfer results in unrealistic experimental time frames and inefficient removal of drug, as a result these apparatuses are not capable of simulating the intestinal absorption process.

Therefore, this research utilizes hollow fiber membrane module, with large membrane surface area, to simulate the absorption process. The goal of the study is to understand the dissolution and membrane mass transport of supersaturating drug delivery systems using the dynamic *in vitro* setup developed herein.

CHAPTER 2.   ABSORPTIVE DISSOLUTION TESTING OF SUPERSATURATING SYSTEMS: IMPACT OF ABSORPTIVE SINK CONDITIONS ON SOLUTION PHASE BEHAVIOR AND MASS TRANSPORT

2.1   Abstract

One of the most commonly used formulation development tools is dissolution testing. However, for solubility enhancing formulations, a simple closed compartment conventional dissolution apparatus operating under sink conditions often fails to predict oral bioavailability and differentiate between formulations. Hence, increasing attention is being paid to combined dissolution-absorption testing. The currently available mass transport apparatuses, however, have certain limitations, the most important being the small membrane surface area which results in slow mass transfer. In this study, a novel high surface area, flow through absorptive dissolution testing apparatus was developed and tested on weakly basic model drug, nevirapine. Following optimization of the experimental parameters, the mass transfer attained for a nevirapine solution was 30 times higher in 60 min as compared to a side-by-side diffusion cell. To further evaluate the system, nevirapine powder and commercial tablets were first dissolved at an acidic pH, followed by pH increase, creating a supersaturated solution. Detailed information related to the extent of supersaturation achieved in crystallizing and non-crystallizing systems could be obtained from the combined dissolution-mass transport measurements. Differences in donor cell compartment concentration-time profiles were noted for absorptive versus closed compartment conditions. It is anticipated that this approach could be a promising tool to identify solubility enabling formulations which perform optimally *in vivo*.

2.2　Introduction

Dissolution testing of drug products is an important formulation performance assessment tool for orally administered drug products and is used for understanding physicochemical properties of the drug substance and drug product attributes.[2,3] Ideally, it can also be used as an alternative to *in vivo* testing, or to provide discrimination between formulations that have potentially different *in vivo* performance.[3,4,7,43] The optimization of drug delivery systems, i.e., forms and formulations, has become increasingly important over the past two decades, as the number of poorly water soluble drugs in drug discovery pipelines has increased to more than 40%.[5] In order to improve solubility and bioavailability of these compounds, formulation scientists have employed different approaches including complexation, micellization, cocrystals and amorphous solid dispersions.[82,99] As many of these enabling formulations are complex in terms of performance prediction, conventional dissolution testing methods are still widely used to assess developmental formulations and often fail to predict *in vivo* performance.[2] The simple basket/paddle USP I/II apparatus is a one-compartment, closed environment setup with a defined volume and lacks absorptive sink conditions, biorelevant fluid volumes and hydrodynamics. Obtaining meaningful dissolution data for better prediction of product performance is imperative to optimize pharmaceutical formulation development and hence there is a substantial need for and interest in improving release testing.

Over the past few years, several designs have been proposed to overcome challenges with compendial dissolution testing. The United States Pharmacopeia has standardized the reciprocating cylinder (USP 3) and flow through cell (USP 4) for dissolution testing in order to incorporate *in vivo* relevant hydrodynamics.[7] To better consider *in vivo* physiological conditions, biorelevant media were first introduced in 1998.[100] Since then several dissolution studies have been carried out in biorelevant media designed to mimic the fasted and fed states and the data used to improve predictions of *in vivo* oral absorption.[8,101] The aforementioned dissolution apparatuses, however, do not capture the complexity of the luminal environment. Moreover, certain drug formulations, particularly complex enabling formulations used for poorly water soluble compounds, tend to result in supersaturation and precipitation during gastrointestinal transit and it is difficult to predict the extent of these events *in vivo* using compendial dissolution methods.[7] Consequently, several multicompartment dissolution models including the artificial stomach

duodenal model[102], the transfer model[9] and the gastrointestinal simulator[103] have been developed to mimic gastric emptying and the change in the environment upon entering the intestinal compartment.

Although numerous developments and modifications have been applied to conventional dissolution methodology, they do not incorporate absorptive sink conditions. The presence of an absorptive compartment in dissolution studies is particularly important for formulations that supersaturate and potentially undergo precipitation during GI transit. This is because the mass transport rate of drug from the dissolution compartment into the receiver compartment not only provides information about the solution thermodynamics, but as drug is continuously removed, it will also impact the supersaturation profile, which in turn will impact dissolution kinetics of any undissolved material, as well as crystallization kinetics. Bevernage et al.[42] demonstrated that precipitation of drug from a supersaturated solution was less extensive when dissolution studies were carried out in the presence of an absorptive compartment. The study also aided in understanding the impact of precipitation inhibitors, further illustrating the importance of combined dissolution/absorption studies. Therefore, appropriate evaluation of the performance of supersaturating formulations *in vitro* is critical, albeit somewhat complex.[5,82,104] Further, it is known that solubilizing additives such as surfactants, complexing agents or cosolvents can reduce the free drug concentration available for oral absorption; this is not reflected by concentration versus time profiles, the typical output of a dissolution experiment, but is seen as a decrease in membrane mass transfer rate at a given concentration in an absorptive experiment. Thus, for such systems it is imperative to consider membrane mass transfer rate, in combination with dissolution testing.[39,40] One approach adopted to incorporate an absorptive compartment is the addition of an upper organic layer to the aqueous medium that can serve as a reservoir for dissolved drug, with this setup termed biphasic dissolution testing.[39,40,47,105] Frank et al.[49] included a pH-shift into the biphasic dissolution test leading to improved prediction of formulation performance as compared to single phase dissolution. Although the biphasic system provided interesting findings, the use of organic solvent and the lack of a physical barrier between the two phases limits its applicability. Solvent volatility, emulsion formation with surfactant-enriched biorelevant media or blocking of sampling lines due to viscous solvents are some of the issues that have been reported for the biphasic system.[46]

An alternative approach to performing dissolution-absorption measurements is the use of a two-compartment system separated by a membrane barrier, wherein drug present in the donor compartment diffuses across the membrane into a receiver compartment. In 1999, Ginski and Polli[43] developed an integrated dissolution/Caco-2 permeation method to study differences between various formulations. The *in vitro* dissolution-absorption results matched with the observed clinical data in contrast to the standard *in vitro* dissolution testing results. Since then dissolution-absorption systems have been employed widely to predict *in vivo* relevant formulation performances.[50,52,53,106] Kobayashi et al.[107] developed a dissolution-absorption assay which incorporated drug dissolution and pH changes. A permeability assessment method was also developed using a flow through dissolution cell to study the influence of dosage form on the permeation process.[108] Kataoka et al.[51] studied the food effect on oral absorption of poorly soluble drug compounds using dissolution-absorption systems and the assay results corresponded well with the *in vivo* observations. A double artificial membrane permeability assay was also developed to incorporate an intracellular compartment in absorption measurements.[55]

The rate of drug absorption across a membrane is evaluated in terms of flux. Typically, flux is described as a function of the concentration gradient of the species across the membrane. However, from a more fundamental perspective, flux is dependent on the gradient in chemical potential, more specifically, thermodynamic activity, of the species across the barrier.[44] Twist and Zatz[109] demonstrated experimentally that a constant flux value was observed for saturated solutions in different solvents having different solute concentrations; this is because the thermodynamic activity of the solute was constant in all the solvents at saturation. Hence it is useful to consider flux in terms of solute activity as given in equation 2.1,

$$J = \frac{1}{A}\frac{dM}{dt} = \frac{D}{h\gamma_m} * a \tag{2.1}$$

where J is the membrane flux, A is surface area of the membrane, dM/dt is rate of mass transfer, a is the activity of species, D is the solute diffusion coefficient, h is the membrane thickness and γ_m is solute activity coefficient in the membrane.

The currently used *in vitro* apparatuses to determine the mass transport of poorly water-soluble drugs, however, have certain limitations which impact their usefulness for absorptive dissolution testing. An important limitation is the small membrane surface area per unit volume. As seen from equation 1, the amount of drug transferred across a membrane over a certain period of time is the product of diffusive flux and membrane surface area; small membrane surface area results in low mass transfer rates. There are several literature reports describing poor prediction or long experimental times required to obtain detectable concentration on the receiver side in a dissolution/permeation setup due to small membrane surface area.[10,110] In addition, the small volumes typically used can make it difficult to maintain sink conditions on the receiver side. Further, in some systems, a static aqueous boundary layer is formed adjacent to either side of the membrane. This aqueous layer, known as the unstirred water layer, acts as an additional barrier to the transport of drug across the membrane, particularly for highly lipophilic drug molecules, and further slows down the measurements.[45] Such experimental conditions and slow flux measurements make it difficult to study the performance of complex formulations, especially supersaturating formulations.

Considering the increasing demand for enabling formulations of poorly soluble drugs, there is a compelling need to develop improved *in vitro* tools to evaluate and optimize the dissolution/absorption behavior of different formulations. The goal of this study was to develop and test a high surface area, flow through, absorptive dissolution testing apparatus, designed to provide *in vivo* relevant information about formulation performance. The central component of this apparatus is a hollow fiber membrane. Hollow fiber membranes offer a large surface area per unit volume of fluid, enabling higher mass transfer in a shorter period of time. Additionally, controlled hydrodynamics can be achieved with fluid flowing on both sides of the membrane. This allows measurement in a continuous system, potentially more similar to that found *in vivo*. The continuous system also reduces additional diffusion barriers created by an aqueous boundary layer adjacent to the membrane surface. The use of a hollow fiber membrane for simulating intestinal absorption has been reported previously.[64,65] However, previous studies have not explored the potential of the membrane module for mass transport measurements or as an *in vitro* tool for formulation development of supersaturating dosage forms. Herein, we have compared the mass transfer across a hollow fiber membrane module using fluid flow to that across a flat-sheet

membrane in a side-by-side diffusion cell. The operating parameters of the flow through apparatus were optimized and mass transport measurements were combined with dissolution testing. Nevirapine, a weakly basic drug with a pKa 2.8 was chosen as the model compound for this investigation. It has relatively poor solubility at pH 6.5 and hence supersaturated solutions can be readily generated by increasing the pH from a low to a higher value. A comparative study between supersaturated nevirapine solutions with differing propensities to crystallize demonstrated that the apparatus was robust and very sensitive to the solution phase behavior, providing a greater level of information about formulation performance than a simple, closed compartment dissolution experiment.

2.3   Materials

Nevirapine was purchased from ChemShuttle (Jiangsu, China). This material was identified as the anhydrous form by comparing the experimental X-ray powder diffraction pattern to the theoretical pattern generated from the nevirapine crystal structure (reference code PABHIJ) in the Cambridge Structural Database. Hydroxypropyl methylcellulose acetate succinate MF grade (HPMC-AS) was supplied by Shin-Etsu Chemical Co. Ltd. (Tokyo, Japan). Polyvinylpyrrolidone/vinyl acetate or Kollidon® VA 64 (PVPVA) was obtained from BASF Corporation (Florham Park, NJ). Methanol and dimethyl sulfoxide (DMSO) were purchased from Fisher Scientific. Nevirapine tablets (200 mg, Camber Pharmaceuticals, Inc) were purchased from the Purdue Pharmacy (West Lafayette, IN). According to the package insert, the tablets also contained the following excipients: microcrystalline cellulose, croscarmellose sodium, corn starch, povidone, sodium starch glycolate, colloidal silicone dioxide and magnesium stearate. Tablet and powder dissolution was carried out in 0.1 N HCl followed by pH-shift to pH 6.5, achieved by addition of an equal volume of 0.17 M Na_2HPO_4. 50 mM pH 6.5 phosphate buffer was used as the aqueous medium in other experiments. All mass transport experiments were carried out at pH 6.5 because nevirapine is weakly basic drug with pKa of 2.8 and is thus substantially unionized at pH 6.5.

2.4   Methods

2.4.1   Crystalline Solubility Measurements

The solubility of anhydrous crystalline nevirapine was measured in 50 mM pH 6.5 phosphate buffer. An excess of drug was equilibrated in the medium for 48 h at 37 °C. Equilibrated samples were then subjected to ultracentrifugation to separate excess solids from the dissolved drug using a Sorvall Legend Micro 21 (Thermo Fisher Scientific Inc., MA) at 14800 rpm for 30 min. The crystal form after slurrying was found to be unchanged based on the X-ray powder diffraction pattern. The supernatant was diluted using 50 mM phosphate buffer and absorbance was measured using an ultraviolet visible (UV/vis) spectrophotometer (SI Photonics, Tuscon, AZ) at 282 nm. Measurements were performed in triplicate. A standard curve was prepared by adding different concentrations of methanolic stock solution to 50 mM phosphate buffer. A good linearity (r_2=0.9997) was observed for the range of concentrations prepared.

2.4.2   Crystallization Inhibition Studies

The nucleation induction time of nevirapine in the presence and absence of dissolved polymer was determined using UV-extinction measurements. The crystallization inhibition studies were performed for supersaturated solutions of nevirapine (500 µg/mL) with no polymer, 0.05% HPMC-AS or 0.1% PVPVA in the solution. The formation of crystals was detected from the increase in extinction at 400 nm, using a UV dip probe whereby the measured induction time is the sum of the true nucleation induction time and the time required for the crystals to grow to a detectable size.

2.4.3   Diffusion Studies in Side-By-Side Diffusion Cell

A side-by-side diffusion cell (PermeGear, Inc., Hellertown, PA), shown in Figure 2.1, consisting of a donor and a receiver compartment separated by a flat-sheet membrane with a surface area of 7.07 cm_2 was used to study nevirapine mass transport in a conventional diffusion cell. A porous semi-permeable hydrophilic polyethersulfone membrane (ST grade) with 10 kDa molecular weight cut-off (MWCO) (Synder Filtration, Inc., Vacaville, CA), corresponding to pore size of approximately 2 nm was used. The concentration of drug in the receiver compartment was monitored as a function of time using a UV dip probe.
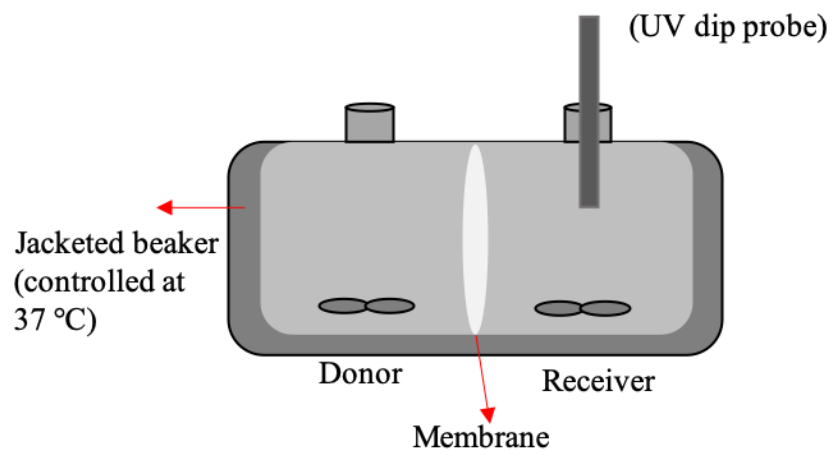
Figure 2.1: Schematic of side-by-side diffusion cell experimental setup

2.4.4 Mass Transport Setup

The dissolution and mass transport studies were carried using the experimental setup shown in Figure 2.2.
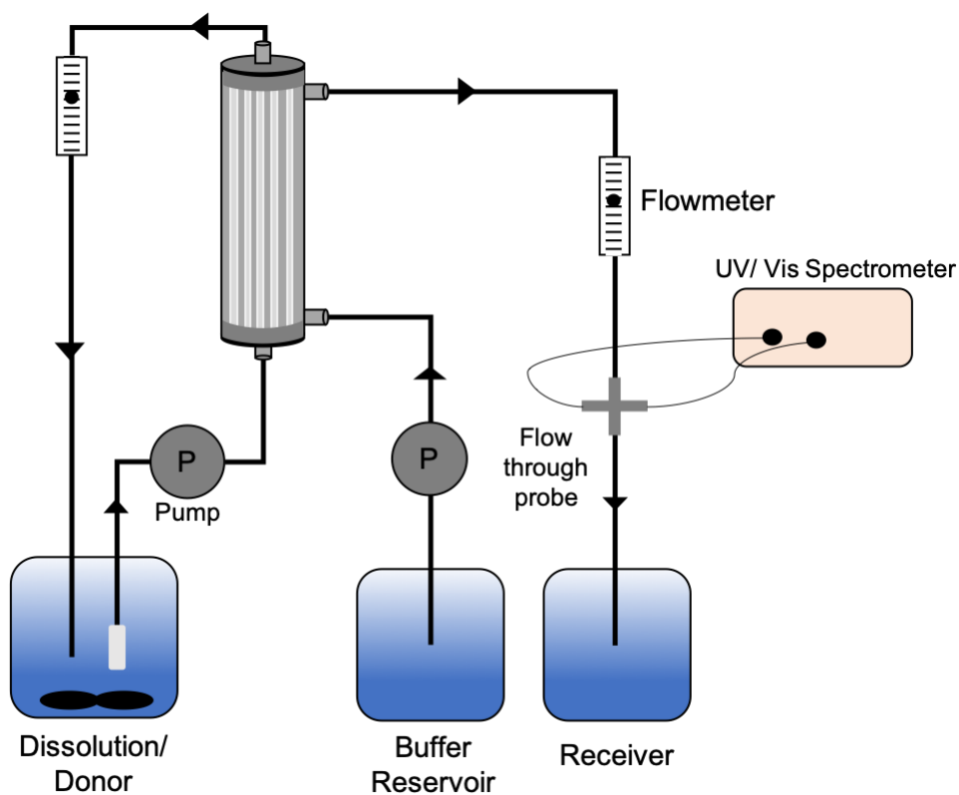
Figure 2.2: Schematic of absorptive dissolution testing apparatus

The apparatus consists of a donor chamber containing the drug dissolved or suspended in the aqueous medium, a hollow fiber membrane module, a buffer reservoir containing the absorption medium and a receiver container to collect drug following diffusion across the membrane. A polyethersulfone hollow fiber membrane procured from Spectrum Laboratories, Inc. (Rancho Dominguez, CA) had a 10 kDa MWCO which corresponds to a pore size of c.a. 2.5 nm. The module has a surface area of 115 cm_2 containing 36 hollow fibers with dimensions of 0.5 mm ID, 0.2 mm thickness and 20 cm length. A two-way peristaltic pump MINIPULS 3 (Gilson Inc., Middleton, WI) was used to pump fluid in both of the channels using parallel, co-current flow. The fluid from the donor container is pumped through tubing into the inner side of the hollow fiber membrane. Simultaneously, buffer solution is pumped from the reservoir on the outer side of the hollow fibers. The drug present in the donor fluid diffuses across the membrane into the receiver fluid which is collected at the end of the receiver channel into the receiver container. The concentration of drug in the receiver fluid was analyzed in-line using a flow-through UV probe (SI Photonics, Tuscon, AZ), before it was collected in the receiver container. The donor fluid emerging from the membrane module was recycled back to the donor container to enable additional diffusion of drug. Flowmeters (Gilmont Instruments, IL) were used to determine any fluctuations in the flow rate. The temperature was maintained at 37 °C. All of the experimental runs were followed by a 50/50 volume % methanol/H_2O wash for 30 min. For all the preliminary and optimization experiments performed on the apparatus, the donor solution volume was kept constant at 50 mL.

2.4.5   Dissolution and Mass Transport Studies

The mass transport apparatus for combined dissolution-absorption analysis was used to study the performance of various nevirapine systems. Closed compartment dissolution experiments were also performed for comparison. Three types of nevirapine samples were evaluated, namely crystalline suspension, powder (active pharmaceutical ingredient powder dissolved initially at low pH) and tablet (commercial formulation, drug also initially dissolved at low pH). The crystalline suspension was prepared by adding an excess of nevirapine powder to the aqueous medium at pH 6.5. Dissolution of tablet and powder was performed at 37 °C in 0.1 N HCl for 30 min (time required to achieve complete dissolution). Following dissolution, the solution pH was adjusted to pH 6.5 by addition of an equal volume of 0.17 M Na_2HPO_4 such that the final

volume was doubled. The adjustment in volume and pH of the medium was performed to achieve a known degree of supersaturation. The final volume of the crystalline suspension and powder formulation was 100 mL, while in the case of the tablet, it was 400 mL. A higher volume was used for the tablet to ensure dissolution of 200 mg of nevirapine in the acidic medium to afford an equivalent supersaturation after pH adjustment. The donor solution was stirred at 300 rpm using a magnetic stirrer. The crystalline suspension and supersaturated solutions evolved from tablet and powder were then evaluated in terms of donor compartment solution concentration-time profiles using both a closed compartment setup and the flow through apparatus shown in Figure 1. The mass flow of drug across the membrane for the dissolution-absorption system was also determined from the receiver compartment concentration profiles as a function of time. Experiments were conducted over a period of 4 h. All of the absorption measurements were performed at a flow rate of 2 mL/min. The donor solution for both dissolution and dissolution-absorption measurements was sampled manually and filtered through 0.45 µm glass fiber filters (Tisch Scientific, OH) and the concentration was determined by UV spectrometry. A 10 µm pore size cannula filter (Agilent Technologies, Inc., Memphis, TN) was inserted at the inlet of the donor fluid channel to filter out solids in the donor solution entering the membrane module. The amount of drug in the receiver fluid was analyzed in-line by UV spectrometry using a flow-through UV cell. For the formulations where the impact of polymer on supersaturation was evaluated, 0.05% HPMC-AS was pre-dissolved in the 0.17 M Na_2HPO_4 solution.

Experimental studies were also carried out to determine differences in crystallization propensity during dissolution in the presence and the absence of an absorptive environment. For this particular study, experiments were carried out in pH 6.5 phosphate buffer with 0.1% PVPVA pre-dissolved in the buffer. The flow rate for these experiments was set to 4 mL/min. A supersaturated solution (500 µg/mL) was prepared by addition of the required amount of concentrated methanolic stock solution of nevirapine to the buffer. The crystallization tendency of the solution was then analyzed with or without absorption measurements using the mass transport apparatus for 120 min.

2.4.6 Mathematical Model

The mass transfer in the hollow fiber membrane module includes mass balances across several parts of the apparatus. A mathematical model to theoretically predict mass transfer is a useful tool for understanding parameters governing these mass balances and for optimization of the apparatus. The overall mass transfer in the membrane module was derived based on relationships provided in the literature.[60,111,112] There are three important mass balances to be considered for this setup: for a fiber segment along the length axis of the fiber, across the entire module and in the reservoir containing drug, i.e., the donor container. For deriving a mass transfer model for the system, we assume that the system is at steady state, no drug is adsorbed onto the membrane surface once the steady state is reached and there exists uniform pore size and wetting properties across the membrane.
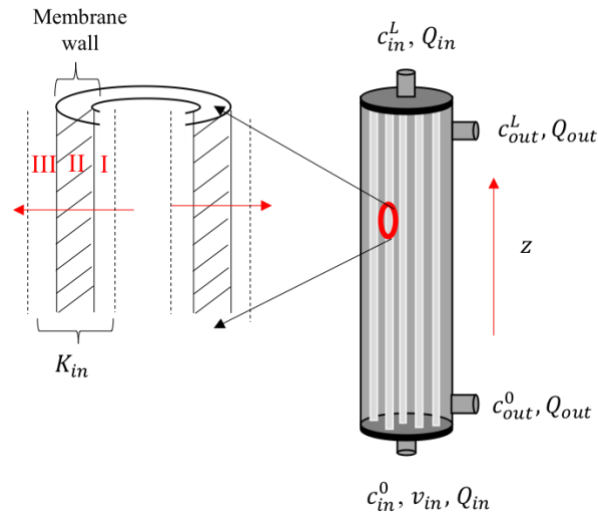
Figure 2.3: Illustration of variables for mass transfer in a hollow fiber membrane

The mass balance across a differential segment dz that accounts for a change in concentration along the fiber length L is given by:

$$[\text{Accumulation}] = [\text{Flow in} - \text{out}] + [\text{mass transferred across porous membrane}]$$
$$0 = Q_{in}dc_{in}^z + K_{in}(\pi d_{in}N)(c_{in}^z - c_{in}^{z*})dz \qquad (2.2)$$

such that, at $z = 0$, $c_{in}^z = c_{in}^0$ and at $z = L$, $c_{in}^z = c_{in}^L$.

Here d_{in} is the internal fiber diameter, N is the number of fibers, K_{in} is the overall mass transfer coefficient, c_{in}^z is the drug concentration inside the fiber at z and c_{in}^{z*} is the concentration at the membrane wall in equilibrium with the outside concentration c_{out}^z at z. The overall mass transfer coefficient, K_{in}, across a single fiber element is dependent on the individual mass transfer coefficients as shown below,

$$\frac{1}{K_{in}} = \frac{1}{k_{in}} + \frac{1}{k_m} + \frac{1}{k_{out}} \tag{2.3}$$

where k_{in}, k_m and k_{out} are mass transfer coefficients in the aqueous layer on the inside of the membrane, across the membrane and in the aqueous layer on the outside of the membrane, respectively. The inverse of mass transfer represents resistance. The three resistances for mass transfer are in series and hence, the overall resistance to mass transfer is the sum of the individual resistances.

As the membrane used in this study is hydrophilic and an aqueous medium is used in both of the fluid channels in the system, the medium wets the membrane well and there is no partitioning of drug compound in the two fluids. Hence, the concentration c_{in}^{z*} simply equals c_{out}^z.

The overall mass balance across the entire module for length z at a given time is,

$$Q_{out}(c_{out}^z - c_{out}^0) = Q_{in}(c_{in}^0 - c_{in}^z) \tag{2.4}$$

where Q_{in} and Q_{out} are the volumetric flow rate inside the fiber and outside the fiber, respectively. In the above equation, as fresh buffer is pumped continuously on the outside of the hollow fiber membranes in the shell region, $c_{out}^0 = 0$.

Therefore, from equation 2.4,

$$c_{out}^z = \frac{Q_{in}}{Q_{out}}(c_{in}^0 - c_{in}^z) \tag{2.5}$$

Substituting equation 2.5 in equation 2.2, and integrating from $z = 0$ to $z = L$ gives,

$$c_{in}^L = \frac{c_{in}^0}{\left(1 + \frac{Q_{in}}{Q_{out}}\right)}\left(\exp\left(-\frac{K_{in}\pi d_{in}NL}{Q_{in}}\left(1 + \frac{Q_{in}}{Q_{out}}\right)\right) + \frac{Q_{in}}{Q_{out}}\right) \tag{2.6}$$

Equation 2.6 provides the concentration of the exit stream from the inside of the membrane, i.e., the donor fluid, in a single pass. It is a function of the flow rate, overall mass transfer coefficient and membrane module properties. The term $\pi d_{in}NL$ represents the total surface area available for absorption across all the hollow fibers in the module and hence, denoted as 'A' in the following equations to simplify the expressions.

As the donor concentration is changing with time due to recirculation of unabsorbed drug, mass balance in the reservoir with volume V_{in} is considered and given by,

$$V_{in}\frac{dc_{in}^0}{dt} = Q_{in}(c_{in}^L - c_{in}^0) \tag{2.7}$$

Substituting equation 2.6 in equation 2.7 and integrating from $t = 0$ to $t = t$ we get,

$$\ln\left(\frac{c_{in}^0(t)}{c_{in}^0(0)}\right) = \frac{t.Q_{in}}{V_{in}\left(1 + \frac{Q_{in}}{Q_{out}}\right)}\left[\exp\left(-\frac{K_{in}A}{Q_{in}}\left(1 + \frac{Q_{in}}{Q_{out}}\right)\right) - 1\right] \tag{2.8}$$

or,

$$c_{in}^0(t) = c_{in}^0(0)\exp\left\{\frac{t.Q_{in}}{V_{in}\left(1 + \frac{Q_{in}}{Q_{out}}\right)}\left[\exp\left(-\frac{K_{in}A}{Q_{in}}\left(1 + \frac{Q_{in}}{Q_{out}}\right)\right) - 1\right]\right\} \tag{2.9}$$

The complex equation obtained above is simply the variation in the donor concentration as a function of time. The concentration of the receiver channel can be obtained by substituting equation 2.9 back into equation 2.5 for $z = L$. The form of these equations is similar to that obtained in the literature.[111]

In order to obtain the theoretical concentration profile using the expression derived in equation 2.9, it is important to know the value of the overall mass transfer coefficient, K_{in}. Theoretically, K_{in} is a function of fluid velocities on either side of the membrane surfaces,

viscosity of the fluids, diffusion coefficient of the molecule, fiber diameter, membrane material properties and length of the membrane module.[60] However, to determine K_{in} from first principles, a gamut of experimental optimizations and validations is required. Therefore, in view of the scope of this study, K_{in} was obtained by non-linear curve fitting of a range of data sets and then used to determine the applicability of the model to the experimental dissolution-absorption results. The data obtained from experiments carried out at similar operating conditions, but with different initial donor concentration ($c_{in}^0(0)$) above and below the crystalline solubility of nevirapine, was used to determine K_{in}. As K_{in} is a function of flow rate and membrane properties and not $c_{in}^0(0)$, the value should essentially remain constant for experiments carried out at different $c_{in}^0(0)$ values. A mean value of K_{in}, $(9.07 \pm 1.06) *10_{-5}$ cm/s was obtained from data fitting. The standard deviation in the fitted value can be attributed to the somewhat imprecise measurements of flow rate in the fluid channels using the employed rotameter: the model was found to be very sensitive to the fluid velocity.

2.5 Results

2.5.1 Solubility Experiments and Induction Studies

The crystalline solubility of anhydrous nevirapine in pH 6.5 50 mM phosphate buffer at 37 °C was found to be 128 µg/mL. Induction time studies were performed to determine the effectiveness of selected polymers as crystallization inhibitors. The nucleation induction time for nevirapine at 500 µg/mL in the absence of polymer was found to be around 5 min. Given the crystalline solubility, this represents a supersaturation ratio (S), defined as the experimental concentration/crystalline solubility, of 3.9. In the presence of 0.05% HPMC-AS crystallization was inhibited for more than 4h and with 0.1% PVPVA in the medium, crystallization occurred at around 60 min.

2.5.2 Preliminary Studies and Optimization of the Apparatus

The preliminary results obtained from the new apparatus were compared with the experiments carried out using a side-by-side diffusion cell. Nevirapine flux at its crystalline solubility in pH 6.5 phosphate buffer at 37 °C was studied in both apparatuses with similar

membrane materials. As shown in Table 2.1, the hollow fiber membrane, with 16-fold higher surface area, showed a considerably faster mass transfer as compared to the flat-sheet membrane.

Table 2.1: Comparative study of mass transfer across flat-sheet and hollow fiber membrane

Parameters	Flat-sheet membrane	Hollow Fiber Membrane
Initial Solution Concentration (μg/mL)	100	100
Solution Volume (mL)	30.0	50.0
Surface Area (cm$_2$)	7.07	115
Volume available for absorption at time t (cm$_3$)	30.0	1.41
Membrane Thickness (mm)	1.52	0.20
% of mass transferred in 60 min	1.50	41.5

Good reproducibility for the flow through apparatus was achieved following optimization of the experimental procedures and process parameters. The optimal flow conditions were found to be co-current flow with similar flow rates in both fluid channels. The co-current flow resulted in minimal flow disturbance and bubble formation, which was caused due to fluid channeling in the module. Considering the volume of the membrane module, the operating flow rate (2 mL/min) was determined by carrying out experiments for a range of flow rates from 0.5 mL/min to 9 mL/min. An optimal range of flow rates was observed whereby the mass transfer increased with an increase in flow rate due to reduction in aqueous boundary layer and improved sink conditions. Beyond a certain flow rate, however, the mass transfer started to decrease due to insufficient residence time. The transmembrane pressure gradient in the membrane module was eliminated so as to avoid any convective mass transfer across the membrane. With the use of the flow-through UV cell, the concentration of drug diffused across the membrane at a certain flow rate was measured in-line at every time point generating a non-cumulative concentration profile as shown in Figure 2.4. The error bars represent triplicate measurements.
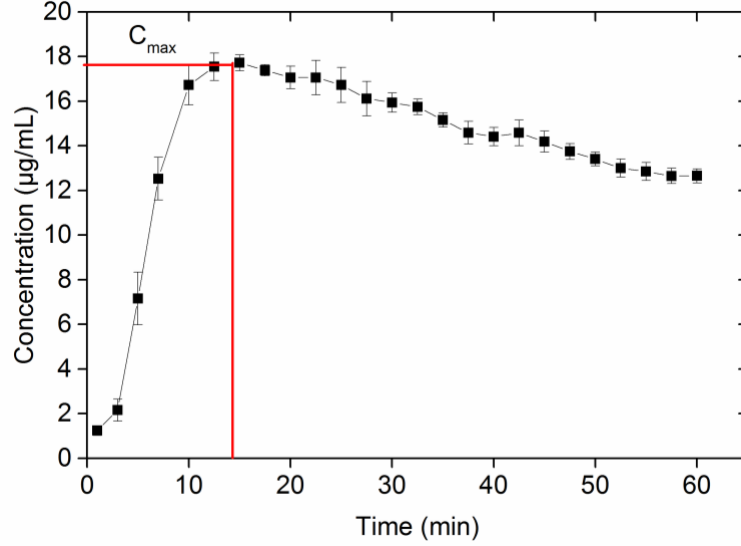
Figure 2.4: A typical concentration profile of receiver channel concentration indicating mass transfer across a hollow fiber membrane at flow rate of 2 mL/min.

At the operating flow rate, the concentration initially increases reaching a maximum value within about 15 minutes, and then slowly declines over the experimental time frame (Figure 2.4). The initial increase in the concentration can be attributed to saturation of the membrane with the drug to attain a steady state. A maximum is then reached followed by a decline. The decline can be attributed to a decrease in the driving force for mass transfer as the donor concentration is simultaneously depleted. The total drug diffused across the membrane over a certain time period is given by equation 2.10,

$$M_{total} = AUC_{total} * Q_{out} \qquad (2.10)$$

where M_{total} is total mass transferred, AUC_{total} is area under the curve for entire concentration-time profile and Q_{out} is volumetric flow rate outside the fiber (receiver fluid in this study). To verify complete mass balance, the system (including membrane module and tubing) was washed with solvent after every experimental run to remove any drug left in the voids of the system or adsorbed on the membrane. Further, the total donor concentration and solvent wash concentration were determined by UV spectrophotometry. The total receiver concentration was calculated from the receiver concentration profile using equation 2.10. Table 2.2 shows a typical mass balance

obtained after an experimental run (performed in duplicate) for 60 min starting with 5 mg of drug indicating that a complete mass balance can be achieved with this system.

Table 2.2: Mass balance of an experiment carried out with 5 mg of drug added to the donor compartment for an experimental run of 60 min.

	Mass balance (mg)	
	Trial 1	Trial 2
Drug left in donor container	2.09	1.78
Drug in receiver container	1.89	2.14
Drug obtained from solvent wash	0.99	1.07
Total Mass	4.97	4.99

Linearity between the amount of drug transferred and initial drug concentration (or more rigorously, the thermodynamic activity of the drug molecule) on the donor side was also evaluated for sub and supersaturated solutions. The amount of nevirapine transferred across the membrane over 60 min was determined. A linear relationship was observed between C_{max} as well as the area under the curve (AUC_{0-60}) and the initial drug concentration (Figure 2.5). As observed previously for other systems, there was no discontinuity between sub and supersaturated solutions.[10,11] Given the linear correlation between C_{max} and the initial donor concentration, as shown in Figure 2.5, these data can serve as a calibration set to determine the degree of saturation or supersaturation in an unknown system, as will be discussed in detail in the next section.
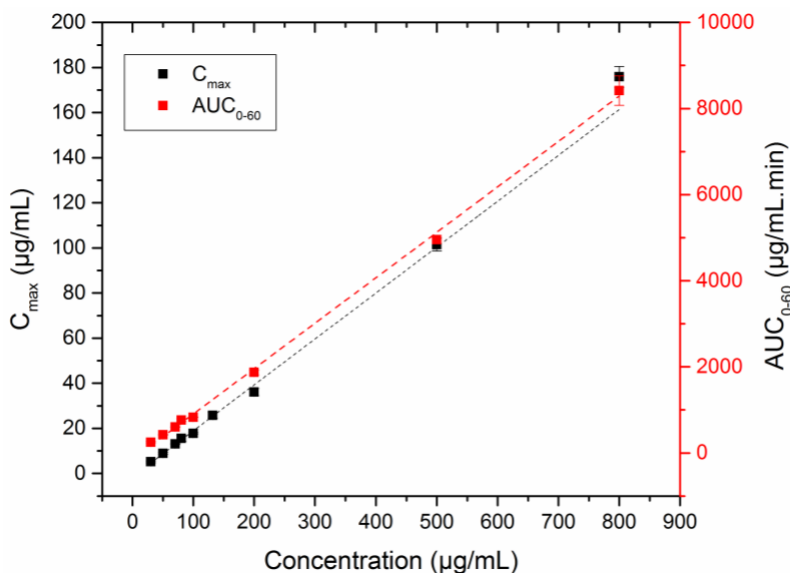
Figure 2.5: A linear correlation of maximum initial donor concentration and area under the curve observed in the receiver compartment.

2.5.3   Dissolution-Absorption Studies

The optimized mass transport apparatus was assessed for its potential to predict formulation performance and help discriminate between different formulations. The three types of nevirapine systems considered in this study were evaluated both for dissolution and absorption using the aforementioned apparatus. Figure 2.6 shows the concentration in the donor container and the receiver channel as a function of time for different systems. The donor profile, Figure 2.6a, shows the concentration-time profile for the first 30 min as the tablet dissolves in the acidic medium. After 30 minutes, the pH was changed to pH 6.5 and absorption measurements were commenced. The concentration profiles after 30 min shows depletion of drug due to mass transfer across the membrane and/or crystallization in the donor compartment. The receiver profile in Figure 4b shows the concentration of nevirapine that has diffused into the receiver channel during absorption measurements. By comparing the donor and receiver concentration profiles, it is possible to extract information about the various processes occurring in the dissolution vessel.
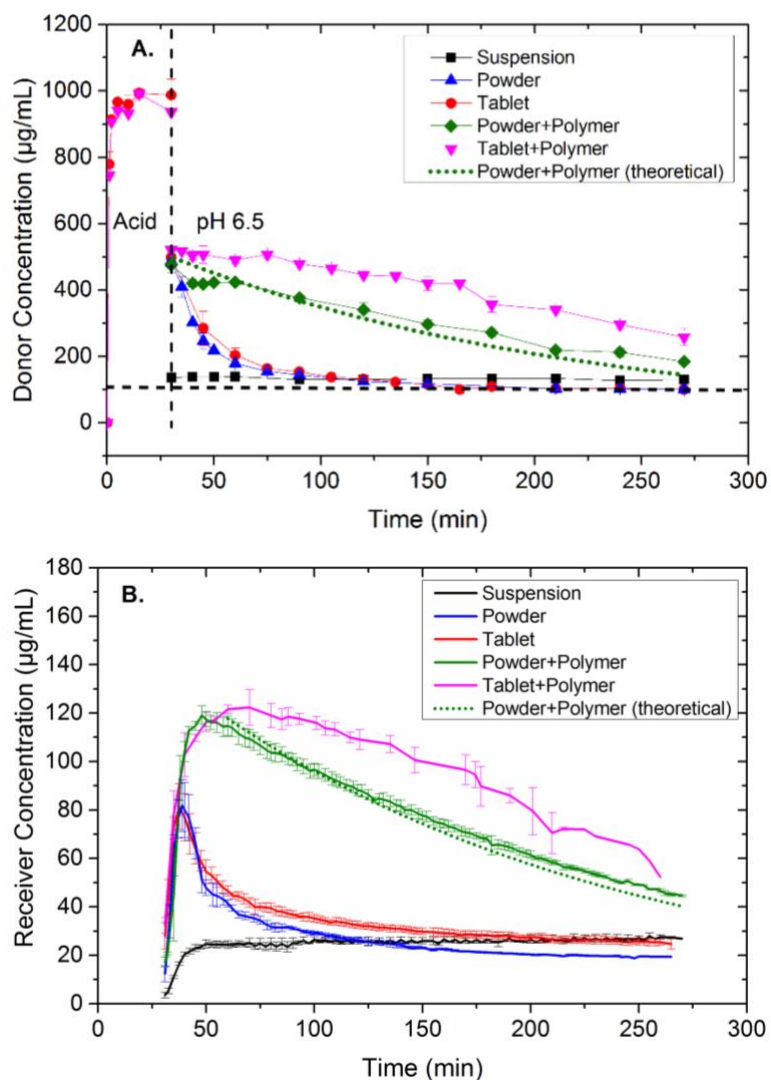
Figure 2.6: The donor (a) and receiver (b) concentration of nevirapine formulations during combined dissolution/mass transport analysis in the presence and absence of polymer (HPMC-AS) pre-dissolved in the solution

The first system evaluated was a control consisting of a crystalline suspension with an excess of undissolved drug. This system was only evaluated at pH 6.5. As expected, the donor and receiver concentration profiles for this system show constant concentration values over the experimental time frame. The concentration in the donor cell corresponds to the crystalline solubility of nevirapine while the C_{max} for the receiver profile reflects the value found for a solution at the crystalline solubility (Figure 2.6).

In the case of drug powder dissolution-absorption studies, the solids were completely dissolved in the acidic medium and the pH change subsequently led to a supersaturated solution (S=3.9). During the absorption measurement, a rapid decrease in drug concentration was noted in the donor concentration-time profile, wherein the concentration dropped to the value observed for the crystalline suspension. The decline in donor compartment concentration can likely be attributed to crystallization, with some contribution from simultaneous absorption across the membrane. The donor compartment solution was sampled, and crystals could be seen using a polarized light microscope. Concurrently, in the receiver concentration profile, the drug concentration increased to a certain C_{max} before it rapidly decreased reaching a value closer to that observed for the crystalline suspension. The C_{max} in this case was found to be approximately 4 times higher than that observed for the crystalline suspension.

The complexity of the system was increased by evaluating the absorptive dissolution profiles of a commercial nevirapine tablet, using the same two-step dissolution process with pH change after 30 minutes. The tablet dissolved completely in the acidic medium, as seen in Figure 2.6a. Upon pH-shift, the drops in the donor and receiver concentrations with time were analogous to those observed for the powder formulation, decreasing until the donor side concentration was equivalent to crystalline solubility. However, C_{max} was again approximately 4 times higher than that observed for crystalline suspension.

Given the rapid crystallization, it was of interest to evaluate the impact of adding a crystallization inhibitor. As seen in Figure 2.6a, the presence of 0.05% HPMC-AS pre-dissolved in the dissolution medium had a substantial impact on the solution concentrations. With the polymer present, the donor drug concentration profile showed a gradual decrease over time as opposed to the rapid decline observed for systems without polymer. No crystals could be observed in the donor solutions for times of up to 160 min. A correspondingly higher receiver compartment C_{max} was achieved in the presence of polymer as compared to in the absence of polymer due to sustained supersaturation in the former. Tablet and drug powder profiles were again generally similar. The slight difference in the magnitude of donor and receiver concentrations generated following pH-shift between the powder and tablet can be attributed to the higher amount of drug

present in tablet; commercial tablets were used hence the exact mass of drug in the tablet can vary whereas the powder sample was accurately weighed.

2.5.4 Data Modeling

The mathematical model derived for the mass transport process in a hollow fiber membrane illustrates the important operating parameters that govern mass transfer in the system and can help select the optimal experimental parameters. The drug concentration in the donor solution is changing continuously due to mass transfer and is predicted by the model to deplete exponentially with time, with the important variables determining the rate of mass transfer comprising of the overall mass transfer coefficient, membrane module properties, volumetric flow rate, total volume of the container and the initial donor concentration. The decrease in the receiver concentration is coupled to the change in the donor compartment concentration and should also follow an exponential decline. Considering the exponential decrease in concentration over time expected theoretically, the validity of the model can be evaluated by plotting experimentally-determined logarithmic values of the ratio of the donor concentration at time t and initial donor concentration as a function of time. A linear correlation of $\ln\left(\frac{c_{in}^0(t)}{c_{in}^0(0)}\right)$ vs time for an experimental data set, as seen in Figure 2.7, provides confidence that the theoretical mass balance model adequately describes the experimental observations.
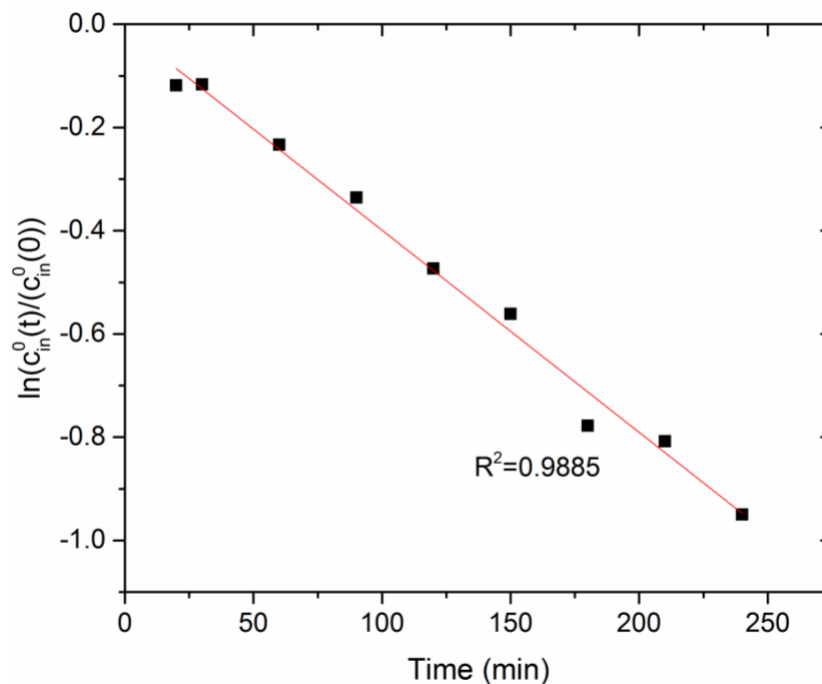
Figure 2.7: A linear correlation of ratio of concentrations of donor versus time on a semi-log scale for a sample data set indicating an exponential decrease in the donor concentration.

An ideal mass transfer unit operation should show a linear correlation between mass transfer coefficient and fluid flow rates.[111] Fitting the model to the experimental data obtained for different flow rates and plotting the estimated K_{in} against flow rate showed a linear correlation as expected (Figure 2.8). This also agrees well with the experimental results observed for different flow rates, wherein the total amount of drug transferred over time increases within the range of flow rates considered here, further confirming the accuracy of the model to predict mass transfer in the apparatus.
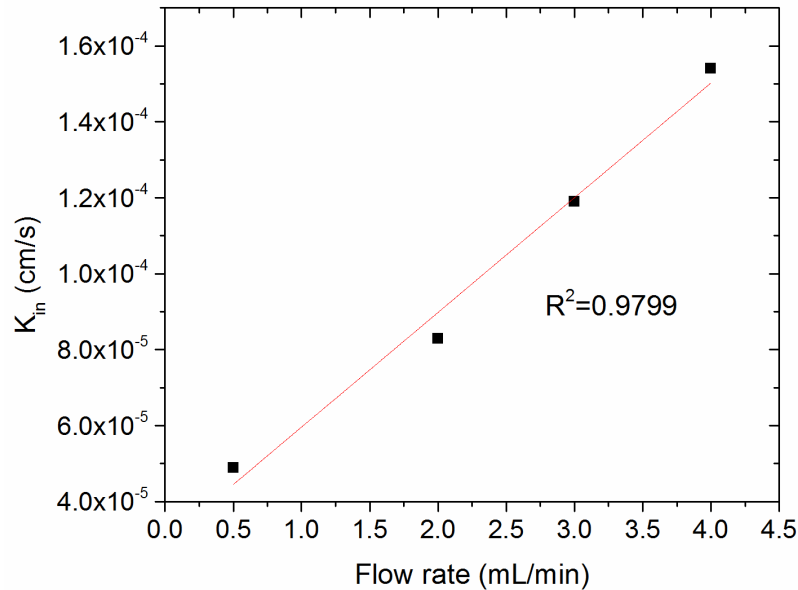
Figure 2.8: The overall mass transfer coefficient K_{in} as a function of flow rate shows a linear correlation.

Having confirmed the apparent validity of the model, donor and receiver concentration profiles for dissolution-absorption of powder in the presence of pre-dissolved polymer in solution was predicted using the model. A comparison between the experimental data and the concentration-time profile predicted by the model is shown in Figure 2.6a and 2.6b (dotted lines). Good agreement between the experimental and predicted curves is seen using a K_{in} of $1.08*10_{-4}$ cm/s, which is within the expected range considering the error. The predicted curve is plotted only after the system reached steady state as the model is valid only for a steady state process. It should be noted that the model can only be used for experiments where no crystallization occurs over the experimental time frame. To predict concentration profiles for formulations undergoing crystallization, accurate crystallization kinetics need to be included in the model, which is beyond the scope of the current study.

2.5.5   Closed compartment dissolution versus dissolution-absorption

The concentration time profiles for the tablet in the donor compartment with and without absorption were compared and found to be fairly similar both in the presence and absence of a

polymer, HPMC-AS. In the absence of polymer, the solution concentration declined rapidly (Figure 2.9), while in the presence of HPMC-AS, it remained constant over the duration of the experiment for the closed compartment and slowly declined in the absorptive system due to mass transfer across the membrane.
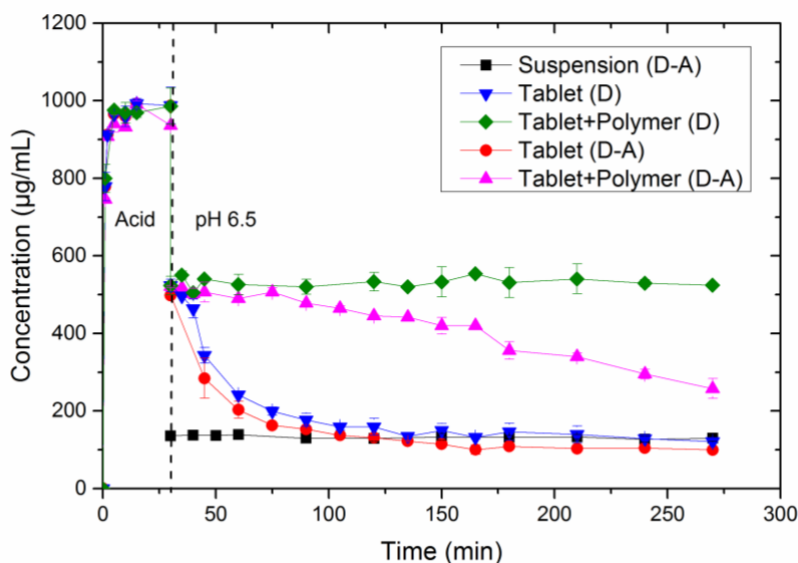
Figure 2.9: A comparative plot of donor concentration-time profiles for the tablets in the presence (D-A, dissolution-absorption) and absence of absorptive compartment (D, dissolution). Data for the suspension is shown for comparison and the polymer used was HPMC-AS.

Thus for these two situations, namely very rapid crystallization and no crystallization, the absorptive compartment did not appear to substantially impact the phase behavior of the donor solution. To explore a system with a moderate potential to undergo crystallization, PVPVA was added to the dissolution medium (based on the induction time data shown above, this polymer has some impact on inhibiting nevirapine crystallization) and a supersaturated solution (S=3.9) was generated. Figure 2.10a shows a comparison of the donor compartment concentrations as a function of time, showing a steeper decline in concentration for absorption relative to closed compartment. Figure 2.10b shows a comparison of the total amount of drug remaining in solution in the donor container and the amount of drug transferred across the membrane and collected in the receiver container as a function of time for the absorptive system relative to the amount of drug in solution for the closed system. From this analysis, it is apparent that the total amount of drug (donor plus receiver compartment) remains constant for 120 min in the presence of an absorptive compartment indicating that no drug is lost through crystallization. On the other hand, in the case

70

of the closed compartment, the total amount of drug decreases after 60 min indicating that crystallization of the drug has occurred. Thus, in this case, the crystallization tendency is reduced by the presence of an absorptive compartment.
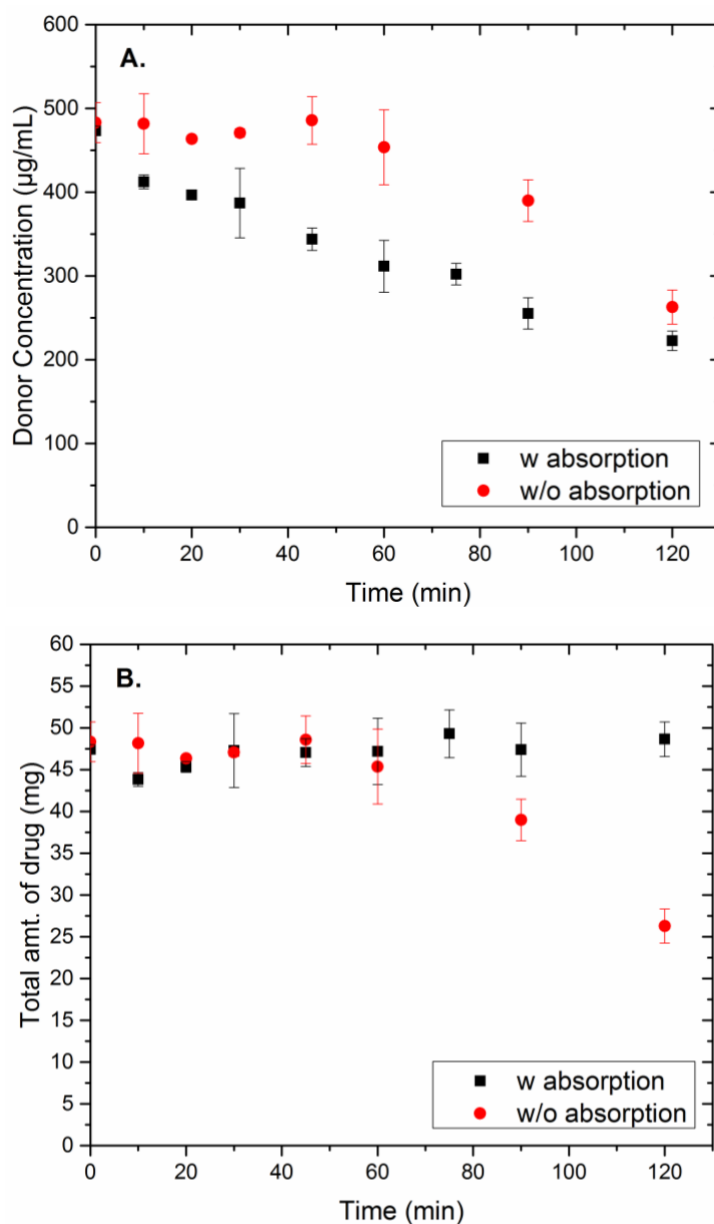
Figure 2.10: Donor concentration (a) and total amount of drug in donor and receiver (b) in the presence and the absence of absorptive environment.

2.6   Discussion

2.6.1   Potential of the New Apparatus for Mass Transport Analysis

An *in vitro* tool that provides improved mechanistic understanding of formulation dissolution performance, and *in vivo* relevant discrimination between various enabling formulations would be of great utility to formulation scientists. The coupling of an absorptive compartment to the dissolution chamber is emerging as an important approach for the evaluation of enabling formulations such as those that are anticipated to undergo supersaturation *in vivo*.[7,113] However, for membrane based systems, a major limitation is the surface area of the membrane employed, which being small, limits the extent of possible mass transfer. Consequently, it is not possible in many instances to truly couple the processes of dissolution and mass transport in a biorelevant manner, since the extent of mass transport is low, which in turn impacts the dissolution process. The use of a hollow fiber membrane to study absorption of drug across the membrane is an attractive approach because the rate of mass transfer is improved substantially as highlighted by the data shown in Table 2.1. These increases are primarily due to the large surface area to volume ratio offered by the membrane module. The improved mass transfer can also be attributed to smaller membrane thickness and the continuous flow setup that reduces the diffusional barrier that can arise from an unstirred water layer formed adjacent to the membrane surface. Finally, the continuous flow of fresh buffer on the outer side of the membrane maintains sink condition and thus offers a high driving force for the mass transfer. Because the use of hollow fiber membranes for evaluation of drug transport is relatively unexplored,[64,65] it is important to consider factors that impact the observed experimental output.

The non-cumulative concentration profile generated by in-line measurement of concentration of drug diffused across the membrane gives a real-time analysis of the rate of appearance of drug across the membrane during absorption (Figure 2.4). The exponential decrease in the concentration profile following attainment of steady state is well predicted by the theoretical model developed (Figure 2.6). Because sink conditions are maintained by supplying a continuous flow of fresh buffer, the donor compartment concentration as a function of time dictates the mass transport rate (equation 2.5). The concentration-time profile observed in the receiver compartment is therefore coupled to the concentration-time profile in the donor compartment and reflects

formulation performance including dissolution rate relative to mass transfer rate, crystallization events, and degree of supersaturation achieved.

2.6.2 Formulation Discrimination and Formulation Performance

The dissolution-absorption analysis of the three types of formulations considered in this study reveal that the apparatus can capture differences between formulations, thus providing mechanistic understanding of phenomena occurring during dissolution and absorption of the drug. An example of the coupling between the dissolution and absorption processes is provided by studies on the crystalline suspension. Following attainment of steady state, this system showed a constant concentration profile for both the donor and receiver compartment due to the reservoir provided by the undissolved excess powder in the solution. Thus, as drug is absorbed across the membrane, solid rapidly dissolves to replenish the solution concentration in the donor compartment to maintain the equilibrium crystalline solubility. Consequently, the constant concentration value observed in the receiver profile following membrane saturation at the C_{max} agrees well with the C_{max} obtained starting from a saturated solution of the drug (Figure 2.5). These observations confirm that the receiver profile accurately reflects the donor concentration. Clearly the dissolution rate of the crystalline material is rapid relative to the absorption of the drug across the membrane and under these experimental conditions, the system is not dissolution rate limited. It should be noted that this reservoir effect cannot be as easily observed with a side-by-side diffusion cell.

Many weakly basic compounds are expected to undergo supersaturation *in vivo* when transfer from the low pH stomach environment to the higher pH small intestinal compartment reduces the extent of ionization of the compound. Thus, two step dissolution tests involving a pH change are increasingly being used to evaluate such systems. The supersaturated solutions thus generated from nevirapine powder and tablet showed interesting donor and receiver concentration profiles. Based on the induction time measurements described above, which were conducted at a comparable supersaturation as is generated upon pH change, it is apparent that nevirapine has a high tendency to crystallize from supersaturated solutions. Hence, the donor concentration dropped to the crystalline solubility and showed a constant value for a certain period of time, indicating that crystallized drug provided a reservoir, and then the concentration dropped to below the

crystalline solubility. Due to the initial generation of supersaturation following pH-shift, whereby a period of about 50 minutes was required for the solution to reach the crystalline solubility, the receiver concentration profile showed a higher C_{max} as compared to the crystalline suspension. However, due to crystallization, the concentration rapidly declined to a value close to that seen for the receiver compartment of crystalline suspension system. Subsequently, the concentration decreases below this value, indicating that all the crystalline material in the donor compartment has dissolved. Both powder and tablet formulations showed similar donor and receiver concentration profiles, with differences in the time taken to reach the crystalline solubility. The difference was due to the different volumes of donor solution (and therefore total mass of drug) used for the two formulations, where a larger volume was used for the tablet formulation. This dependence of the rate of mass transfer on the volume of the donor fluid can be explained based on the model derived. As seen from equation 2.7, the rate of mass transfer is inversely proportional to the volume of the donor compartment. Hence, a longer time was taken for tablet formulation to reach the crystalline solubility in the donor compartment and the effect was reflected in the receiver concentration profile as well.

Given the similar crystallization rate observed for the tablet and powder, it can be noted that the tablet formulation does not include any excipients that reduce the crystallization rate; studies show that nevirapine is well absorbed from the commercial formulation.[114] In the presence of HPMC-AS, based on the induction time studies, both the powder and tablet systems are expected to show sustained supersaturation. For the powder formulation, no crystallization was observed for 4 h. Thus, the donor and the receiver concentration profile showed a slower decline with time and a higher C_{max} as compared to when no polymer was present owing to mass loss from solution due to crystallization as well as membrane transport in the latter system. Tablet dissolution and absorption in the presence of polymer exhibited similar trends in terms of donor and receiver concentration profiles as the powder formulation. Additionally, for the tablet, crystallization was only inhibited for 120 min. The origin of the difference in crystallization behavior of the powder and tablet was not investigated further, but it is speculated that the presence of undissolved excipient particles such as microcrystalline cellulose may have played a role.

The linear correlation observed between C_{max} and the initial donor concentration can be used to extrapolate further details about formulation performance based on the observed receiver concentration profile. As seen in Figure 2.6b, C_{max} observed for powder and tablet formulations in the presence and absence of HPMC-AS differ, even though an equivalent supersaturation was generated initially in the donor compartment in both cases. This is obviously due to immediate crystallization in the donor compartment in the absence of the polymer. The C_{max} for the crystallizing system provides information about the level of supersaturation in the donor compartment when steady state was achieved for the system; this corresponds to the supersaturation in the donor compartment at approximately 10-15 minutes post pH change. Thus, the supersaturation extrapolated from the receiver compartment information can be considered as the maximum effective supersaturation observed for a formulation and can be utilized to discriminate between formulations. The effective supersaturations were calculated for the various nevirapine formulations evaluated in this study using the C_{max} values and the correlation between C_{max} and concentration (Figure 2.5) and are compared with the maximum supersaturation in the donor compartment, which was calculated from the donor concentration observed immediately following pH change. As seen from Table 2.3, in the absence of polymer, a lower effective supersaturation is observed relative to the initial, maximum supersaturation. In contrast, in the presence of polymer, the supersaturation calculated to exist in the donor compartment, based on the value of C_{max} (receiver compartment) is in good agreement with the expected supersaturation based on the donor compartment concentration measurements. The theoretical supersaturation values expected in the donor provide a reference to the observed values.

Table 2.3: Theoretical and observed supersaturation ratios (S) for different formulations deduced from donor and receiver concentration-time profile

Formulation	Theoretical S	Maximum S Observed in Donor	S Observed at t_{max} in Receiver
Suspension	1.0	1.07 ± 0.0	1.00 ± 0.03
Powder	3.9	3.8 ± 0.1	2.8 ± 0.3
Powder + Polymer	3.9	3.9 ± 0.1	4.10 ± 0.06
Tablet	3.9	3.8 ± 0.1	2.9 ± 0.3
Tablet + Polymer	3.9	4.07 ± 0.02	4.0 ± 0.2

2.6.3 Importance of Absorptive Dissolution Testing

Previous studies have highlighted the potential importance of an absorptive compartment.[42] For nevirapine tablets with no polymer additive in the dissolution medium, the concentration-time profile for dissolution only was quite similar to that observed for the combined dissolution-absorption system. This was due to the rapid crystallization of nevirapine in both instances. This observation can be rationalized by the high driving force for nucleation that is present immediately after the pH increase due to the level of supersaturation generated. Thus, crystallization in the donor compartment commences before substantial mass transport can occur, and the presence of an absorptive compartment cannot lead to a reduction in the supersaturation, and consequently reduce the driving force for nucleation. The profiles, however, are not identical. The dissolution only system reaches the crystalline solubility in 140-160 min while this concentration is reached in the dissolution-absorption system in 120 min (Figure 2.9). This difference is due to two processes contributing to depletion of solution drug concentration in the case of the absorptive system, mass transport across the membrane as well as crystallization. In contrast, for the dissolution only system, only crystallization can lead to a reduction in donor solution concentration. Thus, dissolution tests may overestimate the extent of supersaturation at any given time point. This effect can be clearly seen by comparing the corresponding dissolution and dissolution-absorption concentration time profiles for tablets in the presence of HPMC-AS (Figure 2.9). For dissolution-absorption measurements, the donor concentration depletes slowly due to absorption across the membrane, providing information about how the absorption driving force changes with time, while the dissolution only system shows a constant concentration level over the duration of the experiment. Therefore, to better estimate the concentration driving force for oral absorption, dissolution testing in the presence of absorptive compartment is likely to be beneficial.

The data presented in Figure 2.10 further highlights the importance of including an absorptive compartment in dissolution studies, especially for systems that undergo crystallization on a slower timescale, as for the case where PVPVA is used as an inhibitor. Quite different donor concentration time profiles are observed with and without an absorptive compartment. Through mass balance analysis of the absorptive dissolution data, it becomes apparent that crystallization is avoided in this experiment. In contrast, crystallization is observed for the closed compartment system after an hour. Thus, the closed compartment overestimates the risk for crystallization, while

the absorptive compartment experiment provides a depletion in concentration with time which is important to consider when evaluating crystallization risk, and a situation that also occurs *in vivo* in the small intestine. Hence, in agreement with previous observations, it is clear that the presence of an absorptive compartment during dissolution studies can alter crystallization kinetics of a formulation. This observation is readily rationalized on the basis that the mass transfer of drug across the membrane depletes the donor concentration (Figure 2.10a), thus reducing supersaturation and in turn the driving force for nucleation and growth.

The approach described herein offers considerable flexibility in experimental design. Hollow fibers membranes are available in variety of membrane materials and surface areas, enabling different drugs to be evaluated and experimental conditions to be varied to achieve the desired absorption rate. While highly lipophilic drugs may pose challenges, both in terms of adsorption to certain membrane types and low overall solution concentrations, these obstacles should be solvable through appropriate membrane choice and implementation of sensitive analytical techniques or addition of solubilizing additives to receiver fluid. Therefore, the mass transfer can be studied for variety of compounds, although this approach is likely of greatest relevance for drug displaying solubility limited absorption like BCS Class II compounds. Having demonstrated the proof of concenpt, future studies will be conducted with different drug compounds, membrane types and dissolution media, including biorelevant media.

2.7   Conclusion

This study introduces a novel approach to *in vitro* analysis of formulation performance, employing a hollow fiber membrane to study absorption of a drug across a membrane. Preliminary observations highlight several advantages of this system. In particular, the large surface area-to-volume ratio and continuous flow used in the system greatly improves the mass transfer rate, enabling coupling of dissolution and absorption, and allowing these processes to be studied over relevant timeframes. Dissolution-absorption studies of nevirapine formulations demonstrated the utility of including an absorptive compartment to evaluate the supersaturation generated upon pH increase and the impact of polymers on formulation performance. Important parameters governing the rate of mass transport were elucidated through development of a mathematical model which showed a good fit to the experimental observations. Thus, the absorptive-dissolution system can

provide additional information about formulation performance not typically realized with conventional dissolution testing approaches. Although, the *in vivo* relevance of the formulation performance observed in the apparatus still needs to be tested experimentally, these insights may enable better prediction of formulation performance and will allow pharmaceutical scientists to make more informed decisions with respect to form and formulation optimization.

CHAPTER 3.   INSIGHT INTO AMORPHOUS SOLID DISPERSION PERFORMANCE BY COUPLED DISSOLUTION AND MEMBRANE MASS TRANSFER MEASUREMENTS.

3.1   Abstract

The tendency of highly supersaturated solutions of poorly water-soluble drugs to undergo liquid-liquid phase separation (LLPS) into drug-rich and water-rich phases when the concentration exceeds the amorphous solubility, for example, during dissolution of some amorphous solid dispersions, is thought to be advantageous from a bioavailability enhancement perspective. Recently, we have developed a high surface area, flow-through absorptive dissolution testing apparatus that enables fast mass transfer providing more *in vivo* relevant conditions and time frames for formulation testing. Using this apparatus, the absorption behaviors of solutions with different extents of supersaturation below and above the amorphous solubility were evaluated. In addition, simultaneous dissolution-absorption testing of amorphous solid dispersions (ASDs) with varying drug loadings and polymer types was carried out to study and distinguish the absorption behavior of ASDs that do or do not undergo LLPS. When compared with closed-compartment dissolution testing, a significant influence of the absorptive compartment on the dissolution rate of ASDs, particularly at high drug loadings, was observed. The formation of drug-rich nanodroplets, generated by both solvent-addition and ASD dissolution, resulted in a higher amount of drug transferred across the membrane. Moreover, the mass transfer was further enhanced with increasing concentration above the amorphous solubility, thereby showing correlation with an increase in the number of drug-rich particles. The importance of including an absorptive compartment in dissolution testing is highlighted in this study, enabling coupling of dissolution to membrane transport, and providing a more meaningful comparison between different formulations.

3.2   Introduction

Dissolution performance is an important evaluation in the formulation development of oral

solid dosage forms, whereby dissolution is inherently dependent on the compound solubility in the dissolution medium.[33,34] With many poorly water soluble drug candidates, the problem of low oral bioavailability due to insufficient dissolved material is becoming more ubiquitous. In order to address this issue, several formulation strategies are commonly employed including the use of solubility-enhancing additives or supersaturating formulations.[6] Although solubilizing additives are promising formulation strategies for increasing the equilibrium concentration of the drug compound, it has been reported that they either have no impact or tend to decrease membrane transport by lowering the thermodynamic activity of the drug molecule.[115,40] On the other hand, supersaturating formulations are gaining increased interest as they can generate high intraluminal concentrations, significantly higher than the thermodynamic equilibrium solubility and can enhance oral absorption.[116–119]

A solute in a supersaturated solution has a higher thermodynamic activity and chemical potential than the thermodynamically stable crystalline form. The driving force for membrane transport is the difference in the chemical potential of the species across the membrane.[44] Hence, supersaturated systems impart higher membrane flux, particularly when the system does not undergo crystallization over biorelevant time frames.[5,10,11] There are several routes for generating a supersaturated solution *in vivo* including amorphous solids, amorphous solid dispersions, salt dissolution, pH change in the gastrointestinal (GI) tract, dissolution of cocrystals, lipid or surfactant-based formulations.[120] Amorphous solid dispersions (ASDs), containing drug molecules dispersed in a polymer matrix, are of great interest due to their ability to generate and maintain supersaturation for biologically relevant times, whereby the presence of a suitable polymer reduces the risk of crystallization, leading to higher solution concentrations available for absorption.[58,84,121–123] A highly supersaturated solution of a hydrophobic compound may undergo liquid-liquid phase separation (LLPS), leading to the formation of disordered colloidal drug aggregates as a precursor to crystallization.[12–14] LLPS is observed when the solute concentration exceeds the amorphous solubility of the drug in the aqueous medium, and the solution splits into two phases, a drug-rich and a water-rich phase.[10,11,15,76,85] The concentration of the water-rich phase is equal to the amorphous solubility of the compound and the drug-rich phase comprises water-saturated amorphous compound typically in the form of nanodroplets. The thermodynamic activity of the drug is the same in the drug-rich and water-rich phases and hence there is a metastable

equilibrium between the two phases with the amorphous solubility being the maximum achievable free drug concentration for a particular compound.[5,15,75] This metastable equilibrium will be maintained until the system overcomes the thermodynamic barrier to crystal nucleation. The potential effect of these colloidal aggregates on oral absorption has also been studied recently.[11,84] *In vitro* studies demonstrated that, in the absence of crystallization, these drug-rich nanodroplets acted as a reservoir, replenishing drug to the aqueous phase from which absorption across the membrane occurs, until the drug-rich phase was ultimately depleted.[10] High flux was observed for as long as the supersaturation was maintained at a constant level; the duration of this reservoir effect depended on the amount of drug present in the drug-rich phase and its ability to dissolve rapidly. Hence, the formation of drug-rich nanodroplets may potentially enhance the oral bioavailability of poorly soluble drug compounds. It has also been suggested that drug-rich colloids have the potential to reduce the diffusional barrier in the unstirred water layer of the intestinal tract, and thus enhance the effective permeability of the compound *in vivo*.[124]

The standard United States Pharmacopeia (USP) dissolution apparatus is typically employed for testing formulation performance and rank ordering solid forms and formulations. In order to develop effective supersaturating formulations, dissolution testing plays a key role as a formulation development tool particularly at the early stage. However, standard dissolution testing often fails to predict the performance of such complex formulations as it is a closed, one-compartment setup, and lacks absorptive sink conditions. Hence, there is a substantial need for improved release-testing methodology to obtain *in vivo* relevant dissolution data.[125] Numerous modifications have been applied to the conventional dissolution apparatus with respect to biorelevant fluid or hydrodynamics, however, they still lack the absorptive sink condition.[7] The presence of an absorptive compartment is particularly important for formulations that undergo supersaturation and crystallization. The continuous removal of drug from the dissolution medium due to absorption across the membrane can alter both dissolution as well as the crystallization kinetics of the drug. Studies have reported that crystallization of drug from a supersaturated solution was less extensive when dissolution studies were carried out in combination with absorption across a membrane.[42,126] Several approaches have incorporated an absorptive compartment into dissolution studies.[43,50,113,125] The most common approach is to use a two-compartment system that contains a donor and a receiver compartment separated by a membrane.

Dissolution of drug takes place in the donor compartment and drug appearing in the receiver compartment is quantified to study the rate of absorption or permeation of the compound. However, currently used *in vitro* mass transport apparatuses have several limitations. The surface area of the membrane available for absorption in these apparatuses is small. As the membrane surface area is proportional to the rate of mass transfer, slow mass transfer in the system leads to long experimental times and potentially poor prediction of formulation performance.[10,110] Moreover, the small volumes in the receiver compartment can make it difficult to achieve detectable concentrations. Further, the presence of an unstirred water layer barrier due to hydrodynamic constraints further slows down the rate of mass transfer.

Considering the aforementioned limitations of dissolution testing and mass transport measurements, we have developed a novel high surface area, flow-through absorptive dissolution testing apparatus. This apparatus utilizes a hollow fiber membrane module to evaluate the absorption behavior of a drug that is either pre-dissolved or simultaneously dissolving in the dissolution medium. Hollow fiber membranes offer large surface area per unit volume which enhance mass transfer rates significantly. The continuous flow of fluids on either side of the membrane reduces the unstirred water layer barrier and provides controlled hydrodynamics which are potentially more similar to those found *in vivo*.[127–129] Fresh receiver fluid is pumped continuously, maintaining sink conditions on the receiver side. Moreover, the flow-through setup allows in-line measurement of the receiver concentration, thus providing real time analysis of solution behavior during dissolution of formulations. The robustness and sensitivity of the apparatus has been described previously.[126]

The goal of this study was to utilize an *in vitro* absorptive dissolution testing apparatus to understand the dissolution-absorption behavior of supersaturating systems undergoing LLPS with the formation of colloidal drug species. The enhanced mass transfer and reservoir effect due to drug-rich nanodroplets has been demonstrated previously using a static and a flow-through side-by-side diffusion cell.[10,11] However, in the latter study, the experiments had to be carried out over 16 h duration in order to study depletion of the drug-rich phase during absorption measurements due to slow mass transfer. Clearly, this is longer than the biorelevant intestinal absorption time frame of 3 - 4 h. The faster rate of mass transfer in the new apparatus allows understanding of

solution phase behavior and drug membrane transport over more relevant time frames. Atazanavir was used as a model drug compound as it is a relatively slow crystallizer[130] and by adding sufficient amounts of certain polymers, crystallization could be inhibited for more than 4 h. Solutions with different extents of supersaturation, generated by the solvent-shift method, were evaluated for their absorption behavior for concentrations below and above the amorphous solubility. The drug-rich nanodroplets formed at concentrations above the amorphous solubility were characterized in terms of number and size. Simultaneous dissolution and absorption measurements were also evaluated for a set of ASDs. The drug loading and polymer type can influence the drug release rate, and hence solution concentration and phase behavior.[86,131] Moreover, the formation of drug-rich nanodroplets has been observed during dissolution of some ASDs and a higher diffusive flux was noted for these formulations.[58,132] Therefore, concurrent dissolution-absorption measurements of ASDs were performed herein to understand the influence of formulation variables on dissolution rate, speciation and subsequent absorption profiles. A comparative study of closed compartment ASD dissolution was also carried out to understand the effect of the absorptive compartment on the dissolution rate with differences being observed for some systems.

3.3   Materials

Atazanavir (ATZ) was purchased from ChemShuttle (Jiangsu, China). Hydroxypropyl methylcellulose (HPMC) and hydroxypropyl methylcellulose acetate succinate (HPMCAS) MF grade were supplied by Shin-Etsu Chemical Co. Ltd. (Tokyo, Japan). Polyvinylpyrrolidone/ vinyl acetate, also known as Kollidon VA 64 (PVPVA), was obtained from the BASF Corporation (Florham Park, NJ). Nile red was purchased from Sigma Aldrich Co. (St. Louis, MO). Methanol and dichloromethane were purchased from Fisher Scientific (Pittsburgh, PA). Atazanavir is a weakly basic compound with a pKa of 4.52,[133] hence all dissolution and mass transport studies were carried out in pH 6.8 50 mM phosphate buffer such that ATZ was substantially unionized.

3.4 Methods

3.4.1 Crystalline and amorphous solubility determination

The crystalline solubility of ATZ in 50 mM phosphate buffer at pH 6.8 was determined by equilibrating excess solid drug in the aqueous medium for 48 h at 37 °C. The undissolved solids were separated by microcentrifugation using a Sorvall Legend Micro 21 (Thermo Fisher Scientific Inc., MA) at 14800 rpm ($21,100 \times g$ rcf) for 30 min. The supernatant was evaluated for concentration using a UV/vis spectrophotometer (SI photonics, Tuscon, AZ) at 278 nm.

The amorphous solubility of ATZ was determined by the UV-extinction method.[15] A supersaturated solution of atazanavir was generated in 50 mL pH 6.8 phosphate buffer containing 1 mg/mL pre-dissolved HPMCAS. A methanolic stock solution of ATZ (30 mg/mL) was gradually added to the aqueous medium at 37 °C using a syringe pump (Harvard Apparatus, Holliston MA) at a rate of 40 μL/min. The final methanol amount added was approximately 50 - 60 μL. Supersaturated solutions thus generated were monitored for changes in scattering using a UV/Vis spectrophotometer at 400 nm. The concentration where scattering was observed was noted as the amorphous solubility and the onset concentration for LLPS. Amorphous solubility was also determined using a similar method in the presence of 1.8 mg/mL PVPVA pre-dissolved in buffer.

3.4.2 Particle size and particle concentration measurement

The particle size of drug-rich nanodroplets generated due to LLPS was evaluated using dynamic light scattering (DLS) using a Nano-Zetasizer (Nano-ZS) from Malvern Instruments (Westborough, MA) equipped with dispersion technology software. A backscattering detector was used with the scattering light detected at an angle 173°. Samples were filtered using 1 or 0.45 μm glass fiber filters and were filled into disposable plastic cuvettes. The temperature of the sample holder was set at 37 °C. DLS measurements were carried out for different initial donor concentrations above LLPS and also during the absorption measurements to understand nanodroplet depletion during the process.

Particle concentration was evaluated using nanoparticle tracking analysis (NTA) with a Nanosight LM10 (Malvern Instruments, Westborough, MA). A green laser with a wavelength of

532 nm was used as a light source. The nanodroplets were observed using a microscope with 20× magnification and a video camera. The particle size is determined by tracking Brownian motion of the particles and relating the movement to particle size using the Stokes-Einstein equation. In this study, NTA was carried out in fluorescence mode. This is because the buffer containing 1 mg/mL HPMCAS showed high background noise most likely due to the presence of small polymer aggregates at pH 6.8.[134,135] The fluorescence mode allows only fluorescent particles to be detected. Nile red was used to preferentially stain the drug-rich droplets. Nile red is hydrophobic in nature and can be excited at 532 nm. When drug-rich species are formed, nile red partitions into these relatively hydrophobic regions. Thus, after application of the spectral filter, only drug-rich nanodroplets are illuminated. 1 μg/mL of nile red was added to the samples and the samples were then injected into the sample holder, which was equilibrated at 37 °C. The camera intensity was adjusted such that the particles were clearly visible, and the data was captured over a 30 s time frame.

3.4.3   Preparation of amorphous solid dispersions

Powdered ASDs of ATZ were prepared with various drug loadings (10, 30, and 50 wt.%,) in polymers (HPMCAS, HPMC and PVPVA). Drug and polymer were dissolved in methanol (HPMCAS and PVPVA) or 1:1 dichloromethane: methanol (HPMC). Each solution was then subjected to rotary evaporation under vacuum using a Buchi Rotavapor-R (New Castle, NJ) equipped with a Yamato BM-200 water bath which was maintained at 45 °C. Once the solvent was evaporated, the ASDs were dried under vacuum for at least 24 h. The dried ASDs were reduced to powder by cryo-milling (SPEX Sample Prep Freezer Mill 6775, Metuchen, NJ) and stored at 0% RH.

3.4.4   Fluorescence Spectroscopy

Atazanavir is an autofluorescent molecule, showing a peak shift and higher peak intensity when drug-rich species are formed. Hence, fluorescence spectroscopy was carried out at concentrations below and above the amorphous solubility as a means to determine if drug-rich nanodroplets were present or absent. An excitation wavelength of 250 nm was used, and the emission spectrum was recorded. Atazanavir showed a peak at 329 nm for solutions below the

amorphous solubility with a second peak emerging at 369 nm when nanodroplets were formed (Figure S1). The change in ratio of the peak intensities at 328 nm and 369 nm was used to evaluate formation of nanodroplets above LLPS onset concentration and depletion of nanodroplets during the absorption measurement.

3.4.5   Mass transport experiments

The mass transport of atazanavir from solutions of different concentrations was studied in the absorptive dissolution testing apparatus described previously with minor modifications.[126] The solutions in the donor and receiver channels were pumped through a cellulosic hollow fiber membrane (surface area 100 cm2, pore size 15 nm) using a peristaltic pump in parallel, co-current flow. The flow rates in both channels were maintained at 4 mL/min. The receiver concentration was measured using a flow-through UV probe (SI Photonics, Tuscon, AZ). The mass transport experiments were carried out for concentrations above the crystalline solubility. Hence, supersaturated solutions were generated for concentrations below and above the amorphous solubility and subsequent mass transport was evaluated to determine the effect of LLPS on receiver concentration-time profiles. The supersaturated solutions were generated by the solvent-shift method, adding aliquots of methanolic stock solution of atazanavir (25 mg/mL) to aqueous media. The aqueous buffer solution contained pre-dissolved 1 mg/mL HPMCAS. The donor volume was 50 mL and experiments were carried out at 37 °C. All experimental runs were followed by a 50% methanol solution wash for 30 min to remove residual drug in the apparatus. The mass balance was carried out for the apparatus and approximately 5-10% atazanavir was recovered from the solvent wash.

3.4.6   Dissolution and simultaneous dissolution-mass transport experiments

The dissolution of ASDs was first studied in a closed compartment setup. Dissolution was carried out in 50 mM phosphate buffer, pH 6.8. The dissolution volume was 50 mL for all the studies and solution was continuously stirred at 300 rpm at 37 °C. The powdered ASDs were suspended in the aqueous medium and dissolution was studied for 120 min. The concentration was measured by a UV spectrophotometer coupled to a dip probe.

For simultaneous dissolution and absorption studies, ASDs were suspended in the donor container, and absorption measurements were initiated by turning on the fluid flow. Polyethylene cannula filters, 10 μm or 70 μm pore size (Agilent Technologies, Inc., Memphis, TN), were inserted at the entrance of the donor channel tubing to prevent undissolved ASD particles from entering the hollow fiber membrane. The dissolution-absorption behavior was studied for 2 h at 37 °C. The donor volume was 50 mL and the final concentration that would be theoretically generated upon complete (100%) dissolution of ASDs was 200 μg/mL. The concentration in the donor container was measured by a UV spectrophotometer, using a dip probe. The receiver concentration was measured using a flow-through UV cell. The formation and longevity of the drug-rich phase was evaluated using fluorescence spectroscopy, DLS and NTA after filtering the sample through 0.45 μm or 1 μm glass fiber filters. The presence or absence of crystallinity was determined using a polarized light microscope (Version 2.3; Nikon Company, Tokyo, Japan).

3.5   Results

3.5.1   Solubility Measurements

The crystalline solubility of atazanavir in pH 6.8 phosphate buffer at 37 °C was 5 (± 0.5) μg/mL. The amorphous solubility, and in turn the LLPS onset concentration, by the UV extinction method was found to be 78 (± 5) μg/mL. The pKa of atazanavir is 4.42, hence, the solubility values are for unionized species.

3.5.2   Formation of drug-rich nanodroplets

A variety of ATZ concentrations, ranging from above the crystal solubility to above the amorphous solubility, were generated. For concentrations below the amorphous solubility, the solution was a clear, single phase solution. Concentrations above the amorphous solubility led to LLPS and formation of drug-rich nanodroplets and solutions were visibly turbid. The generation of nanodroplets was confirmed using fluorescence spectroscopy. Figure 3.1 shows the peak intensity ratio of the two emission peaks at 329 and 369 nm as a function of concentration. The intensity of the peak at 369 nm, which is characteristic of atazanavir in a drug-rich environment[136], increased with concentration resulting in a higher peak intensity ratio.
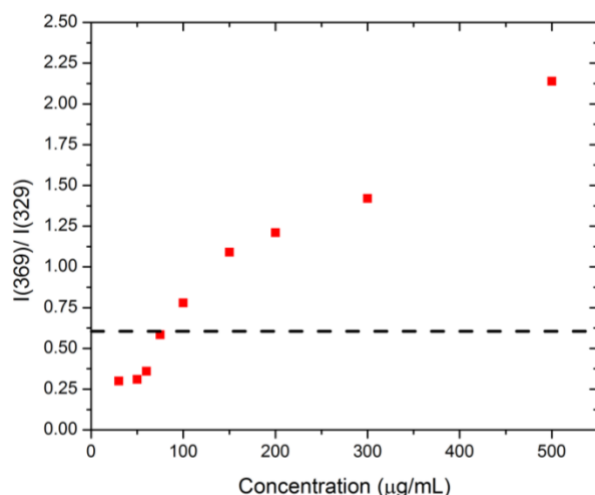
Figure 3.1. The peak intensity ratio of atazanavir emission peaks at 369 and 329 nm as a function of concentration. The horizontal line shows the intensity ratio above which the amorphous solubility is exceeded.

The drug-rich nanodroplets were further analyzed for size using DLS for different concentrations above the amorphous solubility, with results shown in Table 3.1. The PDI is the polydispersity index and indicates the width of particle size distribution. Typically, the lower the PDI, the more monodisperse the system. Above a PDI= 0.7, the sample has a broad particle size distribution.

Table 3.1: Particle size of ATZ at initial donor concentrations above LLPS. The values in the parentheses are standard deviations, n=3.

Conc. (µg/ml)	Average d (nm)	PDI	Derived count rate (kcps)
100	210 (10)	0.15 (0.02)	28633
150	204 (13)	0.13 (0.03)	40219
200	216 (7)	0.12 (0.02)	77464
300	211 (4)	0.12 (0.01)	275831
500	226 (9)	0.08 (0.02)	342132

As observed in Table 3.1, the average size of the nanodroplets did not change with an increase in the initial ATZ concentration, and the nanodroplets were monodisperse for all concentrations, as indicated by the PDI. Since an increase in the donor concentration above the

amorphous solubility generated a similar particle size distribution but higher intensity in fluorescence emission, it was intuitive that the number of droplets increased with concentration. This was confirmed by measuring particle concentration using NTA. Figure 3.2A shows an increase in particle formation with an increase concentration above the amorphous solubility. The scattering images shown in Figure 3.2B-D visually confirm the increased particle density at higher drug concentrations. The particle concentration for concentrations higher than 150 µg/mL was not measured as the particle concentration was too high for individual particles to be tracked.
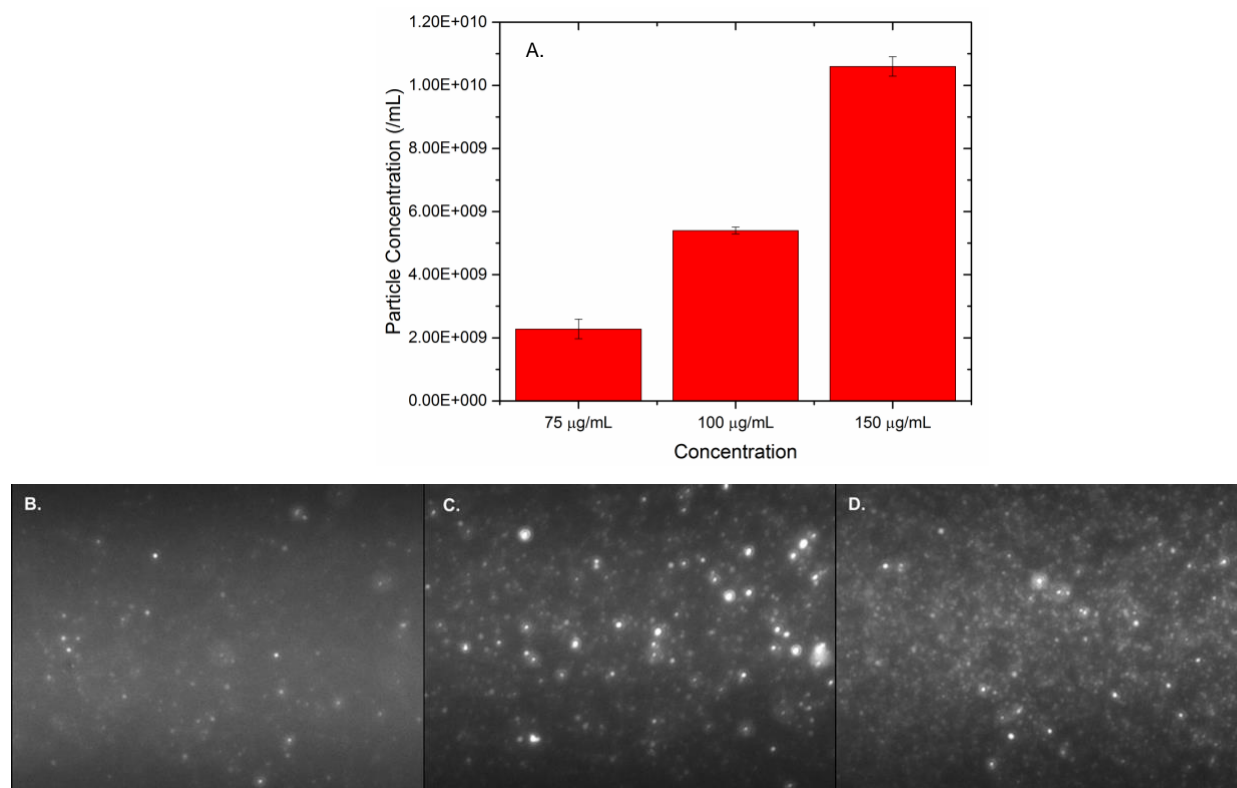
Figure 3.2. A. Particle formation for different ATZ concentrations at and above the amorphous solubility. Images B, C, and D are captured during NTA measurements for 75, 100 and 150 µg/mL ATZ suspensions, respectively, in fluorescence mode.

3.5.3 Mass transport of supersaturated solutions

Figure 3.3 shows the absorption profile for mass transport measurements carried out for a range of ATZ concentrations below and above the amorphous solubility. The mass transport studies were conducted for 100 min to obtain sufficient information about mass transfer across the membrane. The concentration profile represents the non-cumulative concentration in the receiver

channel. The initial increase in concentration represents the time taken to attain steady state in the hollow fiber membrane module (<10 min). With continued mass transfer across the membrane, a maximum concentration (C_{max}) is achieved, after which time the receiver concentration depletes (Figure 3.3) owing to the decrease in the donor concentration. The area under the curve (AUC) at a particular flow rate (4 mL/min) indicates the total amount of drug transferred over time. The increase in AUC with an increase in the donor concentration indicates a subsequent increase in the mass transfer.
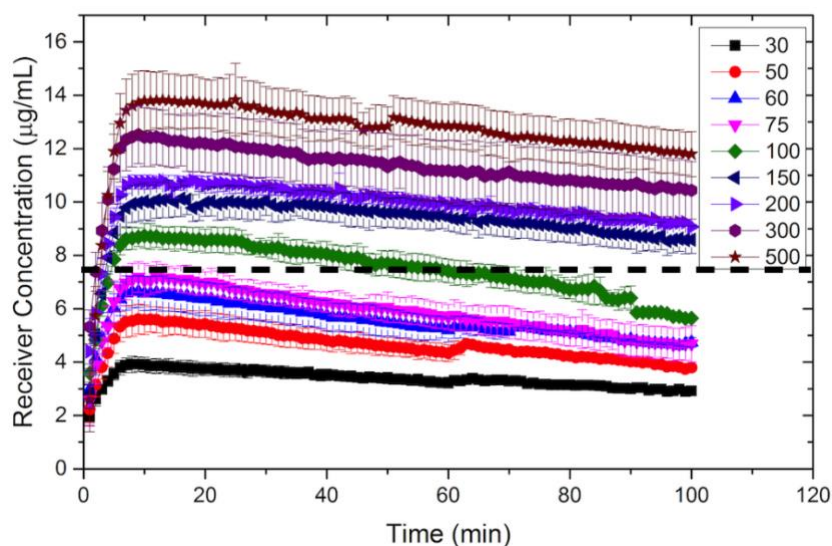
Figure 3.3. The receiver concentration profile of ATZ for a range of initial donor concentrations. The legend shows the initial ATZ concentration in μg/mL. The horizontal line indicates the C_{max} observed in the receiver concentration for a donor concentration initially equivalent to the amorphous solubility.

Higher C_{max} and AUC values were observed, as expected, as the ATZ concentration increased. For concentrations below the LLPS concentration, both C_{max} and AUC increased with an increase in the initial concentration, due to a higher driving force for mass transfer.[126] Above the amorphous solubility (LLPS onset concentration), the drug-rich phase appears and is in metastable equilibrium with the aqueous phase and the thermodynamic activity of the solute is constant, meaning that the concentration of the molecularly dissolved drug in the aqueous solution is equal to the amorphous solubility.[5] If measured in a side-by-side diffusion cell with a similar membrane type, the rate of mass transfer would typically reach a single maximum for concentrations above the amorphous solubility. However, a plateau in the concentration was not observed in the flow-through apparatus. Instead, the receiver concentration continued to increase

with increasing donor concentration, with a notable change in slope of the C_{max} (or AUC) vs donor concentration above the amorphous solubility (Figure 3.4). This shows that there is a difference in the mass transfer coefficient in the presence of drug-rich nanodroplets.
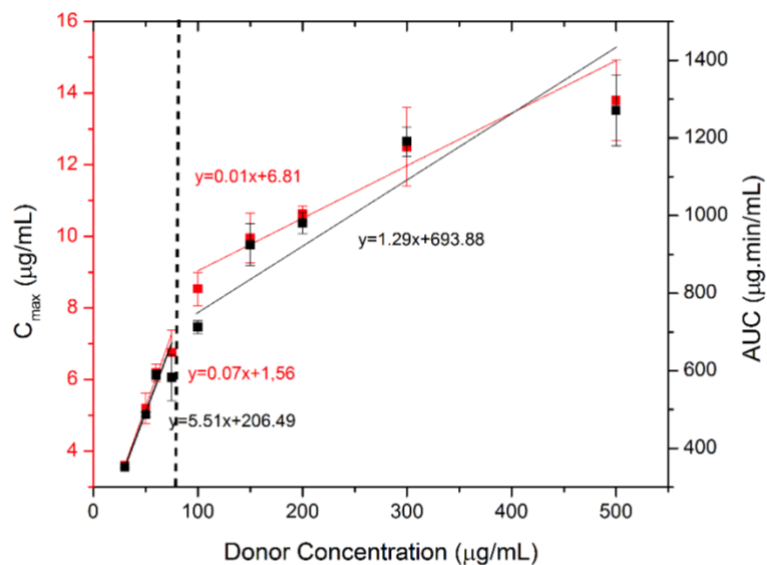
Figure 3.4. The C_{max} and AUC values plotted with respect to the initial donor concentration. The vertical line corresponds to the amorphous solubility.

3.5.4 Dissolution and absorption behavior of ASDs

From Figure 3.3, it is obvious that the amount of drug transferred was higher for concentrations that exceeded the amorphous solubility. Hence, it was of interest to understand the dissolution and absorption performance of different ASDs with dose concentrations above the amorphous solubility, focusing on the ability of ASDs with varying drug loadings and formulated with different polymers to generate drug-rich nanodroplets and enhance mass transfer. For comparison purposes, supersaturated solutions above the amorphous solubility were generated in the presence of 1 mg/mL of pre-dissolved polymer, HPMCAS, HPMC or PVPVA, by the solvent shift method. The properties of the drug-rich nanodroplets thus generated are reported in Table 3.2. The fluorescence ratio was similar for all the solutions, indicating a similar mass of nanodroplets generated for each system, however the particle size of the nanodroplets varied with the polymer. The presence of HPMCAS and PVPVA yielded particles of size 200-250 nm, while with HPMC, slightly larger particles of size 350 nm were generated. For the PVPVA-containing solutions,

agglomeration of nanodroplets was observed, where the size and the PDI increased and the derived count rate decreased with time (Figure S3.3).

Dissolution profiles of different ASDs, shown by powder diffraction to be X-ray amorphous (Figure S3.2), were measured under closed-compartment non-sink conditions, Figure 3.5. The final dose concentration was 200 µg/mL if all of the drug was released, though it should be noted that the apparent concentration measured by UV spectroscopy is not quantitative above the amorphous solubility (>78 µg/mL) as nanodroplets present in the solution can absorb and scatter light.[137] In the case of HPMCAS-based ASDs, 90:10 ASDs dissolved rapidly resulting in the formation of drug-rich nanodroplets and the maximum apparent concentration achieved was close to the dose concentration, exceeding the amorphous solubility. Nanodroplet formation was confirmed by fluorescence spectroscopy and particle size analysis, the latter which showed scattering species with an average size of ~ 300 nm (Table 2). An increase in drug loading (30 and 50% drug loading) resulted in slower dissolution rate with no drug-rich nanodroplets observed, consistent with the observation that the maximum concentration did not exceed the amorphous solubility. The decrease in the dissolution rate and maximum solution concentration achieved with the increase in drug loading has been observed previously and, in some instances, is thought to occur due to formation of a drug-rich layer at the ASD surface which then controls the dissolution. [84,86,131,132,138] For HPMC-based ASDs, dissolution rates for 10% and 30% drug loadings were similar to the corresponding HPMCAS-based ASDs. Dissolution of PVPVA-based ASDs showed similar dissolution trends to HPMCAS-based ASDs for 30% and 50% drug loading, wherein they did not undergo LLPS and showed a moderate and slow dissolution rate, respectively. Interestingly, the solution concentration observed for the 30 and 10% drug loading ASDs was higher than the expected amorphous solubility. Hence the impact of PVPVA on amorphous solubility of atazanavir was evaluated. In the presence of pre-dissolved PVPVA (1.8 mg/mL), the amorphous solubility increased to 94 (± 4) µg/mL, explaining the plateauing of concentrations at or above ~ 90 µg/mL. In the case of 10% drug loading ASDs, although ASDs dissolved immediately to a solution concentration slightly above the amorphous solubility, no nanospecies could be detected; the fluorescence spectra did not show the peak at 369 nm (characteristic for solutions containing nanodroplets) and no scattering species were observed in DLS measurements, as shown in Table 3.2. However, an unfiltered solution showed a peak intensity ratio of 0.89, indicating the presence

of a drug-rich hydrophobic environment. Most likely, the nanodroplets formed in the boundary layer underwent rapid agglomeration and could therefore not be readily detected.
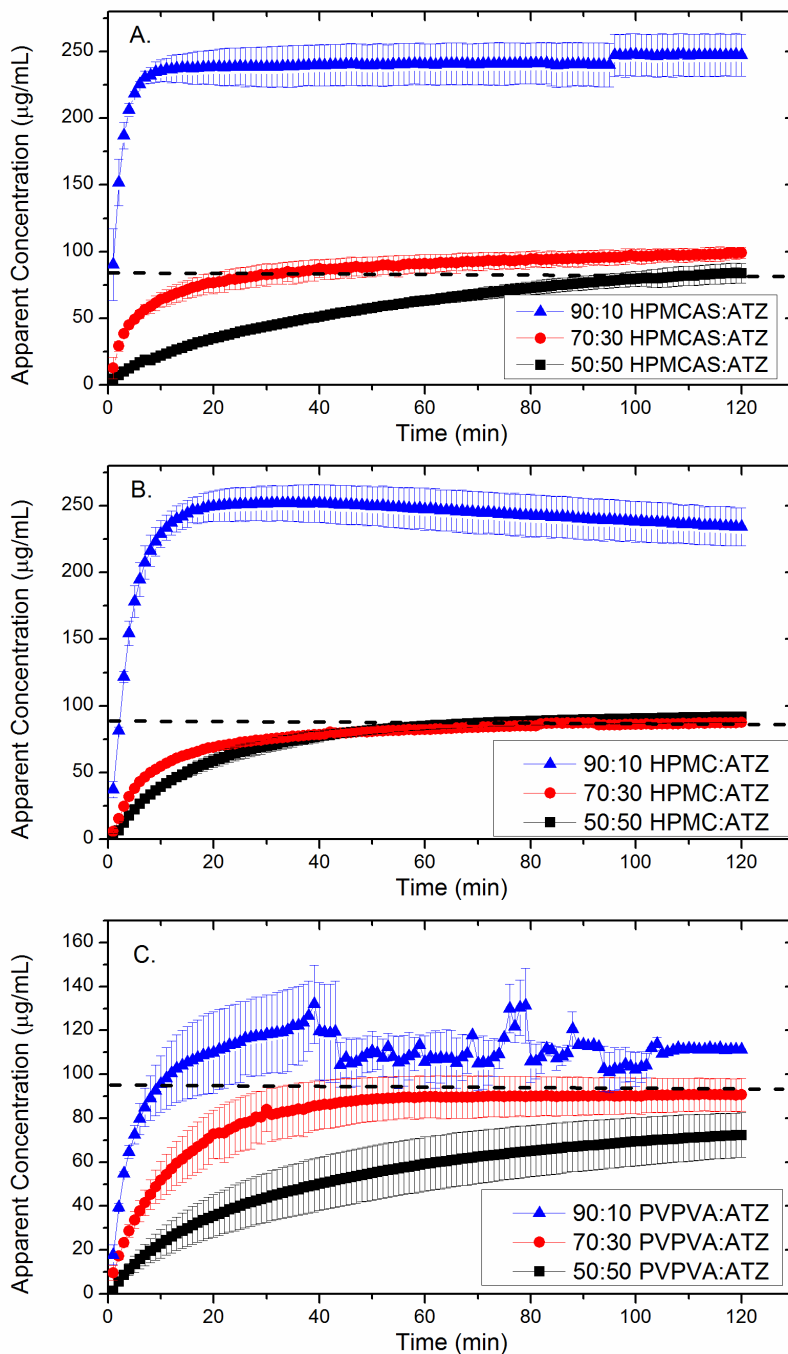
Figure 3.5. Dissolution profiles of different ASDs under closed compartment non-sink dissolution conditions. The horizontal line shows the solution concentration equivalent to the amorphous solubility.

Next, the dissolution behavior of ASDs during simultaneous absorption measurements was evaluated (Figure 3.6). Figure 3.6A and 3.6B show donor and receiver concentrations, respectively, of HPMCAS-based ASDs during simultaneous dissolution-absorption measurements. In general, the dissolution of ASDs followed a similar trend as observed in non-sink dissolution studies. However, in contrast to the plateau in solution concentration observed during closed-compartment dissolution, the donor concentration profile in dissolution-absorption measurements showed a decline in apparent concentration due to simultaneous absorption across the membrane which reduced the number of nanodroplets present in the donor compartment.

The high apparent donor concentration was reflected in the receiver concentration profile, wherein a higher C_{max} was observed which correlated well with the values found in the solvent-shift experiments (at a comparable concentration) shown in Figure 3.3. Although, the apparent donor concentration showed a gradual decline in concentration, the receiver concentration was maintained at a high concentration, above the C_{max} generated for a solution at a concentration equivalent to amorphous solubility (indicated by horizontal line in Figure 3.6), for the duration of the experiment, 120 min. This, in part, can be attributed to the nanodroplets replenishing the drug lost due to absorption, thereby maintaining the solution concentration at the amorphous solubility. In the case of dissolution-absorption of the 30% drug loading system, a relatively slower dissolution rate of the ASD was observed, with a maximum concentration slightly lower than the amorphous solubility and consequently no LLPS. Due to simultaneous dissolution and absorption, the concentrations achieved over time on the donor side were lower than those observed in Figure 3.5A. The donor concentration was relatively constant beyond 30 min, indicating replenishment of drug to the solution by dissolution of residual ASD. The receiver concentration correspondingly showed a C_{max} lower than the amorphous solubility and concentrations plateaued after 30 min reflecting the constant donor concentration. For the 50% drug loading, the drug release was much slower, similar to that found in closed compartment dissolution studies. The donor concentration achieved the amorphous solubility, however only after 100 min. The gradual increase in concentration in the donor container resulted in gradual increase in concentration in the receiver channel. Similar profiles were observed for the HPMC dispersions.

For PVPVA-based ASD, the 10% drug loading again did not result in the discernable formation of drug-rich nanospecies. The donor concentration reached a plateau slightly above amorphous solubility as observed in the closed-compartment dissolution, potentially due to the presence of some agglomerates, combined with some solubilization by the polymer. Interestingly, the receiver concentration profile showed a somewhat lower C_{max} value than that observed for cellulose-based ASDs with 10% drug loading, however, it was slightly above the concentration that was observed for a solution at the amorphous solubility. Most likely, any colloidal species that formed in the donor compartment rapidly agglomerated to form micron-sized species and therefore did not pass through the filter used prior to taking fluorescence or DLS measurements. The receiver concentration remained constant over the duration of the experiment, depicting the reservoir effect of the agglomerates. The 30% drug loading showed a similar dissolution profile to the 10% drug loading, attaining the maximum concentration in 20 min. However, the maximum concentration was close to the experimentally determined amorphous solubility and hence slightly lower than that observed for 10% drug loading. Lower donor concentrations were reflected in the receiver concentration profiles. The 50% drug loading ASD, showed a gradual release of drug over time, whereby the concentration started to drop after 80 min the donor container and hence, in the receiver channel (indicated by red arrow). Further investigation revealed that the donor solution underwent crystallization at this time point, as confirmed by polarized light microscopic analysis of the dissolution medium. Crystallization lowered the donor solution concentration with a concurrent decrease in the receiver concentration.

Figure 3.6G compares the amount of drug transferred over 120 min for each formulation, calculated by multiplying the area under the curve by the flow rate of the receiver fluid. HPMCAS and HPMC-based 10% drug loading systems clearly showed higher amounts of drug transferred as compared to other formulations. 50:50 PVPVA:ATZ showed the least amount of drug transferred, as the formulation underwent crystallization. The integration approach not only enables quantitation of the mass transfer observed for different formulations, but also highlights the impact of formulation dissolution rate, nanodroplet formation and crystallization on absorption behavior, information that is less readily discernable from the dissolution profiles.
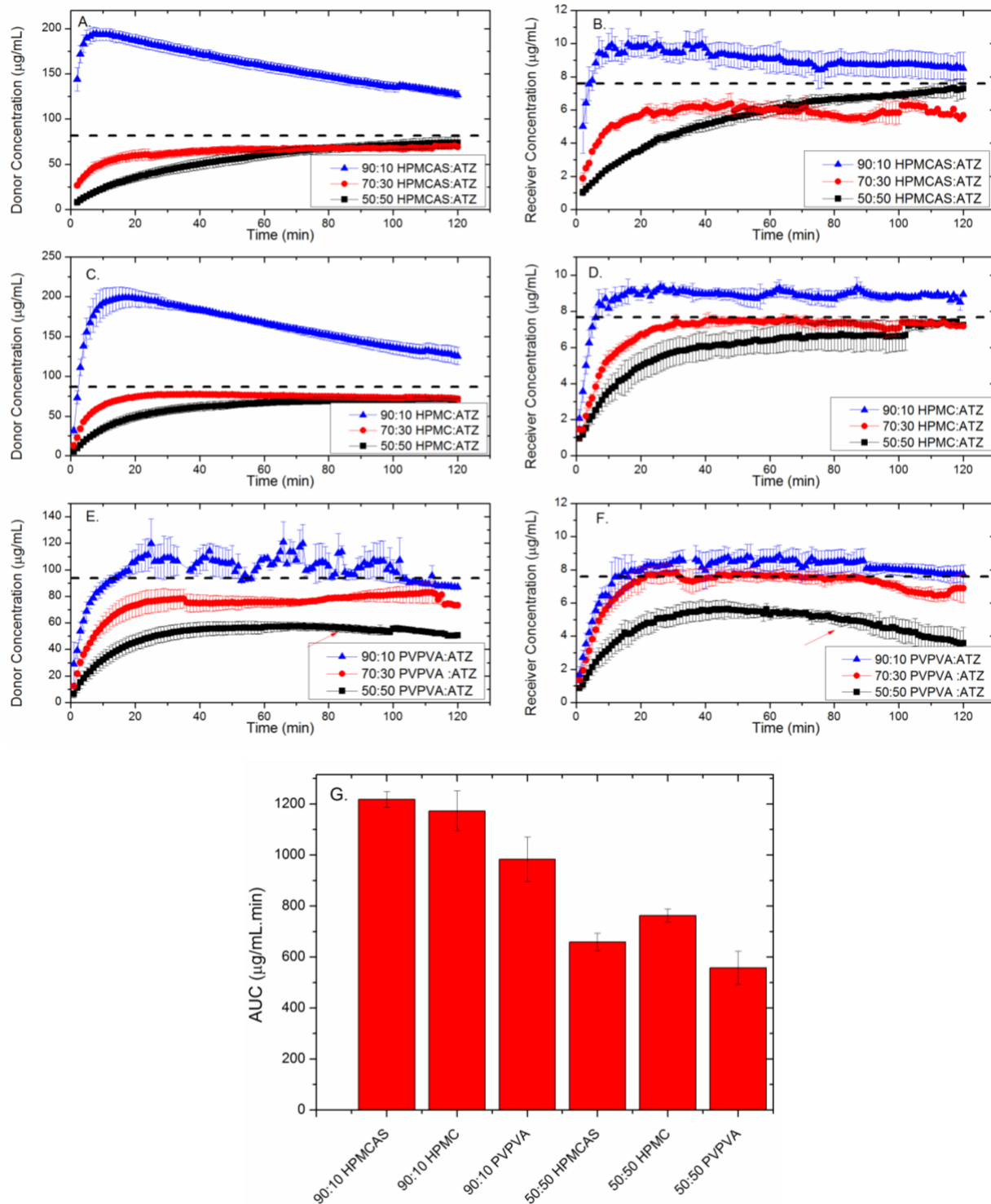
Figure 3.6: (A-F) Donor and receiver concentration profiles during the simultaneous dissolution and absorption of ATZ ASDs with varying drug loadings and different polymers. The horizontal line shows the concentration equivalent to the amorphous solubility in the donor compartment. The arrows denote the point at which crystallization was observed in 50:50 PVPVA:ATZ. (G) Amount of drug transferred across the membrane in 120 min for different formulations.

Table 3.2: Comparison of drug-rich nanodroplet properties generated by the solvent-shift method and during non-sink and sink ASD dissolution.

Formulation		I(369)/ I(329)*		$d_{average}$ (nm)		PDI	
		Diss	Diss-Abs	Diss	Diss-Abs	Diss	Diss-Abs
HPMCAS	Solvent-shift	1.21		221(12)		0.1(0.01)	
	90:10 ASD	1.17	1.19	294(26)	307(28)	0.20(0.06)	0.26(0.05)
HPMC	Solvent-shift	1.24		311(23)		0.07(0)	
	90:10 ASD	1.30	1.29	326(34)	317(42)	0.027(0.01)	0.06(0.01)
PVPVA	Solvent-shift	1.25		254(10)		0.1(0.03)	
	90:10 ASD	0.26**	0.27**	-	-	-	-

* I(369)/I(329) at amorphous solubility (~ 75 µg/mL) is 0.58. All polymers (1 mg/mL) pre-dissolved for solvent-shift experiments.

** The values correspond to filtered solution. Unfiltered solution showed values ~ 0.89.

The mass transport behaviors of the colloidal supersaturated solutions generated by the solvent-shift method and by dissolution of an ASD were compared to understand the impact of different supersaturation routes on the absorption profiles. As seen from Figure 3.7A, the receiver concentration profile was similar for both the routes. Fluorescence spectroscopy was employed to monitor depletion of nanodroplets during absorption measurements. The continuous change in fluorescence intensity ratio indicated a decrease in the amount of drug in a drug-rich environment, consistent with the gradual depletion of nanodroplets as free drug transports across the membrane and the nanodroplets dissolve to maintain the concentration at the amorphous solubility. The rate of nanodroplet depletion was similar, irrespective of the route of supersaturation.
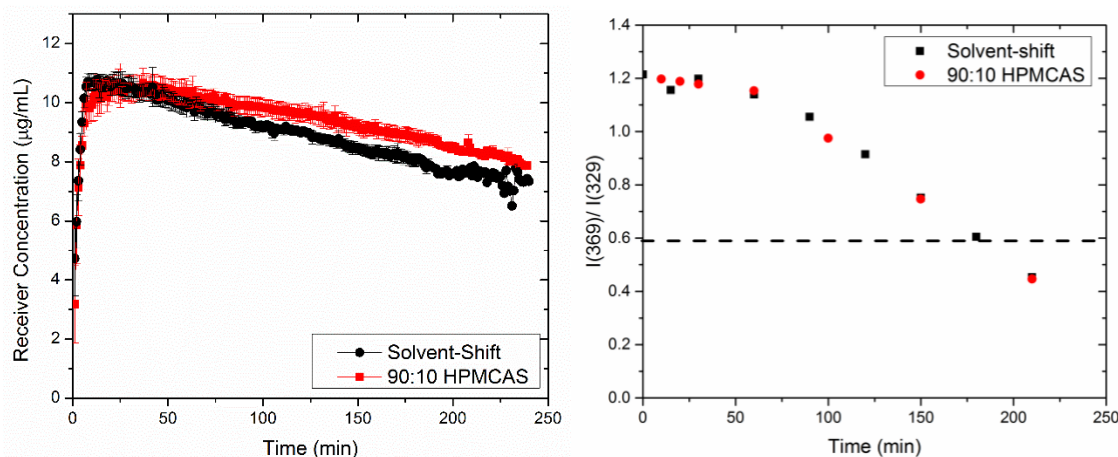
Figure 3.7: (a) Receiver concentration profiles of supersaturated solutions produced by dissolution of 90:10 HPMCAS:ATZ and generated by the solvent-shift method. (b) Fluorescence intensity ratio at 329 nm and 369 nm is plotted over duration of the mass transport measurements.

To explore the impact of ATZ nanodroplet number generated from ASD dissolution on mass transfer and correlate with observations in Figure 3.3, dissolution-absorption measurements for 90:10 HPMCAS:ATZ ASDs with different dose concentrations above the amorphous solubility were undertaken (Figure 3.8). Although the concentration of molecularly dissolved drug is the same for all three dose concentrations, C_{max} increased with increase in the dose concentration, similar to the supersaturated solutions generated by solvent shift method (Figure 3.3). The concentration versus time in the receiver compartment showed a much steeper decline with time for the 100 μg/mL dose, relative to the 200 and 500 μg/mL dose levels. The more sustained transport for the higher dose concentrations can be attributed to a greater number of drug-rich nanodroplets in these systems, maintaining the free drug solution concentration at the amorphous solubility for extended periods of time.
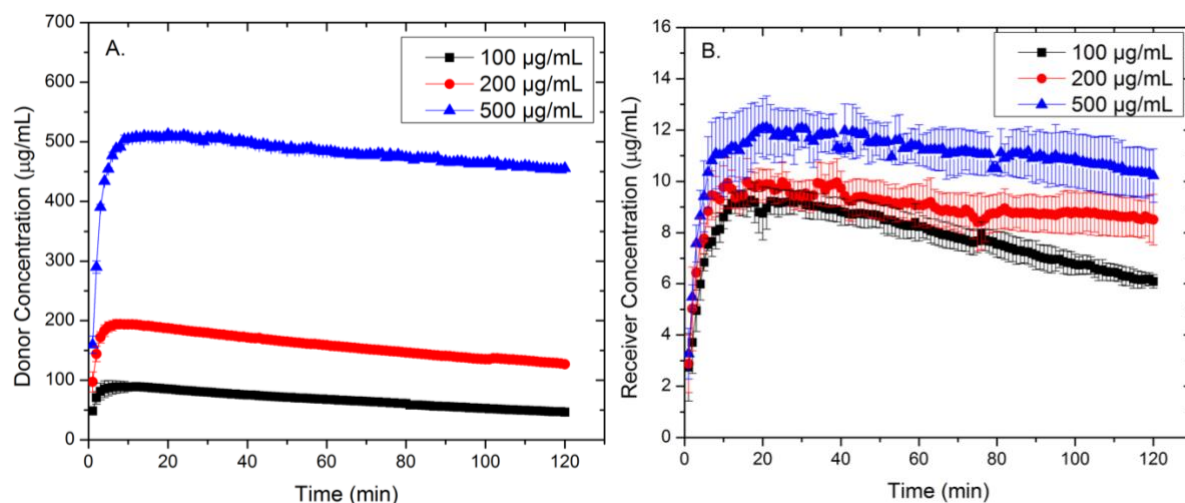
Figure 3.8: Donor and receiver concentrations for 90:10 HPMCAS:ATZ with different dose concentrations.

3.6 Discussion

It is widely recognized that the amount of drug that is available for permeation across a membrane following dissolution from enabling formulations, in particular into complex media, is not well described by the drug concentration due to variations in drug speciation. Speciation describes the many different environments in which the drug can be present after dissolution, and depends on the formulation and media composition. Species include free unionized drug, ionized drug, drug in micellar structures, drug complexes, and other colloidal drug species.[5] For passive diffusion, only free, un-ionized drug permeates through the membrane. To address these issues, dissolution measurements are increasingly being combined with absorption measurements to better evaluate the interplay between dissolution rate, solution concentration time profiles and amount transferred across a membrane. Given the lack of robustness of cell-based membranes to excipients and media components, there is burgeoning interest in developing cell free systems to assess both drug permeation and to conduct simultaneous dissolution absorption measurements.[139] A major limitation of currently available systems is the small permeation area relative to the donor volume. This is a particular issue for dissolution absorption measurements of poorly water soluble compounds whereby, under non-sink conditions, dissolution rate of the dosage form is coupled to mass transport rate. For complex systems, many other processes are also linked to the membrane mass transport rate, including crystallization kinetics for supersaturated solutions, redissolution of precipitated material, drug diffusion out of micelles, and dissociation of complexes. Therefore, it

99

is important for the mass transport rate across the membrane to be sufficiently high to deplete the donor concentration by an appreciable amount, enabling the impact of these coupled processes to be better evaluated. The absorptive dissolution testing approach described herein clearly enables such features to be assessed for amorphous solid dispersion formulations over biorelevant timeframes, with a high extent of sensitivity, enabling real-time insights into the donor compartment solution phase behavior of supersaturated systems and implications for absorption.

3.6.1 Absorption behavior in the presence of drug-rich nanodroplets in the solution

The highly supersaturated solutions of ATZ generated in the aqueous buffer showed interesting absorption behavior in the new absorptive testing apparatus. The flow-through measurements give a non-cumulative concentration profile for drug diffused through the membrane module in a single pass, thereby increasing sensitivity to capture solution dynamics in the donor container. Consequently, the absorption profiles obtained for different concentrations above the amorphous solubility, where drug-rich nanoparticles were present, were unique to this experimental setup. The presence of increasing amounts of nanospecies clearly improves the overall mass transport of the drug (Figure 3.3). Given that the pore size of the membrane was c.a. 15 nm and the mean particle size of the drug-rich phase was c.a. 200 nm, the drug-rich nanodroplets are not diffusing across the membrane. Interestingly, the slope of C_{max} and AUC vs. donor concentration (Figure 3.4) changed above the amorphous solubility. A change in the proportionality between C_{max} or AUC vs. donor concentration above or below the LLPS onset concentration for same set of mass transport conditions indicates a change in the mass transfer coefficient. Since the free drug solution concentration and the thermodynamic driving force for mass transfer is constant above the amorphous solubility, logically, the observed behavior results from the increase in the number of amorphous droplets (Figure 3.2), with an increase in the initial donor concentration above the LLPS concentration. Given that the colloidal species are more than two orders of magnitude larger than molecularly dissolved drugs, increases in overall diffusivity based on an additional population of species (i.e. the nanospecies) are expected to be negligible. For the flow rates used in the apparatus, the flow in the hollow fiber membrane is laminar. Theoretically, laminar flow in tubular geometry results in a parabolic velocity profile with maximum flow at the center and zero at the wall with a corresponding bell-shaped concentration profile.[127,129,140] Possibly, the mass transfer of the colloidal solutions could be enhanced in the

presence of nanoparticles in the aqueous boundary layer of the laminar flow due to nanoscale convection induced by Brownian motion,[141,142] effectively changing the concentration gradient in the boundary layer. Alternatively, there could be some extent of dissolution rate limited absorption in this experimental set-up whereby more nanodroplets mitigate this to some extent by providing a higher surface area. In order to gain further understanding of the influence of nanodroplets on mass transfer rates, a systematic study of the impact of colloidal species on flow properties and the concentration gradient in the boundary layer of laminar flow is required. It is also anticipated that insight into nanodroplet dissolution may shed light upon the underlying mechanism for the mass transfer enhancement above amorphous solubility in the apparatus. Nanodroplet dissolution is expected to be extremely rapid, given the high surface area to volume ratio of these species. Moreover, the solubility of a solid particle is dependent on the size of the particle, volume of the molecule, surface energy of the solid and it increases exponentially as the radius of particle decreases, significantly at nanometer scale.[143] Although the nanodroplets generated in this study are c.a. 200 nm, during their dissolution shrinkage is anticipated,[144,145] which may lead to higher free drug concentrations when the size approaches a few nanometers. Since the residence time of a single pass of the donor solution in a single hollow fiber is approximately 10 s, it is plausible that the apparatus is capturing this phenomenon of enhanced solubility due to size reduction upon dissolution. Importantly, it is apparent from Figure 3 that the presence of colloidal drug species greatly enhances the amount of drug transferred across the membrane in a given time frame. Considering similarities between the apparatus and *in vivo* conditions with respect to the tubular geometry and large surface area available for absorption, if this occurs *in vivo*, (a recent study supports that the presence of colloidal species is beneficial for absorption)[146] then it is clearly important to be able to assess the impact of these colloidal species *in vitro* in order to select the best formulation in terms of optimizing the formation of colloidal species formed.

3.6.2 ASD formulation, solution phase behavior and impact on absorption

ASDs are a widely used formulation strategy to improve bioavailability of poorly soluble drugs. Dissolution of ASDs typically involves several physical processes including supersaturation, liquid-liquid phase separation and crystallization, all of which impact the bioavailability advantage of the formulation.[5] The supersaturation generated by dissolution of a given ASD is highly dependent on, among other factors, the drug loading and polymer type.[58,84,138] Herein, we observe

very different release for ASDs when these factors were varied, with a more complete picture of differences provided by comparing the absorption profiles of the various systems.

Figure3.6 clearly shows the absorption advantage of the low drug-loading ASD formulations versus higher drug-loading dispersions. The lower drug loading ASDs dissolved rapidly, exceeding the amorphous solubility, and undergoing LLPS to form nanodroplets. The presence of nanodroplets resulted in higher amounts transferred to the receiver compartment (Figure 3.6G). Although the ASDs dissolved to yield aggregates with a larger size than the nanodroplets created by the solvent shift method, these variations did not result in significant differences in the absorption behavior of supersaturated solutions generated by the two routes (Figure 3.7). Furthermore, the low drug-loading PVPVA dispersions formed agglomerates following dissolution, but still resulted in a nearly the same amount of drug transported into the receiver compartment as for the low drug loading cellulose-based dispersions, even though this would not necessarily be predicted from the dissolution profiles. Thus, these agglomerated species yielded somewhat improved absorption profiles, at least over a 2 hours absorption window, although their performance diminished over a longer absorption window (Figure S3.5).

The sensitivity of the apparatus to solution speciation allowed us to further explore the phenomena of LLPS following ASD dissolution and the impact of the number of nanospecies on mass transfer, in a manner typically not realized in simple low surface area two-compartment mass transport measurements. The C_{max} and AUC increased for 90:10 HPMCAS:ATZ ASDs with an increase in dose concentration (Figure 3.6). The C_{max} can potentially be dependent on the number of nanodroplets flowing through the membrane module for dose concentrations above the amorphous solubility, which in turn will be dependent on the dose and extent of dissolution of the ASD. Thus, formulations undergoing LLPS may enhance absorption behavior not only by providing a reservoir and replenishing drug lost due to absorption, but also by contributing to enhancements in the mass transfer coefficients. The *in vivo* relevance of this observation, however, needs further investigation.

3.6.3 Influence of absorptive compartment on dissolution rate of ASDs

This study highlights the impact of an absorptive compartment in dissolution testing of supersaturating formulations. The absorption measurements resulted in different donor concentration profiles as compared to the closed-compartment dissolution testing due to the presence of an absorptive sink in the former experiments. As drug is continually removed by absorption across the membrane *in vivo*, the gradually declining drug concentration in the donor chamber during the dissolution-absorption measurement is potentially more *in vivo* relevant as compared to simple dissolution profiles. More quantitative information about the true driving force for mass transfer thus can be obtained from simultaneous dissolution and absorption measurements. The inclusion of the absorption compartment clearly influenced the ASD dissolution rate, in particular for the slow releasing formulations, as illustrated in Figure 3.9. All formulations with 50% drug loading showed higher amounts of drug released when simultaneous dissolution-absorption measurements were carried out. The lowering of concentration in the donor compartment due to removal of drug during absorption promoted greater ASD dissolution relative to the closed compartment system, better reflecting the environment expected *in vivo*. Moreover, when the amount of drug released from these ASDs is compared for the various polymers, the closed-compartment dissolution showed better performance for HPMC ASDs followed by HPMCAS and PVPVA based ASDs, whereas simultaneous measurement showed that all the three formulations had similar drug release rate for over the first 60 min (Figure S3.4).
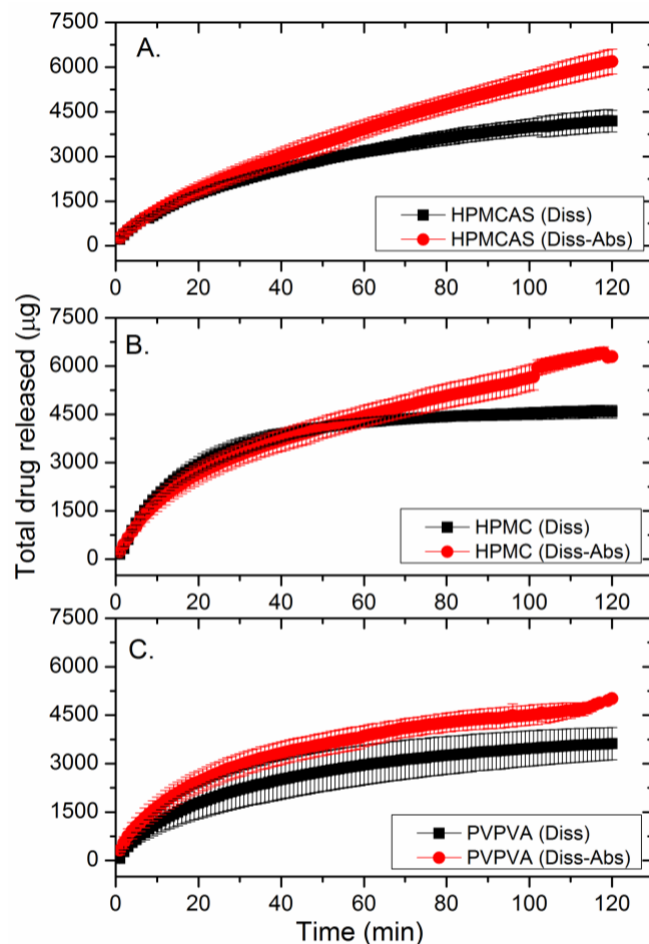
Figure 3.9: Comparison between dissolution and dissolution-absorption profile for 50% drug loading ASDs. In the presence of an absorptive compartment, the total amount of drug dissolved was calculated from the amount of drug present in the donor compartment plus the amount of drug that has been transferred into the receiver compartment.

3.7   Conclusion

This study was focused on the application of an *in vitro* absorptive dissolution testing apparatus to study the absorption behavior of highly supersaturated solutions including those generated by ASD dissolution. Since such highly supersaturated solutions are at high risk of undergoing crystallization, it is crucial to study their membrane transport properties over biorelevant time frames with an appropriate mass transfer rate of the drug. The high rate of mass transfer offered by the hollow fiber absorptive dissolution testing system makes it a suitable tool to gain insight into the impact of formulation factors on membrane transport rates. Furthermore, it is possible to probe the coupling between formulation dissolution, solution phase behavior, and

the amount of drug transferred across the membrane. As expected, mass transfer for supersaturated atazanavir solutions was found to increase linearly with increasing supersaturation. Interestingly, for concentrations above the amorphous solubility where colloidal drug-rich aggregates were formed, further increases in mass transfer was observed. ASDs that dissolved to above the amorphous solubility, forming colloidal species, also showed enhanced mass transfer. Of note, absorption profiles did not always concur with inferences made about formulation performance based on sole consideration of dissolution profiles. In addition, dissolution of more slowly dissolving ASDs was promoted by the presence of an absorption compartment, enabling more realistic measurement of the dissolution process under non-sink conditions, by coupling it with the absorption process. In summary, we believe that the absorptive dissolution testing apparatus is an efficient tool that can improve understanding of the dissolution-absorption behavior of complex, enabling formulations such as amorphous solid dispersions, providing mechanistic understanding of the solution and membrane transport phenomena.

CHAPTER 4.   ABSORPTIVE DISSOLUTION TESTING: AN IMPROVED APPROACH TO STUDY THE IMPACT OF RESIDUAL CRYSTALLINITY ON THE PERFORMANCE OF AMORPHOUS FORMULATIONS

4.1   Abstract

Amorphous solid dispersions typically improve the oral bioavailability of poorly soluble drugs. However, residual crystallinity is always a concern, in terms of potential impact on the product stability and performance. Consequently, *in vitro* tools that allow biorelevant assessment of residual crystallinity are of interest. The goal of the current study was to employ absorptive dissolution testing to evaluate the impact of different levels of crystallinity in an amorphous formulation on membrane mass transport kinetics and supersaturation-time profiles. Partial crystallinity was induced in commercially available tacrolimus formulations by exposure to moderate temperature and high relative humidity. A hollow fiber membrane was coupled to a dissolution vessel to create an absorptive dissolution testing apparatus, and concentration-time profiles were simultaneously monitored during dissolution (donor compartment) and after absorption across the membrane (receiver compartment). The coupled dissolution-absorption measurements indicated that residual crystallinity impacted the absorption profiles in a manner that depended on the volume of fluid used for the dissolution measurement. A high percentage of residual crystallinity hampered the drug release from the formulation. Higher supersaturation in non-sink dissolution conditions improved mass transfer rates, however, the presence of seed crystals led to rapid desupersaturation. Further systematic studies to delineate the interplay between the rate of absorption and desupersaturation revealed that for a given dissolution rate, the crystallization rate would supersede the absorption rate only at high supersaturations. Thus, seeds have a lower impact on absorption when the overall supersaturation generated is lower. This study underscores the importance of considering competing physical processes when evaluating amorphous formulations. A further consideration highlighted is that different fluid volumes may impact the absorption profile for supersaturating dosage forms. Absorptive dissolution testing

appears to be a potentially valuable tool to mechanistically investigate amorphous solid dispersion formulation release and phase behavior under more biorelevant conditions.

4.2   Introduction

Intestinal drug absorption is a highly complex and dynamic process, strongly influenced by the physicochemical properties of the drug and physiological variables in the gastrointestinal (GI) tract.[147] Typical physiological parameters critical to passive drug absorption include GI fluid composition, pH, volume, hydrodynamics, emptying rates and forces, intestinal transit time and surface area of the intestinal membrane.[148] Amongst these, luminal fluid volume is one of the more important parameters as it affects the luminal drug concentration and total amount of drug that can be dissolved from the dosage form. Fluid volumes are influenced by several factors such as the amount of liquid ingested with the dosage form, gastric emptying rate, intestinal transit time and the uptake of fluid across the membrane. Hence, it varies significantly between subjects.[148,149] Recent magnetic resonance imaging (MRI) studies determining luminal fluid volumes have reported a range of volumes for the stomach and small intestine. Adult stomach volumes have been observed to range between 18 – 54 mL in the fasted state with an increase in fluid volume in the fed state.[148,150–152] In the small intestine, studies have reported a range from 30 – 420 mL, with an average of 100 mL in the fasted state and slightly higher volumes in the fed state.[148,153] Additionally, MRI studies have shown that the fluid content in the lumen is discontinuous, existing as multiple fluid pockets with a median pocket volume of 4-12 mL depending upon fed or fasted state.[153] The luminal drug concentration is a key parameter in dictating the rate of drug absorption, whereby the flux across a membrane varies as a function of free unionized drug concentration and permeability.[45] Consequently, intersubject variability in fluid volume can potentially result in a range of drug concentrations in the luminal environment, thereby impacting the rate of absorption across the intestinal membrane, and in turn, bioavailability.

Currently, dissolution testing is the primary analytical tool used to predict drug concentration-time profiles. Besides being used as a surrogate to predict *in vivo* performance, the dissolution test is also an important tool for process development, process validation, drug product development, product quality control and bioequivalence assessment.[154] Typically, compendial dissolution testing is performed in a large dissolution volume, usually 900 mL, to mimic the *in*

vivo sink environment. Such high fluid volumes are generally effective in determining batch-to-batch differences or discriminating between simple formulations of highly or moderately soluble drug compounds.[155] However, the number of poorly soluble drug candidates has increased and many of these require complex enabling formulation strategies to overcome solubility limitations and improve oral bioavailability.[6] Supersaturating drug delivery systems are being increasingly employed due to their ability to generate high intraluminal drug concentrations, appreciably higher than the equilibrium solubility.[116–118,146,156] However, supersaturated solutions are thermodynamically metastable and the drug can crystallize. The extent of supersaturation achieved in the lumen will depend on a variety of factors, including the amount of drug dosed, the volume of fluid present, the solubility of the compound in the local conditions, and the ability of the formulation to dissolve to concentrations higher than the equilibrium solubility. Thus, if a formulation has a tendency to generate supersaturation in a small volume, high luminal concentrations can be expected from the supersaturating drug delivery system *in vivo*. However, the sink conditions employed in compendial dissolution testing do not enable supersaturation and subsequent crystallization tendency to be assessed. Consequently, non-sink dissolution conditions, are gaining increased attention for better prediction of supersaturation and crystallization kinetics.[155]

For supersaturating drug delivery systems to contribute to bioavailability enhancement, the generated supersaturation has to be maintained for long enough so as to provide an absorption advantage.[5] Amorphous solid dispersions (ASDs), which are usually molecular level blends of drug and polymer, release the drug to achieve concentrations higher than the equilibrium solubility. The polymer typically serves as a solution crystallization inhibitor also, maintaining the supersaturation, ideally during the absorption window.[5,72,82,157] However, since the drug is in the amorphous form in the ASD, crystallization may occur over the shelf-life of the product, in particular if higher temperatures and relative humidity are encountered. At elevated humidity, the water absorbed from the surrounding atmospheric environment decreases the glass transition temperature (T_g) of the solid dispersion leading to crystallization due to increased molecular mobility of the compound.[16] Low levels of crystallinity also can result from the manufacturing process itself, either due to incomplete amorphization or partial crystallization caused by selected processing conditions such as unoptimized process temperature or slow solvent evaporation

rates.[17–19,68] The subsequent presence of crystals can lead to further crystallization during storage or upon dissolution. The impact of the residual crystallinity on the extent of supersaturation generated and the subsequent desupersaturation rate via secondary nucleation and crystal growth is expected to depend on seed origin, morphology, and interfacial properties.[158] The desupersaturation rate will also be impacted by any additives that alter crystallization kinetics. Desupersaturation resulting from residual crystallinity can have a negative impact on *in vivo* concentration-time profiles and in turn, bioavailability.[155,158,159] However, *in vivo* studies have shown a variable impact of residual crystallinity on absorption.[146,160,161] To better predict the influence of residual crystallinity on *in vivo* performance, more discriminatory *in vitro* assessments are needed.

Tacrolimus (TAC), an immunosuppressive agent used in organ transplants, is a poorly soluble drug commercially available as amorphous formulations. Currently, in addition to the brand formulation, Prograf®, there are several generic versions available as 0.5, 1 and 5 mg capsules. Tacrolimus has a narrow therapeutic index and has shown large intersubject variability in human pharmacokinetic studies.[17,162] Recently, studies were carried out to understand differences in brand and generic formulations with respect to non-sink dissolution profiles and susceptibility to crystallization under storage conditions.[17] One generic product showed a tendency to undergo crystallization during open dish storage at various conditions. This prompted further studies to determine the impact of crystallinity on the dissolution profiles.[159] The presence of crystalline drug impacted the level and duration of supersaturation achieved during dissolution.

Ideally, dissolution testing under non-sink conditions should be combined with an absorptive compartment to better predict the *in vivo* performance of supersaturating formulations. The absorptive sink can significantly impact the concentration-time profiles achieved during dissolution.[83,126] Recently, we have developed a high surface area, flow-through absorptive dissolution testing apparatus that allows simultaneous measurement of dissolution and membrane transport rate.[126] The apparatus employs a hollow fiber membrane to provide a large surface area allowing rapid mass transfer and thus, dissolution-absorption testing in biorelevant time frames. This flow-through apparatus with in-line measurement of drug concentration has proven to be a robust and sensitive tool to understand solution phase behavior. The goal of this study was to

utilize this system to evaluate the interplay between formulation residual crystallinity and dissolution volume on the relative extent and kinetics of absorption. We hypothesize that a lower dissolution volume will lead to a higher supersaturation, which in turn will enhance the absorption rates. However, it will also amplify the residual crystallinity-induced desupersaturation tendency of the system, potentially lowering the drug available for absorption. Simultaneous dissolution-absorption measurements were performed for Prograf® and generic tacrolimus (Accord) formulations. Due to the susceptibility of Accord formulations to crystallize under stressed storage conditions, partial (20, 50 and 100%) crystallinity was introduced by exposure to 40 °C/ 75% RH. Prograf does not crystallize under similar storage conditions.[17] The dissolution-absorption measurements were carried out for three volumes, 240, 100 and 40 mL. The two higher volumes were chosen as a typical volume of water taken by a patient (240 mL) and the stomach volume after 15 min following ingestion of 240 mL (100 mL).[152] These volumes are sink with respect to the amorphous solubility of tacrolimus. The lowest volume, 40 mL, represents a non-sink condition with respect to the amorphous solubility and approximates the fasted stomach volume.[152] Based on the absorption profiles obtained, a virtual bioequivalence assessment was performed to quantitatively correlate the performance of the brand formulation and the generic formulations with varying extents of residual crystallinity. Upon dissolution of formulations in the aqueous media, there are two competing processes controlling the drug concentration in the dissolution container for the system under consideration, namely absorption and crystal growth (due to the presence of residual crystal seeds). A model was developed to demonstrate the interplay between absorption and desupersaturation, elucidating the extent of the influence of these physical processes on formulation performance.

4.3   Materials

Tacrolimus monohydrate was procured from Molcan Corporation (Toronto, Canada). Prograf® (manufactured by Astellas Pharma Tech. Co., Ltd., Toyama, Japan) and a generic formulation (manufactured for Accord Healthcare Inc., Durham, NC by Intas Pharmaceuticals Ltd., Ahmedabad, India) containing 5 mg of tacrolimus were purchased from Purdue University Pharmacy (West Lafayette, IN). Hydroxypropyl cellulose (Klucel LF Pharm) (HPC) was purchased from Hercules Inc. (Wilmington, DE). Hydroxypropyl methylcellulose (PharmCoat 606) (HPMC) was obtained from Shin-Estu Chemicals (Niigata, Japan). HPLC grade acetonitrile and

methanol were supplied by Fisher Scientific (Chicago, IL). 5 mM Phosphate buffer, pH 4.5 with pre-dissolved 50 µg/mL HPC was used as a dissolution medium, prepared as mentioned in Trasi et al.[17]

4.4   Methods

4.4.1   Powder X-Ray Diffraction

Powder X-ray diffraction (PXRD) of crystalline tacrolimus monohydrate and contents of Prograf and Accord capsules was carried out using a Rigaku Smartlab diffractometer (Rigaku Americas, The Woodlands, TX) with a CuKα radiation source operating at 40 kV and 40 mA. Generic capsules were exposed to accelerated stability conditions (40 °C and 75% RH) for a period of 2-5 weeks in an open container. The contents of 5 capsules were mixed thoroughly before exposure to stress conditions to provide sufficient sample and improve content uniformity with respect to crystalline content. These samples were then periodically analyzed by PXRD to determine % crystallinity induced over time. Similar crystallization kinetics have been observed previously.[17,159] The % crystallinity was determined by generating a calibration curve for samples (fresh generic capsule contents) with a known amount of added crystalline tacrolimus monohydrate. A scan rate of 0.5 °/min with step size of 0.02° was used to scan between 9.5° – 11.5° 2θ. Crystallinity was calculated by taking the ratio of the area under the curve for the peaks between 10° - 10.5° and 9.5° - 10.8°, as described by Trasi et al.[17]

4.4.2   Scanning Electron Microscopy (SEM)

Crystalline tacrolimus monohydrate and the water insoluble components (tacrolimus and croscarmellose sodium) of a maximally crystallized Accord formulation were analyzed using SEM. The maximally crystallized Accord formulation was immersed in 10 mL water for ~5 min to dissolve soluble formulation components. The resultant slurry was then filtered and dried prior to the analysis with SEM. The crystalline samples were placed on SEM pin mount holders, sputter coated with platinum and then imaged with a FEI Nova NanoSEM equipped with an Everhart-Thornley detector (ETD) and through-the-lens detector (TLD). The SEM was operated at a 5 kV accelerating voltage, with 5 mm working distance and beam spot size of 3 nm.

4.4.3 Dissolution and absorption measurements

The dissolution and absorption of Prograf and Accord formulations with 0, 20, 50 and 100% crystallinity were characterized simultaneously using a high surface area, flow-through absorptive dissolution testing apparatus as described previously with minor modifications.[126] Triplicate measurements were carried out using three dissolution volumes (240, 100 and 40 mL) for all formulations. A crystalline suspension of tacrolimus monohydrate was also evaluated for each volume to provide a control. For Prograf and fresh Accord, the capsule contents were added to the dissolution media and absorption measurements were initiated by starting fluid flow through the hollow fiber membrane. In the case of samples with different crystallinity extents, 132 mg of powder was weighed (total amount of powder in one capsule of generic formulation)[17] from the pooled powder of 5 capsules, and added to the dissolution media.

The absorption or mass transport measurements were carried out across a cellulosic hollow fiber membrane (surface area 100 cm_2, pore size 15 nm). Fluid was pumped in the donor and receiver channels at 2 mL/min using a peristaltic pump in parallel, co-current flow. The receiver concentration was measured using an in-line UV flow-through probe (SI Photonics, Tuscon, AZ). The donor concentration was measured by high pressure liquid chromatography (HPLC) analysis (see below) by periodic manual sampling. The dissolution medium was replenished with an equal volume of buffer after every sample acquisition. The samples were filtered using 1 μm glass fiber filters and diluted with 50:50 v/v acetonitrile:water before the analysis. To prevent any solid particles from entering into the hollow fiber membrane module, a 10 μm cannula filter was attached at the donor tube entrance. The donor and receiver concentrations were studied for 2 h and all experiments were carried out at 37 °C.

For dissolution-absorption experiments of supersaturated solutions of TAC, generated by the solvent-shift method, supersaturation equivalent to a completely dissolved 5 mg dose in dissolution media with different volumes was generated by addition of an appropriate amount of a methanolic stock solution (the maximum amount of methanol added was 250 μL). The absorption measurements were carried out in a similar way as described above for 4 h.

4.4.4   Desupersaturation Measurements

Desupersaturation rate was measured experimentally for tacrolimus solutions at different supersaturations in the presence of crystal seeds. To generate crystal seeds with relevant properties, one capsule of the maximally crystallized generic formulation was added to 100 mL of dissolution media and equilibrated overnight. The concentration of TAC in the equilibrated solutions was then analyzed and the desired supersaturation was generated by addition of a methanolic stock solution of TAC (10 mg/mL) to the crystalline suspension. The final methanol amount in the solution ranged between 0.2-0.5 v/v% of the total solution volume. The tacrolimus concentration was measured using UV spectroscopy (SI Photonics, Tuscon, AZ) as a function of time and the slope of concentration vs time profile over the first ~ 40 min was taken as the desupersaturation rate.

4.4.5   HPLC Analysis

The concentration of TAC was analyzed by HPLC using Agilent HPLC 1260 Infinity II system (Agilent Technologies, Santa Clara) and an Ascentis C8 4.6 mm × 15 cm × 5 μm column, with a UV detector operating at wavelength 210 nm. Two different pathlengths were used; 60 mm was used for concentrations below 1 μg/mL, while 10 mm was used for higher concentrations. The column temperature was set to 50 °C. The mobile phase was 70:30 v/v acetonitrile: water and a flow rate of 0.75 mL/min was used for the analysis. The retention time was 12 min. The sample injection volume was 50 μL.

4.5   Results

4.5.1   Characterization of Residual Crystallinity

Accord, the generic formulation, has been observed to undergo crystallization over time under accelerated storage conditions of 40 °C/ 75% RH.[17] The drug potency at these conditions has been confirmed, wherein no degradation of tacrolimus was observed.[159] Herein, the generic capsules were subjected to stress storage conditions to induce 20%, 50% and 100% crystallinity in the amorphous formulation. The % crystallinity was quantified with PXRD with the help of a standard curve (R^2=0.9808) (limit of detection was ~1% and limit of quantification was ~5%). Once the desired crystallinity was obtained, samples were removed from the storage conditions

and stored at room temperature prior to evaluation. PXRD diffractograms for formulations with different extents of crystallinity are shown in Figure 4.1.
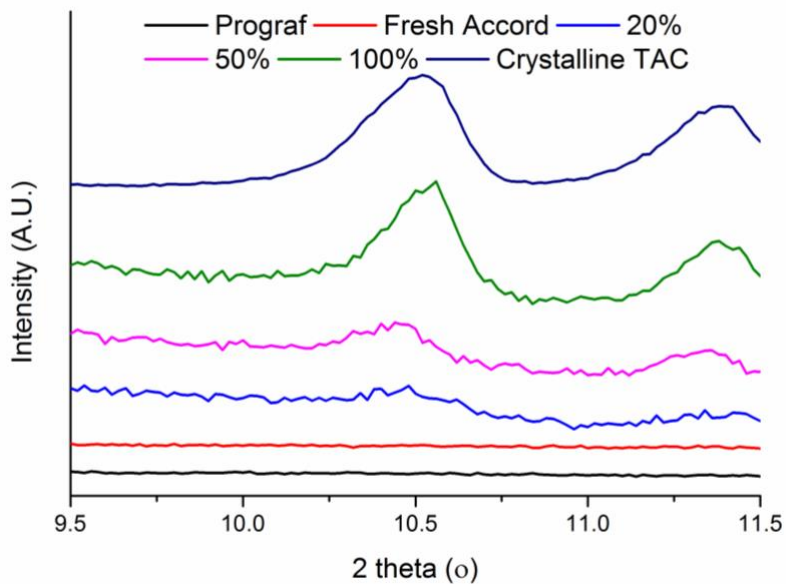
Figure 4.1: X-ray patterns of crystalline tacrolimus monohydrate, Prograf and generic formulations with varying % crystallinity upon storage at 40 °C/ 75% RH.

SEM images (Figure 4.2) show that crystals formed from the generic product were plate-like and of small size, < 1 µm. The as-received tacrolimus crystals are larger with a somewhat similar morphology.
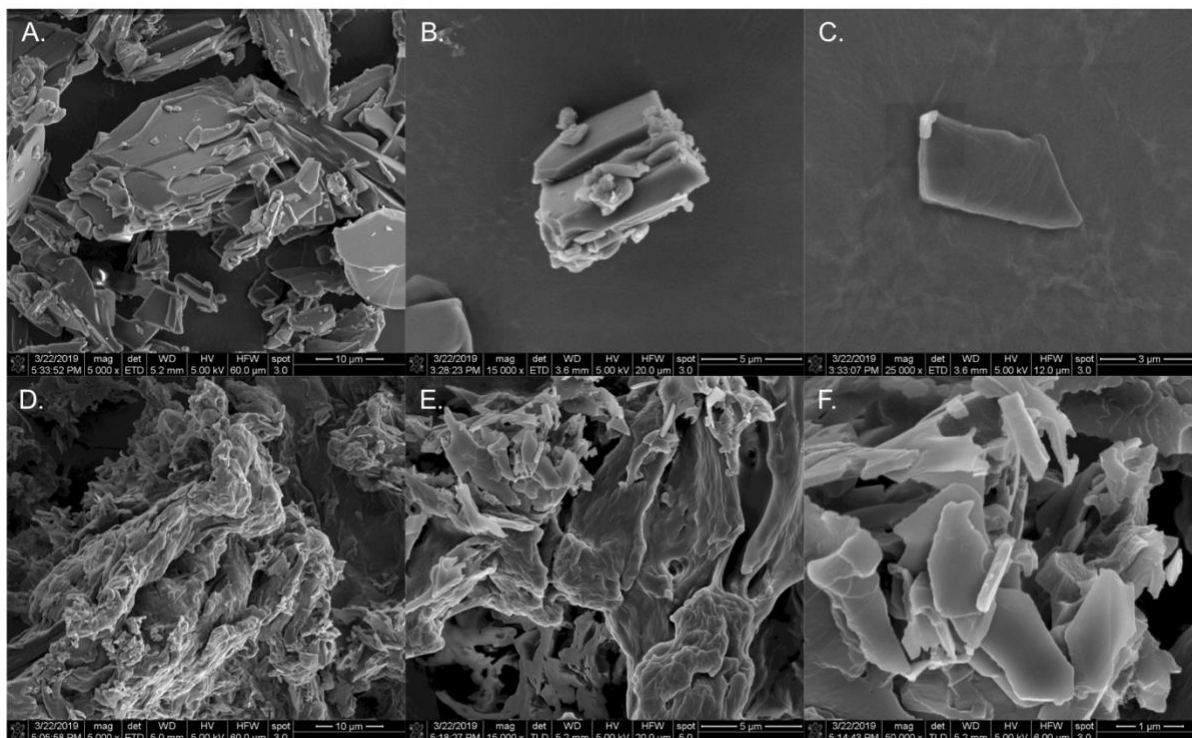
Figure 4.2: SEM images of crystalline as-received TAC (A, B, C) and TAC crystals/croscarmellose Na obtained after exposure of the generic product to 40 °C/ 75% RH followed by washing to remove soluble excipients (D, E, F) at different magnifications.

4.5.2   Dissolution and Absorption Behavior of Tacrolimus Formulations

Dissolution-absorption measurements of Prograf and Accord formulations with varying extents of residual crystallinity were first carried out with a dissolution volume of 240 mL, representing the volume of water typically recommended for clinical testing of oral formulations.[163] The measurements were carried out simultaneously to simulate the absorption environment present *in vivo* as the drug dissolves and then permeates across the enterocytes. Crystalline solubility of TAC at 37 °C in pH 4.5 5 mM phosphate buffer was found to be 2.5 ± 0.4 µg/mL and amorphous solubility has been reported as ~ 50 µg/mL.[162] Considering the dose of 5 mg, the theoretical maximum donor concentration in 240 mL was ~ 21 µg/mL. Thus, the dissolution conditions were sink with respect to the amorphous solubility, but non-sink with respect to the crystalline solubility of tacrolimus. Figure 4.3 shows the donor and receiver concentration profiles for the different formulations tested, which varied in terms of the extent of crystallinity. The donor profile shows the cumulative concentration obtained by manual sampling,

while the receiver concentration is a non-cumulative measurement obtained using a flow-through UV probe. Hence, the receiver concentration consists of initial data points corresponding to the saturation of the membrane and attainment of steady state.126 The subsequent decrease in the donor concentration reflects depletion due to absorption. Prograf showed gradual release of tacrolimus in the donor compartment (Figure 4.3a) which was reflected in the receiver compartment concentration profile. Release was nearly complete after 120 min. In comparison, the fresh generic showed rapid release of tacrolimus within 20 min followed by a slow decline in concentration with time due to subsequent absorption across the hollow fiber membrane. Correspondingly, the receiver concentration profile attained a maximum concentration after 20 min. Due to simultaneous absorption, the maximum donor concentration was lower than the theoretical maximum concentration of 21 µg/mL. The generic formulation containing 20% drug crystallinity showed similar donor and receiver concentration profiles as the fresh generic. However, samples containing 50% crystalline content achieved only half of the maximum attainable concentration, ~ 9 µg/mL. A corresponding low maximum concentration was observed in the receiver compartment. Further increase in the extent of crystallinity to 100% led to additional reduction in the amount of drug released in the donor compartment and a lower C_{max} in the receiver compartment, with the profiles comparable to those observed for the crystalline suspension of tacrolimus monohydrate.
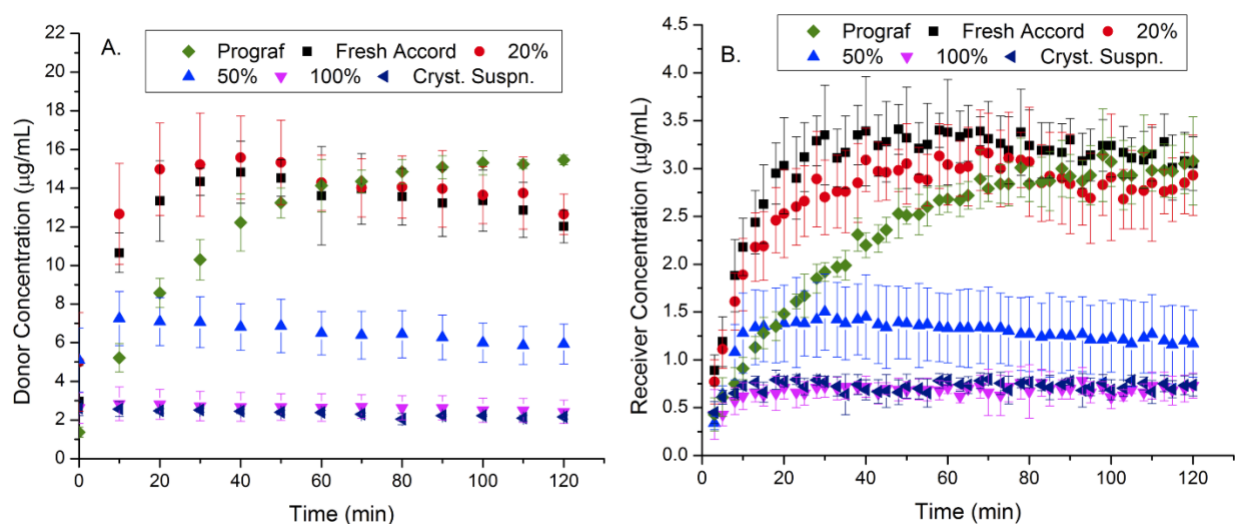
Figure 4.3: (a) Donor and (b) receiver concentration of tacrolimus brand and generic formulations when dissolved in 240 mL. Tacrolimus in the generic formulation underwent crystallization in solid-state and the legend reflects formulations with different weight percentage crystallinity.

In 100 mL of media, complete drug dissolution from the 5 mg formulation generates a donor concentration equal to 50 µg/mL. Hence, the at-sink conditions were maintained with respect to the amorphous solubility but are highly non-sink with respect to crystalline solubility. Furthermore, complete dissolution of the dose would result in a more supersaturated solution relative to the 240 mL volume. For 100 mL volume, similar trends in donor and receiver concentration profiles were observed between the different formulations as for 240 mL, although the rate and extent of absorption were different (Figure 4.4). Thus, Prograf had a slow release profile while both fresh and 20% crystalline generic showed fast release whereby the impact of the crystalline content on the dissolution and absorption profiles was not discernable within experimental error. As observed for 240 mL, the donor concentration did not reach the theoretical maximum concentration of 50 µg/mL for either Prograf or generic due to drug being removed by absorption. This observation highlights how absorption can decrease the extent of supersaturation achieved in the donor compartment. 50% and 100% crystalline Accord formulations once again resulted in lower concentrations in the donor compartment, which was reflected in the lower extent of absorption.
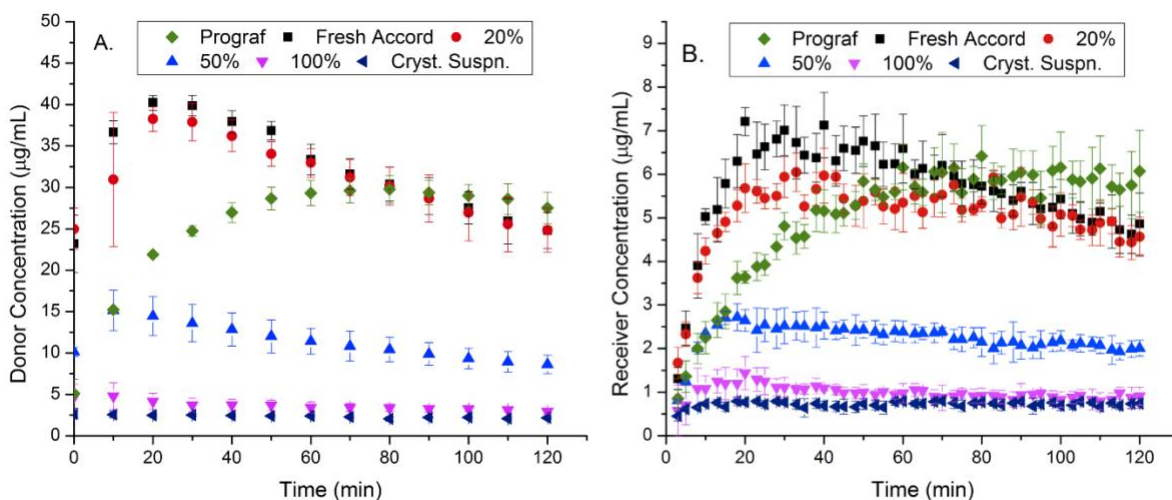
Figure 4.4: (a) Donor and (b) receiver concentration of tacrolimus brand and generic formulations when dissolved in 100 mL. The legend reflects formulations with different weight percentage crystallinity.

The final volume evaluated was 40 mL, with results summarized in Figure 4.5. At this volume, complete dissolution of the single 5 mg dose would theoretically generate a concentration equivalent to 125 µg/mL, thus making the dissolution environment non-sink with respect to both the crystalline and amorphous solubility. However, the amorphous solubility is the maximum concentration of free drug that can be attained, and increases in concentration above this value result in liquid-liquid phase separation (LLPS).[5] For these tacrolimus formulations, LLPS is not observed and the solid stops dissolving when the amorphous solubility is reached.[162] Herein, the fresh generic showed a fast drug release, attaining the amorphous solubility in the donor compartment, followed by a gradual decrease in both the donor and receiver compartment concentrations. For the 20% crystalline generic formulation, a significant decrease in concentration was observed in the donor compartment after 30 min, suggesting that crystallization of TAC occurred simultaneously with absorption across the membrane. The 50% crystalline formulation dissolved to a concentration of approximately half of the amorphous solubility under these highly non-sink dissolution conditions. The resultant receiver profile showed a higher C_{max} as compared to that observed for larger dissolution volumes. Interestingly, the 100% crystalline formulation generated a concentration above the crystalline solubility, suggesting either residual amorphous content or a defective crystal structure. The extent of absorption was also slightly higher than that observed for the crystalline control.
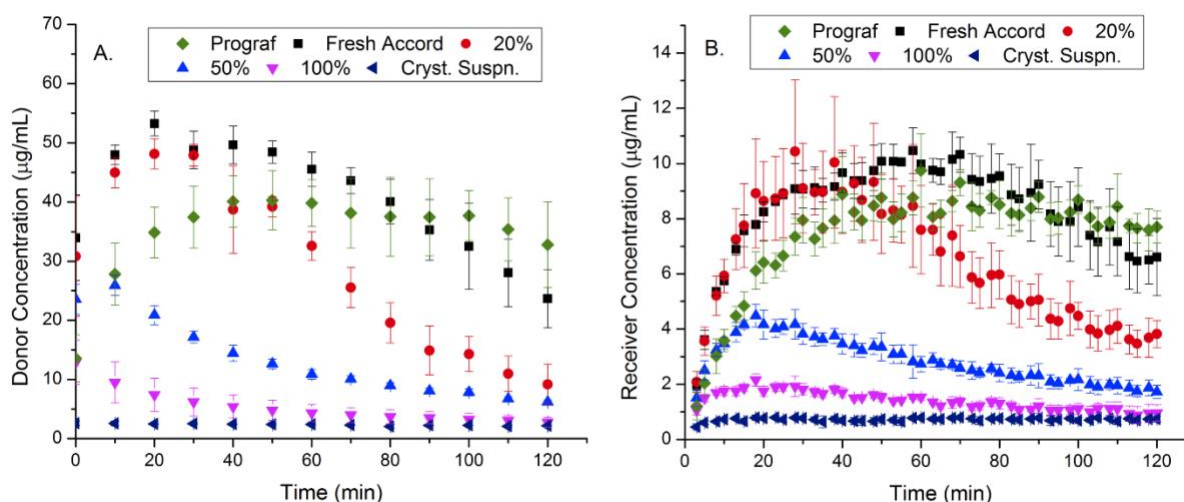
Figure 4.5: (a) Donor and (b) receiver concentration of tacrolimus brand and generic formulations when dissolved in 40 mL.

4.5.3 Solution crystallization during dissolution-absorption measurements

To determine the extent of crystallization occurring during dissolution-absorption measurements, the total amount of drug in the donor and receiver was calculated to achieve a mass balance of the total solution concentration as a function of time. A decrease in the total amount of drug dissolved following attainment of the maximum solution concentration indicates crystallization in the donor compartment with time. Figure 4.6 shows the results for the different formulations for the three dissolution volumes. No change in total concentration with time was observed for any formulation in 240 mL or 100 mL. The total amount of drug in the case of fresh generic and 20% crystalline formulation was less than 5 mg due to some drug adsorbed onto the membrane, drug solution that is retained in the tubing and variability in the drug content across different generic capsules. For 40 mL dissolution volume, the amount of drug increased over time for fresh generic, indicating continuous release of drug in the non-sink condition. However, the total drug amount decreased after 60 min for the 20% crystalline formulation and in the initial 20 min for 50% and 100% crystalline formulations, indicating that additional crystallization was occurring in the dissolution medium. It is important to note that both brand and generic formulations contained ~ 5 mg of HPMC.[17] In the absence of crystalline seeds, tacrolimus is a slow crystallizer and can maintain supersaturation for up to 3 h, and in the presence of HPMC, no crystallization was observed for over 6-8 h.[162] This explains why there was no crystallization of the fresh generic formulation.
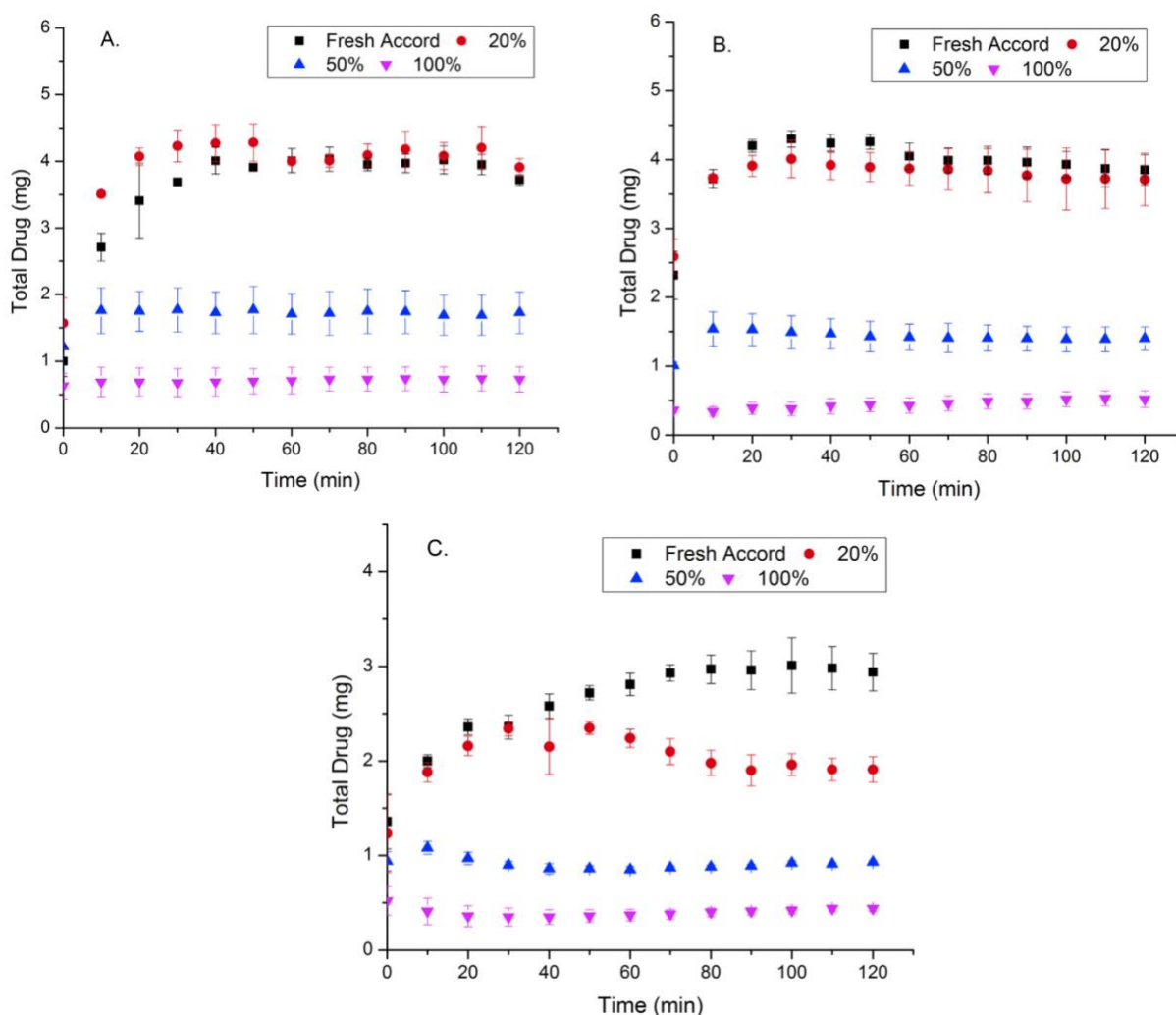
Figure 4.6: Total amount of drug in the donor and receiver in (a) 240 mL, (b) 100 mL, (c) 40 mL.

4.5.4 Impact of residual crystallinity on inter and intra-product variability

The area under the curve (AUC) of the receiver concentration profile can provide a quantitative measure of differences in formulation performance,[126] and values are presented in Figure 7. Overall, AUC decreased with an increase in % crystallinity for the generic formulation for all dissolution volumes. The AUC of Prograf was lower than that of fresh generic due to the slower release profile of the former system. Interestingly, the magnitude of AUC increased with a decrease in dissolution volume, regardless of the extent of crystallinity in the formulations, but was constant for the control suspension.

Virtual bioequivalence was evaluated for the data obtained in this study using receiver AUC as the input metric. According to bioequivalence (BE) criteria, the test-to-reference (T/R) ratio with 90% confidence interval (C.I.) for AUC should lie between 80–125 %. Figure 4.7 shows the T/R ratio for the different formulations studied and was calculated by taking the natural log of AUC_{test}/AUC_{ref}. For inter-product variability, the generic formulations were considered as the test and the reference was Prograf. Intra-product variability was determined by calculating T/R for partially crystalline generic formulations (T) with respect to fresh generic Accord (R). For 240 mL, when generic formulations were compared with Prograf, T/R for fresh generic exceeded the BE criteria. Bioequivalence outcomes for 100 mL dissolution volumes showed BE for fresh generic and 20% crystalline sample with respect to Prograf. In contrast, for 40 mL volume, the 20% crystalline generic was not bioequivalent with respect to either Prograf or the fresh generic based on this *in vitro* test. 50% and 100% crystalline generic formulations were not equivalent to either Prograf or fresh generic for any dissolution volumes considered in this study. Thus, dissolution volumes showed a significant impact on BE outcomes for the generic formulation, particularly for fresh generic and 20% crystalline generic formulation using this virtual approach. It should be noted that the C.I. in this study corresponds to the experimental error from triplicate experiments and does not represent the inter-subject variability observed in *in vivo* BE study. Therefore, we only evaluated the mean value of T/R for the BE criteria, which provides a good insight into differences in brand and generic formulations taking into account differences in the physicochemical properties of the various formulations considered. Intra-subject variability in an *in vivo* BE study is likely to lead to larger C.I. values.
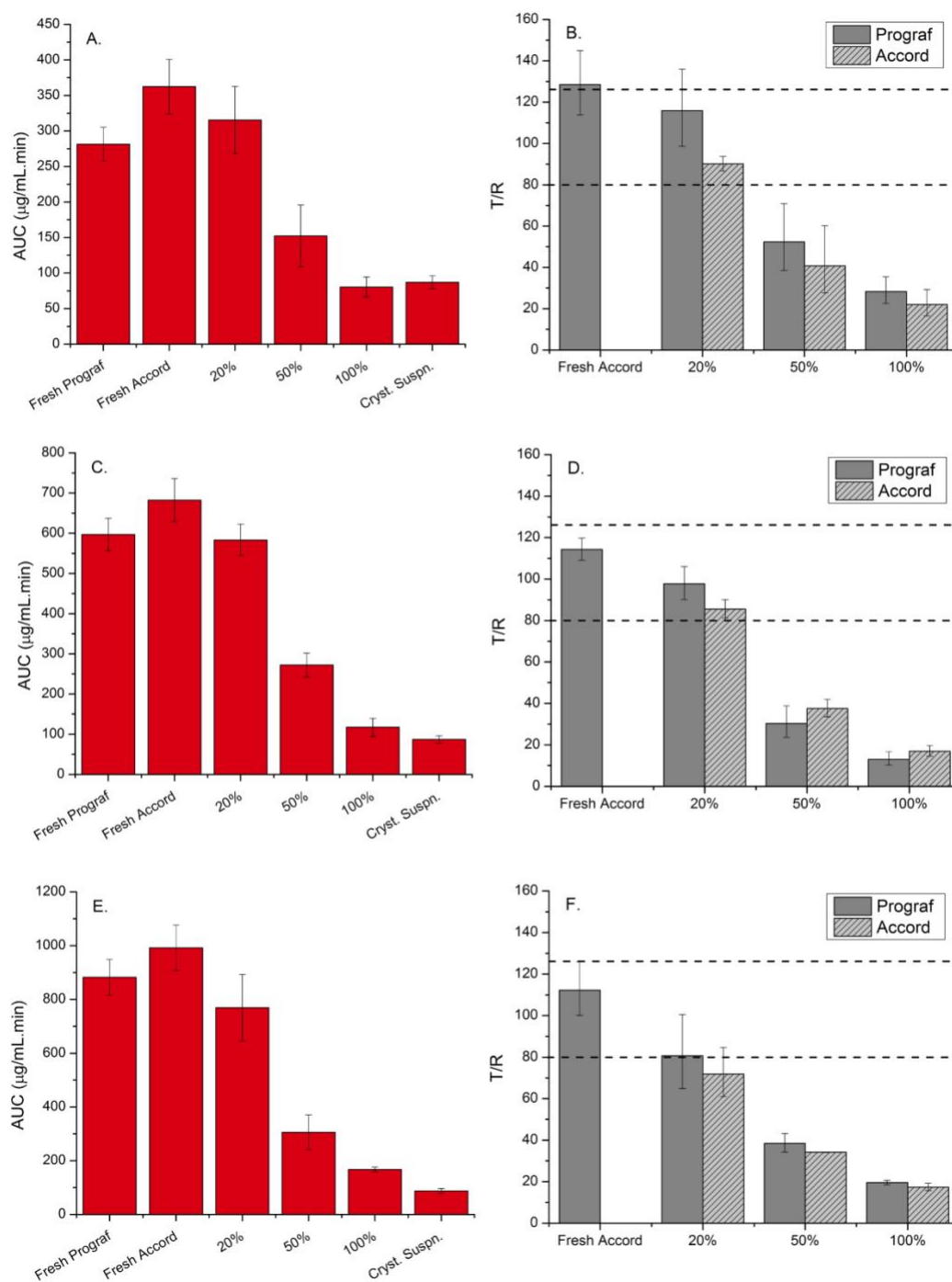
Figure 4.7. AUC$_{0-120}$ of receiver concentration profile in (a) 240 mL, (c) 100 mL, (e) 40 mL. Virtual BE for AUC for (b) 240 mL, (d) 100 mL, (f) 40 mL. The data shows reference-to-test and test-to-test ratio comparing AUC for Prograf and Accord formulations and Accord and crystalline Accord formulations respectively. Error bars indicate 90% C.I.

4.5.5 Depletion in Solution Concentration Due to Absorption

Mass transfer is proportional to supersaturation or, in other words, the solute thermodynamic activity.[11] Hence, to confirm the relationship between mass transfer rates and supersaturation, the mass transport of a supersaturated solution of tacrolimus generated by solvent addition was evaluated. Figure 4.8 shows the donor and receiver concentration profile when the supersaturation ratio (S) equivalent to a 5 mg dose was generated in either 100 (S of 20) or 240 mL (S of 8) of dissolution medium. Here S is given by the ratio of C/C^* where C is the solution concentration and C^* is the equilibrium or crystalline solubility. For the higher supersaturation generated in 100 mL, the donor and receiver concentration profiles showed a steeper decline in the concentration with time. On the other hand, a more gradual decline in the concentration for both compartments was observed in 240 mL where the supersaturation was lower. It should be noted that the decline in concentration in the donor compartment was solely due to absorption across the membrane since no crystallization occurred due to the presence of HPMC, which inhibits tacrolimus nucleation over the duration of the experiment.[17] A quantitative comparison between the extent of mass transfer for the two volumes can be seen in Figure 4.8c. It is clear that a higher amount of drug was absorbed when a lower volume was used, and hence a higher supersaturation was generated. The AUC of receiver profiles shown in Figure 8b when evaluated for 120 min were found to be 871 ± 60 µg/mL.min for 100 mL and 488 ± 37 µg/mL.min for 240 mL. These values corresponded closely with AUCs observed in Figure 7a and 7b (682 ± 54 µg/mL.min for 100 mL and 362 ± 38 µg/mL.min for 240 mL), suggesting little impact of excipients on the dissolution and absorption profiles.
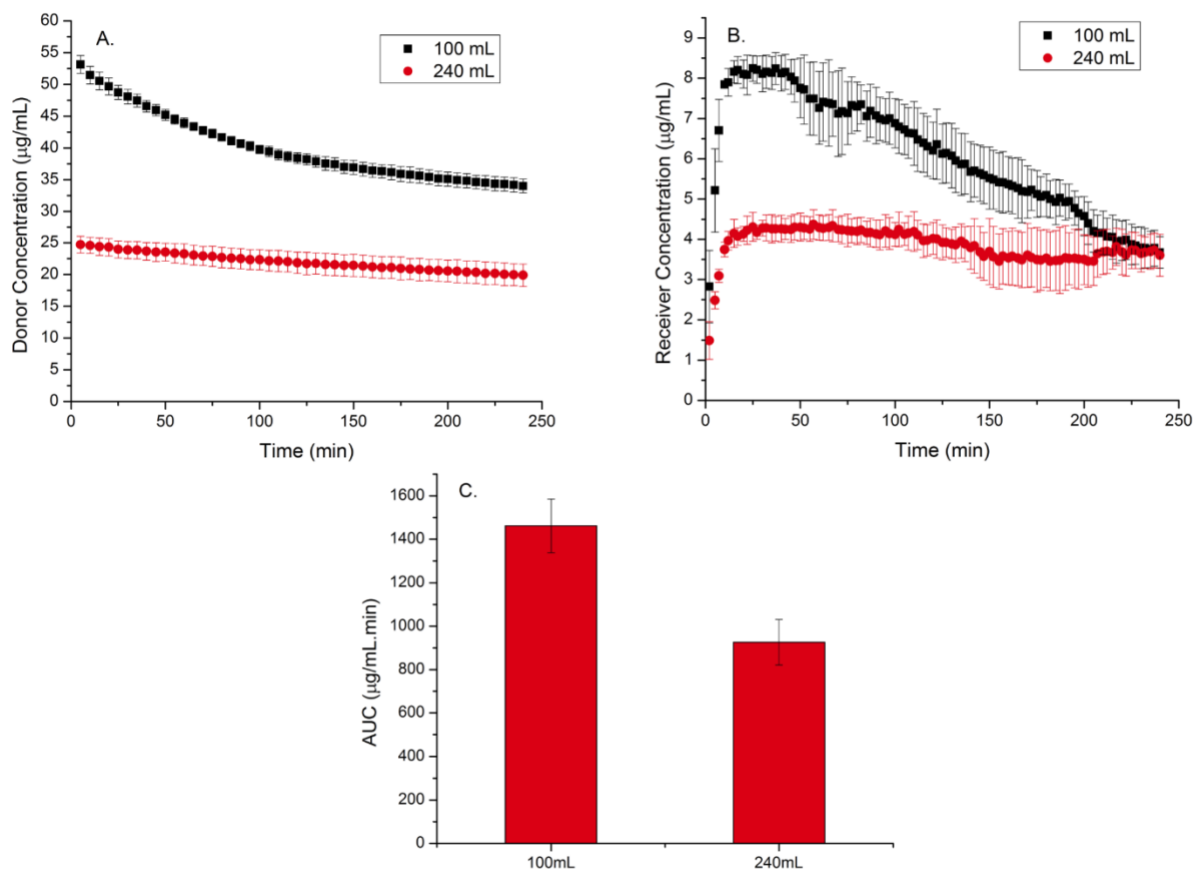
Figure 4.8: Donor (a) and receiver (b) concentration profiles of supersaturated solution of tacrolimus. (c) AUC_{0-240} of receiver coencentration profile.

4.5.6 Depletion in Solution Concentration due to Desupersaturation

Desupersaturation rates were evaluated as a function of supersaturation ratio for seeded solutions. Figure 4.9 shows characteristic desupersaturation profiles for a high and medium supersaturation level in the presence of seeds crystals. These supersaturation levels correspond to a completely dissolved 5 mg dose in 100 and 240 mL, respectively. The crystal seeds were introduced into the solution by adding the 100% crystallized generic formulation, thereby performing seeded crystallization experiments with similar parameters as for the formulations described above, but with a controlled initial supersaturation. Figure 4.9b shows that the desupersaturation rate, which is the slope of the concentration-time profile over the initial 60 min, was much greater for the higher supersaturation.
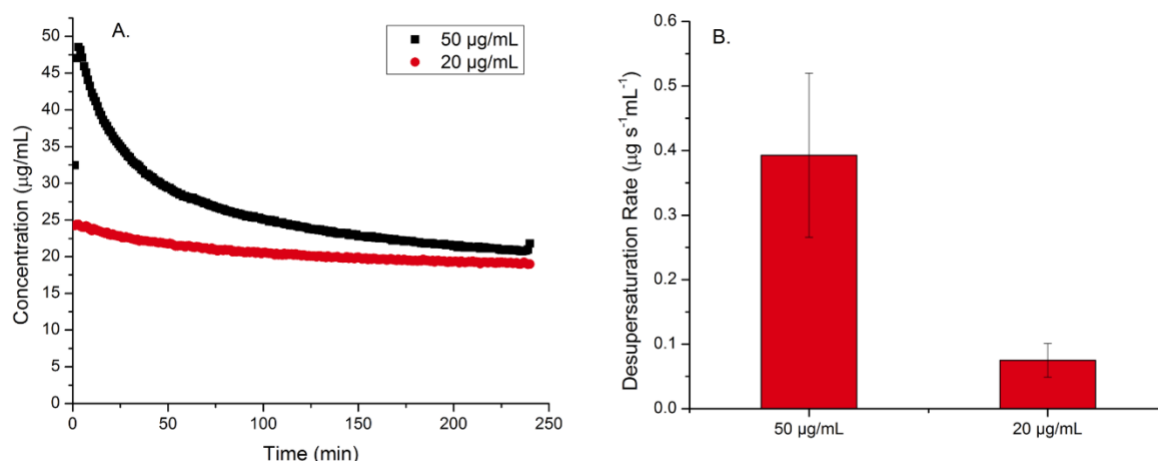
Figure 4.9: (a) Desupersaturation profile at different levels of supersaturation (b) Desupersaturation rate at different level of supersaturation.

4.6 Discussion

4.6.1 Predictive Dissolution Testing for Bioavailability and Bioequivalence Assessment

Dissolution testing guides the decision-making process at several stages of drug product development and manufacturing. Consequently, its discriminatory power is crucial.[164] However, the lack of a dynamic environment, as found *in vivo*, makes it difficult to assess the biopharmaceutical risk of complex formulations, such as those designed to undergo supersaturation, using compendial dissolution systems.[165,166] An absorptive compartment coupled to the dissolution test is particularly crucial for supersaturating formulations to capture competing kinetic processes, notably membrane transfer and crystallization kinetics. An absorptive compartment also leads to removal of material from the compartment in which the formulation is dissolving. In this context, it is additionally important to evaluate dissolution volume, since it will impact the extent of supersaturation generated for some systems, specifically low dose formulations of poorly soluble compounds. The resultant supersaturation will affect both the absorption rate, which depends on the chemical potential gradient across the membrane, as well as crystallization kinetics including nucleation and growth rates. Previous studies demonstrated an interplay between the extent of the dissolution sink and desupersaturation in a closed-compartment setup.[155,159] The present study considers the impact of an absorptive sink.

125

The three dissolution volumes investigated herein generate different sink indices (SI) with respect to the amorphous solubility of TAC (SI = C_sV/Dose where C_s is amorphous solubility and V is volume), and all conditions are non-sink with respect to the crystalline solubility. For 240 mL, 100 mL and 40 mL, the SIs were 2.4, 1 and 0.4, respectively, which corresponds to sink, at-sink and non-sink conditions. The corresponding maximum supersaturation ratios were 8 and 20; for the lowest volume the maximum supersaturation ratio is limited by the amorphous solubility of the drug. For non-sink conditions, only a portion of the dose can dissolve if the dissolution is controlled by the amorphous solubility. For sink conditions, the entire dose can dissolve if fully amorphous, but any crystalline material will not dissolve unless the SI is $\geq$ 1 with respect to the crystalline solubility.

The slower release profile of Prograf as compared to fresh generic formulation observed for all dissolution volumes demonstrated inherent differences in the two formulations. These differences were investigated previously and were attributed to variations in manufacturing processes of the formulations.[17] Prograf is manufactured as an amorphous solid dispersion via solvent impregnation of the drug into the polymer.[167] In contrast, based on reverse engineering, it was concluded that the generic formulation largely exists as amorphous drug deposited as a thin layer on excipients, and is physically mixed with the polymer rather than molecularly dispersed.[17] As such, dissolution is fast, but the drug is susceptible to crystallization upon exposure to stress storage conditions. In this study, by varying the sink indices, distinct differences in supersaturation and absorption profiles between Prograf, fresh generic and partially crystallized generic were highlighted. For SI > 1, there was a significant difference between release profiles of Prograf and fresh generic as observed in Figure 4.3a, with this difference persisting, but becoming more moderate with decreasing volume. These differences in dissolution behavior led to a lower AUC for Prograf relative to the fresh generic, and a higher T_{max}. In a recent *in vivo* study in dogs, it was noted that the T_{max} for Prograf was approximately twice as long as the T_{max} for the fresh Accord formulation, and the AUC also trended lower.[160] Interestingly, the fresh generic did not undergo crystallization during dissolution, a different outcome from that observed in a previous study.[159] This can be explained by the lower supersaturation achieved in the donor compartment due to the simultaneous absorption of drug across the membrane. This clearly reduces the crystallization

tendency and is an important consideration when evaluating formulation robustness to phase changes during release testing.

The crystallinity extent of the various Accord formulations had a significant influence on the amount of drug released. This is readily explained by the rapid dissolution of the amorphous fraction, leading to a supersaturated solution. Consequently, the crystalline content is unable to dissolve once saturation is achieved. Thus, the maximum solution concentration generated is dependent on the amorphous content of the formulation, as well as the tendency of the crystals to grow and consume the solution supersaturation during the dissolution experiment. In terms of the extent of absorption, higher residual crystallinity led to reduced membrane transport due to the lower supersaturation achieved and subsequently a lower AUC for the receiver compartment. The impact of residual crystallinity is more pronounced as the volume is reduced. For instance, the desupersaturation tendency of 20% crystalline generic formulation was observed only for SI < 1. This can be related back to the fact that the rate and extent of supersaturation generation is maximized in the lower volume. This in turn is expected to promote the growth of the crystalline fraction, leading to an increased extent of crystallinity during the dissolution-absorption experiment, and ultimately reducing the supersaturation. Therefore, non-sink conditions can potentially provide more discrimination between formulations with small amounts of residual crystallinity, but observations should clearly be put into perspective relative to expected *in vivo* conditions in terms of minimum and maximum fluid volumes.

The virtual bioequivalence, evaluated from the absorption profiles, showed some interesting differences between the formulations, with the volume playing a pivotal role in the magnitude of these variations in some instances. The bioequivalence outcomes of fresh generic Accord clearly varied with the volume and this formulation failed to be bioequivalent at larger volume. Based on the results obtained for the high crystallinity formulations, the importance of formulating tacrolimus in the amorphous state is highlighted. The 50 and 100% formulations are noticeably not bioequivalent with the fresh generic for any volume based on this *in vitro* test. This was also the outcome of an *in vivo* study in dogs.[160] Moreover, the absorption of the sample with 20% crystallinity is consistently lower than the fresh product for all volumes, and the low volume test leads to a reduction in the mean value to below the 80% limit. It should be noted, however,

that we are not taking into account confidence intervals in this assessment, which would be critically important in an *in vivo* BE study. Clearly, the ramifications of dissolution testing conditions, i.e. absorptive sink and dissolution volume, on virtual bioequivalence outcomes were evident in this study. It is apparent that the dissolution volume can have significant impact on the bioequivalence outcomes, especially for amorphous formulations with residual crystallinity due to variations in the supersaturation generated.

4.6.2 Interplay between Absorption and Desupersaturation

This study has highlighted an interesting interplay between supersaturation generated by formulation dissolution, absorption rate and desupersaturation at different physiologically relevant volumes. After dissolution, the drug concentration-time profile in the donor compartment was dominated by two competing processes; absorption and desupersaturation. Desupersaturation occurred primarily due to growth of crystal seeds in the donor compartment, derived from the formulation, and hence provides information about the crystal growth rate, assuming minimal secondary nucleation. The change in the donor concentration due to absorption across the membrane can be mathematically expressed as shown in equation 1, whereas desupersaturation or crystal growth is given by equation 2.[66,126]

$$\frac{dC}{dt} = C_{in}(0).Z.\exp(Zt) \tag{4.1}$$

such that $Z = \frac{Q_{in}}{V_{in}\left(1+\frac{Q_{in}}{Q_{out}}\right)}\left[\exp\left(-\frac{K_{in}A}{Q_{in}}\left(1+\frac{Q_{in}}{Q_{out}}\right)\right) - 1\right]$

$$\frac{dC}{dt} = k_g A(C_{in}(0) - C^*)^n \tag{4.2}$$

where $\frac{dC}{dt}$ is rate of change of concentration in the donor compartment, $C_{in}(0)$ is the initial donor concentration, C^* is the equilibrium solubility, Q_{in} and Q_{out} are flow rates inside and outside the hollow fiber membrane, V_{in} is the donor volume, K_{in} is the mass transfer coefficient. A is the surface area of the membrane in the hollow fiber module in equation 1 and surface area of crystals in equation 4.2. k_g is the growth rate constant and n is the growth order. According to equations 4.1 and 4.2, the absorption and desupersaturation rates are proportional to the concentration, and

hence supersaturation (S), albeit to different extents. The concentration depletion in the donor can thus be schematically represented as shown in Figure 4.10.

Absorption

$$\frac{dC}{dt} \propto [S]$$

[Formulation Dissolution] $\longrightarrow$ [Drug in Solution] $\longrightarrow$ Crystallization

$$\frac{dC}{dt} \propto [S-1]^n$$
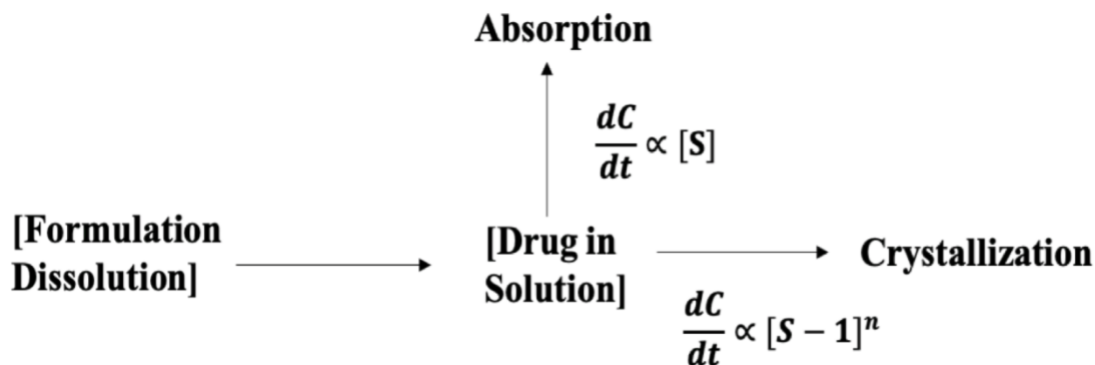
Figure 4.10: Schematic of competing physical processes during dissolution and absorption of supersaturated drug delivery systems.

To further understand the contribution of each of the physical processes, the rate-controlling steps were modeled as a function of supersaturation. To determine the absorption rate (equation 4.1), the mass transfer coefficient (K_{in}) was measured by non-linear curve fitting of the absorption profiles in Figure 8 and was found to be 1.09×10-4 cm/s. The overall crystal growth order n (equation 4.2) was determined by performing desupersaturation measurements in the presence of seeds for a range of supersaturations. Figure 4.11 shows desupersaturation or crystal growth rate plotted as a function of supersaturation on logarithmic scale. The slope of a plot log $\frac{dC}{dt}$ versus log (S-1) yields n, which was found to ~ 1.7. In the presence of an inhibitory polymer, as for these experiments, the crystal growth is integration-controlled due to polymer adsorption on the crystal surface, and n is typically ~ 2,[66,168] in good agreement with our extracted value. The growth rate constant (assuming and including constant crystal surface area) was obtained from the intercept of the plot in Figure 4.11 and was found to be 1.17×10-4 cm/s.
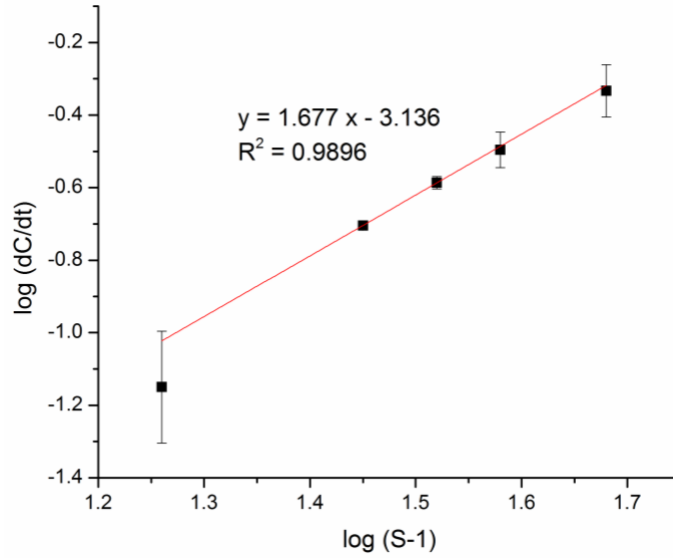
Figure 4.11: Logarithmic plot of desupersaturation rate as function of supersaturation in presence of crystal seeds and polymer in the solution.

Using the extracted constants, $\frac{dC}{dt}$ as a function of supersaturation was simulated, with results shown in Figure 4.12. Absorption is clearly the rate-controlling process at low supersaturation, whereas crystal growth with consequent desupersaturation is the predominant process at higher supersaturations. It is also apparent that the depletion of concentration over time lowers both the absorption and desupersaturation rates as the driving force decreases. It is important to note that $\frac{dC}{dt}$ for absorption is a function of time t (equation 4.1). For simulation purposes, only the initial time point was considered.

130
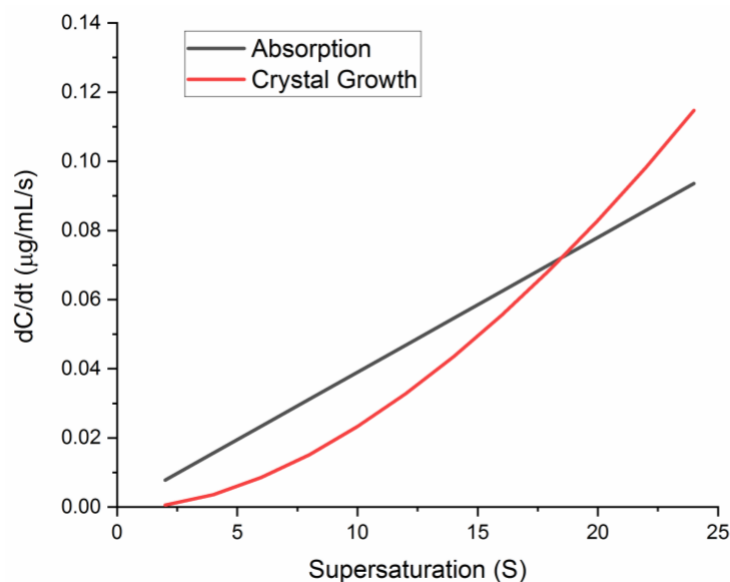
Figure 4.12: Simulation of absorption rate and crystal growth rate as a function of solution concentration. Equilibrium solubility of TAC considered for above calculations was 2.5 ug/mL.

The theoretical predictions of the relative contribution of absorption and desupersaturation to the change in donor concentration helps in explaining our experimental observations in Figures 4.8 and 4.9, wherein higher supersaturation led to faster membrane mass transfer and faster desupersaturation. These relationships also help clarify the observations that crystallization was not always observed, even when crystal seeds were present (Figure 4.6). This can be attributed to the lower maximum supersaturation generated for the higher volumes, and continual reduction in the supersaturation due to simultaneous loss of drug across the membrane, which in turn prevented additional crystal growth. In addition to absorption, the presence of a polymer clearly contributed to the prevention of desupersaturation in the solution, via poisoning the crystal surface and retarding crystal growth.[168] However, the high supersaturation generated in the case of the non-sink condition, combined with dominance of crystal growth in this supersaturation regime explains the rapid solution crystallization observed for partially and fully crystallized generic formulations (Figure 4.5). This interplay highlights that crystal seeds can have different impacts on absorption depending on the supersaturation profile generated following dissolution, which in turn depends on the volume of dissolution medium available. Clearly, these relationships are non-trivial to deconvolute, and will vary as a function of factors such as drug and formulation but are important for understanding what specification should be placed on residual crystalline content.

131

4.6.3   Effect of Fluid Volume on Intersubject Variability

Inter-subject variability for a given formulation can result from numerous factors that can vary such as transit time, GI motility, fluid pH, volume, composition, or drug efflux.[148] Herein, we demonstrate that fluid volume, in the context of amorphous formulations, could be a critical factor to evaluate. The supersaturation generated from amorphous formulations impacts bioavailability via the absorption rate, and, for certain drugs such as tacrolimus, the extent of supersaturation generated will depend on the fluid volume present in the lumen. Apart from the variability in fluid volume due to the amount of fluid ingested between different patients, gastric emptying rate or intestinal transit time, water absorption across the intestinal membrane due to luminal osmolality can also alter the drug concentration in lumen.[149,169] Therefore, absorption profiles could vary considerably for a particular drug product if there is a significant difference in fluid volume between subjects. Figure 13 compares absorption profiles for tacrolimus for different volumes. We suggest that such differences could translate to *in vivo* scenarios, and could contribute to high inter-subject variability, a well-known trait of TAC formulations.[170] Interestingly, and somewhat counterintuitively, higher AUCs are achieved in our *in vitro* test for the lowest volume.
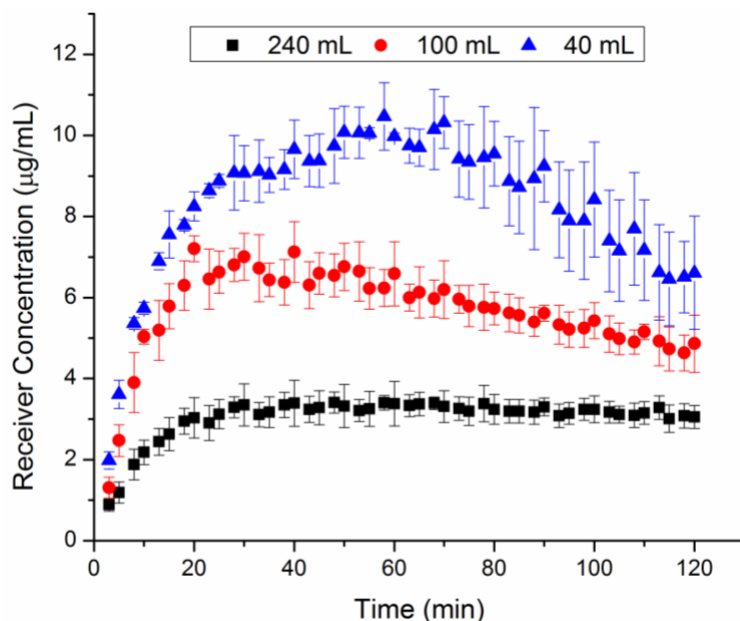
Figure 4.13: Receiver concentration profiles of fresh generic dissolved in different dissolution volumes.

4.7   Conclusions

This study demonstrates the importance of a discriminatory *in vitro* tool to assess factors impacting drug release, crystallization and membrane transport kinetics for amorphous formulations. The extent of supersaturation generated, and the kinetics of any subsequent solution phase transformations are important indicators of likely bioavailability for these formulations. Herein, we demonstrate that the risk presented by residual crystallinity needs to be evaluated in the context of the dosing conditions, specifically, the volume available for dissolution. Absorptive dissolution testing provides an *in vitro* tool to mechanistically investigate the interplay between crystallization kinetics and membrane mass transport as a function of supersaturation over relevant timescales. Variations in the dissolution volume provide further insights into the influence of fluid volume on the performance of thermodynamically labile systems. Mathematical modeling of concentration depletion due to absorption and desupersaturation allowed the individual contributions of competing physical processes during dissolution-absorption studies to be deconvoluted. Our findings clearly demonstrate that crystallization kinetics dominate drug concentration depletion in a seeded environment if supersaturation is significantly high, irrespective of a high absorption rate and the presence of an inhibitory polymer. In contrast, at lower supersaturation, the presence of seeds has a reduced impact. This newly developed *in vitro* absorptive dissolution testing tool thus appears to be well suited for the evaluation of oral formulations with complex phase behavior.

CHAPTER 5.   DISSOLUTION OF MESOPOROUS SILICA-BASED FORMULATIONS: IMPLICATIONS OF ADSORPTION TENDENCY, SUPERSATURATION AND ABSORPTIVE SINK ON DRUG RELEASE

5.1   Abstract

Mesoporous silica-based formulations are an alternative amorphous formulation strategy for the oral delivery of poorly soluble drugs. These formulations have improved physical stability due to drug nanoconfinement, however, their application can be limited by incomplete drug release. Adsorption of drug on the silica surface is a dynamic process, whereby absorption of dissolved drug across the gastrointestinal membrane can potentially drive additional release from mesoporous silica formulations. The goal of this study was to evaluate the adsorption tendency of a poorly soluble drug, atazanavir, on the silica surface (SBA-15) and assess the dissolution behavior of drug-loaded mesoporous silica-based formulations using a recently developed absorptive dissolution testing apparatus. Formulations were prepared with different drug loadings. Solid-state characterization using X-ray diffraction, differential scanning calorimetry, thermogravimetric analysis and infrared spectroscopy showed that all formulations were amorphous. Infrared spectra further suggested intermolecular interactions between silanol groups in SBA-15 and carbonyl groups in atazanavir. Differences in the thermal behavior suggested differences in the extent of nanoconfinement as a function of drug loading. Coupled dissolution-absorption studies showed incomplete drug release, which varied with drug loading. Partial release for low drug loadings was attributed to drug remaining adsorbed to the silica surface, while the increasing hydrophobicity of formulations with increasing drug loading was thought to underpin further reductions in drug release. Coupling dissolution to absorption led to almost complete drug release over 4 h. Dissolution was further improved when the formulation was dissolved first in gastric pH conditions followed by pH-shift to intestinal conditions, highlighting the importance of *in vitro* testing conditions for formulation evaluation.

5.2   Introduction

Poor bioavailability of drugs resulting from insufficient concentrations of dissolved drug has resulted in the development of several solubility-enabling formulation strategies.[6] Typical

formulation strategies include nanosizing, co-formulation with solubilizing agents or formulating as higher energy solid forms such as salts, co-crystals or amorphous solids.[6] In addition to improving the dissolution rate and solubility, generating and maintaining supersaturation can provide a higher driving force for membrane transport and significantly enhance the bioavailability of poorly soluble compounds.[5] One of the common supersaturating delivery systems used for commercial formulations is amorphous solid dispersions (ASDs). These formulations generate supersaturated solutions upon dissolution due to the higher free energy of amorphous solid and the presence of a hydrophilic polymer. Furthermore, the polymer can delay drug crystallization enabling supersaturation to be maintained over biorelevant time frames.[5,72,82]

Mesoporous silica-based drug delivery system (MPS) represent an alternative formulation approach to deliver drugs in amorphous form.[21,88,90] There have been more than 6000 articles published on these drug delivery systems over the past two decades.[94] Ordered mesoporous silica particles are amorphous materials with a periodic hexagonal arrangement of cylindrical pores of 2-50 nm with a narrow pore size distribution.[171,172] These materials offer a large specific surface area, up to 1500 m_2/g, which can effectively encapsulate drug molecules.[20,21] There are several types of mesoporous silica materials typically used for drug delivery application such as MCM-41, SBA-15, with some differences in the pore geometry and method of preparation.[90,173] In these systems, drug is loaded into the porous silica material by either solvent impregnation, incipient wetting, melt impregnation or supercritical CO_2.[174,175] The loading of drug into the nanopores suppresses drug crystallization. This is due to a confinement effect where the surface energy contributions to crystallization are larger (unfavorable) below a critical pore diameter.[176] Moreover, there may be changes in crystallization kinetics following nanopore confinement, either resulting from a change in the nucleation mechanism or because of interactions of drug immobilized on the pore wall surface.[22] The extent of amorphization depends on the drug-loading, drug-silica interaction, silica pore size and pore geometry.[22–26] The drug loading capacity of these delivery systems similarly depends on the pore volume, pore diameter, specific surface area, presence of silanol groups on the silica surface, functional groups of drug molecule, drug molecule size and solvent used for drug loading.[173,177,178] The theoretical amount of drug adsorbed onto silica can be estimated by evaluating the specific surface area of the silica material, the drug molecular weight

and the surface area occupied by a single drug molecule.[179] Materials with higher specific surface area generally shows higher adsorption capacity, and thus higher drug loading capacity.[180]

The application of mesoporous silica for drug delivery was introduced in 2001[88] and subsequently multiple studies have explored the potential of these materials for local drug delivery for bone tissue repair, cell-specific drug delivery for cancer treatment and as stimuli-responsive controlled release delivery systems.[90,181,182] Additionally, mesoporous silica materials have been explored for oral drug delivery of poorly soluble drugs where the drug is encapsulated as an amorphous solid, with good physical stability against crystallization and rapid drug release, thereby offering solubility and bioavailability advantages. Itraconazole release in simulated gastric fluid was observed to be faster when the drug was incorporated in the mesoporous silica particles as compared to crystalline drug.[91,175] Similarly, several weakly acidic and basic poorly soluble drugs were reported to release rapidly when formulated with MPS.[21,183–185] The supersaturation generated upon dissolution of an amorphous formulation is critical to its absorption behavior. The drug release rate from mesoporous silica particles depends on several factors including the surface area, pore size or pore geometry, strength of drug-silica interaction, the extent of water penetration into the pores to displace the adsorbed drug, drug solubility and hence dissolution rate in the aqueous medium, and diffusion of the dissolved drug into the release medium.[173,186,187] Larger pore sizes showed slightly faster release as compared to smaller pore size.[93,188,189] The drug release is observed to be slower for smaller pore size as it restricts the water diffusion into the drug/silica matrix.[178] Similarly, higher drug loading may slow down the water penetration and thus, the drug release rate, as the hydrophobicity of the pores increases with the increase in drug loading.[190] Surface-functionalization of the silica surface also allows control of drug release by altering drug-silica interactions, a strategy typically used for stimuli-responsive drug release.[30,96,182]

Dissolution of mesoporous silica-based formulations shows an immediate burst release, however, the total percent release is variable. Some studies report complete drug release, , particularly when dissolution was carried out under sink conditions.[21,174,191,192] On the other hand, other studies have shown incomplete drug release, particularly when dissolution generated a supersaturated solution. Vallet-Regi et al. in their seminal work of mesoporous silica-based drug delivery systems reported incomplete release of itraconazole from MCM-41.[88] Similarly, Mellaerts

et al. showed that itraconazole release plateaued at 60% when released from ordered mesoporous silica.[91,175,193] Indomethacin release from MCM-41 and Syloid 244 FP EU in pH 5.5 buffer was observed to plateau at 40-80% depending on how the formulations were prepared.[194] Recent work from our group explored the release of ritonavir from mesoporous silica-based formulation in a basic pH environment, under conditions where supersaturation was generated, and noted that only 50% of drug was released.[27] The incomplete release in supersaturated solutions was attributed to ritonavir-silica interactions whereby some drug remained adsorbed on the silica surface, even in the presence of the bulk aqueous phase.[27] The generation of supersaturated solutions from amorphous formulations is a highly likely *in vivo* due to the low GI fluid volume available and higher solubility of amorphous solids.[195] Clearly, incomplete drug release is not desirable from an oral bioavailability perspective, as the extent of supersaturation generated in the solution is critical to the mass transport rate. Therefore, a better understanding of MPS formulations is imperative to maximize their drug delivery performance.

In vivo, as the oral formulation undergoes dissolution, there are several physiological factors that impact the release of drug from the silica matrix including the pH in the gastrointestinal environment, the composition of the gastrointestinal fluid and the fluid volume.[196] Another important consideration for understanding drug release behavior from the silica matrix is the coupling between absorption of dissolved drug across the intestinal membrane and the promotion of additional drug release. Drug removal due to absorption decreases the solution concentration in the lumen, which in turn may alter the amount of drug adsorbed onto the silica surface based on consideration of the adsorption isotherm. In recent studies on flubendazole-loaded mesoporous silica formulations, a lack of correlation was observed between *in vitro* and *in vivo* results.[197] In addition to the differences in the composition of *in vitro* dissolution media and GI fluids, the lack of correlation suggests that absorption of drug may have an impact on drug release from these formulations. *In vitro*, mesoporous silica-based drug delivery systems are generally studied using single compartment dissolution testing, which lacks an absorptive sink compartment. Thus, it is difficult to assess the true performance of these complex formulations using current *in vitro* methods, necessitating a more dynamic *in vivo*-relevant testing methodology.

Recently, we have developed an absorptive dissolution testing apparatus that simulates the intestinal absorption process and provides simultaneous measurement of drug release and absorption.[126] The central component of the apparatus is a hollow fiber membrane that has a large surface per unit volume, offering faster mass transfer and absorption measurements in biorelevant time frames. The apparatus has shown great sensitivity to phase behavior such as crystallization, and its impact on the absorption behavior of formulations.[83,126,195] In addition, drug absorption promotes the dissolution of slow releasing formulations and also mitigates the risk of crystallization in supersaturated drug solutions. Utilizing this apparatus, the goal of this study was to evaluate drug release from mesoporous silica-based formulations under absorptive dissolution conditions. Atazanavir (ATZ), a poorly water-soluble and lipophilic compound, was used as the model drug and SBA-15 was employed as the silica carrier. ATZ was loaded in SBA-15 at varying drug loadings to understand the impact of drug loading on the formulation dissolution behavior. The solid-state properties of the formulations were evaluated using differential scanning calorimetry and X-ray powder diffraction, while infrared spectroscopy was used to probe drug-silica interactions. The dissolution behavior was evaluated in the presence of absorptive compartment, to test the hypothesis that better overall drug release would be observed with drug removal from the donor compartment. Finally, the formulation performance of mesoporous silica-based system was compared with ATZ ASDs using absorptive dissolution testing.

5.3 Materials

Atazanavir was purchased from Gojira Fine Chemicals, LLC (Bedford Heights, OH). SBA-15 with pore size of 7.1 nm and specific surface area of 586 m_2/g was purchased from Glantero (Cork, Ireland). Hydroxypropyl methylcellulose (PharmCoat 606) (HPMC) was obtained from Shin-Estu Chemicals (Niigata, Japan). HPLC grade acetonitrile and methanol were supplied by Fisher Scientific (Chicago, IL). Dissolution in acidic medium was carried out in 0.1 N HCl and in near-neutral medium using pH 6.8 50 mM phosphate buffer. The dissolution medium contained pre-dissolved HPMC at a concentration of 100 µg/mL. pH 6.8 50 mM phosphate buffer was used as buffer reservoir for the receiver compartment in the absorption measurements.

5.4 Methods

5.4.1 Drug loading procedure

Atazanavir was loaded into SBA-15 particles by the incipient wetness impregnation method,[175] wherein, depending upon the drug-loading, the desired volume of concentrated methanolic stock solution (10 – 35 mg/mL) of ATZ was added to SBA-15 and was vigorously mixed using a spatula. The sample was dried by storage in an oven at 40 °C overnight, followed by vacuum drying for 48 h. Samples were prepared at five different drug loadings: 5, 10, 20, 30 and 50% w/w. The drug content was confirmed by dispersing a known amount of sample in methanol under sonication for 30 min. The sample was then centrifuged at $21,1000 \times$ g for 10 min and the supernatant was analyzed by HPLC.

5.4.2 Powder X-ray Diffraction

Powder X-ray Diffraction (PXRD) of the ATZ-loaded mesoporous silica system was carried out using a Rigaku Smartlab diffractometer (Rigaku Americas, The Woodlands, TX) with a CuKα radiation source operating at 40 kV and 40 mA to determine any crystalline content in the formulation. A scan rate of 10°/min with a step size of 0.02° was used to scan between 5° – 40° 2θ. All the fresh samples were analyzed after 24 h of storage at 40 °C followed by 48 h storage under low pressure.

5.4.3 Differential Scanning Calorimetry

Thermal analysis of the ATZ-loaded mesoporous silica formulations was performed in a TA Q2000 differential scanning calorimeter (DSC) (TA Instruments, New Castle, DE) to determine the thermal events undergone by the formulations. The instrument was calibrated for temperature and enthalpy using indium. Nitrogen was purged at 50 mL/min. 2-4 mg of sample was weighed into an aluminum Tzero pan. The samples were heated at a rate of 10 °C/ min from 25 to 210 °C with a modulation amplitude of 1 °C/min every 60 s.

5.4.4 Thermogravimetric analysis

Thermogravimetric analysis (TGA) was performed in a TGA 5500 (TA Instruments, New Castle, DE) to determine degradation temperature of ATZ for pure drug and formulations with different drug loadings. The samples were placed in the platinum sample pans and were heated to 600 °C at a heating rate of 10 °C/min. The analysis was performed under nitrogen gas.

5.4.5 Fourier Transform – Infrared Spectroscopy

The infrared spectra were collected using a Bruker Vertex 70 Fourier Transform Infrared (FT-IR) spectrometer (Bruker Co., Billerica, MA) with a Golden Gate diamond Attenuated Total Reflectance (ATR) accessory (Specac Inc., Kent, United Kingdom). The sample was placed in contact with the diamond crystal. 128 scans were collected for both the background scan and the sample over the scan range of 1000 to 4000 cm$_{-1}$ with a resolution of 4 cm$_{-1}$. The data were analyzed using OPUS software (Version 7.2, Bruker Optik GmbH).

5.4.6 Dissolution and Absorption Studies

The dissolution studies of ATZ-loaded mesoporous silica formulations were carried out in a 50 mL aqueous media (either acidic or pH 6.8). The dose concentration was equivalent to the amorphous solubility of atazanavir, 75 µg/mL.[83] The concentration was determined by periodically withdrawing samples from the dissolution vessel and filtering through 1 µm glass fiber filters (Macherey-Nagel, Inc., Bethlehem, PA). For two-step dissolution studies, pH adjustments were done by addition of concentrated HCl and NaOH solutions following 30 min dissolution in acidic medium.

The mass transport studies were carried out in the flow-through, high surface area absorptive dissolution testing apparatus described previously.[83,126,195] A cellulosic hollow fiber membrane module (surface area 100 cm$_2$, pore size 15 nm) was used to simulate the absorption process. The receiver fluid was pH 6.8 50 mM phosphate buffer. The flow rate in the donor and receiver channel was maintained at 4 mL/min. The measurements were carried out at 37 °C. The receiver concentration was measured in-line using a flow-through UV probe, connected to a UV-Vis spectrometer (SI Photonics, Tuscon, AZ). The donor volume was 50 mL and a 10 µm cannula

filter (Agilent, Santa Clara, CA) was used at the entrance of the donor channel tubing to prevent water-insoluble silica particles from entering the hollow fibers. The donor concentration was measured by high pressure liquid chromatography (HPLC) following manual periodic sampling and filtration through 1 µm glass fiber filters. All measurements were carried out in triplicate.

5.4.7 Adsorption Isotherm

To generate an adsorption isotherm for the ATZ – SBA-15 system, a known amount of SBA-15 was added to the aqueous media such that SBA-15 concentration was either 300 µg/mL or 25 µg/mL. An aliquot of a concentrated methanolic stock solution of ATZ was added to the aqueous media containing SBA-15 and the suspension was equilibrated for 2 h (rapid equilibrium was observed for the ATZ-silica system) at 37 °C. Adsorption of ATZ was evaluated for a wide range of concentrations between its crystalline and amorphous solubility. Hence, the concentrations generated were supersaturated with respect to ATZ crystalline solubility. The equilibrium achieved in this case was a metastable equilibrium as the solution was supersaturated.[198] No crystallization was observed over the timeframe of the experiment (0.1 mg/mL of hydroxypropyl methyl cellulose, was added to prevent crystallization). The amount of methanol added was below 0.5% and hence there was no significant contribution of methanol on the adsorption. Following equilibration, the samples were filtered through 1 µm glass fiber filters and analyzed using HPLC. The amount of ATZ adsorbed was determined by evaluating the difference in the concentrations of ATZ initially and after equilibration, and the amount of SBA-15 used.

5.4.8 High Pressure Liquid Chromatography

The concentration of ATZ was analyzed by high pressure liquid chromatography (HPLC) using an Agilent HPLC 1260 Infinity II system (Agilent Technologies, Santa Clara) and an Eclipse Plus C18 4.6 mm × 30 cm × 5 µm column, with a UV detector operating at wavelength 210 nm. The calibration curve was generated for the concentration range of 2 to 30 µg/mL. The mobile phase was 60:40 v/v acetonitrile: pH 2.5 water (acidified with orthophosphoric acid) and a flow rate of 0.7 mL/min was used for the analysis. The run time was 7 min. The sample injection volume was 15 µL. All the samples were diluted with 50:50 v/v acetonitrile: water prior to the analysis.

5.5 Results

5.5.1 Adsorption Isotherm of Atazanavir

Prior to evaluating the adsorption tendency of ATZ onto the silica surface, the theoretical monolayer layer coverage of ATZ on SBA-15 was determined using the approach described by Azais et al.[179] The molecular dimensions of ATZ (shown in Figure 5.1) were obtained from Cambridge Crystallographic Data Center (CCDC) database as (17.53 × 14.07 × 7 Å) (Reference code: LISTEP). Assuming the larger dimensions of ATZ are in contact with the SBA-15 pore surface and considering the SSA of SBA-15 as 586 m_2/g, the theoretical monolayer coverage can be estimated as (SSA × mol. weight of drug) /(drug molecular surface area × Avogadro's number N_A). Based on this geometric approach, the theoretical monolayer coverage for ATZ was found to be 278 mg/g or ~28% w/w.
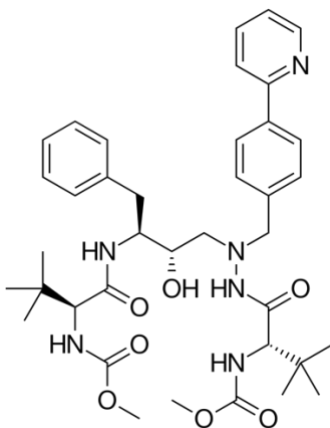
Figure 5.1: Molecular structure of atazanavir.

The adsorption of ATZ onto the silica surface was investigated to understand potential correlations between adsorption tendency and drug release during dissolution studies. Figure 5.2 shows the adsorption isotherm of ATZ. ATZ has crystalline solubility of 5 (± 0.5) µg/mL and amorphous solubility of 78 (± 5) µg/mL.[83] Based on Figure 5.2a, ATZ showed a non-linear adsorption tendency. The overall adsorption of ATZ on the silica surface was significantly lower when compared to the theoretically estimated monolayer coverage, with the maximum amount of drug adsorbed equivalent to 25 mg/g at the maximum solute thermodynamic activity (i.e. the amorphous solubility). The adsorption isotherm showed type II behavior, wherein the amount of

ATZ adsorbed increased with an increase in the solution concentration, reaching a plateau and then further increasing non-linearly at higher solution concentrations.[199] A similar adsorption isotherm was also observed for the structural analog, ritonavir.[198]

The experimental data shown in Figure 5.2 was fitted to Brunauer-Emmett-Teller (BET) isotherm equation by non-linear least square fitting. The BET equation for adsorption from solution is given as follows:[200]

$$Q_a = Q_m \frac{K_{BET}X}{(1-X)(1+(K_{BET}-1)X)} \qquad (5.1)$$

where Q_a is the total amount of drug adsorbed (mg/g), Q_m is monolayer coverage, K_{BET} is the equilibrium constant of adsorption and desorption and X is the ratio of the equilibrium concentration to the saturation concentration (C_e/C_s, where Cs is taken as the amorphous solubility). From the BET equation, the monolayer coverage (Q_m) was found to be 4.5 mg/g. This value was much lower than estimated theoretical monolayer coverage based on geometric considerations (SSA of SBA-15 and molecular dimensions of ATZ). During additional experiments, it was also observed that for a given ATZ concentration, the amount of drug adsorbed depended on the amount of SBA-15 present. The amount of ATZ adsorbed was significantly higher when low amount of SBA-15 (25 µg/mL) was used, although it followed a similar type II adsorption isotherm (Figure 5.2b). This seemingly counterintuitive observation can be rationalized as follows: Although mg of ATZ adsorbed per g of silica was significantly higher for a lower amount of silica, the percentage ATZ adsorbed was much lower. This is because the inherent adsorption capacity of silica is a constant (and dependent on the surface properties) and and hence a lower number of active sites should result in a lower percentage of drug adsorbed. Typically, the percentage of solute adsorbed increases with an increase in the amount of adsorbent and eventually attains a plateau, indicating the maximum amount of adsorbent required for efficient solute adsorption.[201–205] The difference in adsorption isotherms observed herein highlights that during the release studies, the amount of silica used in the experiment should be considered when correlating the adsorption tendency to rationalize the incomplete drug release.
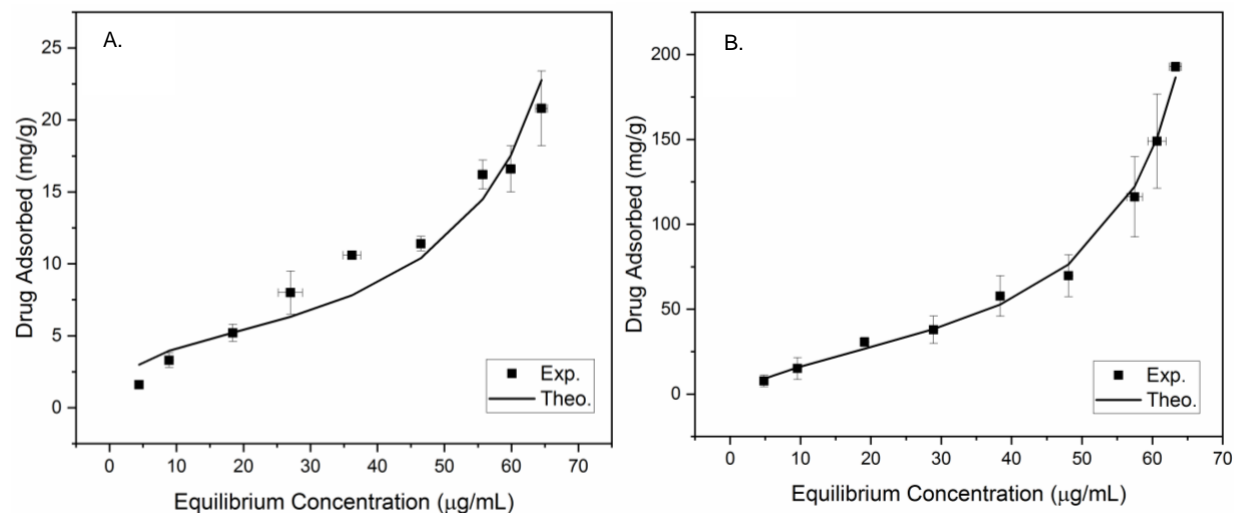
Figure 5.2: Adsorption isotherm of ATZ with (a) 300 µg/mL SBA-15 and (b) 25 µg/mL SBA-15.

5.5.2 Evaluation of ATZ-loaded mesoporous silica formulations

Solid-state characterization

PXRD of ATZ-loaded mesoporous silica systems (ATZ-MPS) are shown in Figure 5.3. The halo in the X-ray diffractograms for all the ATZ-MPS formulations suggested that the drug was amorphous following preparation. Following storage in a desiccator at room temperature for a week, the 50% drug-loaded ATZ-MPS system showed diffraction, indicating drug crystallization (data not shown). All the other ATZ-MPS systems were found to be stable for over 3 months. Stability was not evaluated beyond 3 months.
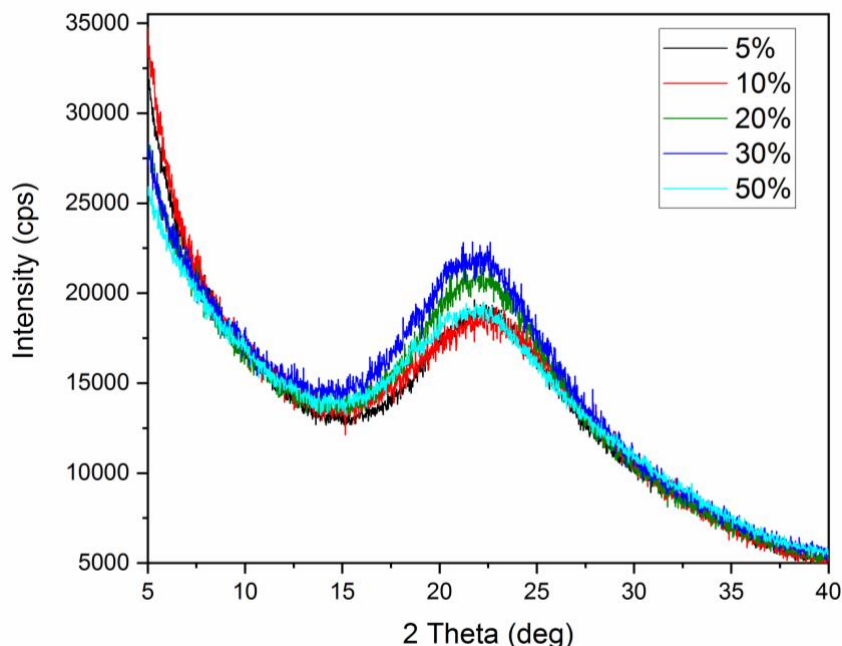
Figure 5.3: Powder X-ray Diffractograms of ATZ-MPS formulations with varying drug loadings. The legend indicates % drug loading. Samples analyzed after 24 h of storage at 40 °C followed by 48 h storage under low pressure

To further confirm the physical state of ATZ in the mesoporous silica, thermal analysis was carried out using DSC. Figure 5.4 shows DSC thermograms of ATZ-MPS formulations obtained after single heating cycle. The physical mixture of amorphous ATZ and SBA-15 was first assessed to obtain a control dataset. A clear glass transition at 105 °C and a melting endotherm at 208 °C were observed. Thus, amorphous ATZ underwent crystallization during heating above Tg, although the crystallization exotherm appears broad and not well distinguished from the baseline. For 5, 10 and 20% ATZ-MPS formulations, there was no indication of the glass transition or melting events in the thermograms. A small glass transition and melting event were observed for the 30% drug loading, while a clear T_g at 105 °C and melting peak at 208 °C was observed for the 50% ATZ-MPS formulation. The confinement of molecules in nanopores is known to significantly alter thermal events such as the glass transition or crystallization.[206,207] Therefore, the results suggest a difference in the molecular environment in the formulations as a function of drug loading.
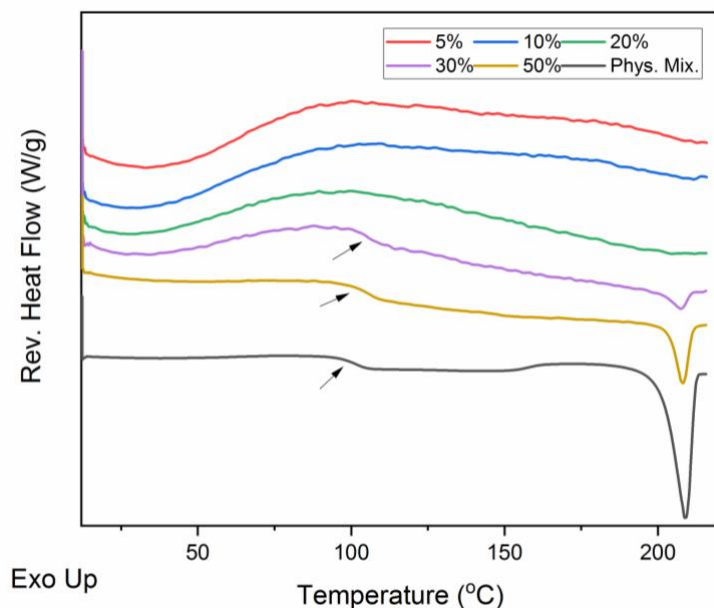
Figure 5.4: DSC thermograms of ATZ-MPS formulations. The arrow indicates T_g. The legend indicates % drug loading.

The drug loading in the mesoporous silica particles was assessed by measuring the dissolved content by HPLC. All formulations showed a percent drug loading close to the theoretical amount of drug added (data not shown). To further confirm the drug loading, TGA was also performed for all the ATZ-MPS formulations prepared (Figure 5.5). Pure ATZ showed degradation at 340 °C. An initial small drop in weight was observed for SBA-15, which can be attributed to the loss of adsorbed water present on the silica surface. The amount of drug loaded in the mesoporous silica particles was inferred based on the percent weight loss for the different formulations and was similar to the theoretical drug, with a standard deviation of $\pm$ 3% from the theoretical value. The second derivative of the weight loss profile was evaluated to obtain an accurate degradation temperature of ATZ in the formulations. Interestingly, the degradation temperature of ATZ-MPS formulations was slightly different from that of pure ATZ and varied with drug loading. A higher degradation temperature was observed for lower drug loadings (5 and 10%) formulations while an increase in the drug loading led to a decrease in the degradation temperature towards that seen for ATZ alone. The 50% ATZ-MPS system exhibited similar degradation to that seen for bulk ATZ. The difference in thermal degradation between low and high drug loading ATZ-MPS formulations suggested a similar confinement effect as observed in DSC studies.

146
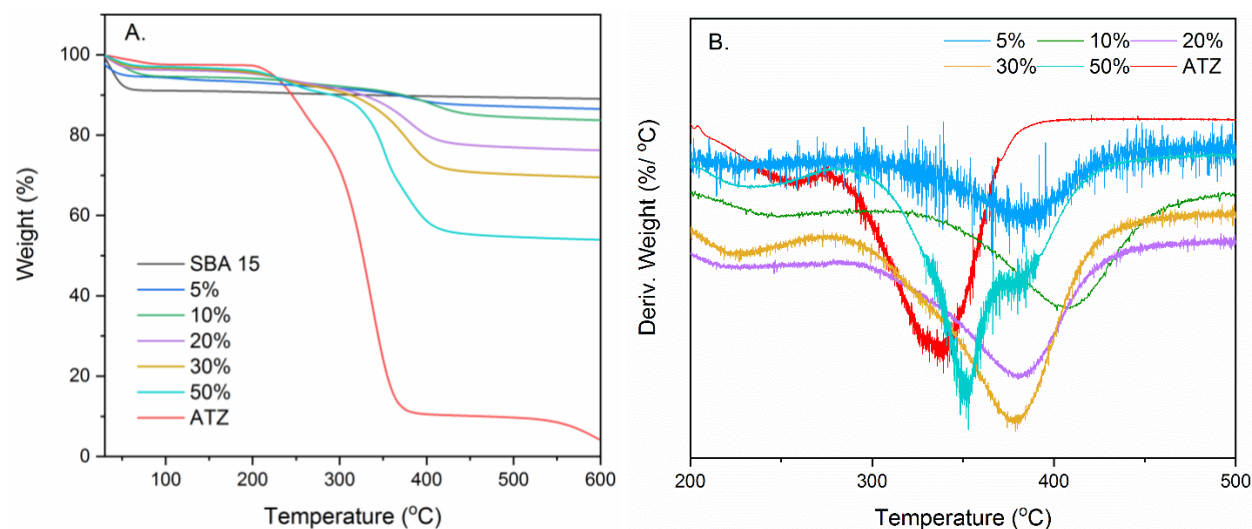
Figure 5.5: (a) Weight loss as a function of time and (b) derivative of degradation of ATZ-MPS formulations

Molecular interactions between ATZ and SBA-15

Molecular interactions between atazanavir and SBA-15 in solid-state were studied using infrared spectroscopy. Figure 5.6 shows FT-IR spectra of crystalline ATZ, amorphous ATZ (prepared by melt quenching), SBA-15 and ATZ-MPS formulations with different drug loadings. Pure crystalline atazanavir shows strong peaks at 3400 and 3350 cm-1 that corresponds to N-H and O-H stretching. The peaks appearing in the range of 3000-2800 cm-1 corresponds to aromatic and aliphatic C-H stretch. The characteristic peaks at 1707, 1688 and 1670 cm-1 can be attributed to C=O stretching and the peak at 1530 cm-1 corresponds to arene C-C stretch. The IR spectra of amorphous ATZ showed a significant broadening of peaks in the regions corresponding to N-H, O-H and C=O stretching as compared to crystalline solid. In addition to peak broadening, the peak at 1707 cm-1 shifted to a higher wavenumber and the peak at 1670 cm-1 shifted to a lower wavenumber. This suggested a change in hydrogen bonding in the amorphous form as compared to the crystalline solid.[208] The IR spectra of pure SBA-15 showed a small peak at 3749 cm-1, characteristic of an isolated (i.e. non hydrogen-bonded) silanol group. A strong, broad peak was observed at 1000-1300 cm-1 which corresponded to an asymmetric Si-O vibration. The region 3600 – 3000 cm-1 was characterized by a broad absorption band and overlapped with the N-H and O-H stretching in ATZ.

ATZ loaded into mesoporous silica in general showed broader peaks as observed for amorphous ATZ, consistent with a disordered structure. For low drug loadings, the C=O peak, seen at 1707 cm^{-1} in amorphous ATZ, shifted to a lower wavenumber, while the peak at 1688 cm^{-1} was broadened with a loss of intensity. The 50% ATZ-MPS system showed a similar spectrum as amorphous ATZ. The peak at 1530 cm^{-1} which corresponded to aromatic carbon stretch showed no peak shift, indicating no interactions of this functional group with the silica surface. Similarly, the peaks between 3000 – 2800 cm^{-1}, corresponding to C-H stretch, showed no peak shift. The region between 3400 and 3350 cm^{-1} showed very broad peaks and no conclusions could be drawn from this region. The peak at 3749 cm^{-1}, corresponding to isolated silanol in SBA-15, was visible in 5% and 10% ATZ-MPS formulations, albeit at low intensity. Further increases in ATZ drug loading resulted in the disappearance of the peak, suggesting drug-silanol interactions.
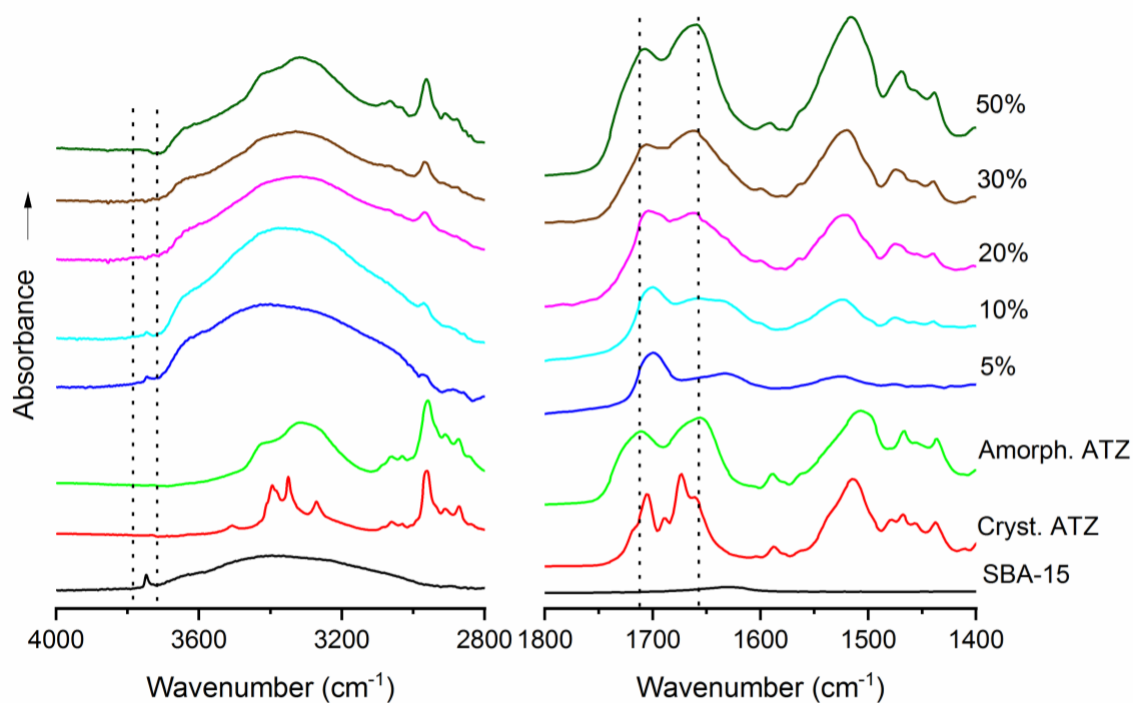
Figure 5.6: FT-IR spectra of crystalline ATZ, amorphous ATZ, SBA-15 and ATZ-MPS systems.

Dissolution and Absorption studies

Simultaneous dissolution and absorption measurements were carried out in a high surface area, flow through absorptive dissolution testing apparatus.[126] Figure 5.6 shows dissolution and absorption profiles of ATZ-MPS formulations with varying drug loadings. All the formulations

were dissolved at a target concentration of 75 µg/mL. Figures 5.7a and 5.7b show donor and receiver concentrations respectively. The donor concentration is the cumulative concentration profile and the receiver concentration profile is the non-cumulative concentration with initial data points corresponding to the period required for membrane saturation. Due to slow dissolution in the donor compartment, the maximum in the receiver concentration was not attained until significant drug release had occurred in the donor. Figure 5.7c is the total % drug released, which was calculated by considering the amount of drug in the donor and the amount of drug transferred across the membrane. The 5 and 10% DL ATZ-MPS formulation showed similar release profiles (Figure 5.7a), wherein the donor compartment drug concentration reached the maximum value in 40 min. The subsequent concentration profile showed a slow decline as drug permeated across the membrane. Herein, the drug release rate was slower than the drug permeation rate across the membrane resulting in a decline in the donor concentration. The total drug release from 5 and 10% DL ATZ-MPS formulations was approximately 80% (Figure 5.7c). The 20% drug loading formulation showed a slightly slower drug release and a lower concentration in the receiver profiles where the total drug release was 66% after 90 min. For these three formulations, 25 – 30% of drug was released instantaneously after adding the formulation to the aqueous media. The 30% drug loading formulation released only 50% of the drug in 90 min while the 50% DL system reached a maximum release of 35% over the same time period. Consequently, the receiver concentrations were much lower for the high DL systems than for the low drug loading ATZ-MPS formulations and the amount of drug absorbed was approximately halved. The incomplete release observed from all systems can likely be partially attributed to the adsorption tendency of ATZ onto the silica surface.
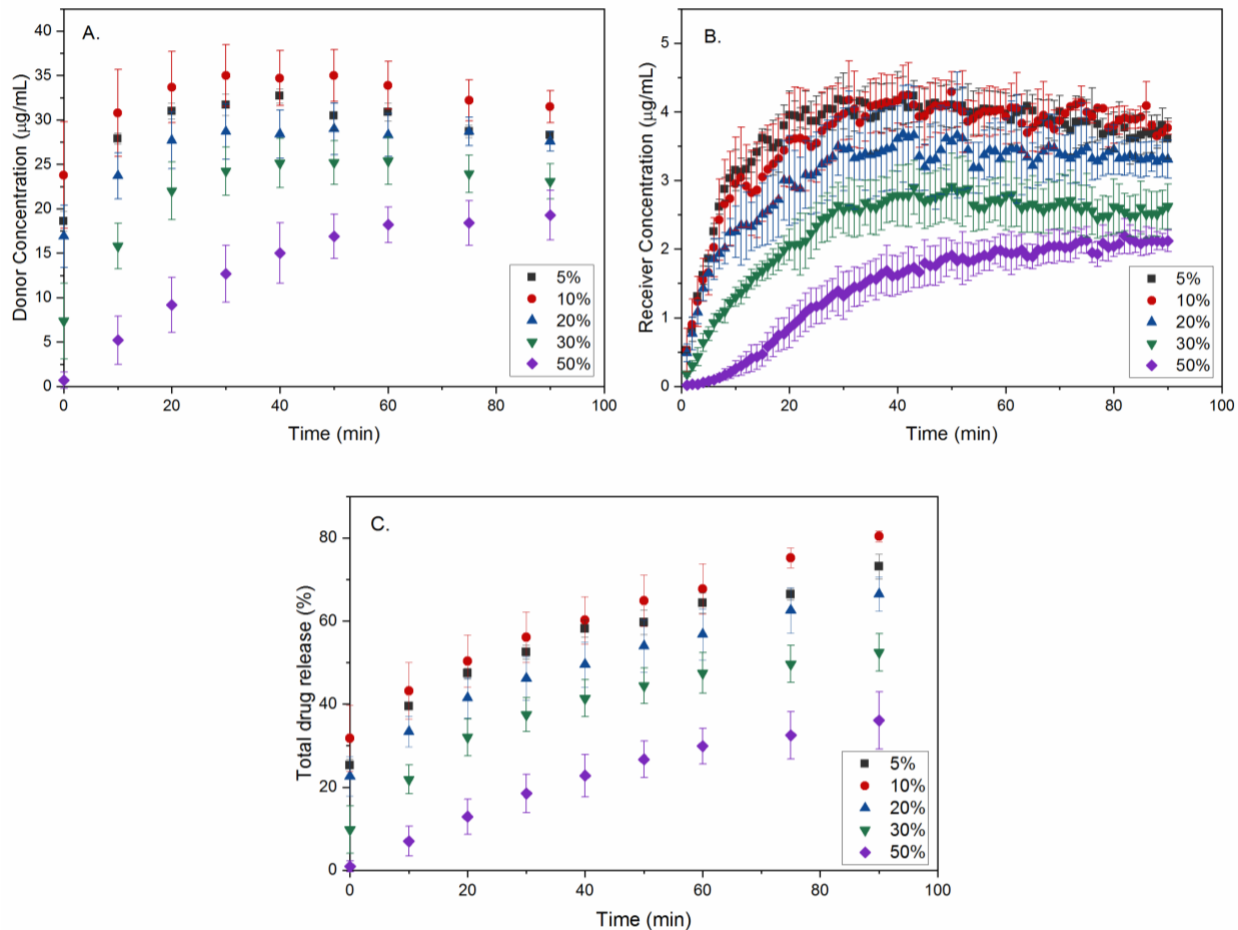
Figure 5.7: (a) Donor, (b) receiver concentration and (c) total drug release during dissolution and absorption studies of ATZ-MPS formulations. The legend indicates % drug loading.

The incomplete release of drug from the silica formulations required further investigation. Hence, dissolution of ATZ-MPS formulation was performed with pre-dissolved ATZ in the aqueous media, with the aim of understand the driving force for drug release. A closed-compartment dissolution of the 20% DL ATZ-MPS formulation was studied in the presence of 20 µg/ml and 40 µg/ml pre-dissolved ATZ in pH 6.8 phosphate buffer as shown in Figure 8. In both the cases, an initial burst release was observed as in the above studies. The burst release suggested that the pre-dissolved drug did not show net adsorption onto the silica surface. However, the extent of initial release decreased with an increase in pre-dissolved ATZ concentration. Comparing the dissolution profile in buffer, the presence of pre-dissolved drug suppressed drug release, with 40 µg/mL pre-dissolved ATZ having a larger impact. However, it is important to note that the final total concentration was highest for the case of 40 µg/mL pre-dissolved ATZ.
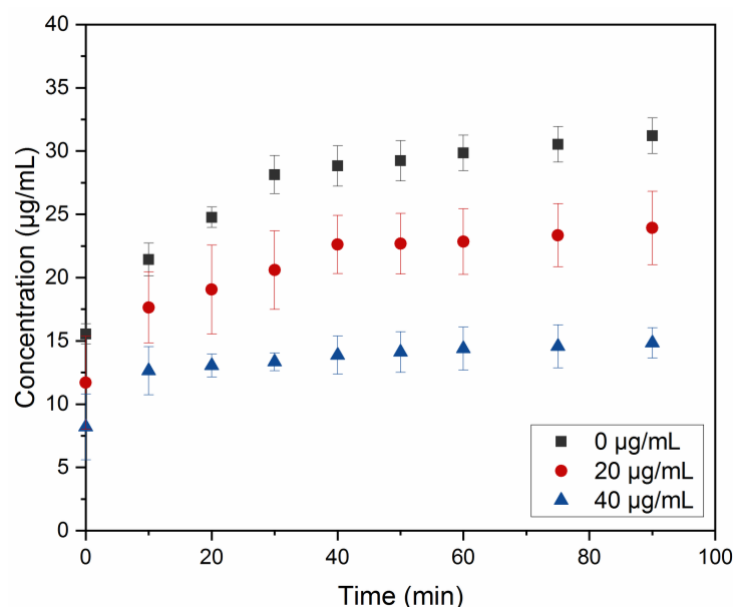
Figure 5.8: Dissolution profile of 20% ATZ-MPS in the presence of pre-dissolved 20 µg/mL and 40 µg/mL ATZ in pH 6.8 phosphate buffer. The y-axis indicates the concentration in the dissolution medium after subtracting the initial pre-dissolved concentration.

Dissolution-absorption measurements were also performed over a longer duration. The continuous removal of drug due to absorption across the membrane should deplete the solution concentration in the donor and result in further release of drug from the formulation. Figure 5.9 shows donor and receiver concentrations of the 20% DL ATZ-MPS formulation for dissolution-absorption measurements over 240 min. As shown in Figure 5.9a, the donor concentration reached a maximum value and declined with time due to subsequent membrane transport. As a result, the maximum concentration in the receiver profile (Figure 5.9b) was followed by a gradual decline in the concentration. Evaluating the total drug release over 240 min, the drug was released constantly during the simultaneous dissolution-absorption measurements, reaching almost 90%. In comparison, for closed-compartment dissolution, only 40% drug was released, with a plateau reached after 60 min (as shown in Figure 5.9c). These observations suggest that removal of drug due to permeation across the membrane promotes additional drug release from the MPS.
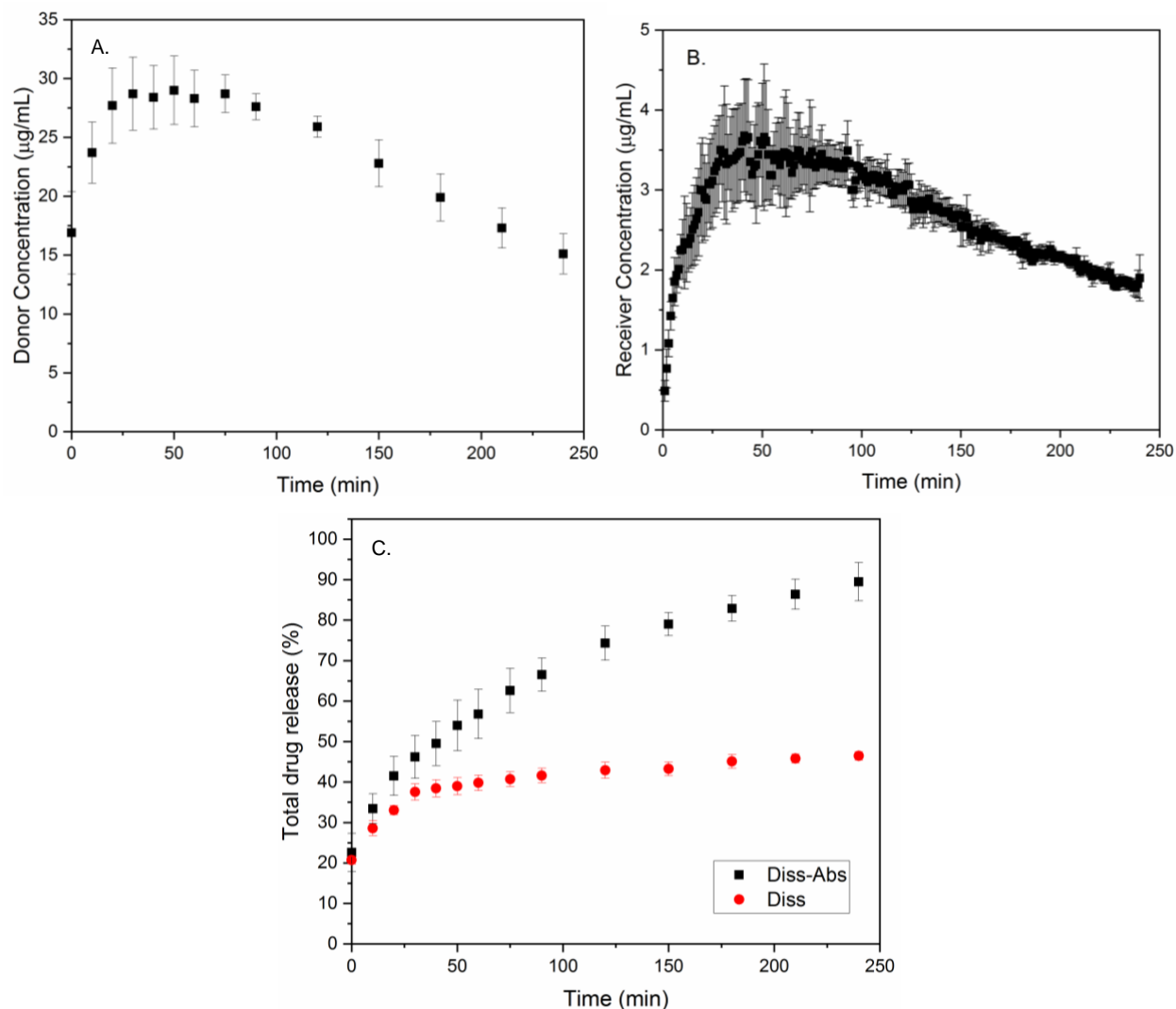
Figure 5.9: (a) Donor, (b) receiver and (c) total drug release during dissolution-absorption measurements over 240 min.

Next, two-step dissolution studies involving a pH shift were conducted. 20% DL ATZ-MPS was first exposed to an acidic medium for 30 min, followed by pH shift to pH 6.8 with initiation of absorption measurements (Figure 5.10). Dissolution in the acidic medium resulted in almost 80% drug release in 30 min. This was significantly higher than the release extent observed for pH 6.8 and can be attributed to the higher solubility of the weakly basic ATZ at a lower pH. Upon pH shift, the donor concentration declined over time owing to simultaneous absorption across the membrane, however, there was only a small extent of additional release. The higher overall concentration in the donor compartment increased the amount of drug reaching the receiver

compartment (relative to pH 6.8 only, Figure 5.7). Clearly, the greater extent of supersaturation generated in the intestinal compartment for the two-step dissolution has a notable impact on the absorption behavior, shown by comparing receiver concentrations of single-step and two-step studies in Figure 5.10c.
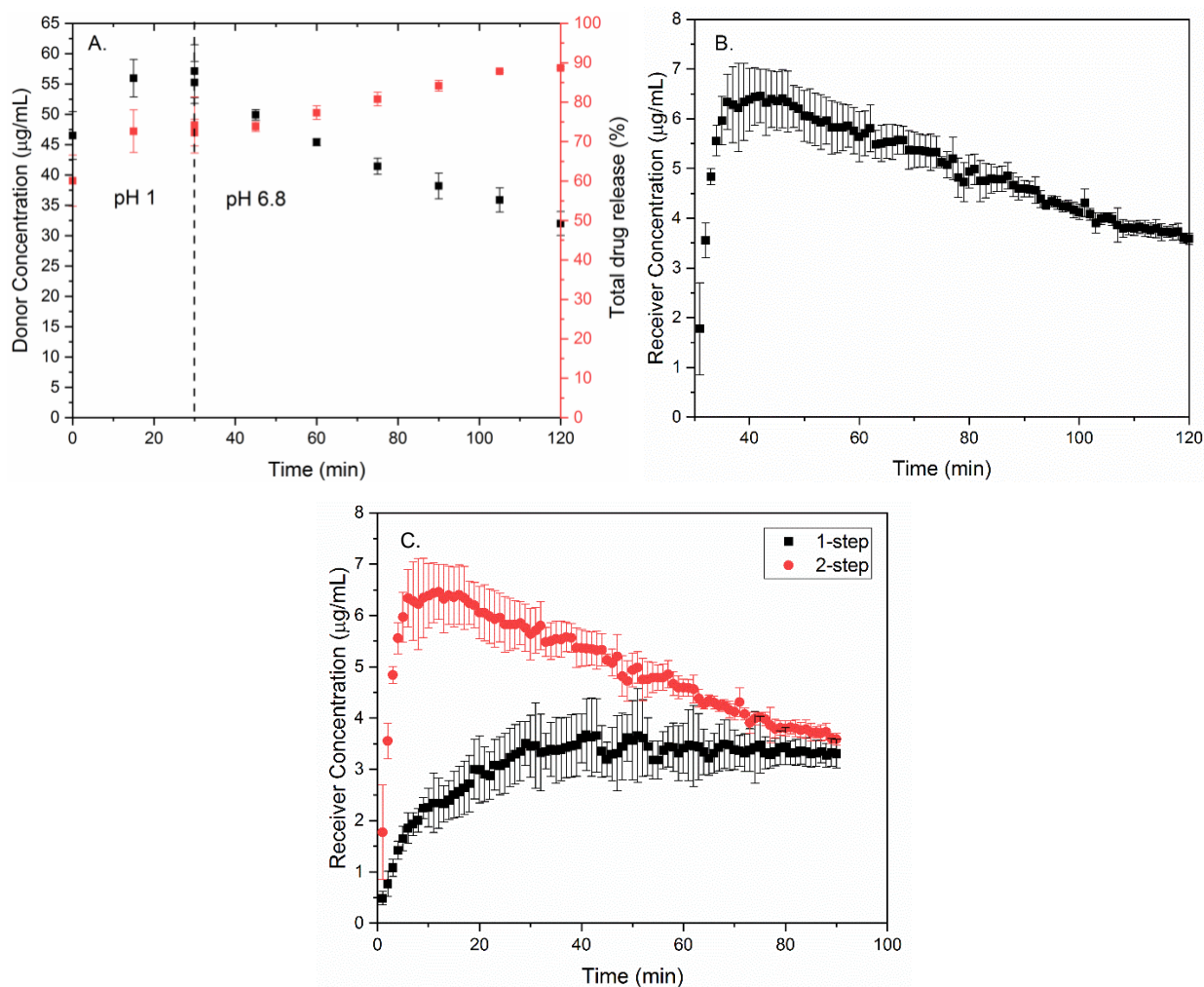
Figure 5.10: (a) Donor concentration, total % drug release, (b) receiver concentration of 20% ATZ-MPS in two-step dissolution-absorption and (c) Receiver concentration profile in single-step and two-step dissolution absorption studies of 20% ATZ-MPS formulation.

The performance of the ATZ-MPS formulation was also compared with that of an ATZ amorphous solid dispersion to provide a direct comparison of two types of amorphous formulation, using a drug loading of 10% in for both formulations and a dose concentration of 200 µg/mL. The dose concentration exceeds the amorphous solubility, and hence formulations can potentially

153

undergo liquid-liquid phase separation (LLPS), as observed previously for the 10% drug loaded HPMC dispersion of ATZ.[83] As shown in Figure 5.11, the donor concentration for the MPS formulation plateaued at a concentration considerably below the amorphous solubility. In contrast, the ASD dissolved to a concentration higher than the amorphous solubility and underwent LLPS (this was also observed visually since the ASD dissolved to form a turbid solution). The ASD formulation provided substantially enhanced absorption relative to the MPS system.
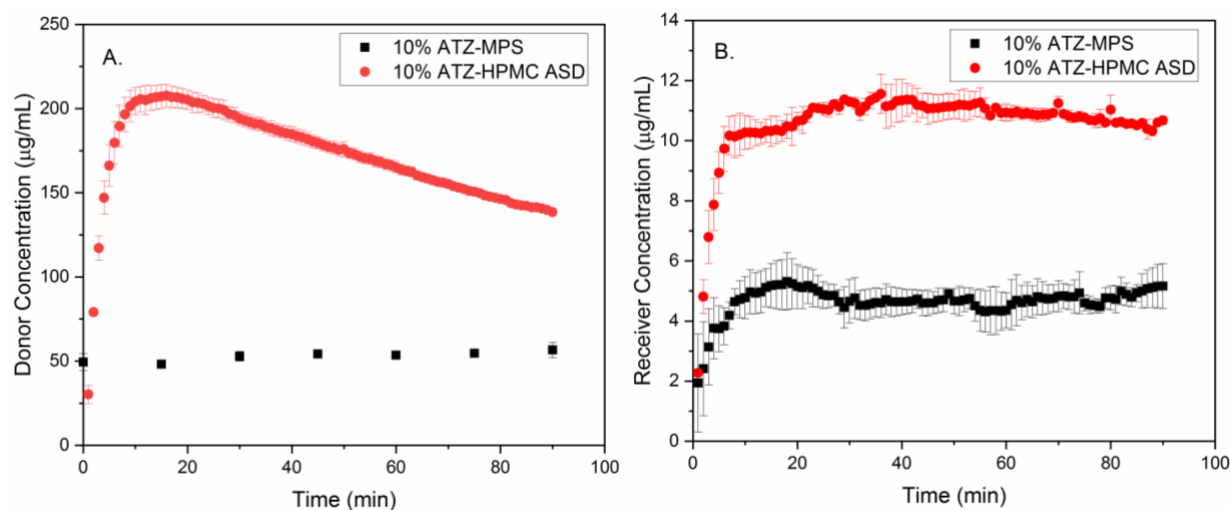
Figure 5.11: (a) Donor and (b) receiver concentration profile of 10% ATZ-MPS and 10% HPMC based ASD formulations.

5.6 Discussion

5.6.1 Nanoconfinement effect in solid-state

Formulating a drug as an amorphous solid is often challenging due to their tendency to crystallize. Crystallization kinetics are highly dependent on the molecular mobility, which in turn varies strongly with the storage temperature relative to the glass transition temperature (T_g). The molecular mobility in a glassy material is notably reduced below T_g, resulting in a lower crystallization tendency.[16,79] Increases in molecular mobility occur when the temperature is increased or following absorption of water from the surroundings.[209] Formulation efforts are consequently typically centered around reducing the drug molecular mobility in the amorphous system. Mesoporous silica is an attractive delivery carrier for amorphous solids as the drug is confined in the nanopores. Confinement can improve stability against crystallization particularly

if the pore size is smaller than critical nucleus size.[25,92,176] Furthermore, the confinement effect can increase the boiling temperature due to capillary condensation and decrease the melting temperature due to increase in the surface energy contributions, reducing the thermodynamic driving force for phase transformation to the crystal.[25,210]

In addition to pore size and specific surface area, intermolecular interactions between silica and the drug also play a role in the amorphization of drugs in mesoporous silica materials. Strong interactions of drug molecules with the pore walls can hinder the molecular arrangement required for crystallization, due to surface immobilization.[22,175,211] The silica surface primarily has silanol groups (Si-OH), which are important for the adsorption of guest molecules. Because silanols are both hydrogen bond donors and acceptors, hydrogen bonding is typically the primary interaction mechanism. The surface reactivity is highly dependent on the number and functionalities of the silanol groups, with isolated silanols being the most reactive sites for adsorption.[212] ATZ has several nitrogen lone pairs and carbonyl moieties that serve as potential hydrogen bond acceptors (Figure 5.1). The alterations in the C=O peaks of ATZ and disappearance of the isolated silanol peak at 3749 cm$_{-1}$ with increasing drug loading, observed from the FT-IR studies, clearly support hydrogen bonding between ATZ and SBA-15 in the MPS formulations. The lack of thermal events for the low drug loading ATZ-MPS formulations are also consistent with nanoconfinement and drug-pore wall interactions. Nanoconfinement of molecules is known to alter thermal events such as T_g and melting temperature,[25] or lead to an absence of thermal events.[175,213] The thermal transitions observed for higher DLs (30 and 50%) can be attributed to overfilling of the pores, with some drug residing on the exterior surface of the silica particles.[25] This is also consistent with the more bulk-like IR spectra observed for these systems. Further evidence of the differences in drug molecular environment as a function of drug loading is provided by the TGA observations. The nanoconfinement effect is expected to result in a higher activation energy for degradation due to the stronger interactions between the drug molecules and the silica surface.[214,215] Indeed, higher degradation temperatures are observed for the low drug loading formulations (5, 10 and 20%) when compared with neat amorphous ATZ.

5.6.2 Interplay between adsorption tendency and dissolution behavior

The utility of an amorphous formulation in oral drug delivery is determined by the extent of the solubility and dissolution rate advantages. Mesoporous silica-based ATZ formulations dissolved fairly rapidly to concentrations above the crystalline solubility of the drug, generating supersaturated solutions. However, the amorphous solubility was not achieved, diminishing the potential bioavailability advantage. In particular, the extent of supersaturation was reduced with increased drug loading. Typically, incomplete drug release from mesoporous silica-based formulations is attributed to drug-silica interactions leading to drug adsorption.[97,198] The adsorption isotherm for ATZ (Figure 5.2a) provides an indication of the adsorption tendency of the drug to MPS in an aqueous environment where the drug is supersaturated. It is apparent that the amount of ATZ remaining in the MPS following dissolution was much greater than expected based on the adsorption isotherm, especially for higher drug loading formulations. The low extent of adsorption in an aqueous environment may be due to competition between the adsorption of two species, i.e. drug and water.[28,216] As the adsorbent surface is covered initially with the water molecules, for drug molecules to adsorb onto the silica surface, displacement of the water molecules is an essential step.[217] Hence, drug adsorption on the surface is thermodynamically favorable only when the increase in the free energy due to displacement of water molecules is balanced by the decrease in the free energy due to drug adsorption on the surface. As a result, a complete coverage of drug molecules alone on the silica surface is unlikely if the drug is adsorbing from the aqueous solution. Therefore, the monolayer coverage observed during drug-silica adsorption in aqueous solution does not indicate complete coverage by drug molecules as there are likely a large number of water molecules still present on the surface. The interplay between drug release and drug adsorption is evident from the dissolution studies that were carried out with pre-dissolved ATZ in the buffer (Figure 5.8). A decrease in the ATZ concentration released with an increase in the amount of pre-dissolved ATZ highlighted the impact of a dynamic equilibrium between solution concentration and the drug release. Higher pre-dissolved drug concentration resulted in a lower driving force for drug to release from the silica surface.

Poor wetting of the formulations may also contribute to the suboptimal release seen for the high drug loading ATZ-MPS formulations.[97] This is because the drug release rate is also controlled by the transport of water into the pores, which then displaces the drug adsorbed onto the surface,

which in turn depends on the balance between the free energy of adsorption and free energy of displacement of drug molecules. Drug release from mesoporous silica surface is a diffusion controlled process and depends on the rate of diffusion of water into the pores and diffusion of desorbed drug molecules out of the pores and into the bulk aqueous media.[93,95] As more drug is loaded into the mesoporous silica particles, because atazanavir is a hydrophobic molecule, the surface will become more hydrophobic due to accumulation of drug in the pores.[97,178] Based on these consideration, at low drug loadings (5% and 10%), a reduced extent of incomplete release can be attributed largely to the drug-silica interactions. However, as the drug loading was increased (20-50%), the lower drug release can be attributed in large part to the increased hydrophobicity of the formulation, rather than as a result of strong ATZ-SBA-15 interactions. This is consistent with the bulk-like behavior observed for higher drug loading MPS formulations in the solid-state characterization, indicating overfilling of the pores, and an increased extent of drug-drug interactions. Further, the 5% DL ATZ-MPS showed 30% burst release while negligible burst release was observed for the 50% DL ATZ-MPS.

5.6.3 Impact of absorptive sink on drug release

Incomplete drug release from mesoporous silica-based formulations impacts membrane permeation behavior as highlighted by recent mass transport studies on ritonavir-loaded silica formulations, wherein the formulation showed a significantly lower mass flow rate across a cellulose membrane due to incomplete release when compared with the control maximally supersaturated solution.[27] Since the dynamic equilibrium between drug adsorbed on the surface and drug in the solution is likely to affect the amount of drug released, it was hypothesized that absorption of drug across a membrane would improve drug release by continually reducing the amount of drug in the donor solution, driving the desorption process. A clear enhancement in the extent of drug release was observed under absorptive dissolution conditions over prolonged time periods (Figure 5.9). Thus, according to the Le Chatelier's principle, the removal of drug by transport across the membrane, and the subsequent decrease in drug concentration may improve the release of drug in the lumen as the equilibrium shifts towards desorption.[218] These results highlight an important consideration for *in vitro* testing of mesoporous silica-based formulations. An absorptive compartment during dissolution studies can provide more *in vivo* relevant insights into the formulation performance when compared with a conventional closed-compartmental

157

dissolution setup. Figure 9c clearly demonstrates the difference in formulation performance, wherein the drug release plateaued at 40% in a closed compartmental dissolution test, relative to 90% release under absorptive conditions.

Evaluation of pH impact on the release properties is also an important consideration to better predict *in vivo* performance. As a basic compound with a pKa of 4.49, ATZ has significantly higher solubility in acidic condition.[133] Since silica has isoelectric point at pH 2, in solutions below pH 2, silica shows a positive surface charge, with most of the silanol groups being protonated.[219] Thus, the rapid ATZ release in acidic conditions can be attributed to the significantly higher ATZ solubility at pH 1 and electrostatic repulsion between positively charged ATZ and positively charged silica. This in turn leads to the generation of a high extent of supersaturation when the pH is increased to 6.8, where the solubility of the drug is reduced. Indeed, as shown in Figure 10c, the supersaturation generated in the two-step dissolution experiment, and consequently the mass transfer rate, is much higher than that observed if the dissolution is performed at pH 6.8 (i.e. 1 step dissolution). These studies clearly highlighted gastrointestinal pH as another physiological factor impacting drug release from mesoporous silica-based formulations which should be considered when designing *in vitro* dissolution studies.

5.6.4 Application of mesoporous silica-based drug delivery systems for oral delivery

Mesoporous silica offers several advantages as a drug delivery system for poorly soluble drugs including greater physical stability to drug crystallization, rapid release and generation of supersaturation. However, it appears that the extent of supersaturation generated may be limited. Thus, similar to ritonavir systems, dissolution of ATZ mesoporous silica-based formulations at a dose concentration above the drug amorphous solubility did not result in attainment of the amorphous solubility, which marks the maximum supersaturation. This contrasts with other amorphous formulations, namely ASDs, which yield a higher supersaturation level following dissolution, and consequently a greater extent of drug permeated across a membrane in a given time period, as demonstrated in Figure 11. Although drug release from mesoporous silica is dynamic and is driven by the removal of drug by transport across the membrane, this is insufficient to compensate for the lower extent of supersaturation achieved. However, higher supersaturation from ATZ-MPS formulation may be generated by first dissolving in an acidic medium. The pH-

shift to pH 6.8 renders the solution supersaturated, with the solution concentration plateauing at the amorphous solubility whereby the solution may undergo LLPS. Preliminary studies of two-step dissolution (pH 1 followed by transfer to pH 6.8) were carried out for a 10% ATZ-MPS formulation. Upon pH-shift, the solution concentration plateaued at the amorphous solubility, although no LLPS formation was observed. Hence, the reservoir effect arising from the presence of drug-rich nanodroplets formed via LLPS[10,83] may not occur with MPS formulation. Nevertheless, atazanavir is typically administered with food.[220] Hence, the formulation would not be exposed to low gastric pH, and thus the advantage from dissolution at a low pH may not be obtained, due to the buffering effect of ingested food. This type of pH-dependent dissolution behavior is less of a concern for ASDs where formulations are often designed to release in the intestinal environment.

5.7 Conclusions

Atazanavir, present in amorphous form in mesoporous silica, demonstrated a complex release behavior, which depends on a number of factors. The extent of release and level of supersaturation achieved depended on drug loading, pH, and the presence or absence of an absorptive compartment in the dissolution test. Low pH, low drug loading, and the presence of an absorptive compartment were found to be favorable for driving drug release of atazanavir from mesoporous silica formulation. However, a comparable driving force for membrane transport, i.e. the extent of supersaturation that could be generated, could not be achieved when compared to alternative amorphous formulations, namely an amorphous solid dispersion. Given the multiple factors impacting drug release, design of an appropriate *in vitro* evaluation methodology is clearly critical to better evaluate mesoporous silica-based formulations for oral drug delivery.

CHAPTER 6.   INFLUENCE OF ELECTROSTATIC INTERACTION BETWEEN DRUG AND SILICA ON DISSOLUTION BEHAVIOR OF MESOPOROUS SILICA-BASED ORAL DRUG DELIVERY SYSTEMS

6.1   Abstract

Mesoporous silica particles are attractive carriers for poorly soluble drugs whereby confinement of drug in the mesopores leads to amorphization and the potential for enhanced oral delivery However, interactions between drug molecules and the silica surface can lead to incomplete drug release. The strength of the interaction depends on the silica surface chemistry, which varies as a function of pH, as well as on drug ionization. Herein, the adsorption and dissolution behavior of weakly basic drugs was evaluated as a function of pH to understand the impact of electrostatic interactions on the performance of mesoporous silica-based formulations. Higher adsorption was noted when the drug interacted with the silica surface via electrostatic interaction versus hydrogen bonding. Higher adsorption, in turn, led to a lower extent of drug release. In two-stage release studies, for drugs with a pKa close to intestinal pH values, pH-shift from low to higher pH solutions resulted in a decrease in solution concentration. Further investigations demonstrated that this was due to re-adsorption of drug released in the acidic medium. Two-stage release studies were also coupled with the mass transport measurements. Only a slight improvement in drug release due to simultaneous absorption across the membrane was observed, suggesting strong drug adsorption to the silica surface arising from favorable electrostatic interactions. This study distinctly highlights physiological parameters such as solution pH as important considerations in designing mesoporous silica-based formulation for poorly soluble drugs. It also underscores the importance of incorporating *in vivo* relevant conditions in i*n vitro* testing to better evaluate these complex formulations due to the significant effect of dissolution media on the release behavior.

6.2   Introduction

In recent years, interest in supersaturating drug delivery systems as a means to enhance the delivery of poorly water-soluble drugs have grown. The supersaturated solution generated by dissolution of these formulations leads to a higher driving force for absorption across the gastrointestinal membrane, thereby improving the bioavailability of drug.5 Mesoporous silica-

based drug delivery systems, wherein the drug is encapsulated in mesoporous silica particles, are attracting increasing attention in this context.[181] Mesoporous silica materials offer a large specific surface area, high pore volume and an ordered pore network, making them attractive as a drug carrier system. Loading drug into the silica nanopores suppresses drug crystallization due to confinement effects,[24,25,176] leading to an amorphous formulation with enhanced physical stability in particular for pore sizes smaller than the drug critical nucleus size.[25,176] The maximum drug loading in these formulations depends on the properties of both the drug and the silica material including excipient specific surface area, pore diameter, pore volume, interactions between drug and silica surface, size of the drug molecule and the solvent used for drug loading.[173,177,178] Due to their amorphous nature, mesoporous formulations often show dissolution profiles with rapid burst release of the drug and generation of a supersaturated solution, leading to improved bioavailability relative to crystalline drug.[27,184]

Drug release from mesoporous silica formulations surface depends on several factors including as pore size, pore volume, drug-silica intermolecular interactions, formulation hydrophobicity and drug loading.[187,190] The strength of the interaction between drug molecules and the silica surface is a critical factor impacting both drug loading and release. Silica surfaces display complex chemistry and are typically covered by silanol groups which exist as isolated silanols ($\equiv$Si-OH), vicinal silanols (HO-Si-O-Si-OH) and geminal silanols (=Si(OH)$_2$).[28] Silanols can serve as both hydrogen bond donors and acceptors. Thus, hydrogen bonding is the most common mechanism for interactions with the guest molecule.[28,29] As isolated silanols do not participate in hydrogen bonding with other silanols, they are the most reactive sites for interaction with the drug.[29] Depending on solution pH, silanols can show different extents of protonation leading to positive, negative or neutral surface charge. The isoelectric point of silica lies around pH 2, with positive and negative charges below and above this pH respectively.[221] Thus, at certain pH conditions, silica and guest molecules can interact via electrostatic interactions. Drugs have been shown to interact with the silica surface either through electrostatic interaction or hydrogen bonding depending on drug chemistry and pH conditions.[30] Strong interactions between drug and silica typically result in higher drug loading and sustained drug release. Poor drug-silica interactions, on the other hand, lead to lower drug loading and a burst release.[97,222] Typically, drug loading and drug release are adjusted by functionalization of the silica surface or release kinetics

are modulated using environmental stimuli such as pH or temperature.[90] Silanol-drug hydrogen bonding interactions are relatively weak, hindering attainment of sustained drug release.[30] Consequently, silica surfaces are functionalized by grafting organic silanes to the silanol groups. This alters the isoelectric point of the silica material, inducing stronger electrostatic interactions between drug molecules and the silica surface or hydrophobicity to the material which results in a controlled or site-specific release.[90,223] For instance, amine-functionalization of the silica surface generally results in isoelectric point around pH 7.[97] Hence, these materials can be used to control the release of weakly acidic drugs at higher pH conditions due strong electrostatic interactions between negatively charged drug and positively charged silica.[30,224] Similarly, stimuli-responsive drug release utilizes environmental stimuli to release drug at a particular site.[96] The most common stimuli used to control the release profile is the pH of the environment.[225]

Clearly, pH is an important factor that can influence the performance, and ultimately the oral bioavailability of drugs delivered using mesoporous silica-based formulations (MPS), given the variable pH environment of the gastrointestinal tract. Notably, poorly soluble ionizable drugs exhibit pH-dependent solubility whereby a change in the ionization and solubility of the drug during GI transit can also alter the extent of adsorption to silica. Dissolution studies of ibuprofen loaded in mesoporous silica showed slower release in pH 1.2, and improved release at pH 7.4.[226] Ibuprofen is a weakly acidic compound with a pKa of 5.6, and the improved release was attributed to the higher solubility at higher pH. Similarly, indomethacin and glibenclamide release from MPS formulations was observed to improve upon pH-shift from gastric to intestinal pH conditions. In addition to an increase in solubility, rapid drug release at higher pH was attributed to electrostatic repulsion between negatively charged drug molecules and the negatively charged silica surface.[227] The pH-sensitive release of drug from mesoporous silica was also employed to achieve colon-specific drug delivery systems of an anionic drug. Sulfasalazine was loaded into mesoporous silica modified with triethylammonium groups. Since modification of the silica surface shifted the isoelectric point to pH 7.38, drug release was minimized in gastric conditions while significant release was observed at pH 7.4 and pH 8, thus affording drug delivery to the colon.[228]

Few studies have focused on the pH-dependent adsorption and release of weakly basic compounds for mesoporous silica systems. An important consideration for basic drugs is the

supersaturation that can be generated upon transit from gastric to intestinal pH conditions which results from the higher drug solubility at pH conditions lower than the drug pKa. Supersaturated solutions are known to improve membrane absorption due to higher driving force for membrane transport.[5] However, for MPS formulations, supersaturation can increase the amount of drug adsorbed onto the silica surface, thereby lowering the amount of molecularly dissolved drug available for membrane absorption.[199] The effect of transition from gastric to intestinal pH conditions was observed in dissolution studies of itraconazole MPS formulations, wherein the itraconazole concentration declined rapidly due to crystallization from the supersaturated solution generated upon pH-shift.[184] In our recent studies with the weak base, atazanavir, drug release from mesoporous silica was improved significantly when dissolution was carried out first in acidic conditions prior to pH-shift to intestinal pH. (ref) By adding a polymer to the dissolution medium, the supersaturated solution generated upon pH-shift could be maintained for experimental time frame and improved in vitro absorption was observed relative to single step dissolution at higher pH conditions. The goal of the current study was to further investigate the influence of pH on the adsorption and release of poorly soluble weakly basic drugs compounds from mesoporous silica. Three weakly basic drugs, atazanavir (pKa 4.49)[133], ketoconazole (pKa 2.9 and 6.5)[229,230] and clozapine (pKa 7.5)[231], were evaluated for their adsorption behavior at various physiologically-relevant gastrointestinal pH values.[148] Each drug was loaded in mesoporous silica (SBA-15) at a 20% (w/w) drug loading (DL) and the release performance was evaluated in different pH conditions. Drug release was also evaluated using a two-step dissolution test, simulating gastric to intestinal pH transitions in fasted and fed states, in combination with mass transport measurement using a recently developed absorptive dissolution testing apparatus. Absorptive dissolution testing has been observed to alter the kinetics of competing processes involving mass transfer, such as crystallization or adsorption to a surface due to removal of drug via membrane transport.[83,195] Herein, the impact of concurrent absorption across a membrane on drug release extent and kinetics was evaluated.

6.3 Materials

Atazanavir (ATZ) was purchased from Gojira Fine Chemicals, LLC (Bedford Heights, OH) and ketoconazole (KET) and clozapine (CLZ) were obtained from Hawkins, Inc. (Minneapolis, MN). SBA-15 with pore size of 7.1 nm and specific surface area of 586 m_2/g was purchased from

Glantero (Cork, Ireland). Hydroxypropyl methylcellulose (PharmCoat 606) (HPMC) was obtained from Shin-Estu Chemicals (Niigata, Japan). HPLC grade acetonitrile and methanol were supplied by Fisher Scientific (Chicago, IL). Concentrated HCl, NaOH, buffer salts and triethylamine (TEA) were also purchased from Fisher Scientific (Chicago, IL). Aqueous media at four different pH values were used and 100 µg/mL HPMC was pre-dissolved to prevent drug crystallization. The acidic medium consisted of 0.1 N HCl, 50 mM acetate buffer was used for pH 4.5 and pH 5.5 and 50 mM phosphate buffer was used for pH 6.8 solutions.

6.4   Methods

6.4.1   Drug loading procedure

Atazanavir, ketoconazole and clozapine were loaded into SBA-15 particles by the incipient wetness impregnation method,[175] wherein depending upon the drug, the desired volume of concentrated methanolic stock solution (20 – 40 mg/mL) was added to SBA-15 such that final drug loading was 20%. The addition of stock solution was followed by vigorously mixing using a spatula. The samples were dried by storing in an oven at 40 °C overnight, followed by storage under vacuum for 48 h. The drug content was confirmed by dispersing a known amount of sample in methanol under sonication for 30 min. The sample was then centrifuged at $21,1000 \times$ g for 10 min and the supernatant were analyzed by HPLC.

6.4.2   Adsorption Isotherms

Adsorption isotherms for ATZ, KET and CLZ were generated by adding a small aliquot of a concentrated methanolic stock solution of each drug to an aqueous solution containing a known amount of SBA-15. The suspension was equilibrated for 2 h (rapid equilibrium was observed for all systems in the preliminary studies) at 37 °C. The amount of SBA-15 added in the aqueous media was equivalent to the amount of silica present after dissolution of 20% DL formulation. Adsorption was evaluated for a wide range of drug concentrations, at different solution pH values, namely pH 1, 4.5, 5.5 and 6.8. The amount of methanol added was less than 0.5%. Following equilibration, the samples were centrifuged in a Sorvall Legend Micro 21 Centrifuge (Thermo Scientific, Inc., IL) at 14,800 rpm ($21,100 \times$g rcf) for 10 min and analyzed by high pressure liquid

chromatography as detailed below. The amount of drug adsorbed was determined by evaluating the difference in the amount of drug at the initial and equilibrium concentrations.

6.4.3   Zeta Potential Measurements

The zeta potential of SBA-15 particles was measured using a Nano-Zetasizer (Malvern Instruments, Westborough, MA) for pHs ranging from 1 to 10, using concentrated HCl and NaOH solutions to adjust pH. The measurements were carried out at 37 °C using disposable capillary zeta cells.

6.4.4   Dissolution studies

20% DL mesoporous silica formulations of ATZ, KET and CLZ were analyzed for drug release behavior in different media. The target drug concentration was approximately equivalent to the amorphous solubility of the free base form of the drug, i.e. 75 µg/mL for ATZ, 50 µg/mL for KET and 150 µg/mL for CLZ.[83,232] Dissolution studies were performed in 0.1 N HCl, pH 4.5 50 mM acetate buffer, pH 5.5 50 mM acetate buffer and pH 6.8 50 mM phosphate buffer. Two step dissolution tests were carried out by first suspending the formulations in acidic media for 30 min followed by pH increase to pH 4.5, 5.5 or 6.8, by addition of concentrated NaOH solution, and drug release was monitored for an additional 90 min. Two-step dissolution studies were also carried out by initial suspension in pH 4.5 media followed by pH shift to 5.5. All the dissolution studies were carried out in 50 mL of fluid at 37 °C.

To perform dissolution in the presence of an absorptive compartment, two-step dissolution testing was carried out using a previously developed flow-through, high surface area absorptive dissolution testing apparatus.[126] A cellulosic hollow fiber membrane module (surface area 100 cm2, pore size 15 nm) was used to simulate the absorption process. Following dissolution in an acidic medium, the absorption measurements were initiated after pH-shift to 6.8. The receiver fluid was pH 6.8 50 mM phosphate buffer. The flow rate in the donor and receiver channel was maintained at 4 mL/min. The measurements were carried out at 37 °C. The receiver concentration was measured in-line using a flow-through UV probe, connected to a UV-Vis spectrometer (SI Photonics, Tuscon, AZ). The donor volume was 50 mL and a 10 µm cannula filter (Agilent, Santa

Clara, CA) was used at the entrance of the donor channel tubing to prevent water-insoluble silica particles from entering the hollow fibers. The donor concentration was measured by high pressure liquid chromatography following periodic sampling and centrifugation. All measurements were carried out in triplicate.

6.4.5   High Pressure Liquid Chromatography

The drug concentration was analyzed by high pressure liquid chromatography (HPLC) using an Agilent HPLC 1260 Infinity II system (Agilent Technologies, Santa Clara) and an Eclipse Plus C18 4.6 mm × 30 cm × 5 µm column, with a UV detector. ATZ analysis was performed using mobile phase of 60:40 v/v acetonitrile: pH 2.5 water (acidified with orthophosphoric acid) and a flow rate of 0.7 mL/min with a run time of 7 min. The sample injection volume was 15 µL and concentrations were detected at 210 nm. For KET, samples from dissolution in acidic medium were analyzed using a mobile phase of 50:50 v/v acetonitrile: pH 2.5 water (acidified with orthophosphoric acid), a flow rate of 0.7 mL/min and a run time of 6 min. Samples from all other pH media were analyzed using a mobile phase of 60:40 v/v acetonitrile: water, a flow rate of 1 mL/min and a run time of 8 min. The sample injection volume was 20 µL and the UV-detector wavelength was set to 230 nm. Similarly, for CLZ, acidic samples were analyzed using a mobile phase of 40:60 v/v acetonitrile: pH 2.5 water (acidified with orthophosphoric acid), a flow rate of 0.7 mL/min and a run time of 7 min while all the other samples were analyzed using a mobile phase of 70:30 v/v acetonitrile: water, a flow rate of 1 mL/min and a run time of 7 min. 20 µL sample injection volume was used and CLZ concentration was detected at 254 nm. All the samples were diluted with 50:50 v/v acetonitrile: water prior to analysis.

6.5   Results

6.5.1   Adsorption isotherms as a function of pH

To investigate drug adsorption at different pHs and the resultant impact on the release performance of MPS formulations, weakly basic model compounds with different pK_as were selected to enable the impact of different types of drug-silica interactions to be evaluated. The percent ionization of each drug as a function of pH was determined using the Henderson-

Hasselbalch equation (Figure 6.1). KET has two pKa values (piperazine nitrogen and imidazole nitrogen), while the other drugs have a single pKa.
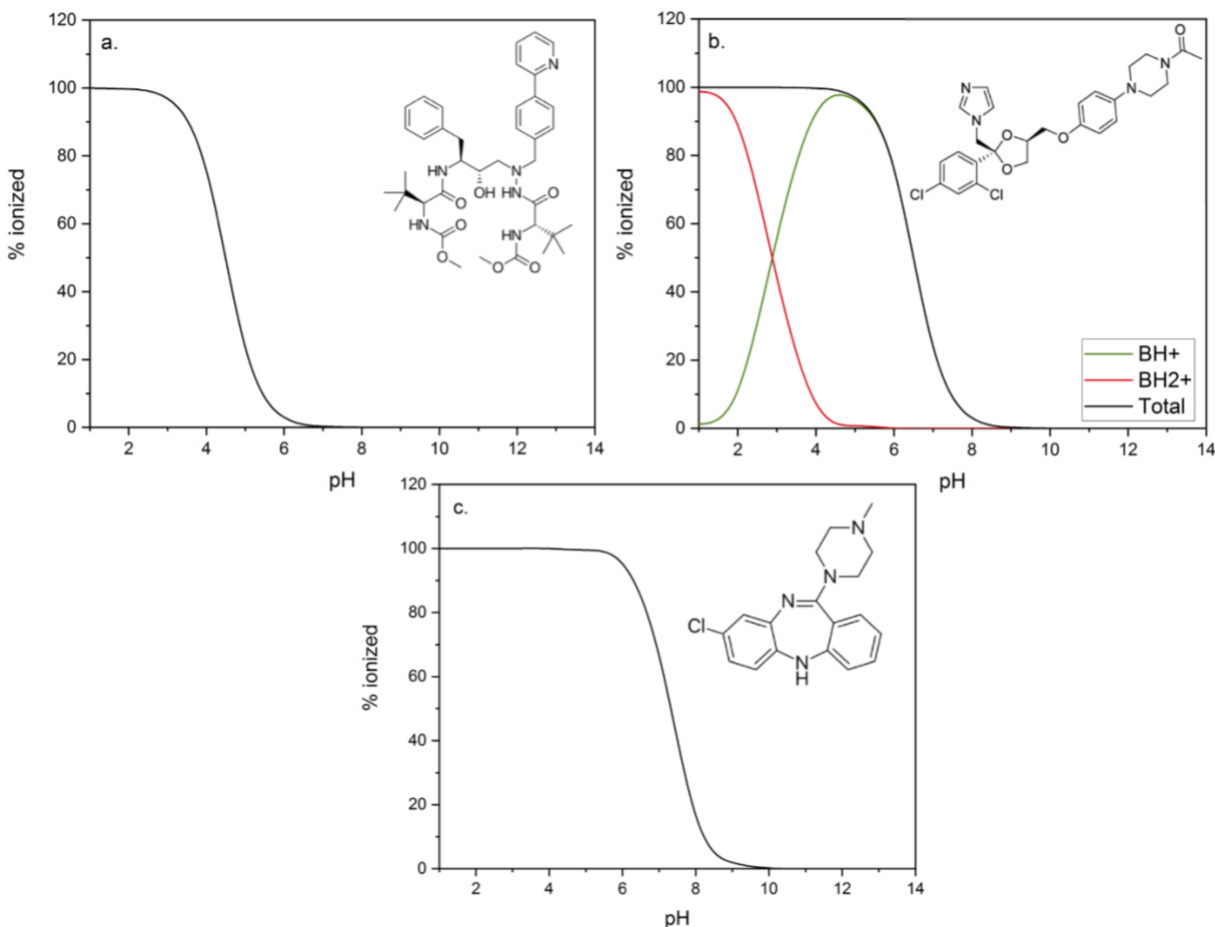
Figure 6.1: The percentage of drug ionized as a function of pH for (a) atazanavir (pKa 4.49), (b) ketoconazole (pKa 2.9 and 6.5) and (c) clozapine (pKa 7.3). The molecular structures are shown as inserts.

The surface chemistry of SBA-15 in an aqueous environment was probed by determining zeta potential as a function of solution pH. As seen in Figure 6.2, SBA-15 showed a small positive charge below pH 2. Above pH 2, the silica surface became negatively charged as the silanol groups became deprotonated and the electric charge increased with further increase in pH. The isoelectric point of SBA-15 was found to be at pH 2, consistent with that reported in the literature.

167
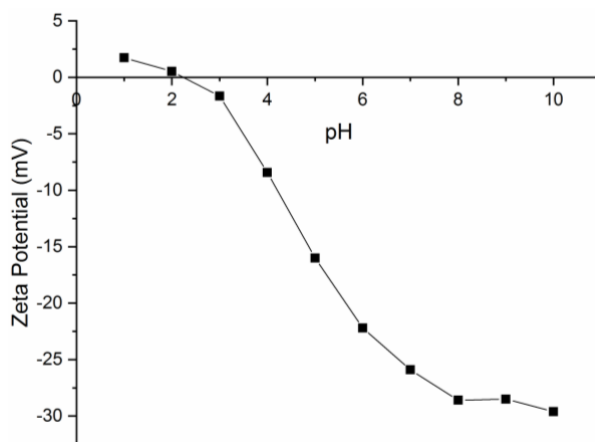
Figure 6.2: The zeta potential of SBA-15 as a function of pH of the aqueous media.

Figure 6.3 shows adsorption isotherms of ATZ, KET and CLZ at four different physiologically-relevant pHs. Each drug displayed a distinctive adsorption behavior as a function of pH. ATZ showed higher adsorption at pH 1 and 4.5 as compared to pH 5.5. At pH 6.8, the amount of ATZ adsorbed decreased by half. In the case of KET, low adsorption was observed at pH 1, however, adsorption increased notably at pH 4.5 with further slight increases at pH 5.5 and pH 6.8. CLZ, on the other hand, showed no adsorption in acidic media (hence, is not included in Figure 6.3) and the adsorption increased substantially from pH 4.5 to pH 6.8. It was evident that the deprotonation of silica and the ionization of the drugs altered the strength of interactions between the drug and the silica surface and hence impacted the adsorption tendency.
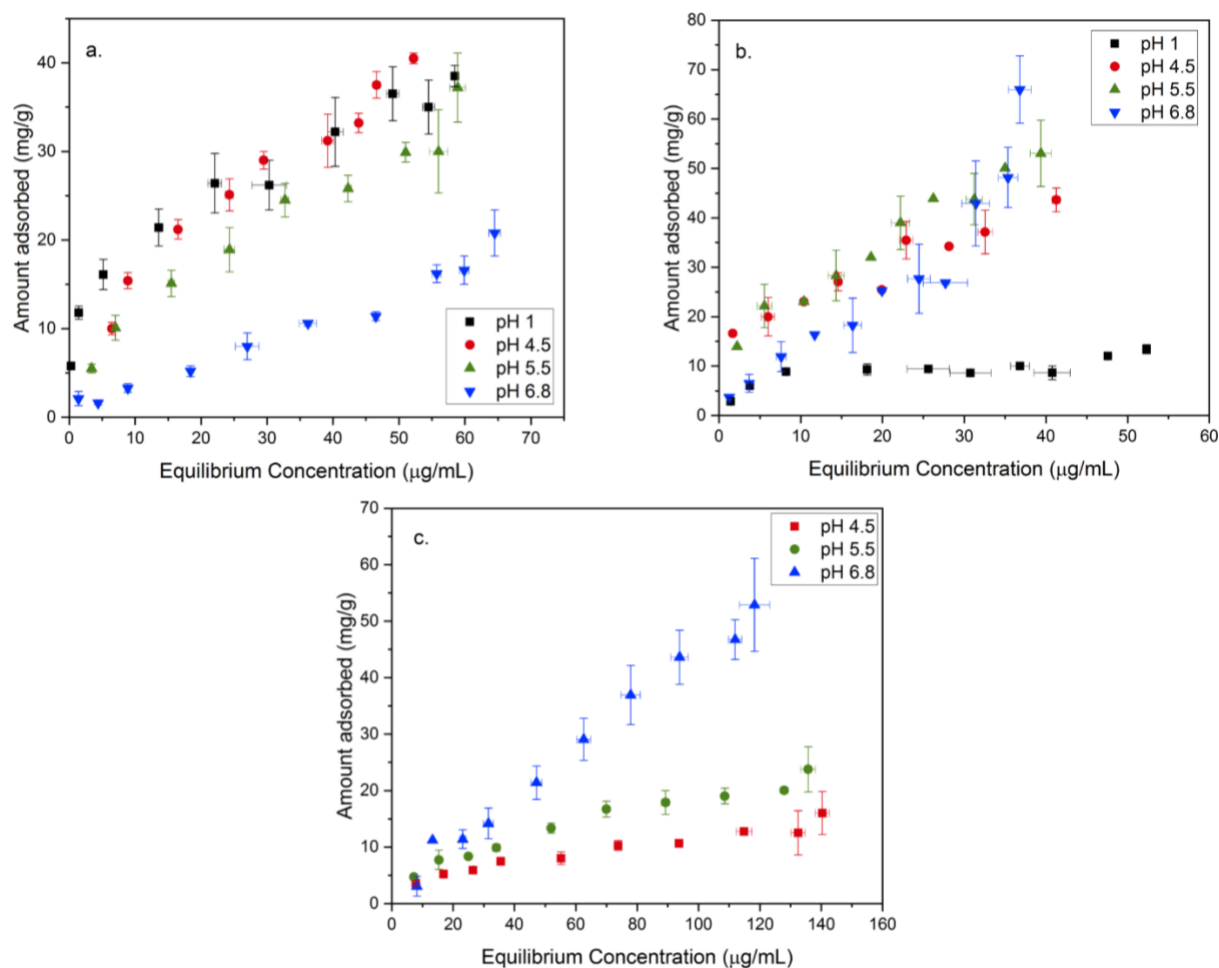
Figure 6.3: Adsorption isotherms of a) ATZ, b) KET and c) CLZ on SBA-15 in aqueous solutions of different pH values.

6.5.2 Dissolution of MPS formulations in different pH environment

20% DL MPS formulations were confirmed to be amorphous using powder X-ray diffraction and confinement effect was observed in differential scanning calorimetry (Figure S6.1 and S6.2). Figure 6.4 shows the dissolution profile of ATZ, KET and CLZ-loaded MPS formulations at various pH conditions, with different release profiles being observed. ATZ-MPS formulations showed a burst release in acidic media, releasing 70% of drug immediately. Thereafter, no further release was observed over a 60 min period. At pH 4.5, 5.5 and 6.8, a smaller extent of burst release (10 – 20%) was observed, followed by gradual drug release which plateaued at about 40% release after 60 min. Thus, at higher pHs, ATZ-MPS formulations displayed notably lower drug release. KET-MPS systems showed immediate and almost complete release (80-90%)

at pH 1 and 4.5. Interestingly, at pH 5.5 and pH 6.8 release was substantially reduced. Dissolution of CLZ-MPS showed rapid and complete release at pH 1 and pH 4.5, with a slight reduction at pH 5.5, and a considerably lowered release at pH 6.8. Clearly, solution pH had a significant impact on dissolution behavior.
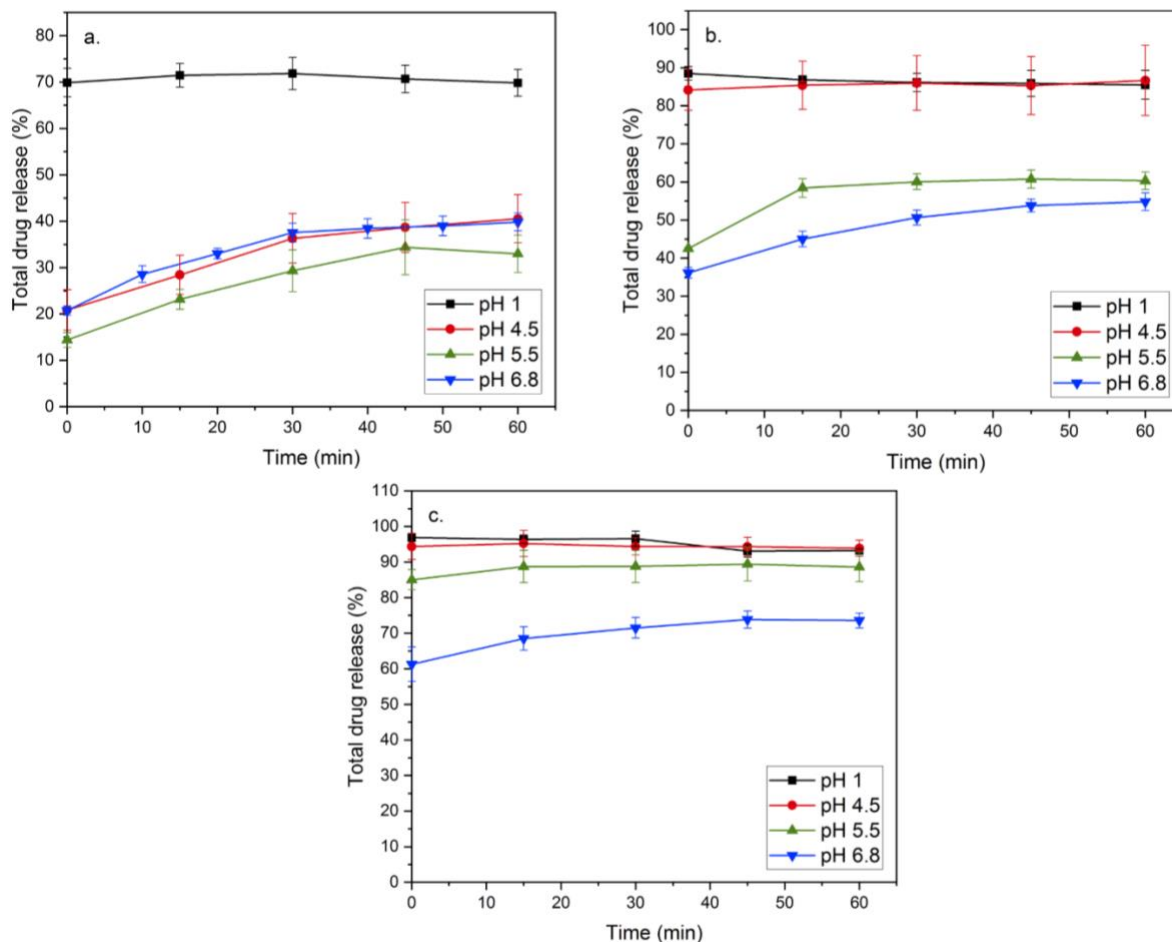
Figure 6.4: Dissolution of 20% drug loaded mesoporous silica particles of (a) atazanavir, (b) ketoconazole and (c) clozapine in pH 1, pH 4.5, pH 5.5 and pH 6.8.

Next, two-step release testing was performed wherein the formulations were first suspended in acidic medium for 30 min followed by an increase in solution pH, mimicking the pH increase experienced during transit from gastric to intestinal conditions (Figure 6.5). In the case of ATZ, the formulation showed 70% release at pH 1, (consistent with single step dissolution, Figure 6.4a). Following pH-shift to 4.5, a small decline in concentration was observed, with total release plateauing at 60%. With pH-shift to pH 5.5 and 6.8, no change in the concentration was observed

over 120 min. For a fed state pH environment (pH 4.5 with shift to pH 5.5), poor release of ATZ was observed, with only a small increase in the release upon pH shift. Different patterns of release behavior were observed for KET and CLZ. KET showed complete release in low pH media, with a notable decrease in solution concentration occurring following pH-shift to pH 5.5 or pH 6.8, whereby almost 30-35% of dissolved drug was lost from the solution. A similar pattern of dissolution behavior was observed for CLZ. Complete drug release was observed at low pH conditions and change to higher pH once again decreased the solution concentration. For example, there was an approximately 30% decrease in CLZ concentration upon pH-shift from 1 to 6.8. For dissolution studies in a fed-state pH environment, CLZ showed complete release at pH 4.5, with a 15% reduction in solution concentration when the pH was increased to 5.5. The concentration drop upon pH change was certainly of interest and warranted further investigation.
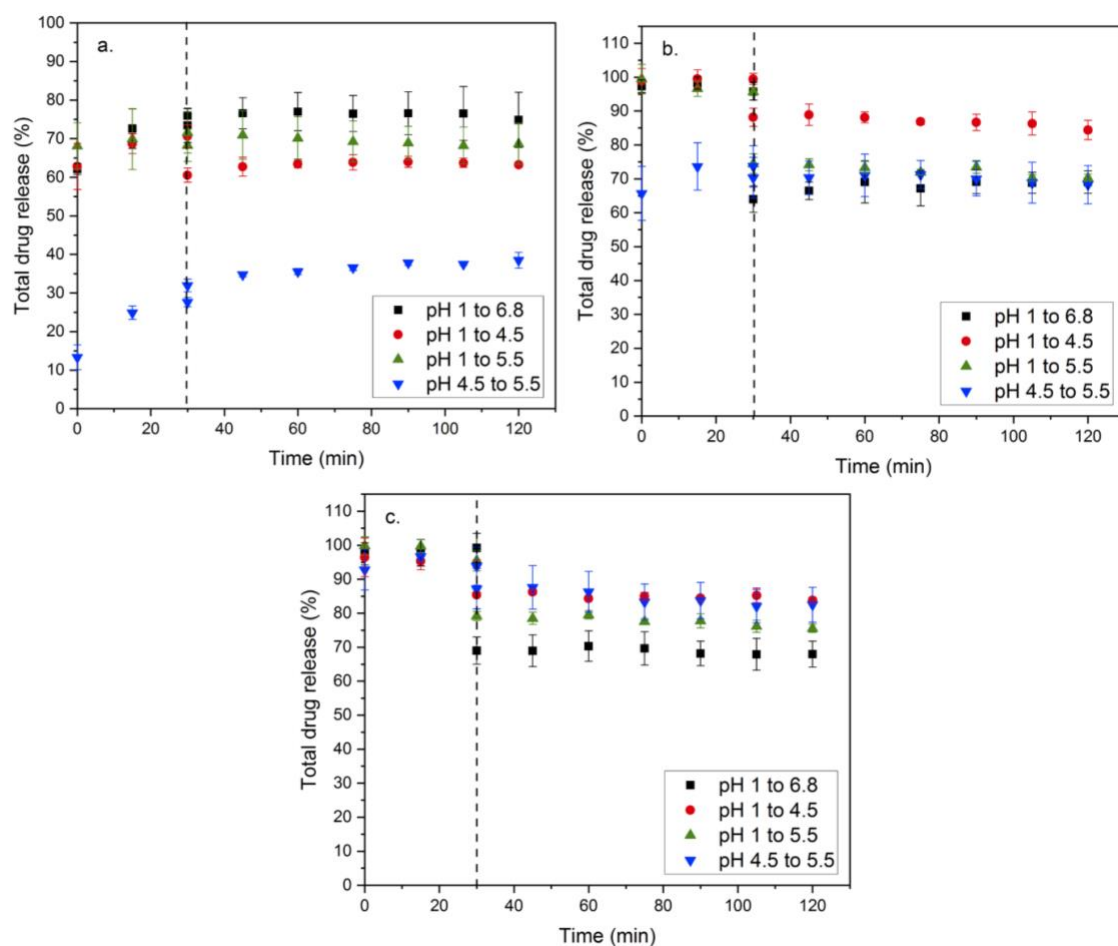
Figure 6.5: Two-step dissolution of (a) ATZ-MPS, (b) KET-MPS and (c) CLZ-MPS. The vertical line indicates the time of pH-shift.

6.5.3 Effect of competing adsorbate species on adsorption and dissolution

The decrease in KET and CLZ concentration upon pH-shift to higher pH values suggested that the drug might be undergoing crystallization. However, X-ray powder diffraction of the precipitate obtained at the end of the experiment showed no diffraction peaks (Figure S6.3). An alternative explanation for the immediate drop in concentration is re-adsorption of the released drug onto the silica surface.[27] Drugs typically interact with the silica surface via hydrogen bonding or electrostatic interactions.[30,90] According to the adsorption isotherms of KET and CLZ at different pHs, drug adsorption is favored at higher pH conditions relative to in acidic media. As KET and CLZ are weakly basic drugs with pK$_a$s of 6.5 and 7.3, respectively, both drugs were ionized to some extent in the higher pH dissolution media (i.e. at pH 5.5 and 6.8). Concurrently, silanol groups in SBA-15 are deprotonated above pH 2 (Figure 6.2). This suggests that the presence of electrostatic interactions between the drug molecules and silica surface for the higher pH conditions. To test this hypothesis and further probe the type of drug-silica interaction present, adsorption of KET and CLZ was studied in the presence of 50 mM triethylamine (TEA) or 0.5 M urea. TEA, being positively charged, was added to serve as a competitive adsorbate, interacting via electrostatic interaction with the silica surface, such that TEA would result in a reduction of KET or CLZ -silica interaction. Adsorption in the presence of urea was studied to assess the extent of competitive adsorption via hydrogen bonding. As observed in Figure 6.6, the amount of KET and CLZ adsorbed onto SBA-15 at pH 6.8 reduced drastically in the presence of TEA indicating competitive adsorption of TEA on the silica surface. In the presence of urea, on the other hand, there was only small reduction in the adsorption of KET while no difference in the amount of drug adsorbed was observed for CLZ.
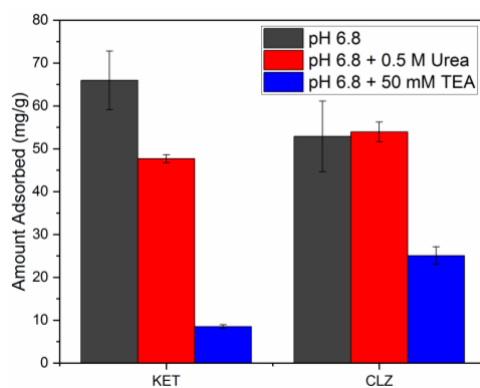
Figure 6.6: Amount of KET and CLZ adsorbed on to SBA-15 at pH 6.8 in the presence of TEA and urea.

Two-step dissolution of KET-MPS and CLZ-MPS was carried out in the presence of TEA to support the contention that the decrease in solution concentration upon pH increase was due to re-adsorption of drug. TEA was added to the aqueous media at the time of pH-shift, i.e., after 30 min. Figure 6.7a shows that, in contrast to the observation in Figure 6.5b, in the presence of TEA and following pH-shift to pH 6.8, KET concentration did not decrease, plateauing at 95% release. Similarly, CLZ concentration decreased to a lesser extent in the presence of TEA when compared to Figure 5c. The lower extent of solution decrease in the presence of TEA is consistent with a lower extent of re-adsorption of KET and CLZ, due to competitive adsorption by TEA.
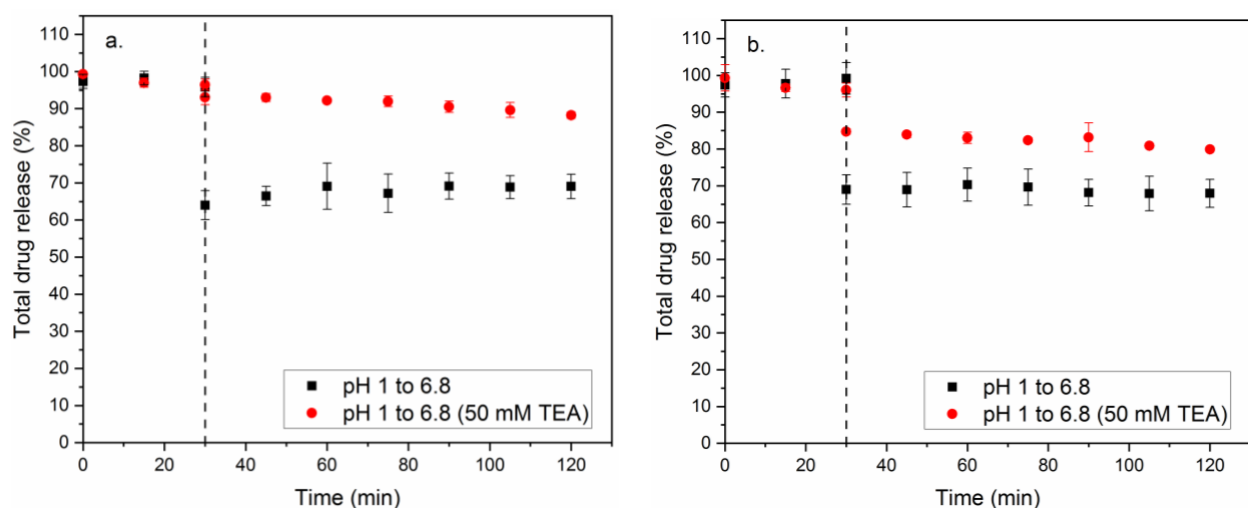
Figure 6.7: Dissolution of (a) KET-MPS and (b) CLZ-MPS in pH 1 and pH 6.8 (in the presence of TEA).

6.5.4 Absorptive Dissolution Testing

The pH transition from acidic to higher pH conditions had a notable impact on the solution concentrations of KET and CLZ, particularly for pH-shift from pH 1 to pH 6.8. The KET-MPS formulation was further studied in an absorptive dissolution testing apparatus to determine if the removal of drug by transport across a membrane would promote further release, mitigating the re-adsorption of drug onto the silica surface. Figure 6.8 shows donor and receiver concentrations from dissolution-absorption studies along with the total drug release over the experimental time frame. The absorption measurements were commenced after pH-shift. The donor concentration showed an abrupt decline in concentration upon pH-shift to pH 6.8, and a further gradual decline in concentration, which can be attributed to the simultaneous absorption of drug across the membrane.

173

The receiver concentration showed a maximum value followed by a gradual decline in concentration, reciprocating the decreasing donor concentration. When assessing the total drug release, the drug release increased only slightly (by 10%) over the 4 h period of absorption measurements. This observation suggested that decrease in the solution concentration due to simultaneous absorption resulted only in small amount of additional drug release, at least over biorelevant time frames.
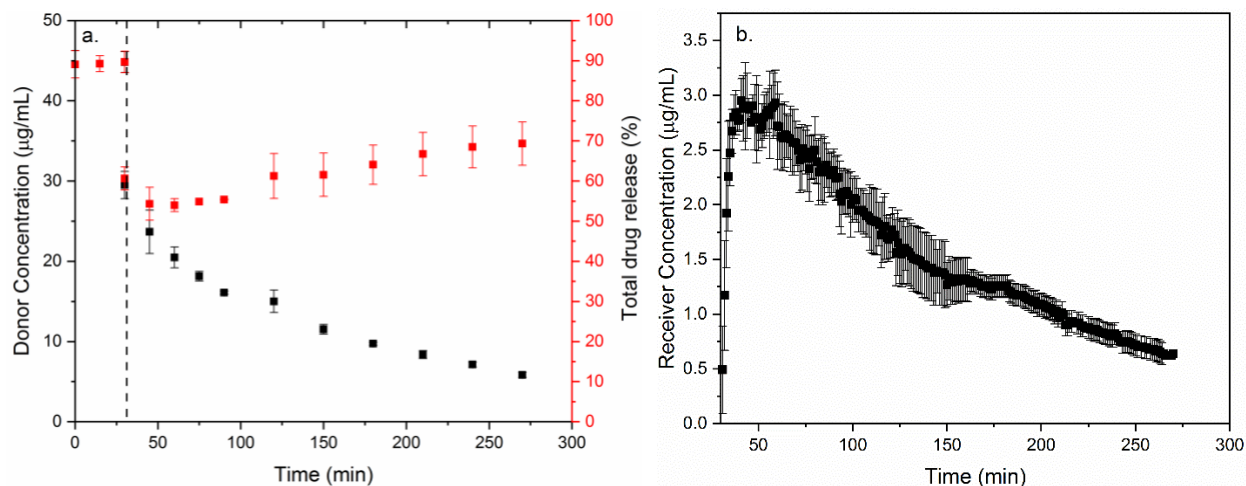
Figure 6.8: (a) Donor, total drug release and (b) receiver concentration of KET-MPS during dissolution-absorption measurements with pH-shift from pH 1 to pH 6.8 after 30 min.

6.6 Discussion

6.6.1 Interplay between drug-silica interaction and drug release

Mesoporous silica is an interesting formulation strategy for poorly soluble drugs considering the improved amorphous physical stability arising from confinement in the silica pores, the potential for rapid release, and the solubility advantage derived from drug amorphization. However, silica is a highly adsorbent material, whereby silanol groups serve as active sites for adsorption of guest molecules. The chemistry of adsorption sites varies in an aqueous environment due to protonation and deprotonation of silanol groups, as follows:[98]

$$\equiv SiOH \ \rightarrow \equiv SiO^- + H^+ \tag{1}$$
$$= Si(OH)_2 \ \rightarrow \equiv SiO_2H^- + H^+ \tag{2}$$
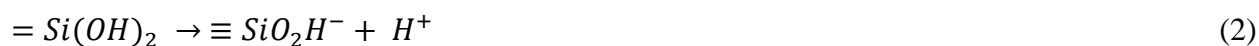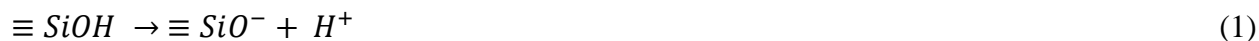
The first dissociation reaction, associated with isolated silanol groups, occurs above pH 2 and the second reaction, associated with geminal silanol groups, occurs at pH > 8.5.[233] The negative charge observed in the zeta potential measurements of SBA-15 in Figure 6.2 is consistent with the value reported in the literature[221] and suggests deprotonation of isolated silanol groups above pH 2. Below pH 2, the silica surface is slightly positively charged with higher concentration of $\equiv SiOH_2^+$, along with some $\equiv SiOH$ and $\equiv SiO^-$ groups. A zeta potential of zero suggests an equal number of positively and negatively charged silanol groups, making the surface electrically neutral. At higher pH, the silica surface becomes predominantly negatively charged with $\equiv SiO^-$ groups.[98] Hence, the surface chemistry of silica in the presence of water largely depends on the ionization state of the silanol groups and is a critical consideration for drug delivery application, in particular for ionizable poorly soluble drugs delivered orally. Because the silica surface chemistry is sensitive to environmental pH, which in turn impacts drug release, the gastrointestinal pH variation is one of the most crucial parameters for MPS formulations. The results obtained herein provide considerable insight into the influence of pH variations on the release of weakly basic drugs from MPS formulations, and the interplay between release and adsorption to the silica surface

The adsorption isotherm for ATZ showed much higher drug adsorption at a lower pH. ATZ with a pKa 4.49, was completely ionized (positively charged) for pH values < pH 3 (Figure 6.1a). SBA-15 has net positive charge positive charge below pH 2, although there is some fraction of $\equiv SiO^-$ species available. Hence, at lower pH values, ATZ is presumably interacting with silica through electrostatic interactions with deprotonated silanol groups. The simultaneous presence of some fraction of positively charged ATZ and negatively charged silica species thus explains the higher levels of adsorption seen at pH 1 and 4.5. Adsorption is then decreased with further increases in pH as the concentration of ionized ATZ decreases. The variation in the interactions between ATZ and silica versus between ATZ and water as a function of pH were reflected in the dissolution profiles of the MPS formulation. The rapid burst release of ATZ in acidic condition can be attributed to higher solubility of ionized ATZ at pH 1, while the incomplete release is explained by the fraction of ATZ that remains adsorbed to the silica surface[27] via electrostatic interactions. The drug release at pH 4.5, 5.5 and 6.8 was much lower, due to a reduction in the extent of ATZ ionization, and the reduced ATZ solubility.[234] At higher pH, the hydrophobicity of ATZ-MPS formulations is increased. Given that drug release from mesoporous silica particles is

essentially a diffusion-controlled process and depends on the diffusion rate of water into the pores to displace the drug adsorbed,[93] increased formulation hydrophobicity is expected to retard water penetration, lowering the drug release. Thus, exposing ATZ-MPS formulations to an acidic environment prior to encountering intestinal pH conditions clearly improves the amount of drug released, as seen by comparing the single-step dissolution data at pH 4.5, 5.5 and pH 6.8 (Figure 6.4), to the two-step data (Figure 6.5). Furthermore, pH-shift from acidic to basic condition results in supersaturation due to the poor solubility of ATZ above pH 3.[234] While fasted state gastric pH conditions drive ATZ release from MPS formulations, fed state pH conditions of pH 4.5 show a considerable reduction in the amount of drug released. Therefore, based solely on the consideration of pH, a negative food effect would be predicted. However, the impact of solubilizing species is not considered in this analysis.

The interaction between KET and SBA-15 was clearly visible in the adsorption isotherms at pH 4.5, 5.5 and 6.8. Considering the positively charged KET (Figure 6.1b) and negatively charged SBA-15 above pH 2, this can be attributed to electrostatic interactions between the two species. Increase in pH from pH 4.5 to pH 6.8 showed a slight increase in the amount of KET adsorbed, which suggested that the decrease in ionized KET species with an increase in pH was balanced by an increase in the number of deprotonated silanol groups. The reduced adsorption of KET due to competitive adsorption of TEA onto the silica surface at pH 6.8 confirmed that KET primarily interacted with silica via electrostatic interaction between positively charged KET and $\equiv SiO^-$ groups. Furthermore, the small impact of urea on decreasing KET adsorption suggested some extent of hydrogen bonding between uncharged KET and silanol groups in addition to the electrostatic interaction. The rapid, complete release of KET during dissolution of the KET-MPS formulation in acidic conditions (pH 1 and 4.5, Figure 6.4) can be attributed to the higher KET solubility and lower adsorption tendency. On the other hand, the lower drug release of KET-MPS in pH 5.5 and pH 6.8 is most likely the result of a higher adsorption tendency, combined with the diminishing KET solubility with increasing pH. The interplay between the tendency of the drug to adsorb onto the silica surface and the tendency to interact with the media and dissolve is clearly highlighted by the two-step dissolution studies. At low pH, the driving force for dissolution is high due to greater solubility at low pH, with little tendency for adsorption. Increasing the pH results in a reduced solubility, together with an enhanced adsorption tendency due to change in the silica

surface chemistry which leads to strong electrostatic interactions between KET and silica. Remarkably, this change in the balance between competing factors leads to drug being re-adsorbed from the solution onto the silica surface upon pH increase, with an appreciable 30% drop in the solution concentration. Support for the conjecture that the concentration decrease is due to drug re-adsorption is provided by the observations that this can be mitigated by addition of the competitive adsorbate, TEA (Figure 6.7). Adsorption of KET to the silica surface at higher pH seems to result from a strong interaction given that absorptive dissolution measurements did not improve the drug release substantially (Figure 6.8), unlike previous observations. Thus, removal of drug due to absorption across the membrane did not drive further desorption of drug from the surface and adsorption appears to be at least partially irreversible at high pH. Unlike in ATZ-MPS, two-step dissolution using fed state pH conditions showed similar performance as for fasted state pH conditions, predicting no food effect on the formulation performance from a pH perspective. Clearly, the dissolution profile of KET-MPS formulation underscores the need to probe the effect of pH on the solution concentration of a weakly basic drug with a high pKa value. Although dissolution under acidic conditions is expected to improve drug release from the MPS formulation, the solution concentration may decline upon transfer to intestinal conditions due to re-adsorption to the silica surface, which is ultimately expected to reduce the drug bioavailability.

CLZ adsorption onto silica followed a similar trend as KET and seemed to interact primarily via electrostatic interactions as the amount of CLZ adsorbed increased at higher pH in Figure 6.3a. This is consistent with the ionization of CLZ and deprotonation of SBA-15 as a function of pH. Moreover, the reduction in adsorption in the presence of TEA and no change in the presence of urea indicated electrostatic interaction as the dominant mechanism for CLZ-silica interaction. A negligible adsorption of CLZ in acidic condition can be attributed to the electrostatic repulsion between CLZ and silica surface. The trend in the amount of drug release during dissolution studies of CLZ-MPS was consistent with the adsorption isotherm for different solution pHs. A complete burst release in acidic condition and pH 4.5 can be attributed to the poor adsorption tendency of CLZ at low pH combined with a high solubility. Lower release at higher pH suggests poor release due to stronger adsorption of ionized CLZ with the increasingly negatively charged silica surface. Similar to KET, in two-step dissolution studies CLZ concentration decreased upon pH-shift to higher pH, which is attributed the increase in electrostatic interactions between CLZ and silica.

Furthermore, the amount of CLZ re-adsorbed was consistent with the trend observed in the adsorption isotherms. Again, TEA reduced the amount of CLZ re-adsorbed at high pH, improving the overall drug release due to competitive adsorption of positively charge TEA. Thus, CLZ provides support for the concept that pH-shift from acidic to intestinal pH conditions may deplete the amount of drug available for absorption for weakly basic compounds that show substantial ionization at intestinal pH conditions. The impact of re-adsorption on the effectiveness of mesoporous silica formulations needs to be evaluated in greater depth in an *in vivo* context.

6.6.2 *In vivo* considerations for MPS formulations

In vivo studies of mesoporous silica-based formulations have shown improved bioavailability for poorly soluble drugs when compared to crystalline formulations. For instance, itraconazole-loaded MPS formulation showed two-fold increase in the area under the curve and a two-fold reduction in T_{max} in comparison to crystalline itraconazole.[91] Similarly, carbamazepine and telmisartan bioavailability was improved using MPS formulations as compared to the commercially available tablets.[235,236] This is expected as the drug in MPS formulations is in an amorphous solid form, hence, the formulations are expected to offer a transient solubility and dissolution advantage, resulting in improved absorption behavior. However, the dissolution of amorphous solids results in generation of supersaturated solution. In such cases, the bioavailability is determined by the extent of supersaturation maintained over biorelevant time frames. *In vivo* studies of fenofibrate-loaded MPS formulations showed better performance for more slowly releasing drug formulation as compared to faster releasing system.[183] This was because the higher supersaturation generated in the latter formulation resulted in rapid drug crystallization. Similarly, itraconazole-loaded silica formulation underwent a rapid decline in the concentration upon gastrointestinal transit due to crystallization of itraconazole.[91] Therefore, in order to achieve enhanced performance from mesoporous silica-based formulations, it is imperative to maintain supersaturation in the solution and this may necessitate addition of a polymer to the formulation to inhibit crystallization.[193,237] In addition to supersaturation due to gastrointestinal (GI) transit, *in vivo* performance of MPS formulations can be significantly influenced by other physiological factors. The pH of the GI tract depends on several variables such as prandial condition, time, meal volume, secretion volume and the region of GI tract.[148] Gastrointestinal fluid conditions are predicted to have an impact on the bioavailability from MPS formulations, as for other

formulations, with considerations specific to MPS formulations highlighted by the observations noted in this study. MPS specific considerations are predominantly the interplay between adsorption to the silica surface versus dissolution into the solution phase. This balance will be impacted not only by local pH conditions, but also by the presence of other species that can adsorb competitively to the silica surface, namely other positively charged species or biological surfactants, and the presence/absence of solubilizing species such as bile salt micelles.[27] Thus, considering the influence of physiological factors on drug release from mesoporous silica-based formulations, it is evident that predicting *in vivo* formulation performance in an *in vitro* setting is a significant challenge. The influence of various *in vivo* factors needs to be carefully considered to develop MPS formulations with optimal performance.

6.7 Conclusions

Herein, the impact of solution pH, drug adsorption extent, drug pKa and the presence or absence of an absorptive sink on the release performance of mesoporous silica-based formulations of weakly basic drugs was explored. The surface properties of silica in aqueous environment vary with the environmental pH and are critical to the release performance of drug-loaded MPS formulations. The change in ionization and solubility of ionizable drugs as a function of pH further influences drug release. A significant impact of solution pH was observed on both the drug adsorption isotherm and the dissolution behavior of MPS formulations. A complex interplay between the pH-dependent drug solubility, ionization of drug and silica as a function of pH, adsorption extent, and release behavior was observed. Since all the three compounds were weakly basic in nature, they primarily interacted with silica via electrostatic interaction. Increases in solution pH resulted in an increase in the negative charge of the silica surface and improved adsorption of positively charged drugs. Poor drug-silica interaction and higher solubility in acidic condition resulted in a complete drug release of all formulations at pH 1. However, re-adsorption to the silica material was observed for two compounds upon pH increase, decreasing the free drug concentration available for absorption across a membrane. This pattern of behavior has potential bioavailability implications for weakly basic drugs formulated using MPS, which would be expected to show good release in fasted state gastric conditions but may have reduced availability upon transit to intestinal conditions due to enhanced interaction with silica. This study clearly

highlights important considerations for *in vitro* formulation testing and overall formulation development of mesoporous silica-based formulations for oral drug delivery applications.

CHAPTER 7.   CONCLUSIONS AND RECOMMENDATIONS

7.1   Research Summary

This research introduces a novel approach for *in vitro* measurements of form and formulation performance, particularly for poorly soluble drugs. An apparatus that can couple dissolution-absorption measurements and provide more *in vivo* relevant mass transfer rates, can be an effective tool at several stages of drug product development including drug design, formulation development, process development, process validation, quality control and bioequivalence. In chapter 2, the design and working principle of the absorptive dissolution testing apparatus was described in detail. The study introduced an application of a hollow fiber membrane, with 16-fold higher membrane surface area as compared to the conventional flat-sheet membrane, to simulate the absorption process. The preliminary studies showed significant enhancement in the mass transfer over conventional apparatuses. A mathematical model was developed to understand the important parameters that governs mass transport rates and was validate using experimental results. The study successfully evaluated dissolution and absorption of an immediate release formulation of nevirapine, elucidating the impact of the extent of supersaturation on absorption profiles. Additionally, the apparatus was able to demonstrate subtle differences in the formulations that are typically difficult to obtain in traditional dissolution or mass transport apparatuses.

The robustness and sensitivity of the apparatus evaluated in chapter 2 suggested that the apparatus can offer better discrimination between complex enabling formulations and insights into the impact of solution phase transformations on the absorption behavior. Therefore, in chapter 3, the apparatus was used to assess the absorption behavior of complex highly supersaturated solutions of poorly soluble drug. In this study, we successfully demonstrated coupling between formulation dissolution, solution phase behavior and absorption. Owing to the high sensitivity of the absorption measurements, the apparatus demonstrated improved mass transfer due to the formation of drug-rich phase following LLPS in the solution. This was speculated to be due to the reservoir effect of drug-rich species and improved concentration gradients in the laminar flow in hollow fibers. Enhanced mass transfer was also observed from ASDs undergoing LLPS upon

dissolution, providing better discrimination between ASDs based on the drug loading and polymer type.

The bioavailability advantage from amorphous formulations can be limited due to the presence of residual crystalline content. In chapter 4, we evaluated dissolution and absorption of amorphous formulations containing some extent of residual crystallinity, induced *in situ* by exposing formulations to stressed storage conditions. In addition to an absorptive sink, the formulations were evaluated with different dissolution volumes to understand the impact of supersaturation generated on the formulation performance. Formulations with higher residual crystalline content generated lower supersaturation and in turn, showed poorer absorption profiles. Larger dissolution volume resulted in lower supersaturation and simultaneous membrane absorption further reduced the solution concentration. As a result, no desupersaturation was observed. On the other hand, smaller volume and non-sink dissolution conditions resulted in higher supersaturation and higher membrane mass transfer. However, the desupersaturation rate dominated over absorption rate due to large driving force for drug crystallization. With the help of mathematical models, we were able to show the interplay between two competing processes, absorption and desupersaturation, on solution concentration as a function of supersaturation.

In chapter 5, mesoporous silica-based amorphous formulations were evaluated in the absorptive dissolution testing apparatus. These formulations are limited by incomplete drug release due to interaction between drug and silica surface. The adsorption of drug on the silica surface is a dynamic process and simultaneous absorption of drug across the membrane can alter the adsorption kinetics due to lowering of the adsorption driving force. Hence, the study focused on determining the interplay between drug adsorption kinetics and membrane absorption process on the overall drug release. Using the absorptive dissolution measurements, we observed a significant improvement in the drug release, thus proving the hypothesis. Additionally, we were able to correlate the intermolecular interactions between drug and silica in the formulation to the dissolution behavior which varied with drug loading. The study clearly highlighted several factors that could impact the performance of mesoporous silica-based formulations such as drug loading, drug-silica interactions, solution pH, absorptive sink and therefore, a need for careful design of *in vitro* measurements for formulation assessment.

On the basis of the effect of solution pH observed on the dissolution and absorption performance of mesoporous silica formulation in chapter 5, the influence of solution pH on mesoporous silica-based formulations of weakly basic compound was further investigated in chapter 6. Adsorption tendency of the drug molecules on the silica surface was found to be dependent on the solution pH and as a result, dissolution profiles varied with the pH. Consequently, a significant difference was observed in the dissolution profile for one-step (dissolution in intestinal pH) vs. two-step dissolution (dissolution in gastric and intestinal pH environment). At higher pH, the drug adsorption increased significantly for drugs with high pKa, while the drug release decreased due to ionization of the drug and protonation/deprotonation of the silica surface. The study demonstrated that physiological parameters such as solution pH are important considerations in the evaluation of mesoporous silica formulations due to complex surface chemistry and reactivity of silica.

Overall, this dissertation highlights the significance of absorptive sink in the dissolution testing of formulations, particularly for poorly soluble drugs. Obtaining meaningful dissolution data for better prediction of product performance is imperative to the formulation development. Absorption of drug across gastrointestinal membrane can alter and be altered by several competing physical processes occurring in the gastrointestinal lumen. The novel methodology developed in this research enables thorough investigation of these competing kinetics in a dynamic *in vitro* setting.

7.2   Recommendations for future work

This research has provided with an *in vitro* methodology to better simulate the membrane absorption process and clearly highlights the importance of incorporating an absorptive sink in the evaluation of dissolution behavior of complex supersaturating formulations.

With a robust mass transport apparatus, the future studies can be focused on combining the compendial dissolution apparatus (USP I/II) with the hollow fiber membrane module to assess its potential as a biorelevant testing apparatus. Formulation optimization is critical to the bioavailability of a drug compound. Hence, such an apparatus with combined dissolution-

absorption testing can be of great utility at formulation design and development stage for the pharmaceutical industry.

In vivo, there are several physical processes such as crystallization, supersaturation, liquid-liquid phase separation or micellization occurring in the lumen along with the dissolution and absorption of drugs. The mathematical model for mass transport in the apparatus developed in this work can be combined with the rate of other physical processes to better predict the formulation performance. In particular, incorporation of the dissolution rate and crystallization kinetics in the mass transfer model can provide a thorough predictive model to assess the performance of a supersaturating formulations. Further studies can focus on the development and validation of the mathematical models.

This study provides a framework for mass transport studies using hollow fiber membrane module. Considering the wide range of surface area and size of the hollow fiber membrane module available from the manufactures, the application of the apparatus can be further extended by incorporating *in vivo* relevant absorption rate for a specific drug. The interplay between complex solution phase behavior and absorption kinetics can then be studied in the presence of *in vivo* relevant conditions to better optimize the formulation design.

The biorelevant experimental conditions for *in vitro* dissolution and absorption testing are becoming increasingly important for complex formulations. Furthermore, biorelevant media can serve as solubilizing agents or crystallization inhibitors, which can in turn alter bioavailability of the formulations. Hence, performing coupled dissolution-absorption studies of supersaturating formulations using biorelevant media would be worth investigating to improve predictions. Absorptive dissolution testing apparatus can also be employed to assess the effect of solubilizing agents such as surfactants, cyclodextrins or other excipients such as polymers on the amount of free drug available for absorption. These additives can either improve the formulation performance by maintaining supersaturation or impair the performance by promoting crystallization or solubilization of drugs.

The formation of drug-rich phase upon dissolution of ASDs due to LLPS offers bioavailability advantage from these formulations. However, LLPS is typically observed from ASDs with low drug loading and there exist a threshold drug loading (also known as congruency limit) above which the dissolution of ASDs does not result in LLPS. Absorptive dissolution testing of ASDs showed improvement in the dissolution rate of slow releasing formulations in the current research. It would be interesting to investigate the congruency limit of ASDs using absorptive dissolution testing apparatus. The simultaneous removal of drug due to absorption may improve the dissolution rate of ASDs, particularly for slow releasing ASDs, and in turn improve the congruency limit of the formulation for LLPS to occur.

APPENDIX A

Supporting Information for Chapter 3
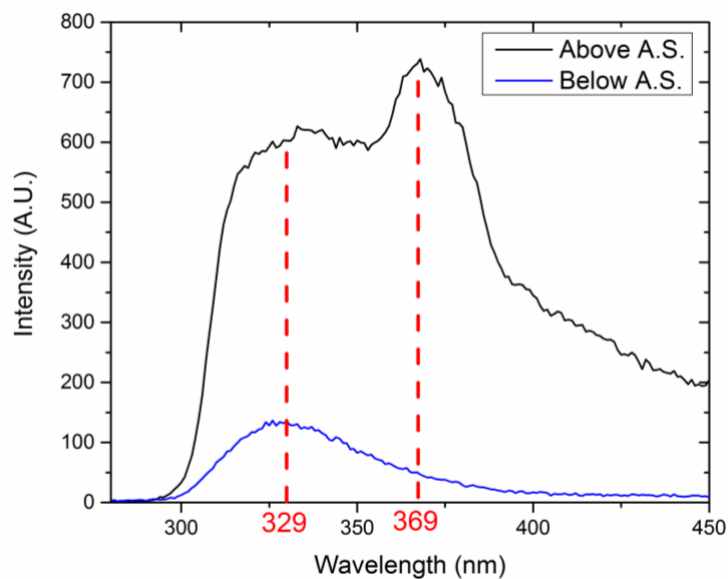
Figure S3.1: Fluorescence spectra of ATZ below and above LLPS onset concentration. A.S. refers to amorphous solubility.
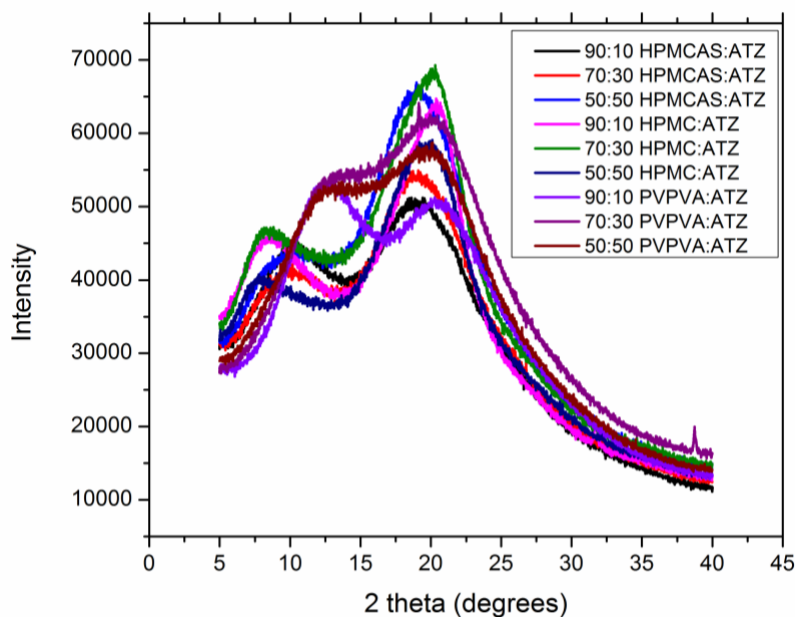
Figure S3.2: Powder X-ray diffraction patterns for ASDs prepared in the study. Powder X-ray diffraction was performed on ASDs prepared in this study using Rigaku Smartlab diffractometer (Woodlands, Texas). Data was obtained over scan range of 5- 40° 2θ with scan rate 4° 2θ/min using CuK$_\alpha$ radiation source operating at 40 kV and 44 mA.
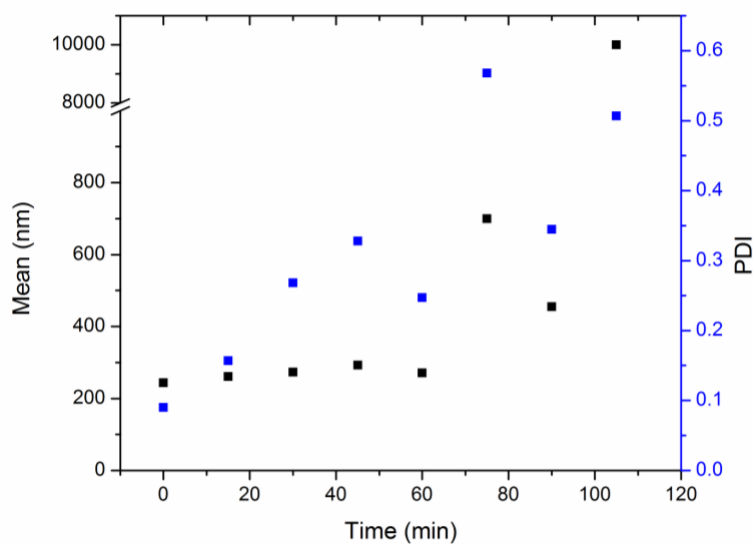
Figure S3.3: Particle size measurement using DLS during dissolution-absorption of supersaturated solution with initial concentration of 200 µg/mL containing 1 mg/mL PVPVA pre-dissolved in pH 6.8 buffer.
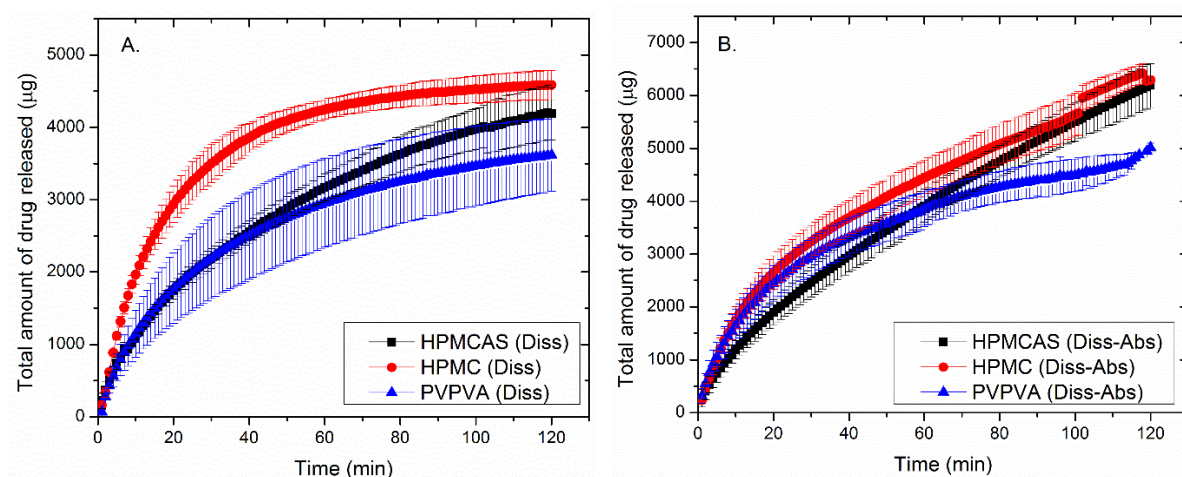
Figure S3.4: Comparison of amount of drug released from 50% drug loading ASDs with different polymers in the absence (A) and presence (B) of absorptive compartment.

Longer duration dissolution-absorption experiments of ASDs

The 10% drug loading ASDs had the most promising dissolution-absorption behavior, as a result of their rapid dissolution and formation of drug-rich nanodroplets. Dissolution of ASDs prepared with cellulose derivatives showed clear evidence of LLPS, while PVPVA-based ASD resulted in agglomerate formation (Figure S4). Agglomeration was supported by fluorescence studies whereby the filtered solution showed a peak ratio of 0.27, while an unfiltered solution showed a peak intensity ratio of 0.89, indicating the presence of a drug-rich hydrophobic environment. The difference in the absorption behavior of these three ASDs was, however, not significant over this time period. Experiments conducted for a longer duration showed donor and receiver concentration profiles with increased discrimination between these formulations. In the case of the ASDs with cellulose derivatives, the apparent donor concentration declined gradually, eventually decreasing to the amorphous solubility of ATZ after c.a. 200 min, indicating depletion of the drug-rich phase. Since the donor molecularly dissolved drug concentration was equivalent to the amorphous solubility up until the nanodroplets depleted, the receiver concentration was also maintained above the concentration corresponding to amorphous solubility until 200 min, as shown in Figure S6B. In contrast, the 90:10 PVPVA:ATZ ASD, saturated at a concentration slightly above the amorphous solubility. The concentration depleted after 150 min. We speculate this could be due to decrease in the amount of amorphous agglomerates to replenish the drug lost

188

during absorption at an equivalent rate. The receiver concentration profile for 90:10 PVPVA:ATZ reflected this decline in concentration beyond amorphous solubility after 150 min. The difference in the AUC of receiver concentration was more obvious in the long duration measurements, with HPMCAS and HPMC showing higher AUCs as compared to PVPVA. Therefore, although all the three formulations attained similar free drug concentrations, the formation of nanodroplets resulted in longer reservoir effect and hence higher AUC as compared to reservoir provided by amorphous agglomerated solid, indicating higher amount of mass transfer.
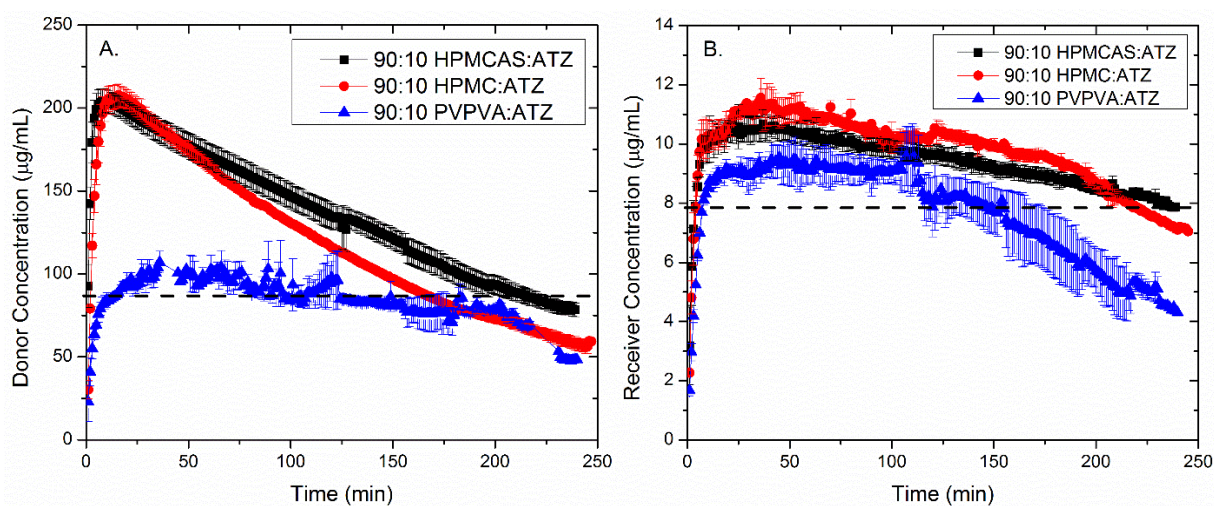
Figure S3.5: Donor and receiver concentration of 10% drug loading ASDs with different polymers over a duration of 4 h.

Supporting Information for Chapter 6
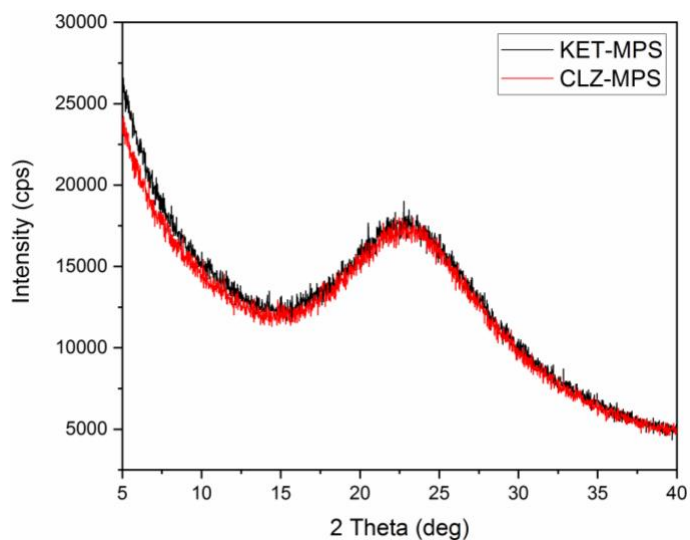
Figure S6.1: Powder X-ray diffraction of 20% KET and CLZ-loaded mesoporous silica formulation.
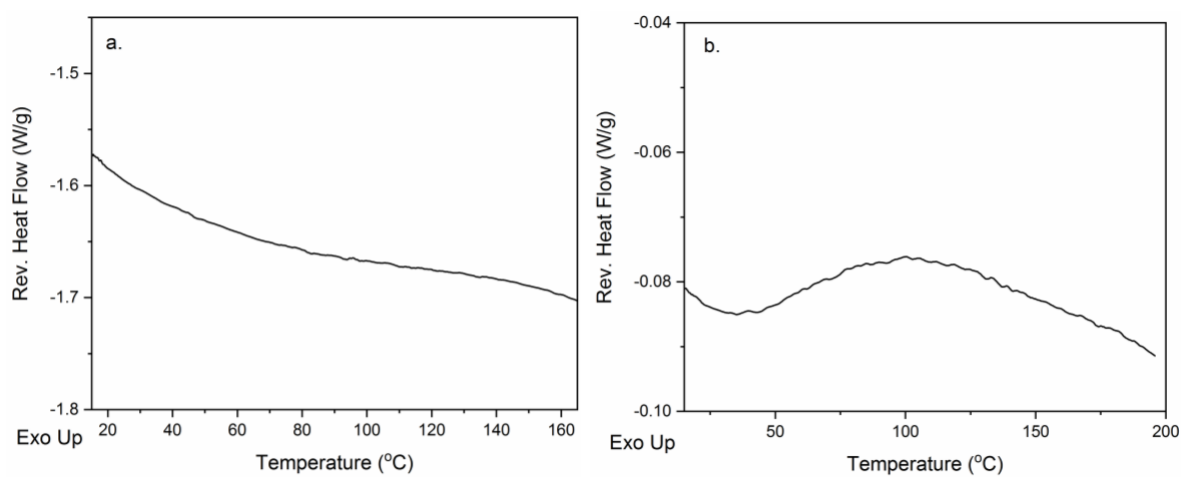
Figure S6.2: DSC thermograms of (a) KET-MPS and (b) CLZ-MPS formulations. No evidence of T_g suggests nanoconfinement of drug in silica pores.
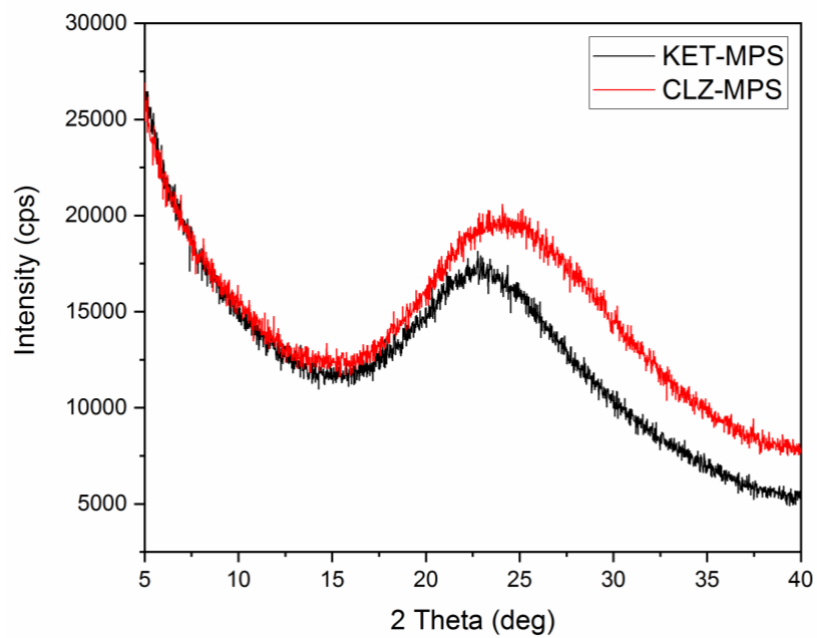
Figure S6.3: Powder X-ray diffraction of precipitate collected after two-step dissolution of 20% KET and CLZ-loaded mesoporous silica formulation with pH-shift from pH 1 to pH 6.8.

REFERENCES

(1) Vivian Gray Min Xia, Chris Butler, Saji Thomas, and Stephen Mayock, G. K. The Science of USP 1 and 2 Dissolution: Present Challengesand Future Relevance. *Pharm. Res.* **2009**, *26* (6), 1289–1302.

(2) McAllister, M. Dynamic Dissolution: A Step Closer to Predictive Dissolution Testing? *Mol. Pharm.* **2010**, *7* (5), 1374–1387.

(3) Dickinson, P. A.; Lee, W. W.; Stott, P. W.; Townsend, A. I.; Smart, J. P.; Ghahramani, P.; Hammett, T.; Billett, L.; Behn, S.; Gibb, R. C. Clinical Relevance of Dissolution Testing in Quality by Design. *AAPS J.* **2008**, *10* (2), 380–390.

(4) Dressman, J. B.; Amidon, G. L.; Reppas, C.; Shah, V. P. Dissolution Testing as a Prognostic Tool for Oral Drug Absorption: Immediate Release Dosage Forms. *Pharm. Res.* **1998**, *15* (1), 11–22.

(5) Taylor, L. S.; Zhang, G. G. Z. Physical Chemistry of Supersaturated Solutions and Implications for Oral Absorption. *Adv. Drug Deliv. Rev.* **2016**, *101*, 122–142.

(6) Williams, H. D.; Trevaskis, N. L.; Charman, S. A.; Shanker, R. M.; Charman, W. N.; Pouton, C. W.; Porter, C. J. H. Strategies to Address Low Drug Solubility in Discovery and Development. *Pharmacol. Rev.* **2013**, *65* (1), 315 LP – 499.

(7) Kostewicz, E. S.; Abrahamsson, B.; Brewster, M.; Brouwers, J.; Butler, J.; Carlert, S.; Dickinson, P. A.; Dressman, J.; Holm, R.; Klein, S. In Vitro Models for the Prediction of in Vivo Performance of Oral Dosage Forms. *Eur. J. Pharm. Sci.* **2014**, *57*, 342–366.

(8) Kostewicz, E. S.; Brauns, U.; Becker, R.; Dressman, J. B. Forecasting the Oral Absorption Behavior of Poorly Soluble Weak Bases Using Solubility and Dissolution Studies in Biorelevant Media. *Pharm. Res.* **2002**, *19* (3), 345–349.

(9) Kostewicz, E. S.; Wunderlich, M.; Brauns, U.; Becker, R.; Bock, T.; Dressman, J. B. Predicting the Precipitation of Poorly Soluble Weak Bases upon Entry in the Small Intestine. *J. Pharm. Pharmacol.* **2004**, *56* (1), 43–51.

(10) Indulkar, A. S.; Gao, Y.; Raina, S. A.; Zhang, G. G. Z.; Taylor, L. S. Exploiting the Phenomenon of Liquid–Liquid Phase Separation for Enhanced and Sustained Membrane Transport of a Poorly Water-Soluble Drug. *Mol. Pharm.* **2016**, *13* (6), 2059–2069.

(11) Raina, S. A.; Zhang, G. G. Z.; Alonzo, D. E.; Wu, J.; Zhu, D.; Catron, N. D.; Gao, Y.; Taylor, L. S. Enhancements and Limits in Drug Membrane Transport Using Supersaturated Solutions of Poorly Water Soluble Drugs. *J. Pharm. Sci.* **2014**, *103* (9), 2736–2748.

(12) Deneau, E.; Steele, G. An In-Line Study of Oiling Out and Crystallization. *Org. Process Res. Dev.* **2005**, *9* (6), 943–950.

(13) Veesler, S.; Lafferrère, L.; Garcia, E.; Hoff, C. Phase Transitions in Supersaturated Drug Solution. *Org. Process Res. Dev.* **2003**, *7* (6), 983–989.

(14) Ceolin, R.; Barrio, M.; Tamarit, J. L.; Veglio, N.; Perrin, M. A.; Espeau, P. Liquid-Liquid Miscibility Gaps and Hydrate Formation in Drug-Water Binary Systems: Pressure-Temperature Phase Diagram of Lidocaine and Pressure-Temperature-Composition Phase Diagram of the Lidocaine-Water System. *J. Pharm. Sci.* **2010**, *99* (6), 2756–2765.

(15) Ilevbare, G. A.; Taylor, L. S. Liquid–Liquid Phase Separation in Highly Supersaturated Aqueous Solutions of Poorly Water-Soluble Drugs: Implications for Solubility Enhancing Formulations. *Cryst. Growth Des.* **2013**, *13* (4), 1497–1509.

(16) Hancock, B. C.; Shamblin, S. L.; Zografi, G. Molecular Mobility of Amorphous Pharmaceutical Solids below Their Glass Transition Temperatures. *Pharm. Res.* **1995**, *12* (6), 799–806.

(17) Trasi, N. S.; Purohit, H. S.; Taylor, L. S. Evaluation of the Crystallization Tendency of Commercially Available Amorphous Tacrolimus Formulations Exposed to Different Stress Conditions. *Pharm. Res.* **2017**, *34* (10), 2142–2155.

(18) Moseson, D. E.; Taylor, L. S. The Application of Temperature-Composition Phase Diagrams for Hot Melt Extrusion Processing of Amorphous Solid Dispersions to Prevent Residual Crystallinity. *Int. J. Pharm.* **2018**, *553* (1–2), 454–466.

(19) Haser, A.; Cao, T.; Lubach, J.; Listro, T.; Acquarulo, L.; Zhang, F. Melt Extrusion vs. Spray Drying: The Effect of Processing Methods on Crystalline Content of Naproxen-Povidone Formulations. *Eur. J. Pharm. Sci.* **2017**, *102*, 115–125.

(20) Kurdyukov, D. A.; Eurov, D. A.; Kirilenko, D. A.; Kukushkina, J. A.; Sokolov, V. V; Yagovkina, M. A.; Golubev, V. G. High-Surface Area Spherical Micro-Mesoporous Silica Particles. *Microporous Mesoporous Mater.* **2016**, *223*, 225–229.

(21) Speybroeck, M. Van; Barillaro, V.; Thi, T. Do; Mellaerts, R.; Martens, J.; Humbeeck, J. Van; Vermant, J.; Annaert, P.; Den Mooter, G. Van; Augustijns, P. Ordered Mesoporous Silica Material SBA-15: A Broad-Spectrum Formulation Platform for Poorly Soluble Drugs. *J. Pharm. Sci.* **2009**, *98* (8), 2648–2658.

(22) Rengarajan, G. T.; Enke, D.; Steinhart, M.; Beiner, M. Stabilization of the Amorphous State of Pharmaceuticals in Nanopores. *J. Mater. Chem.* **2008**, *18* (22), 2537–2539.

(23) Xia, X.; Zhou, C.; Ballell, L.; Garcia-Bennett, A. E. In Vivo Enhancement in Bioavailability of Atazanavir in the Presence of Proton-Pump Inhibitors Using Mesoporous Materials. *ChemMedChem* **2012**, *7* (1), 43–48.

(24) Alcoutlabi, M.; McKenna, G. B. Effects of Confinement on Material Behaviour at the Nanometre Size Scale. *J. Phys. Condens. Matter* **2005**, *17* (15), R461.

(25) Jackson, C. L.; McKenna, G. B. Vitrification and Crystallization of Organic Liquids Confined to Nanoscale Pores. *Chem. Mater.* **1996**, *8* (8), 2128–2137.

(26) Strømme, M.; Brohede, U.; Atluri, R.; Garcia-Bennett, A. E. Mesoporous Silica-based Nanomaterials for Drug Delivery: Evaluation of Structural Properties Associated with Release Rate. *Wiley Interdiscip. Rev. Nanomedicine Nanobiotechnology* **2009**, *1* (1), 140–148.

(27) Dening, T. J.; Taylor, L. S. Supersaturation Potential of Ordered Mesoporous Silica Delivery Systems. Part 1: Dissolution Performance and Drug Membrane Transport Rates. *Mol. Pharm.* **2018**, *15* (8), 3489–3501.

(28) Delle Piane, M.; Corno, M.; Ugliengo, P. Chapter 9 - Ab Initio Modeling of Hydrogen Bond Interaction at Silica Surfaces With Focus on Silica/Drugs Systems; Catlow, C. R. A., Van Speybroeck, V., van Santen, R. A. B. T.-M. and S. in the S. of M. M.-P. M., Eds.; Elsevier, 2018; pp 297–328.

(29) Zhuravlev, L. T. The Surface Chemistry of Amorphous Silica. Zhuravlev Model. *Colloids Surfaces A Physicochem. Eng. Asp.* **2000**, *173* (1–3), 1–38.

(30) Song, S.-W.; Hidajat, K.; Kawi, S. Functionalized SBA-15 Materials as Carriers for Controlled Drug Delivery: Influence of Surface Properties on Matrix− Drug Interactions. *Langmuir* **2005**, *21* (21), 9568–9575.

(31) Samuel H. Yalkowsky. Solubility and Solubilization in Aqueous Media. *J. Am. Chem. Soc.* **2000**, *122* (40), 9882.

(32) Murdande, S. B.; Pikal, M. J.; Shanker, R. M.; Bogner, R. H. Aqueous Solubility of Crystalline and Amorphous Drugs: Challenges in Measurement. *Pharmaceutical Development and Technology*. 2011, pp 187–200.

(33) Noyes, A. A.; Whitney, W. R. THE RATE OF SOLUTION OF SOLID SUBSTANCES IN THEIR OWN SOLUTIONS. *J. Am. Chem. Soc.* **1897**, *19* (12), 930–934.

(34) Dokoumetzidis, A.; Macheras, P. A Century of Dissolution Research: From Noyes and Whitney to the Biopharmaceutics Classification System. *Int. J. Pharm.* **2006**, *321* (1), 1–11.

(35) Sugano, K.; Okazaki, A.; Sugimoto, S.; Tavornvipas, S.; Omura, A.; Mano, T. Solubility and Dissolution Profile Assessment in Drug Discovery. *Drug Metab. Pharmacokinet.* **2007**, *22* (4), 225–254.

(36) Siepmann, J.; Siepmann, F. Mathematical Modeling of Drug Dissolution. *International Journal of Pharmaceutics*. 2013, pp 12–24.

(37) Fotaki, N. Flow-through Cell Apparatus (USP Apparatus 4): Operation and Features. *Dissolution Technol.* **2011**, *18* (4), 46–49.

(38) Carino, S. R.; Sperry, D. C.; Hawley, M. Relative Bioavailability Estimation of Carbamazepine Crystal Forms Using an Artificial Stomach-Duodenum Model. *J. Pharm. Sci.* **2006**, *95* (1), 116–125.

(39) Dahan, A.; Miller, J. M. The Solubility–Permeability Interplay and Its Implications in Formulation Design and Development for Poorly Soluble Drugs. *AAPS J.* **2012**, *14* (2), 244–251.

(40) Miller, J. M.; Beig, A.; Krieg, B. J.; Carr, R. A.; Borchardt, T. B.; Amidon, G. E.; Amidon, G. L.; Dahan, A. The Solubility–Permeability Interplay: Mechanistic Modeling and Predictive Application of the Impact of Micellar Solubilization on Intestinal Permeation. *Mol. Pharm.* **2011**, *8* (5), 1848–1856.

(41) DiNunzio, J. C.; Miller, D. A.; Yang, W.; McGinity, J. W.; Williams III, R. O. Amorphous Compositions Using Concentration Enhancing Polymers for Improved Bioavailability of Itraconazole. *Mol. Pharm.* **2008**, *5* (6), 968–980.

(42) Bevernage, J.; Brouwers, J.; Annaert, P.; Augustijns, P.; Jan Bevernage Pieter Annaert, Patrick Augustijns, J. B. Drug Precipitation–Permeation Interplay: Supersaturation an Absorptive Environment. *Eur. J. Pharm. Biopharm.* **2012**, *82* (2), 424–428.

(43) Ginski, M. J.; Polli, J. E. Prediction of Dissolution–Absorption Relationships from a Dissolution/Caco-2 System. *Int. J. Pharm.* **1999**, *177* (1), 117–125.

(44) Cussler, E. L. *Diffusion: Mass Transfer in Fluid Systems*; Cambridge university press, 2009.

(45) Amidon, G. L.; Lee, P. I.; Topp, E. M. *Transport Processes in Pharmaceutical Systems*; CRC Press, 1999.

(46) Phillips, D. J.; Pygall, S. R.; Cooper, V. B.; Mann, J. C. Overcoming Sink Limitations in Dissolution Testing: A Review of Traditional Methods and the Potential Utility of Biphasic Systems. *J. Pharm. Pharmacol.* **2012**, *64* (11), 1549–1559.

(47) Shi, Y.; Gao, P.; Gong, Y.; Ping, H.; Shi Gao, P., Gong, Y., Ping, H., Y. Application of a Biphasic Test for Characterization of in Vitro Drug Release of Immediate Release Formulations of Celecoxib and Its Relevance to in Vivo Absorption. *Mol. Pharm.* **2010**, *7* (5), 1458–1465.

(48) Xu, H.; Vela, S.; Shi, Y.; Marroum, P.; Gao, P. In Vitro Characterization of Ritonavir Drug Products and Correlation to Human in Vivo Performance. *Mol. Pharm.* **2017**, *14* (11), 3801–3814.

(49)   Frank, K. J.; Locher, K.; Zecevic, D. E.; Fleth, J.; Wagner, K. G. In Vivo Predictive Mini-Scale Dissolution for Weak Bases: Advantages of PH-Shift in Combination with an Absorptive Compartment. *Eur. J. Pharm. Sci.* **2014**, *61*, 32–39.

(50)   Makoto Kataoka Yukako Yamazaki, Toshiyasu Sakane, Hitoshi Sezaki, and Shinji Yamashita, Y. M.; Kataoka, M.; Masaoka, Y.; Yamazaki, Y.; Sakane, T.; Sezaki, H.; Yamashita, S. In Vitro System to Evaluate Oral Absorption of Poorly Water-Soluble Drugs: Simultaneous Analysis on Dissolution and Permeation of Drugs. *Pharm. Res.* **2003**, *20* (10), 1674–1680.

(51)   Kataoka, M.; Masaoka, Y.; Sakuma, S.; Yamashita, S. Effect of Food Intake on the Oral Absorption of Poorly Water-soluble Drugs: In Vitro Assessment of Drug Dissolution and Permeation Assay System. *J. Pharm. Sci.* **2006**, *95* (9), 2051–2061.

(52)   Kataoka, M.; Sugano, K.; da Costa Mathews, C.; Wong, J. W.; Jones, K. L.; Masaoka, Y.; Sakuma, S.; Yamashita, S. Application of Dissolution/Permeation System for Evaluation of Formulation Effect on Oral Absorption of Poorly Water-Soluble Drugs in Drug Development. *Pharm. Res.* **2012**, *29* (6), 1485–1494.

(53)   Kataoka, M.; Yano, K.; Hamatsu, Y.; Masaoka, Y.; Sakuma, S.; Yamashita, S. Assessment of Absorption Potential of Poorly Water-Soluble Drugs by Using the Dissolution/Permeation System. *Eur. J. Pharm. Biopharm.* **2013**, *85* (3), 1317–1324.

(54)   Motz, S. A.; Schaefer, U. F.; Balbach, S.; Eichinger, T.; Lehr, C.-M. Permeability Assessment for Solid Oral Drug Formulations Based on Caco-2 Monolayer in Combination with a Flow through Dissolution Cell. *Eur. J. Pharm. Biopharm.* **2007**, *66* (2), 286–295.

(55)   Kataoka, M.; Tsuneishi, S.; Maeda, Y.; Masaoka, Y.; Sakuma, S.; Yamashita, S. A New in Vitro System for Evaluation of Passive Intestinal Drug Absorption: Establishment of a Double Artificial Membrane Permeation Assay. *Eur. J. Pharm. Biopharm.* **2014**, *88* (3), 840–846.

(56)   Kansy, M.; Senner, F.; Gubernator, K. Physicochemical High Throughput Screening: Parallel Artificial Membrane Permeation Assay in the Description of Passive Absorption Processes. *Journal of Medicinal Chemistry*. 1998, pp 1007–1010.

(57)   Avdeef, A. High-Throughput Measurement of Permeability Profiles. *Drug Bioavailab. Estim. Solubility, Permeability, Absorpt. Bioavailab.* **2003**, 46–71.

(58)   Jackson, M. J.; Kestur, U. S.; Hussain, M. A.; Taylor, L. S. Dissolution of Danazol Amorphous Solid Dispersions: Supersaturation and Phase Behavior as a Function of Drug Loading and Polymer Type. *Mol. Pharm.* **2015**, *13* (1), 223–231.

(59)   Berben, P.; Brouwers, J.; Augustijns, P. The Artificial Membrane Insert System as Predictive Tool for Formulation Performance Evaluation. *Int. J. Pharm.* **2018**, *537* (1–2), 22–29.

(60) Prasad, R.; Sirkar, K. K. Membrane-Based Solvent Extraction. In *Membrane Handbook*; Springer, 1992; pp 727–763.

(61) Reed, B. W.; Semmens, M. J.; Cussler, E. L. Membrane Contactors. *Sci. Technol. Sep. Membr.* **1995**, 467–498.

(62) Dahuron, L. DESIGNING LIQUID-LIQUID EXTRACTIONS IN HOLLOW FIBER MODULES, University of Minnesota, 1987.

(63) Minekus, M.; Marteau, P.; Havenaar, R.; Huis in 't Veld, J. H. J. A Multicompartmental Dynamic Computer-Controlled Model Simulating the Stomach and Small Intestine. *Altern. to Lab. Anim.* **1995**, *23* (August 2015), 197–209.

(64) Blanquet, S.; Zeijdner, E.; Beyssac, E.; Meunier, J.-P.; Denis, S.; Havenaar, R.; Alric, M. A Dynamic Artificial Gastrointestinal System for Studying the Behavior of Orally Administered Drug Dosage Forms under Various Physiological Conditions. *Pharm. Res.* **2004**, *21* (4), 585–591.

(65) Lamberti, G.; Cascone, S.; Iannaccone, M.; Titomanlio, G. In Vitro Simulation of Drug Intestinal Absorption. *Int. J. Pharm.* **2012**, *439* (1), 165–168.

(66) Mullin, J. W. W. *Crystallization (4th Ed.)*; 2001.

(67) Byrn, S. R.; Zografi, G.; Chen, S. *Solid State Properties of Pharmaceutical Materials*; Wiley Online Library, 2017.

(68) Yu, L. Amorphous Pharmaceutical Solids: Preparation, Characterization and Stabilization. *Adv. Drug Deliv. Rev.* **2001**, *48* (1), 27–42.

(69) Zhang, G. G. Z.; Zhou, D. Crystalline and Amorphous Solids. In *Developing solid oral dosage forms*; Elsevier, 2009; pp 25–60.

(70) Murdande, S. B.; Pikal, M. J.; Shanker, R. M.; Bogner, R. H. Solubility Advantage of Amorphous Pharmaceuticals, Part 3: Is Maximum Solubility Advantage Experimentally Attainable and Sustainable? *J. Pharm. Sci.* **2011**, *100* (10), 4349–4356.

(71) Hancock, B. C.; Parks, M. What Is the True Solubility Advantage for Amorphous Pharmaceuticals? *Pharm. Res.* **2000**, *17* (4), 397–404.

(72) Murdande, S. B.; Pikal, M. J.; Shanker, R. M.; Bogner, R. H. Solubility Advantage of Amorphous Pharmaceuticals: I. a Thermodynamic Analysis. *J. Pharm. Sci.* **2010**, *99* (3), 1254–1264.

(73)   Bogner, R. H.; Murdande, S. B.; Pikal, M. J.; Shanker, R. M. Solubility Advantage of Amorphous Pharmaceuticals: II. Application of Quantitative Thermodynamic Relationships for Prediction of Solubility Enhancement in Structurally Diverse Insoluble Pharmaceuticals. *Pharm. Res.* **2010**, *27* (12), 2704–2714.

(74)   Bonnett, P. E.; Carpenter, K. J.; Dawson, S.; Davey, R. J. Solution Crystallisation via a Submerged Liquid–Liquid Phase Boundary: Oiling Out. *Chem. Commun.* **2003**, No. 6, 698–699.

(75)   Deneau, E.; Steele, G. An In-Line Study of Oiling out and Crystallization. *Org. Process Res. Dev.* **2005**, *9* (6), 943–950.

(76)   Mosquera-Giraldo, L. I.; Taylor, L. S. Glass–Liquid Phase Separation in Highly Supersaturated Aqueous Solutions of Telaprevir. *Mol. Pharm.* **2015**, *12* (2), 496–503.

(77)   Newman, A. *Pharmaceutical Amorphous Solid Dispersions*; John Wiley & Sons, 2015.

(78)   Baird, J. A.; Taylor, L. S. Evaluation of Amorphous Solid Dispersion Properties Using Thermal Analysis Techniques. *Adv. Drug Deliv. Rev.* **2012**, *64* (5), 396–421.

(79)   Hancock, B. C.; Zografi, G. Characteristics and Significance of the Amorphous State in Pharmaceutical Systems. *J. Pharm. Sci.* **1997**, *86* (1), 1–12.

(80)   Marsac, P. J.; Rumondor, A. C. F.; Nivens, D. E.; Kestur, U. S.; Stanciu, L.; Taylor, L. S. Effect of Temperature and Moisture on the Miscibility of Amorphous Dispersions of Felodipine and Poly (Vinyl Pyrrolidone). *J. Pharm. Sci.* **2010**, *99* (1), 169–185.

(81)   Hancock, B. C.; Zografi, G. The Relationship between the Glass Transition Temperature and the Water Content of Amorphous Pharmaceutical Solids. *Pharm. Res.* **1994**, *11* (4), 471–477.

(82)   Brouwers, J.; Brewster, M. E.; Augustijns, P. Supersaturating Drug Delivery Systems: The Answer to Solubility-limited Oral Bioavailability? *J. Pharm. Sci.* **2009**, *98* (8), 2549–2572.

(83)   Hate, S. S.; Reutzel-Edens, S. M.; Taylor, L. S. Insight into Amorphous Solid Dispersion Performance by Coupled Dissolution and Membrane Mass Transfer Measurements. *Mol. Pharm.* **2018**.

(84)   Mosquera-Giraldo, L. I.; Li, N.; Wilson, V. R.; Nichols, B. L. B.; Edgar, K. J.; Taylor, L. S. Influence of Polymer and Drug Loading on the Release Profile and Membrane Transport of Telaprevir. *Mol. Pharm.* **2018**.

(85)   Indulkar, A. S.; Waters, J. E.; Mo, H.; Gao, Y.; Raina, S. A.; Zhang, G. G. Z.; Taylor, L. S. Origin of Nanodroplet Formation Upon Dissolution of an Amorphous Solid Dispersion: A Mechanistic Isotope Scrambling Study. *J. Pharm. Sci.* **2018**, *106* (8), 1998–2008.

(86) Simonelli, A. P.; Mehta, S. C.; Higuchi, W. I. Dissolution Rates of High Energy Polyvinylpyrrolidone (PVP)-Sulfathiazole Coprecipitates. *J. Pharm. Sci.* **1969**, *58* (5), 538–549.

(87) Indulkar, A. S.; Lou, X.; Zhang, G. G. Z.; Taylor, L. S. Insights into the Dissolution Mechanism of Ritonavir–Copovidone Amorphous Solid Dispersions: Importance of Congruent Release for Enhanced Performance. *Mol. Pharm.* **2019**, *16* (3), 1327–1339.

(88) Vallet-Regi, M.; Ramila, A.; Del Real, R. P.; Pérez-Pariente, J. A New Property of MCM-41: Drug Delivery System. *Chem. Mater.* **2001**, *13* (2), 308–311.

(89) Kresge, C. T.; Leonowicz, M. E.; Roth, W. J.; Vartuli, J. C.; Beck, J. S. Ordered Mesoporous Molecular Sieves Synthesized by a Liquid-Crystal Template Mechanism. *Nature* **1992**, *359* (6397), 710–712.

(90) Vallet-Regí, M.; Balas, F.; Arcos, D. Mesoporous Materials for Drug Delivery. *Angew. Chemie Int. Ed.* **2007**, *46* (40), 7548–7558.

(91) Mellaerts, R.; Mols, R.; Jammaer, J. A. G.; Aerts, C. A.; Annaert, P.; Van Humbeeck, J.; Van den Mooter, G.; Augustijns, P.; Martens, J. A. Increasing the Oral Bioavailability of the Poorly Water Soluble Drug Itraconazole with Ordered Mesoporous Silica. *Eur. J. Pharm. Biopharm.* **2008**, *69* (1), 223–230.

(92) Cheng, S.; McKenna, G. B. Nanoconfinement Effects on the Glass Transition and Crystallization Behaviors of Nifedipine. *Mol. Pharm.* **2019**, *16* (2), 856–866.

(93) Mellaerts, R.; Aerts, C. A.; Van Humbeeck, J.; Augustijns, P.; Van den Mooter, G.; Martens, J. A. Enhanced Release of Itraconazole from Ordered Mesoporous SBA-15 Silica Materials. *Chem. Commun.* **2007**, No. 13, 1375–1377.

(94) Vallet-Regí, M.; Colilla, M.; Izquierdo-Barba, I.; Manzano, M. Mesoporous Silica Nanoparticles for Drug Delivery: Current Insights. *Molecules* **2018**, *23* (1), 47.

(95) Higuchi, T. Mechanism of Sustained-Action Medication. Theoretical Analysis of Rate of Release of Solid Drugs Dispersed in Solid Matrices. *J. Pharm. Sci.* **1963**, *52* (12), 1145–1149.

(96) Yang, P.; Gai, S.; Lin, J. Functionalized Mesoporous Silica Materials for Controlled Drug Delivery. *Chem. Soc. Rev.* **2012**, *41* (9), 3679–3698.

(97) Rosenholm, J. M.; Lindén, M. Towards Establishing Structure–Activity Relationships for Mesoporous Silica in Drug Delivery Applications. *J. Control. release* **2008**, *128* (2), 157–164.

(98) Sjöberg, S. Silica in Aqueous Environments. *J. Non. Cryst. Solids* **1996**, *196*, 51–57.

(99) Augustijns, P.; Brewster, M. E. Supersaturating Drug Delivery Systems: Fast Is Not Necessarily Good Enough. *J. Pharm. Sci.* **2012**, *101* (1), 7–9.

(100) Galia, E.; Nicolaides, E.; Hörter, D.; Löbenberg, R.; Reppas, C.; Dressman, J. B. Evaluation of Various Dissolution Media for Predicting in Vivo Performance of Class I and II Drugs. *Pharm. Res.* **1998**, *15* (5), 698–705.

(101) Klein, S. The Use of Biorelevant Dissolution Media to Forecast the in Vivo Performance of a Drug. *AAPS J.* **2010**, *12* (3), 397–406.

(102) Vatier, J.; MALIKOVA-SEKERA, E.; Vitre, M. T.; Mignon, M. An Artificial Stomach-duodenum Model for the In-vitro Evaluation of Antacids. *Aliment. Pharmacol. Ther.* **1992**, *6* (4), 447–458.

(103) Matsui, K.; Tsume, Y.; Amidon, G. E.; Amidon, G. L. The Evaluation of in Vitro Drug Dissolution of Commercially Available Oral Dosage Forms for Itraconazole in Gastrointestinal Simulator with Biorelevant Media. *J. Pharm. Sci.* **2016**, *105* (9), 2804–2814.

(104) Jan Bevernage Marcus E. Brewster, Patrick Augustijns, J. B. Evaluation of Gastrointestinal Drug Supersaturation and Precipitation: Strategies Issues. *Int. J. Pharm.* **2013**, *453*, 25–35.

(105) Gibaldi, M.; Feldman, S. Establishment of Sink Conditions in Dissolution Rate Determinations. Theoretical Considerations and Application to Nondisintegrating Dosage Forms. *J. Pharm. Sci.* **1967**, *56* (10), 1238–1242.

(106) Buch, P.; Langguth, P.; Kataoka, M.; Yamashita, S. IVIVC in Oral Absorption for Fenofibrate Immediate Release Tablets Using a Dissolution/Permeation System. *J. Pharm. Sci.* **2009**, *98* (6), 2001–2009.

(107) Kobayashi, M.; Sada, N.; Sugawara, M.; Iseki, K.; Miyazaki, K. Development of a New System for Prediction of Drug Absorption That Takes into Account Drug Dissolution and PH Change in the Gastro-Intestinal Tract. *Int. J. Pharm.* **2001**, *221* (1), 87–94.

(108) Motz, S. A.; Schaefer, U. F.; Balbach, S.; Eichinger, T.; Lehr, C. M. Permeability Assessment for Solid Oral Drug Formulations Based on Caco-2 Monolayer in Combination with a Flow through Dissolution Cell. *Eur. J. Pharm. Biopharm.* **2007**, *66* (2), 286–295.

(109) Twist, J. N.; Zatz, J. L. Influence of Solvents on Paraben Permeation through Idealized Skin Model Membranes. *J. Soc. Cosmet. Chem.* **1986**, *37* (6), 429–444.

(110) Sironi, D.; Rosenberg, J.; Bauer-Brandl, A.; Brandl, M. Dynamic Dissolution-/Permeation-Testing of Nano-and Microparticle Formulations of Fenofibrate. *Eur. J. Pharm. Sci.* **2017**, *96*, 20–27.

(111) D'elia, N. A.; Dahuron, L.; Cussler, E. L. Liquid-Liquid Extractions with Microporous Hollow Fibers. *J. Memb. Sci.* **1986**, *29* (3), 309–319.

(112) Prasad, R.; Sirkar, K. K. Hollow Fiber Solvent Extraction of Pharmaceutical Products: A Case Study. *J. Memb. Sci.* **1989**, *47* (3), 235–259.

(113) Buckley, S. T.; Fischer, S. M.; Fricker, G.; Brandl, M. In Vitro Models to Evaluate the Permeability of Poorly Soluble Drug Entities: Challenges and Perspectives. *Eur. J. Pharm. Sci.* **2012**, *45* (3), 235–250.

(114) Lamson, M. J.; Sabo, J. P.; Macgregor, T. R.; Pav, J. W.; Rowland, L.; Hawi, A.; Cappola, M.; Robinson, P. Single Dose Pharmacokinetics and Bioavailability of Nevirapine in Healthy Volunteers. *Biopharm. Drug Dispos.* **1999**, *20* (6), 285–291.

(115) Raina, S. A.; Zhang, G. G. Z.; Alonzo, D. E.; Wu, J.; Zhu, D.; Catron, N. D.; Gao, Y.; Taylor, L. S. Impact of Solubilizing Additives on Supersaturation and Membrane Transport of Drugs. *Pharm. Res.* **2015**, *32* (10), 3350–3364.

(116) Takano, R.; Takata, N.; Saito, R.; Furumoto, K.; Higo, S.; Hayashi, Y.; Machida, M.; Aso, Y.; Yamashita, S. Quantitative Analysis of the Effect of Supersaturation on in Vivo Drug Absorption. *Mol. Pharm.* **2010**, *7* (5), 1431–1440.

(117) Kohri, N.; Yamayoshi, Y.; Xin, H. E.; Iseki, K. E. N.; SATO, N.; TODO, S.; MIYAZAKI, K. Improving the Oral Bioavailability of Albendazole in Rabbits by the Solid Dispersion Technique. *J. Pharm. Pharmacol.* **1999**, *51* (2), 159–164.

(118) Yamashita, K.; Nakate, T.; Okimoto, K.; Ohike, A.; Tokunaga, Y.; Ibuki, R.; Higaki, K.; Kimura, T. Establishment of New Preparation Method for Solid Dispersion Formulation of Tacrolimus. *Int. J. Pharm.* **2003**, *267* (1–2), 79–91.

(119) Miller, M. A.; DiNunzio, J.; Matteucci, M. E.; Ludher, B. S.; Williams, R. O.; Johnston, K. P. Flocculated Amorphous Itraconazole Nanoparticles for Enhanced in Vitro Supersaturation and in Vivo Bioavailability. *Drug Dev. Ind. Pharm.* **2012**, *38* (5), 557–570.

(120) Almeida e Sousa, L.; Reutzel-Edens, S.; Stephenson, G.; S. Taylor, L. *Supersaturation Potential of Salt, Co-Crystal, and Amorphous Forms of a Model Weak Base*; 2016; Vol. 16.

(121) Kennedy, M.; Hu, J.; Gao, P.; Li, L.; Ali-Reynolds, A.; Chal, B.; Gupta, V.; Ma, C.; Mahajan, N.; Akrami, A.; et al. Enhanced Bioavailability of a Poorly Soluble VR1 Antagonist Using an Amorphous Solid Dispersion Approach: A Case Study. *Mol. Pharm.* **2008**, *5* (6), 981–993.

(122) Newman, A.; Knipp, G.; Zografi, G. Assessing the Performance of Amorphous Solid Dispersions. *J. Pharm. Sci.* **2011**, *101* (4), 1355–1377.

(123) Vasconcelos, T.; Sarmento, B.; Costa, P. Solid Dispersions as Strategy to Improve Oral Bioavailability of Poor Water Soluble Drugs. *Drug Discov. Today* **2007**, *12* (23), 1068–1075.

(124) Stewart, A. M.; Grass, M. E.; Brodeur, T. J.; Goodwin, A. K.; Morgen, M. M.; Friesen, D. T.; Vodak, D. T. Impact of Drug-Rich Colloids of Itraconazole and HPMCAS on Membrane Flux in Vitro and Oral Bioavailability in Rats. *Mol. Pharm.* **2017**, *14* (7), 2437–2449.

(125) McAllister, M. Dynamic Dissolution: A Step Closer to Predictive Testing? *Mol. Pharm.* **2010**, *7* (5), 1374–1387.

(126) Hate, S. S.; Reutzel-Edens, S. M.; Taylor, L. S. Absorptive Dissolution Testing of Supersaturating Systems: Impact of Absorptive Sink Conditions on Solution Phase Behavior and Mass Transport. *Mol. Pharm.* **2017**.

(127) Amidon, G. L.; Kou, J.; Elliott, R. L.; Lightfoot, E. N. Analysis of Models for Determining Intestinal Wall Permeabilities. *J. Pharm. Sci.* **1980**, *69* (12), 1369–1373.

(128) Levitt, M. D.; Kneip, J. M.; Levitt, D. G. Use of Laminar Flow and Unstirred Layer Models to Predict Intestinal Absorption in the Rat. *J. Clin. Invest.* **1988**, *81* (5), 1365–1369.

(129) Elliott, R. L.; Amidon, G. L.; Lightfoot, E. N. A Convective Mass Transfer Model for Determining Intestinal Wall Permeabilities: Laminar Flow in a Circular Tube. *J. Theor. Biol.* **1980**, *87* (4), 757–771.

(130) Indulkar, A. S.; Gao, Y.; Raina, S. A.; Zhang, G. G. Z.; Taylor, L. S. Crystallization from Supersaturated Solutions: Role of Lecithin and Composite Simulated Intestinal Fluid. *Pharm. Res.* **2018**, *35* (8), 158.

(131) Simonelli, A. P.; Mehta, S. C.; Higuchi, W. I. Dissolution Rates of High Energy Sulfathiazole-Povidone Coprecipitates II: Characterization of Form of Drug Controlling Its Dissolution Rate via Solubility Studies. *J. Pharm. Sci.* **1976**, *65* (3), 355–361.

(132) Alonzo, D. E.; Gao, Y.; Zhou, D.; Mo, H.; Zhang, G. G. Z.; Taylor, L. S. Dissolution and Precipitation Behavior of Amorphous Solid Dispersions. *J. Pharm. Sci.* **2011**, *100* (8), 3316–3331.

(133) Indulkar, A. S.; Box, K. J.; Taylor, R.; Ruiz, R.; Taylor, L. S. PH-Dependent Liquid–Liquid Phase Separation of Highly Supersaturated Solutions of Weakly Basic Drugs. *Mol. Pharm.* **2015**, *12* (7), 2365–2377.

(134) Friesen, D. T.; Shanker, R.; Crew, M.; Smithey, D. T.; Curatolo, W. J.; Nightingale, J. A. S. Hydroxypropyl Methylcellulose Acetate Succinate-Based Spray-Dried Dispersions: An Overview. *Mol. Pharm.* **2008**, *5* (6), 1003–1019.

(135) Chen, R.; Ilasi, N.; Sekulic, S. S. Absolute Molecular Weight Determination of Hypromellose Acetate Succinate by Size Exclusion Chromatography: Use of a Multi Angle Laser Light Scattering Detector and a Mixed Solvent. *J. Pharm. Biomed. Anal.* **2011**, *56* (4), 743–748.

(136) Indulkar, A. S.; Mo, H.; Gao, Y.; Raina, S. A.; Zhang, G. G. Z.; Taylor, L. S. Impact of Micellar Surfactant on Supersaturation and Insight into Solubilization Mechanisms in Supersaturated Solutions of Atazanavir. *Pharm. Res.* **2017**, *34* (6), 1276–1295.

(137) Van Eerdenbrugh, B.; Alonzo, D. E.; Taylor, L. S. Influence of Particle Size on the Ultraviolet Spectrum of Particulate-Containing Solutions: Implications for in-Situ Concentration Monitoring Using UV/Vis Fiber-Optic Probes. *Pharm. Res.* **2011**, *28* (7), 1643–1652.

(138) Purohit, H. S.; Taylor, L. S. Phase Behavior of Ritonavir Amorphous Solid Dispersions during Hydration and Dissolution. *Pharm. Res.* **2017**, *34* (12), 2842–2861.

(139) Berben, P.; Bauer-Brandl, A.; Brandl, M.; Faller, B.; Flaten, G. E.; Jacobsen, A.-C.; Brouwers, J.; Augustijns, P. Drug Permeability Profiling Using Cell-Free Permeation Tools: Overview and Applications. *Eur. J. Pharm. Sci.* **2018**.

(140) Bird, R. B.; Stewart, W. E.; Lightfoot, E. N. *Transport Phenomena*; Wiley International edition; Wiley, 2007.

(141) Krishnamurthy, S.; Bhattacharya, P.; Phelan, P. E.; Prasher, R. S. Enhanced Mass Transport in Nanofluids. *Nano Lett.* **2006**, *6* (3), 419–423.

(142) Pang, C.; Lee, J. W.; Kang, Y. T. Review on Combined Heat and Mass Transfer Characteristics in Nanofluids. *Int. J. Therm. Sci.* **2015**, *87*, 49–67.

(143) Yalkowsky, S. H. *Solubility and Solubilization in Aqueous Media*; ACS Professional Reference Book Series; American Chemical Society, 1999.

(144) Higuchi, W. I.; Hiestand, E. N. Dissolution Rates of Finely Divided Drug Powders I. Effect of a Distribution of Particle Sizes in a Diffusion-controlled Process. *J. Pharm. Sci.* **1963**, *52* (1), 67–71.

(145) Elzey, S.; Grassian, V. H. Nanoparticle Dissolution from the Particle Perspective: Insights from Particle Sizing Measurements. *Langmuir* **2010**, *26* (15), 12505–12508.

(146) Wilson, V.; Lou, X.; Osterling, D. J.; Stolarik, D. F.; Jenkins, G.; Gao, W.; Zhang, G. G. Z.; Taylor, L. S. Relationship between Amorphous Solid Dispersion In Vivo Absorption and In Vitro Dissolution: Phase Behavior during Dissolution, Speciation, and Membrane Mass Transport. *J. Control. Release* **2018**.

(147) Golub, A. L.; Frost, R. W.; Betlach, C. J.; Gonzalez, M. A. Physiologic Considerations in Drug Absorption from the Gastrointestinal Tract. *J. Allergy Clin. Immunol.* **1986**, *78* (4), 689–694.

(148) Mudie, D. M.; Amidon, G. L.; Amidon, G. E. Physiological Parameters for Oral Delivery and in Vitro Testing. *Mol. Pharm.* **2010**, *7* (5), 1388–1405.

(149) Tanaka, Y.; Goto, T.; Kataoka, M.; Sakuma, S.; Yamashita, S. Impact of Luminal Fluid Volume on the Drug Absorption after Oral Administration: Analysis Based on in Vivo Drug Concentration–Time Profile in the Gastrointestinal Tract. *J. Pharm. Sci.* **2015**, *104* (9), 3120–3127.

(150) Steingoetter, A.; Fox, M.; Treier, R.; Weishaupt, D.; Marincek, B.; Boesiger, P.; Fried, M.; Schwizer, W. Effects of Posture on the Physiology of Gastric Emptying: A Magnetic Resonance Imaging Study. *Scand. J. Gastroenterol.* **2006**, *41* (10), 1155–1164.

(151) Kwiatek, M. A.; Menne, D.; Steingoetter, A.; Goetze, O.; Forras-Kaufman, Z.; Kaufman, E.; Fruehauf, H.; Boesiger, P.; Fried, M.; Schwizer, W. Effect of Meal Volume and Calorie Load on Postprandial Gastric Function and Emptying: Studies under Physiological Conditions by Combined Fiber-Optic Pressure Measurement and MRI. *Am. J. Physiol. Liver Physiol.* **2009**, *297* (5), G894–G901.

(152) Mudie, D. M.; Murray, K.; Hoad, C. L.; Pritchard, S. E.; Garnett, M. C.; Amidon, G. L.; Gowland, P. A.; Spiller, R. C.; Amidon, G. E.; Marciani, L. Quantification of Gastrointestinal Liquid Volumes and Distribution Following a 240 ML Dose of Water in the Fasted State. *Mol. Pharm.* **2014**, *11* (9), 3039–3047.

(153) Schiller, C.; Fröhlich, C.; Giessmann, T.; Siegmund, W.; Mönnikes, H.; Hosten, N.; Weitschies, W. Intestinal Fluid Volumes and Transit of Dosage Forms as Assessed by Magnetic Resonance Imaging. *Aliment. Pharmacol. Ther.* **2005**, *22* (10), 971–979.

(154) Zaborenko, N.; Shi, Z.; Corredor, C. C.; Smith-Goettler, B. M.; Zhang, L.; Hermans, A.; Neu, C. M.; Alam, M. A.; Cohen, M. J.; Lu, X.; et al. First-Principles and Empirical Approaches to Predicting In Vitro Dissolution for Pharmaceutical Formulation and Process Development and for Product Release Testing. *AAPS J.* **2019**, *21* (3), 32.

(155) Sun, D. D.; Wen, H.; Taylor, L. S. Non-Sink Dissolution Conditions for Predicting Product Quality and In Vivo Performance of Supersaturating Drug Delivery Systems. *J. Pharm. Sci.* **2016**, *105* (9), 2477–2488.

(156) Liu, C.; Chen, Z.; Chen, Y.; Lu, J.; Li, Y.; Wang, S.; Wu, G.; Qian, F. Improving Oral Bioavailability of Sorafenib by Optimizing the "Spring" and "Parachute" Based on Molecular Interaction Mechanisms. *Mol. Pharm.* **2016**, *13* (2), 599–608.

(157) Van den Mooter, G. The Use of Amorphous Solid Dispersions: A Formulation Strategy to Overcome Poor Solubility and Dissolution Rate. *Drug Discov. Today Technol.* **2012**, *9* (2), e79–e85.

(158) Que, C.; Gao, Y.; Raina, S. A.; Zhang, G. G. Z.; Taylor, L. S. Paclitaxel Crystal Seeds with Different Intrinsic Properties and Their Impact on Dissolution of Paclitaxel-HPMCAS Amorphous Solid Dispersions. *Cryst. Growth Des.* **2018**, *18* (3), 1548–1559.

(159) Purohit, H. S.; Trasi, N. S.; Sun, D. D.; Chow, E. C. Y.; Wen, H.; Zhang, X.; Gao, Y.; Taylor, L. S. Investigating the Impact of Drug Crystallinity in Amorphous Tacrolimus Capsules on Pharmacokinetics and Bioequivalence Using Discriminatory In Vitro Dissolution Testing and Physiologically Based Pharmacokinetic Modeling and Simulation. *J. Pharm. Sci.* **2018**, *107* (5), 1330–1341.

(160) Purohit, H. S.; Trasi, N. S.; Osterling, D. J.; Stolarik, D. F.; Jenkins, G. J.; Gao, W.; Zhang, G. G. Z.; Taylor, L. S. Assessing the Impact of Endogenously Derived Crystalline Drug on the in Vivo Performance of Amorphous Formulations. *Mol. Pharm.* **2019**, *16* (8), 3617–3625.

(161) Knopp, M. M.; Wendelboe, J.; Holm, R.; Rades, T. Effect of Amorphous Phase Separation and Crystallization on the in Vitro and in Vivo Performance of an Amorphous Solid Dispersion. *Eur. J. Pharm. Biopharm.* **2018**, *130*, 290–295.

(162) Trasi, N. S.; Purohit, H. S.; Wen, H.; Sun, D. D.; Taylor, L. S. Non-Sink Dissolution Behavior and Solubility Limit of Commercial Tacrolimus Amorphous Formulations. *J. Pharm. Sci.* **2017**, *106* (1), 264–272.

(163) Administration, F. and D. Guidance for Industry: Bioavailability and Bioequivalence Studies for Orally Administered Drug Products—General Considerations. *Food Drug Adm. Washington, DC* **2003**.

(164) Gray, V. A. Power of the Dissolution Test in Distinguishing a Change in Dosage Form Critical Quality Attributes. *AAPS PharmSciTech* **2018**, *19* (8), 3328–3332.

(165) Grady, H.; Elder, D.; Webster, G. K.; Mao, Y.; Lin, Y.; Flanagan, T.; Mann, J.; Blanchard, A.; Cohen, M. J.; Lin, J. Industry's View on Using Quality Control, Biorelevant, and Clinically Relevant Dissolution Tests for Pharmaceutical Development, Registration, and Commercialization. *J. Pharm. Sci.* **2018**, *107* (1), 34–41.

(166) Forrest, W. P.; Reuter, K. G.; Shah, V.; Kazakevich, I.; Heslinga, M.; Dudhat, S.; Patel, S.; Neri, C.; Mao, Y. USP Apparatus 4: A Valuable In Vitro Tool to Enable Formulation Development of Long-Acting Parenteral (LAP) Nanosuspension Formulations of Poorly Water-Soluble Compounds. *AAPS PharmSciTech* **2018**, *19* (1), 413–424.

(167) Yamashita, K.; Hashimoto, E.; Nomura, Y.; Shimojo, F.; Tamura, S.; Hirose, T.; Ueda, S.; Saitoh, T.; Ibuki, R.; Ideno, T. Sustained Release Formulations Containing Tacrolimus. Google Patents June 10, 2003.

(168) Schram, C. J.; Smyth, R. J.; Taylor, L. S.; Beaudoin, S. P. Understanding Crystal Growth Kinetics in the Absence and Presence of a Polymer Using a Rotating Disk Apparatus. *Cryst. Growth Des.* **2016**, *16* (5), 2640–2645.

(169) Ichijo, K.; Oda, R.; Ishihara, M.; Okada, R.; Moteki, Y.; Funai, Y.; Horiuchi, T.; Kishimoto, H.; Shirasaka, Y.; Inoue, K. Osmolality of Orally Administered Solutions Influences Luminal Water Volume and Drug Absorption in Intestine. *J. Pharm. Sci.* **2017**, *106* (9), 2889–2894.

(170) Ensor, C. R.; Trofe-Clark, J.; Gabardi, S.; McDevitt-Potter, L. M.; Shullo, M. A. Generic Maintenance Immunosuppression in Solid Organ Transplant Recipients. *Pharmacother. J. Hum. Pharmacol. Drug Ther.* **2011**, *31* (11), 1111–1129.

(171) Zhao, D.; Sun, J.; Li, Q.; Stucky, G. D. Morphological Control of Highly Ordered Mesoporous Silica SBA-15. *Chem. Mater.* **2000**, *12* (2), 275–279.

(172) Florek, J.; Guillet-Nicolas, R.; Kleitz, F. Ordered Mesoporous Silica: Synthesis and Applications. *Funct. Mater. Energy, Sustain. Dev. Biomed. Sci. ed. M. Leclerc R. Gauvin, Gruyter* **2014**, 61–100.

(173) Wang, S. Ordered Mesoporous Materials for Drug Delivery. *Microporous mesoporous Mater.* **2009**, *117* (1–2), 1–9.

(174) Ahern, R. J.; Hanrahan, J. P.; Tobin, J. M.; Ryan, K. B.; Crean, A. M. Comparison of Fenofibrate–Mesoporous Silica Drug-Loading Processes for Enhanced Drug Delivery. *Eur. J. Pharm. Sci.* **2013**, *50* (3), 400–409.

(175) Mellaerts, R.; Jammaer, J. A. G.; Van Speybroeck, M.; Chen, H.; Humbeeck, J. Van; Augustijns, P.; Van den Mooter, G.; Martens, J. A. Physical State of Poorly Water Soluble Therapeutic Molecules Loaded into SBA-15 Ordered Mesoporous Silica Carriers: A Case Study with Itraconazole and Ibuprofen. *Langmuir* **2008**, *24* (16), 8651–8659.

(176) Prasad, B. R.; Lele, S. Stabilization of the Amorphous Phase inside Carbon Nanotubes: Solidification in a Constrained Geometry. *Philos. Mag. Lett.* **1994**, *70* (6), 357–361.

(177) Zhang, Y.; Zhi, Z.; Jiang, T.; Zhang, J.; Wang, Z.; Wang, S. Spherical Mesoporous Silica Nanoparticles for Loading and Release of the Poorly Water-Soluble Drug Telmisartan. *J. Control. Release* **2010**, *145* (3), 257–263.

(178) Andersson, J.; Rosenholm, J.; Areva, S.; Lindén, M. Influences of Material Characteristics on Ibuprofen Drug Loading and Release Profiles from Ordered Micro-and Mesoporous Silica Matrices. *Chem. Mater.* **2004**, *16* (21), 4160–4167.

(179) Azaïs, T.; Tourné-Péteilh, C.; Aussenac, F.; Baccile, N.; Coelho, C.; Devoisselle, J.-M.; Babonneau, F. Solid-State NMR Study of Ibuprofen Confined in MCM-41 Material. *Chem. Mater.* **2006**, *18* (26), 6382–6390.

(180) Horcajada, P.; Ramila, A.; Perez-Pariente, J.; Vallet-Regı, M. Influence of Pore Size of MCM-41 Matrices on Drug Delivery Rate. *Microporous Mesoporous Mater.* **2004**, *68* (1–3), 105–109.

(181) Vallet-Regí, M.; Balas, F.; Colilla, M.; Manzano, M. Bioceramics and Pharmaceuticals: A Remarkable Synergy. *Solid state Sci.* **2007**, *9* (9), 768–776.

(182) Rosenholm, J. M.; Sahlgren, C.; Lindén, M. Towards Multifunctional, Targeted Drug Delivery Systems Using Mesoporous Silica Nanoparticles–Opportunities & Challenges. *Nanoscale* **2010**, *2* (10), 1870–1883.

(183) Van Speybroeck, M.; Mellaerts, R.; Mols, R.; Do Thi, T.; Martens, J. A.; Van Humbeeck, J.; Annaert, P.; Van den Mooter, G.; Augustijns, P. Enhanced Absorption of the Poorly Soluble Drug Fenofibrate by Tuning Its Release Rate from Ordered Mesoporous Silica. *Eur. J. Pharm. Sci.* **2010**, *41* (5), 623–630.

(184) Mellaerts, R.; Mols, R.; Kayaert, P.; Annaert, P.; Van Humbeeck, J.; Van den Mooter, G.; Martens, J. A.; Augustijns, P. Ordered Mesoporous Silica Induces PH-Independent Supersaturation of the Basic Low Solubility Compound Itraconazole Resulting in Enhanced Transepithelial Transport. *Int. J. Pharm.* **2008**, *357* (1–2), 169–179.

(185) McCarthy, C. A.; Ahern, R. J.; Devine, K. J.; Crean, A. M. Role of Drug Adsorption onto the Silica Surface in Drug Release from Mesoporous Silica Systems. *Mol. Pharm.* **2017**, *15* (1), 141–149.

(186) Jambhrunkar, S.; Qu, Z.; Popat, A.; Yang, J.; Noonan, O.; Acauan, L.; Ahmad Nor, Y.; Yu, C.; Karmakar, S. Effect of Surface Functionality of Silica Nanoparticles on Cellular Uptake and Cytotoxicity. *Mol. Pharm.* **2014**, *11* (10), 3642–3655.

(187) Jambhrunkar, S.; Qu, Z.; Popat, A.; Karmakar, S.; Xu, C.; Yu, C. Modulating in Vitro Release and Solubility of Griseofulvin Using Functionalized Mesoporous Silica Nanoparticles. *J. Colloid Interface Sci.* **2014**, *434*, 218–225.

(188) Qu, F.; Zhu, G.; Huang, S.; Li, S.; Sun, J.; Zhang, D.; Qiu, S. Controlled Release of Captopril by Regulating the Pore Size and Morphology of Ordered Mesoporous Silica. *Microporous Mesoporous Mater.* **2006**, *92* (1–3), 1–9.

(189) Munoz, B.; Ramila, A.; Perez-Pariente, J.; Diaz, I.; Vallet-Regi, M. MCM-41 Organic Modification as Drug Delivery Rate Regulator. *Chem. Mater.* **2003**, *15* (2), 500–503.

(190) Smirnova, I.; Mamic, J.; Arlt, W. Adsorption of Drugs on Silica Aerogels. *Langmuir* **2003**, *19* (20), 8521–8525.

(191) Kumar, D.; Sailaja Chirravuri, S. V; Shastri, N. R. Impact of Surface Area of Silica Particles on Dissolution Rate and Oral Bioavailability of Poorly Water Soluble Drugs: A Case Study with Aceclofenac. *Int. J. Pharm.* **2014**, *461* (1), 459–468.

(192) McCarthy, C. A.; Ahern, R. J.; Devine, K. J.; Crean, A. M. Role of Drug Adsorption onto the Silica Surface in Drug Release from Mesoporous Silica Systems. *Mol. Pharm.* **2018**, *15* (1), 141–149.

(193) Van Speybroeck, M.; Mols, R.; Mellaerts, R.; Thi, T. Do; Martens, J. A.; Humbeeck, J. Van; Annaert, P.; Mooter, G. Van den; Augustijns, P. Combined Use of Ordered Mesoporous Silica and Precipitation Inhibitors for Improved Oral Absorption of the Poorly Soluble Weak Base Itraconazole. *Eur. J. Pharm. Biopharm.* **2010**, *75* (3), 354–365.

(194) Limnell, T.; Santos, H. A.; Mäkilä, E.; Heikkilä, T.; Salonen, J.; Murzin, D. Y.; Kumar, N.; Laaksonen, T.; Peltonen, L.; Hirvonen, J. Drug Delivery Formulations of Ordered and Nonordered Mesoporous Silica: Comparison of Three Drug Loading Methods. *J. Pharm. Sci.* **2011**, *100* (8), 3294–3306.

(195) Hate, S. S.; Reutzel-Edens, S. M.; Taylor, L. S. Absorptive Dissolution Testing: An Improved Approach to Study the Impact of Residual Crystallinity on the Performance of Amorphous Formulations. *J. Pharm. Sci.* **2019**.

(196) Florek, J.; Caillard, R.; Kleitz, F. Evaluation of Mesoporous Silica Nanoparticles for Oral Drug Delivery – Current Status and Perspective of MSNs Drug Carriers. *Nanoscale* **2017**, *9* (40), 15252–15277.

(197) Vialpando, M.; Smulders, S.; Bone, S.; Jager, C.; Vodak, D.; Van Speybroeck, M.; Verheyen, L.; Backx, K.; Boeykens, P.; Brewster, M. E.; et al. Evaluation of Three Amorphous Drug Delivery Technologies to Improve the Oral Absorption of Flubendazole. *J. Pharm. Sci.* **2016**, *105* (9), 2782–2793.

(198) Dening, T. J.; Zemlyanov, D.; Taylor, L. S. Application of an Adsorption Isotherm to Explain Incomplete Drug Release from Ordered Mesoporous Silica Materials under Supersaturating Conditions. *J. Control. Release* **2019**.

(199) Parfitt, G. D.; Rochester, C. H. *Adsorption from Solution at the Solid/Liquid Interface*; Academic press London, 1983; Vol. 122.

(200) Brunauer, S.; Emmett, P. H.; Teller, E. Adsorption of Gases in Multimolecular Layers. *J. Am. Chem. Soc.* **1938**, *60* (2), 309–319.

(201) Kara, S.; Aydiner, C.; Demirbas, E.; Kobya, M.; Dizge, N. Modeling the Effects of Adsorbent Dose and Particle Size on the Adsorption of Reactive Textile Dyes by Fly Ash. *Desalination* **2007**, *212* (1–3), 282–293.

(202) Sivaraj, R.; Namasivayam, C.; Kadirvelu, K. Orange Peel as an Adsorbent in the Removal of Acid Violet 17 (Acid Dye) from Aqueous Solutions. *Waste Manag.* **2001**, *21* (1), 105–110.

(203) Xu, Y.; Ohki, A.; Maeda, S. Adsorption and Removal of Antimony from Aqueous Solution by an Activated Alumina: 1. Adsorption Capacity of Adsorbent and Effect of Process Variables. *Toxicol. Environ. Chem.* **2001**, *80* (3–4), 133–144.

(204) Yapar, S.; Özbudak, V.; Dias, A.; Lopes, A. Effect of Adsorbent Concentration to the Adsorption of Phenol on Hexadecyl Trimethyl Ammonium-Bentonite. *J. Hazard. Mater.* **2005**, *121* (1–3), 135–139.

(205) Pradhan, J.; Das, S. N.; Thakur, R. S. Adsorption of Hexavalent Chromium from Aqueous Solution by Using Activated Red Mud. *J. Colloid Interface Sci.* **1999**, *217* (1), 137–141.

(206) Ellison, C. J.; Torkelson, J. M. The Distribution of Glass-Transition Temperatures in Nanoscopically Confined Glass Formers. *Nat. Mater.* **2003**, *2* (10), 695.

(207) Park, J.-Y.; McKenna, G. B. Size and Confinement Effects on the Glass Transition Behavior of Polystyrene/o-Terphenyl Polymer Solutions. *Phys. Rev. B* **2000**, *61* (10), 6667.

(208) Tang, X. C.; Pikal, M. J.; Taylor, L. S. A Spectroscopic Investigation of Hydrogen Bond Patterns in Crystalline and Amorphous Phases in Dihydropyridine Calcium Channel Blockers. *Pharm. Res.* **2002**, *19* (4), 477–483.

(209) Ahlneck, C.; Zografi, G. The Molecular Basis of Moisture Effects on the Physical and Chemical Stability of Drugs in the Solid State. *Int. J. Pharm.* **1990**, *62* (2–3), 87–95.

(210) Jackson, C. L.; McKenna, G. B. The Melting Behavior of Organic Materials Confined in Porous Solids. *J. Chem. Phys.* **1990**, *93* (12), 9002–9011.

(211) Babonneau, F.; Yeung, L.; Steunou, N.; Gervais, C.; Ramila, A.; Vallet-Regi, M. Solid State NMR Characterisation of Encapsulated Molecules in Mesoporous Silica. *J. sol-gel Sci. Technol.* **2004**, *31* (1–3), 219–223.

(212) Catlow, C. R. A.; Van Speybroeck, V.; van Santen, R. *Modelling and Simulation in the Science of Micro-and Meso-Porous Materials*; Elsevier, 2017.

(213) Paolone, A.; Palumbo, O.; Rispoli, P.; Cantelli, R.; Autrey, T.; Karkamkar, A. Absence of the Structural Phase Transition in Ammonia Borane Dispersed in Mesoporous Silica: Evidence of Novel Thermodynamic Properties. *J. Phys. Chem. C* **2009**, *113* (24), 10319–10321.

(214) Yang, S.; Liu, Z.; Jiao, Y.; Liu, Y.; Ji, C.; Zhang, Y. New Insight into PEO Modified Inner Surface of HNTs and Its Nano-Confinement within Nanotube. *J. Mater. Sci.* **2014**, *49* (12), 4270–4278.

(215) Chen, K.; Wilkie, C. A.; Vyazovkin, S. Nanoconfinement Revealed in Degradation and Relaxation Studies of Two Structurally Different Polystyrene−Clay Systems. *J. Phys. Chem. B* **2007**, *111* (44), 12685–12692.

(216) Sulpizi, M.; Gaigeot, M.-P.; Sprik, M. The Silica–Water Interface: How the Silanols Determine the Surface Acidity and Modulate the Water Properties. *J. Chem. Theory Comput.* **2012**, *8* (3), 1037–1047.

(217) Fu, Y.; Hansen, R. S.; Bartell, F. E. Thermodynamics of Adsorption from Solutions. I. The Molality and Activity "Co-Efficient of Adsorbed Layers. *J. Phys. Colloid Chem.* **1948**, *52* (2), 374–386.

(218) Joos, P.; Serrien, G. The Principle of Braun—Le Châtelier at Surfaces. *J. Colloid Interface Sci.* **1991**, *145* (1), 291–294.

(219) Tao, Q.; Xu, Z.; Wang, J.; Liu, F.; Wan, H.; Zheng, S. Adsorption of Humic Acid to Aminopropyl Functionalized SBA-15. *Microporous Mesoporous Mater.* **2010**, *131* (1–3), 177–185.

(220) Achenbach, C. J.; Darin, K. M.; Murphy, R. L.; Katlama, C. Atazanavir/Ritonavir-Based Combination Antiretroviral Therapy for Treatment of HIV-1 Infection in Adults. *Future Virol.* **2011**, *6* (2), 157–177.

(221) Colilla, M.; Izquierdo-Barba, I.; Sánchez-Salcedo, S.; Fierro, J. G.; Hueso, J.; Vallet-Regí, M. Synthesis and Characterization of Zwitterionic SBA-15 Nanostructured Materials. *Chem. Mater.* **2010**, *22* (23), 6459–6466.

(222) McCarthy, C. A.; Ahern, R. J.; Dontireddy, R.; Ryan, K. B.; Crean, A. M. Mesoporous Silica Formulation Strategies for Drug Dissolution Enhancement: A Review. *Expert Opin. Drug Deliv.* **2016**, *13* (1), 93–108.

(223) Doadrio, J. C.; Sousa, E. M. B.; Izquierdo-Barba, I.; Doadrio, A. L.; Perez-Pariente, J.; Vallet-Regí, M. Functionalization of Mesoporous Materials with Long Alkyl Chains as a Strategy for Controlling Drug Delivery Pattern. *J. Mater. Chem.* **2006**, *16* (5), 462–466.

(224) Lee, C.; Lo, L.; Mou, C.; Yang, C. Synthesis and Characterization of Positive-charge Functionalized Mesoporous Silica Nanoparticles for Oral Drug Delivery of an Anti-inflammatory Drug. *Adv. Funct. Mater.* **2008**, *18* (20), 3283–3292.

(225) Muhammad, F.; Guo, M.; Qi, W.; Sun, F.; Wang, A.; Guo, Y.; Zhu, G. PH-Triggered Controlled Drug Release from Mesoporous Silica Nanoparticles via Intracelluar Dissolution of ZnO Nanolids. *J. Am. Chem. Soc.* **2011**, *133* (23), 8778–8781.

(226) Charnay, C.; Bégu, S.; Tourné-Péteilh, C.; Nicole, L.; Lerner, D. A.; Devoisselle, J.-M. Inclusion of Ibuprofen in Mesoporous Templated Silica: Drug Loading and Release Property. *Eur. J. Pharm. Biopharm.* **2004**, *57* (3), 533–540.

(227) Van Speybroeck, M.; Mellaerts, R.; Thi, T. Do; Martens, J. A.; Van Humbeeck, J.; Annaert, P.; Van den Mooter, G.; Augustijns, P. Preventing Release in the Acidic Environment of the Stomach via Occlusion in Ordered Mesoporous Silica Enhances the Absorption of Poorly Soluble Weakly Acidic Drugs. *J. Pharm. Sci.* **2011**, *100* (11), 4864–4876.

(228) Cheng, S.-H.; Liao, W.-N.; Chen, L.-M.; Lee, C.-H. PH-Controllable Release Using Functionalized Mesoporous Silica Nanoparticles as an Oral Drug Delivery System. *J. Mater. Chem.* **2011**, *21* (20), 7130–7137.

(229) Esclusa-Diaz, M. T.; Guimaraens-Méndez, M.; Pérez-Marcos, M. B.; Vila-Jato, J. L.; Torres-Labandeira, J. J. Characterization and in Vitro Dissolution Behaviour of Ketoconazole/β- and 2-Hydroxypropyl-β-Cyclodextrin Inclusion Compounds. *Int. J. Pharm.* **1996**, *143* (2), 203–210.

(230) Vojić, M. P.; Popović, G.; Sladić, D.; Pfendt, L. Protolytic Equilibria in Homogeneous and Heterogeneous Systems of Ketoconazole and Its Direct Spectrophotometric Determination in Tablets. *J. Serbian Chem. Soc.* **2005**, *70* (1), 67–78.

(231) El Tayar, N.; Van de Waterbeemd, H.; Testa, B. Lipophilicity Measurements of Protonated Basic Compounds by Reversed-Phase High-Performance Liquid Chromatography: II. Procedure for the Determination of a Lipophilic Index Measured by Reversed-Phase High-Performance Liquid Chromatography. *J. Chromatogr. A* **1985**, *320* (2), 305–312.

(232) Hsieh, Y.-L.; Ilevbare, G. A.; Van Eerdenbrugh, B.; Box, K. J.; Sanchez-Felix, M. V.; Taylor, L. S. PH-Induced Precipitation Behavior of Weakly Basic Compounds: Determination of Extent and Duration of Supersaturation Using Potentiometric Titration and Correlation to Solid State Properties. *Pharm. Res.* **2012**, *29* (10), 2738–2753.

(233) Rosenholm, J. M.; Czuryszkiewicz, T.; Kleitz, F.; Rosenholm, J. B.; Lindén, M. On the Nature of the Brønsted Acidic Groups on Native and Functionalized Mesoporous Siliceous SBA-15 as Studied by Benzylamine Adsorption from Solution. *Langmuir* **2007**, *23* (8), 4315–4323.

(234) Saxena, A.; Shah, D.; Padmanabhan, S.; Gautam, S. S.; Chowan, G. S.; Mandlekar, S.; Desikan, S. Prediction of PH Dependent Absorption Using in Vitro, in Silico, and in Vivo Rat Models: Early Liability Assessment during Lead Optimization. *Eur. J. Pharm. Sci.* **2015**, *76*, 173–180.

(235) Wang, Z.; Chen, B.; Quan, G.; Li, F.; Wu, Q.; Dian, L.; Dong, Y.; Li, G.; Wu, C. Increasing the Oral Bioavailability of Poorly Water-Soluble Carbamazepine Using Immediate-Release Pellets Supported on SBA-15 Mesoporous Silica. *Int. J. Nanomedicine* **2012**, *7*, 5807.

(236) Zhang, Y.; Wang, J.; Bai, X.; Jiang, T.; Zhang, Q.; Wang, S. Mesoporous Silica Nanoparticles for Increasing the Oral Bioavailability and Permeation of Poorly Water Soluble Drugs. *Mol. Pharm.* **2012**, *9* (3), 505–513.

(237) Dressman, J. B.; Herbert, E.; Wieber, A.; Birk, G.; Saal, C.; Lubda, D. Mesoporous Silica-based Dosage Forms Improve Release Characteristics of Poorly Soluble Drugs: Case Example Fenofibrate. *J. Pharm. Pharmacol.* **2016**, *68* (5), 634–645.

VITA

Siddhi Santosh Hate received her Bachelors in Chemical Technology from Institute of Chemical Technology in Mumbai, India in May 2013. Shortly after, she moved to the United States to pursue Masters in Chemical Engineering at Rutgers University, New Brunswick. At Rutgers, her research was focused on process system engineering of particulate process such as wet granulation and fluid bed coating. During her Masters studies, Siddhi also visited Research Center for Pharmaceutical Engineering in Graz, Austria for six months of research. Upon graduation, Siddhi joined PhD program in Department of Industrial and Physical Pharmacy at Purdue University, West Lafayette in Fall 2015. Here, her research was focused on the design and evaluation of an *in vitro* apparatus for dissolution and absorption measurements of supersaturating drug delivery systems. During her PhD, she was a recipient of several travel grants and presentation awards at international conferences. She has also been awarded McKeehan Graduate Fellowship in Physical Pharmacy. Following her PhD studies, Siddhi joined Eli Lilly and Company, Indianapolis as a Research Scientist in the Drug Developability group.

PUBLICATIONS

- **Hate S**., Reutzel-Edens S, Taylor L. S., 'Effect of electrostatic interaction between drug and silica on dissolution behavior in mesoporous silica-based drug delivery systems'. (*Under Preparation*)

- **Hate S**., Reutzel-Edens S, Taylor L. S., 'Dissolution of Mesoporous Silica-Based Formulations: Implications of Adsorption Tendency, Supersaturation and Absorptive Sink on Drug Release'. (*Under Preparation*)

- **Hate S**., Reutzel-Edens S, Taylor L. S., 'Absorptive dissolution testing: An improved approach to study the impact of residual crystallinity on the performance of amorphous formulations'. *J. Pharm. Sci.* 2020, 109 (3), 1312-1323.

- **Hate S**., Reutzel-Edens S., Taylor L. S., 'Insight into amorphous solid dispersion performance by coupled dissolution and membrane mass transfer measurements'. *Mol. Pharm.* 2019, *16 (1)*, 448-461.

- **Hate S.**, Reutzel-Edens S., Taylor L. S., 'Absorptive dissolution testing of supersaturating systems: Impact of absorptive sink conditions on solution phase behavior and mass transport'. *Mol. Pharm.* 2017,*14 (11)* 4052-63.